



Engineering Analysis Report for the Climate Change Engineering Vulnerability Assessment

FINAL REPORT



BRITISH COLUMBIA

BC Ministry of Transportation and Infrastructure
Engineering Branch
P.O. Box 9850 Stn Prov Govt
4B – 940 Blanshard Street
Victoria, BC
V8W 9T5

With support from Natural Resources Canada through the Adaptation Platform



Natural Resources
Canada

Ressources naturelles
Canada

Canada

11 August 2014

nhc

northwest hydraulic consultants

water resource specialists



PACIFIC CLIMATE IMPACTS CONSORTIUM

Acknowledgements

Trevor Murdock and Markus Schnorbus of PCIC (Pacific Climate Impacts Consortium) contributed significantly to this work. They recommended the selection of the three global climate model runs used in this study (CNRM-CM5 RCP8.5 run 1, CanESM2 RCP8.5 run 1, and ACCESS1-0 RCP8.5 run 1) and the downscaling methodology most appropriate for a study focusing on extreme events (Bias Correction and Constructed Analogues, or BCCA). They made available the three (3) projected climatic time daily series of precipitation and temperature that formed the basis of our climate scenarios; and provided all necessary information pertaining to the methodology by which those projections had been downscaled.

Stephen Sobie of PCIC clipped the large original datasets to a smaller region encompassing this study's watersheds and nearby meteorological stations, thereby reducing our work effort.

We gratefully acknowledge the assistance of the above individuals and organization.

Table of Contents

1	Introduction	1
1.1	Background and scope	1
1.2	A note regarding uncertainty as it pertains to this study.....	2
2	PART I – Climate change impacts on streamflow.....	4
2.1	Global climate models (GCMs) considered in this study.....	4
2.2	Interpreting comparisons between GCM grid cell data and historical observations at climate stations	5
2.3	Highway 97 East of Pine Pass	7
2.3.1	The observed historical climate record	7
2.3.2	Historical observations of climate vs. GCM simulations and future projections.....	7
2.4	Highway 37A near Stewart	19
2.5	Highway 20 near Bella Coola	29
2.6	Hydrologic modelling of streamflow in Fisher Creek	39
2.6.1	Overview of the HEC-HMS Model	39
2.6.2	Limitations of the modelling.....	39
2.6.3	Modelling Approach	40
2.6.4	Simulations using the Fisher Creek Model	43
2.6.5	Development of future climate data for input to the Fisher Creek Model.....	44
2.6.6	Fisher Creek Model results.....	45
2.6.7	Analyses of historical and future maximum hourly flow in Fisher Creek.....	54
2.7	Climate change impacts to future streamflow at other locations	59
2.7.1	Fur Thief Creek Culvert at Highway 97 east of Pine Pass	59
2.7.2	Bitter Creek Bridge No. 0554 at Highway 37A near Stewart.....	59
2.7.3	Medby Creek Culverts at Highway 20 near Bella Coola	61

3	PART II - Vulnerability analysis	63
3.1	Estimates of total load and total capacity at selected structures	63
3.1.1	Fisher Creek Bridge No. 7110 at Highway 97 east of Pine Pass	63
3.1.2	Fur Thief Creek Culvert at Highway 97 east of Pine Pass	64
3.1.3	Bitter Creek Bridge 0554 at Highway 37A near Stewart	64
3.1.4	Medby Creek Culverts at Highway 20 near Bella Coola	65
3.2	Vulnerability and Capacity Deficit at the selected structures	66
4	PART III - Impact of recent extreme climate on selected structures	68
4.1	Fisher Creek Bridge No. 7110 at Highway 97 east of Pine Pass	68
4.2	Fur Thief Creek Culvert at Highway 97 east of Pine Pass	70
4.3	Bitter Creek Bridge 0554 at Highway 37A near Stewart	71
4.4	Medby Creek Culverts at Highway 20 near Bella Coola	72
4.5	Summary	74
5	PART IV - Commentary on current practice and best practice for the future	75
5.1	Current practice in hydrotechnical design of stream crossings	75
5.1.1	Hydrologic Analysis	75
5.1.2	Hydraulic Design	75
5.2	Best Practice for the future	76
5.2.1	Hydrologic Analysis	76
5.2.2	Hydraulic Design	77
5.3	Recommendations for future studies	79
6	References	82

List of Tables

Table 1. The three global climate model (GCM) runs considered in this report.....	4
Table 2. Summary of selected model processes	41
Table 3. Watershed characteristics for Windrem Creek (Proxy) and Fisher Creek.....	43
Table 4. Annual peak hourly discharges (m ³ /s) from the seven scenario simulations (historic climate and six future climate projections).	53
Table 5. Estimates of the 200-year hourly peak flow based on simulations of historic climate and future climate projections, with changes relative to the simulated historic baseline. Values in parentheses are from simulation with an alternate CNRM-CM5 climate scenario, developed with the exclusion of an exceptionally high daily precipitation value (details in Appendix A).	55
Table 6. Fisher Creek HEC-HMS Model sensitivity to adjustment of precipitation gradient and time of concentration	58
Table 7. Estimated increase in 200-year maximum hourly flow at Fur Thief Creek.	59
Table 8. Comparison of GCM Projections for the areas of Highway 97 east of Pine Pass and Highway 37A near Stewart (from Figures 3 and 10).....	60
Table 9. Estimated increase in 200-year maximum hourly flow at Bitter Creek.....	61
Table 10. Comparison of GCM Projections for the areas of Highway 97 east of Pine Pass and Highway 20 near Bella Coola (from Figures 3 and 15).....	61
Table 11. Estimated increase in 200-year maximum hourly flow at Medby Creek.	62
Table 12. Vulnerability and Capacity Deficit at the selected structures	67
Table 13. Summary of extreme climate event rainfall and estimated flows at the four structures.....	74
Table 14. Summary of future changes in design discharge at the four structures with low and high estimates (CanESM2 late century and CNRM-CM5 mid-century) removed.....	78

List of Figures

Figure 1. Superposition of the 1/12° spatial grid of the downscaled GCM simulations onto a topographic map of Highway 97 east of Pine Pass, showing the Fisher Creek watershed (red) and two regional meteorological stations (green)	6
Figure 2. Highway 97 east of Pine Pass; Watersheds and climate station location.....	8
Figure 3. Mean temperature and annual precipitation for the observed historical record and GCM hindcasts and projections for Highway 97 east of Pine Pass.....	9

Figure 4. Observed and GCM-simulated mean number of wet days per year and mean precipitation intensity on wet days for Highway 97 east of Pine Pass; the area of the rectangles shown gives the mean annual precipitation.10

Figure 5. Probability of non-exceedance plots for daily precipitation at Highway 97 east of Pine Pass (showing observed, GCM hindcasted, and GCM projected)11

Figure 6. Non-exceedance probability for the duration of a wet period at Highway 97 east of Pine Pass.....13

Figure 7. Non-exceedance probability of the duration of a dry period at Highway 97 east of Pine Pass.....15

Figure 8. Simulated historical and projected precipitation totals over multiple-day periods at Highway 97 east of Pine Pass17

Figure 9. Highway 37A near Stewart, BC; Bitter Creek Watershed and climate station location.....20

Figure 10. Mean temperature and annual precipitation for the observed historical record and GCM hindcasts and projections for Highway 37A near Stewart21

Figure 11. Observed and GCM-simulated mean number of wet days per year and mean precipitation intensity on wet days for Highway 37A near Stewart; the area of the rectangles shown gives the mean annual precipitation.22

Figure 12. Probability of non-exceedance plots for daily precipitation at Highway 37A near Stewart (showing observed, GCM hindcasted and GCM projected)23

Figure 13. Simulated historical and projected precipitation totals over multiple-day periods for Highway 37A near Stewart26

Figure 14. Highway 20 near Bella Coola, BC; Medby Creek Watershed and climate station location.....30

Figure 15. Mean temperature and annual precipitation for the observed historical record and GCM hindcasts and projections for Highway 20 near Bella Coola.31

Figure 16. Observed and GCM-simulated mean number of wet days per year and mean precipitation intensity on wet days, for Highway 20 near Bella Coola.32

Figure 17. Probability of non-exceedance plots for daily precipitation at Highway 20 near Bella Coola, showing observed, GCM hindcasted and GCM projected.....33

Figure 18. Simulated historical and projected precipitation totals for different accumulation periods for Highway 20 near Bella Coola.36

Figure 19. Summary of the procedure used for creating time series of daily precipitation and temperature for future climate scenarios.....45

Figure 20. Fisher Creek watershed hydrologic model simulation inputs (temperature and precipitation) and outputs (SWE and discharge) for the historic climate record.46

Figure 21. Fisher Creek watershed hydrologic model simulation inputs (temperature and precipitation) and outputs (SWE and discharge) for the ACCESS1 2040-2069 climate scenario.....	47
Figure 22. Fisher Creek watershed hydrologic model simulation inputs (temperature and precipitation) and outputs (SWE and discharge) for the ACCESS1 2070-2100 climate scenario.....	48
Figure 23. Fisher Creek watershed hydrologic model simulation inputs (temperature and precipitation) and outputs (SWE and discharge) for the CanESM2 2040-2069 climate scenario.....	49
Figure 24. Fisher Creek watershed hydrologic model simulation inputs (temperature and precipitation) and outputs (SWE and discharge) for the CanESM2 2070-2100 climate scenario.....	50
Figure 25. Fisher Creek watershed hydrologic model simulation inputs (temperature and precipitation) and outputs (SWE and discharge) for the CNRM-CM5 2040-2069 climate scenario.....	51
Figure 26. Fisher Creek watershed hydrologic model simulation inputs (temperature and precipitation) and outputs (SWE and discharge) for the CNRM-CM5 2070-2100 climate scenario.....	52

Appendices

Appendix A. Development of Future Climate Scenarios for Fisher Creek’s Hydrologic Model (Detailed Write-up)	
Appendix B. Development, calibration and testing of the Proxy (Windrem Creek) HEC-HMS Model	
Appendix C. Fisher Creek HEC-HMS Model: Simulated Annual Peak Hourly Discharge Frequency Analysis Fits	
Appendix D. Sensitivity Analysis of Fisher Creek HEC-HMS Model: Simulated Annual Peak Hourly Discharge Frequency Analysis Fits	

1 INTRODUCTION

1.1 BACKGROUND AND SCOPE

The BC Ministry of Transportation and Infrastructure (MOTI) has been developing vulnerability studies and reports to determine the implications and impacts that future climate change will have on its infrastructure. Past studies and reports were prepared in several parts of the province that follow the PIEVC Engineering Protocol for Infrastructure Vulnerability Assessment and Adaptation to a Changing Climate (Protocol) and which provided guidance through the steps of the vulnerability assessments. As part of that protocol, this current study involves a detailed engineering vulnerability assessment of three British Columbia Highway segments: (i) Highway 20 in the Bella Coola Region; (ii) Highway 37A in the Stewart Region; and, (iii) Highway 97 in the Pine Pass Region.

Following consecutive large and damaging floods in BC in 2010 and 2011, MOTI has decided to conduct additional engineering analysis of the infrastructure components most severely affected by these floods. Northwest Hydraulic Consultants Ltd. (NHC) has been retained to carry out those analyses to help meet the following objectives:

- Gain an enhanced understanding of the circumstances that contributed to the service interruptions along the highway segments, both climatic and those related to infrastructure design, operation and maintenance;
- Evaluate and predict risk outcomes from future climate conditions based on applying the PIEVC Step 4 (Engineering Analysis) process on select infrastructure components that have been impacted by climate events;
- Inform the development of a Best Practice Document that will assist highway infrastructure owners, operators, maintenance personal and engineering staff address impacts associated with extreme precipitation.

The following report is divided into 4 parts. Part I is focused on how future changes in precipitation and temperature will affect annual maximum hourly streamflow at the following stream crossing structures:

- Fisher Creek Bridge No. 7117 on Highway 97 east of Pine Pass
- Fur Thief Creek Culvert on Highway 97 east of Pine Pass
- Bitter Creek Bridge on Highway 37A near Stewart; and,
- Medby Creek Culvert on Highway 20 near Bella Coola

The Pacific Climate Impacts Consortium (PCIC) has provided NHC with 150 years (1950-2099) of simulated historical (hindcasts) and future (projections) daily precipitation and temperature data for the 49 km² grid cell(s) (grid cells are defined by 1/12° of latitude and longitude, which corresponds roughly to 49 km at the latitude of interest) that includes the climate stations used as historical climate reference for each highway segment. NHC has studied the PCIC datasets and characterized projected changes in precipitation and temperature for the future mid-century period, 2040-2069, and the late-century period, 2070-2099 as compared to observed and GCM-simulated precipitation and temperature in the historical (reference) period.

For the Highway 97 segment, synthetic time series of precipitation and temperature were created using quantile to quantile mapping to mimic each of the 6 GCM-future time period combinations (scenarios). The historic time series and the synthetic time series for each scenario were used as input to a hydrologic model of Fisher Creek to predict changes to the 200-year annual maximum hourly flow that occur as a result of the projected climate change. NHC has made inferences regarding climate change impacts on streamflow for the other stream crossing locations (Fur Thief, Bitter Creek and Medby Creek) using the results of the Fisher Creek Model simulations and the characterization of projected climate changes along the other highway segments.

Part II of the report uses the results from Part I as the input data to performing the PIEVC Step 4 Vulnerability Analysis at the four crossing locations.

Part III provides an assessment of the impact of the extreme climate events on selected structures.

Part IV is an opportunity to review current practice and to provide guidance on changes to future best practice as it can be inferred from the results of this report and also some recommendations on future work.

1.2 A NOTE REGARDING UNCERTAINTY AS IT PERTAINS TO THIS STUDY

While there is a need to provide quantitative information for infrastructure planning and flood protection planning, the underlying projections of climate change are subject to large and unquantifiable uncertainty. The main sources of uncertainty are unknown future emissions of greenhouse gases, uncertain response of the global climate system to increases in greenhouse gas concentrations, and incomplete understanding of regional manifestations that will result from global changes (e.g., Hawkins and Sutton 2010).

The downscaling, in space and time, of GCM-projected climate variables, and the application of the hydrologic model, represent additional (albeit smaller) sources of uncertainty. The hydrologic projections developed in this work should therefore be considered to be plausible representations of the future, given the best current scientific information, and do not represent specific predictions.

The actual future realizations of streamflow at the watersheds studied here will differ from any of these scenarios, and their difference compared to historical streamflow may be greater or smaller than the differences projected in this work. To gain a wider perspective on issues related to uncertainty associated with extreme streamflow projections, the reader is referred to the analysis by Kundewicz et al. (2013) which is based on a vast body of literature, including the IPCC SREX report on climate extremes. The analysis by Kundewicz et al. (2013) concludes that "...presently we have only low confidence in numerical projections of changes in flood magnitude or frequency resulting from climate change".

The results produced by this study highlight the potential large variations in future flood estimates and illustrate the possible deviations from the APEGBC (2012) recommendation of applying a 10% increase to present design flows to account for climate change impacts by the end of the century.

2 PART I – CLIMATE CHANGE IMPACTS ON STREAMFLOW

2.1 GLOBAL CLIMATE MODELS (GCMs) CONSIDERED IN THIS STUDY

Selection of the three GCMs to use was based on the recommendation by Trevor Murdock of the Pacific Climate Impacts Group (PCIC). This recommendation was supported by PCIC’s work, reported in Murdock et al. (2013). In Murdock et al. (2013), the CMIP5 GCM simulations (i.e., those GCM simulations that formed the basis for the recent IPCC Fifth Assessment Report) were first subjected to elimination of those simulations which had performed worst in reproducing climatic extremes in their historical simulations when compared against observations. This was based on 27 indices of extremes (Sillman et al., 2013). This eliminated 12 GCM runs from the original 48 GCM runs.

Among the remaining 36 GCM runs, some are sufficiently similar to be seen as containing redundant information. On this basis, the set can be reduced to a smaller number of GCM runs which nevertheless is representative of the range of climate projections by the complete set. To obtain such a representative smaller set, Murdock et al. (2013) used a clustering algorithm which ordered the 36 GCM runs. The GCM runs ordered 1 through 12 are sufficient to capture nearly 90% of the variability of projections among all runs.

For this project, a maximum of three GCM runs was desired. Thus, the recommendation by Trevor Murdock was that we use the GCMs ordered 1, 2 and 3 by the above clustering algorithm. These three GCM runs are identified in Table 1.

Table 1. The three global climate model (GCM) runs considered in this report

GCM	Representative greenhouse gas concentration pathway (RCP)	Model run	Institution developing the GCM
ACCESS1-0	RCP 8.5 Wm ²	Run 1	CSIRO (Commonwealth Scientific and Industrial Research Organisation, Australia), and BOM (Bureau of Meteorology, Australia)
CanESM2	RCP 8.5 Wm ²	Run 1	Canadian Centre for Climate Modelling and Analysis, Canada.
CNRM-CM5	RCP 8.5 Wm ²	Run 1	Centre National de Recherche Météorologique, France.

PCIC provided downscaled results for the three GCM runs listed in Table 1. The spatial resolution of these downscaled simulations is $1/12^\circ$ (5 arc minutes) and the temporal resolution is daily.

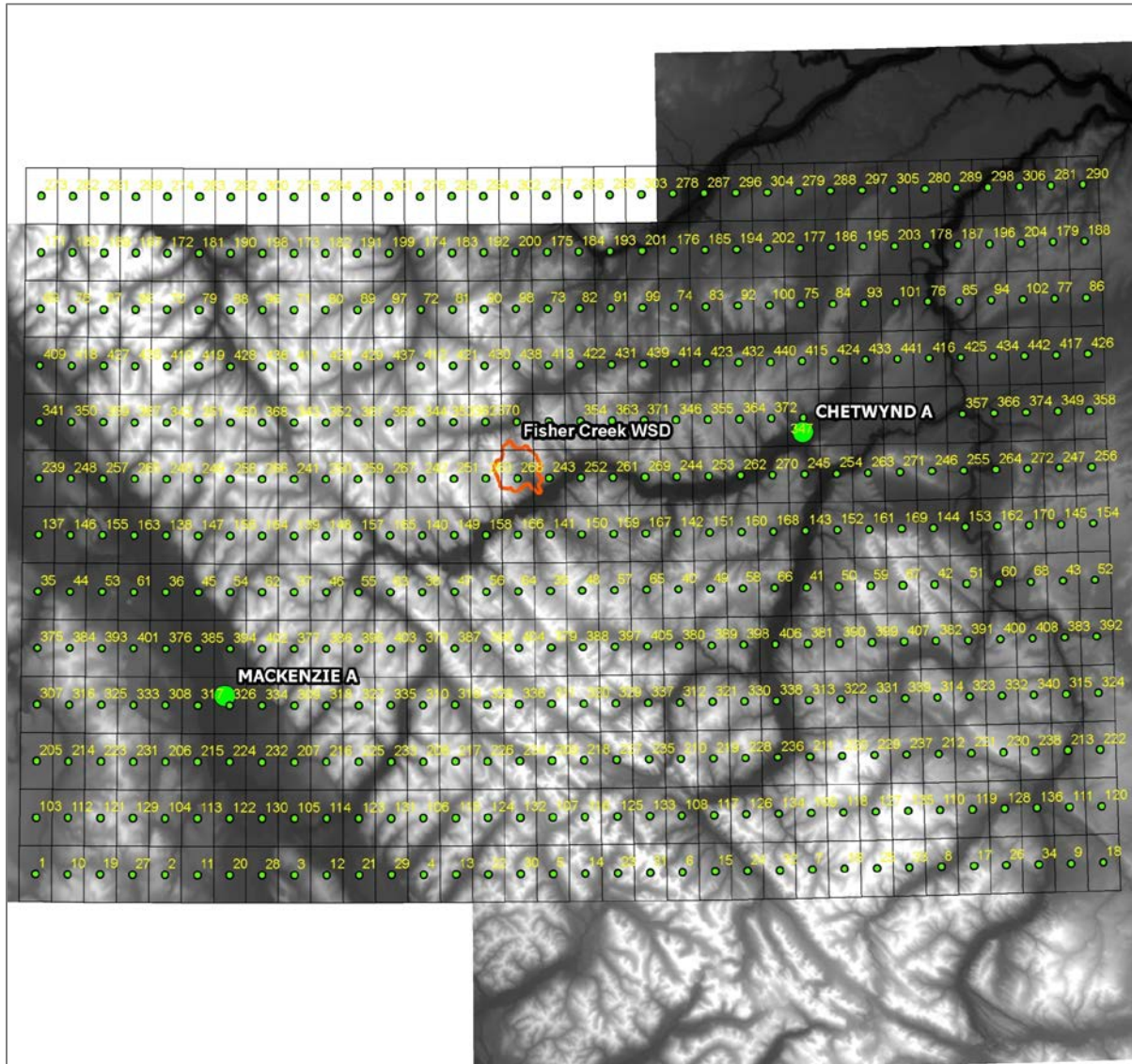
The downscaling technique employed by PCIC, designated BCCAQ, is similar to the BCCA technique followed by the BCSD technique. The reader is referred to Murdock et al. (2013) for further information and references on these techniques.

2.2 INTERPRETING COMPARISONS BETWEEN GCM GRID CELL DATA AND HISTORICAL OBSERVATIONS AT CLIMATE STATIONS

The downscaled simulations of the GCMs are grid cell values, not point values. Grid cells are defined by geographical coordinates with a spacing of 5 arc minutes ($1/12^\circ$) along parallels (longitude) and meridians (latitude). At the latitude of Fisher Creek east of Pine Pass for example, each grid cell has a surface area of about 49 km^2 (Figure 1). A dry day (precipitation = 0) can only occur where precipitation fell nowhere at all within the area of the grid cell. At a meteorological station, which may be approximated as a point rather than an area, we can expect there will be more dry days than for the entire grid cell that surrounds it. We can also expect to see more extremely high precipitation intensity at a point location than we will see averaged over an area. While one portion of the terrain area corresponding to a grid cell may experience very intense precipitation, other portions of the grid cell terrain may receive only moderate precipitation; hence the extreme values are lower when we consider larger areas. The averaging effect over large areas lowers the extremes of intense precipitation, and shortens dry spells, when compared to a point location such as a meteorological station.

With the above considerations in mind, we see that GCM simulations of precipitation over the historical period should not match station observations either in intensity or dry period and wet period duration. It is the annual average precipitation which ought to match more closely, which implies that the larger number of wet days over a grid cell compared to a station is expected to compensate for the lower mean precipitation intensity. Excepted are those cases where the precipitation gradient within a grid cell is very steep – such as when the terrain increases rapidly in elevation. The latter is markedly the case for Highway 37A near Stewart (Section 2.4). In such cases, even the annual values of average precipitation and temperature can differ considerably between grid cell estimates and station observations.

Figure 1. Superposition of the 1/12° spatial grid of the downscaled GCM simulations onto a topographic map of Highway 97 east of Pine Pass, showing the Fisher Creek watershed (red) and two regional meteorological stations (green)



2.3 HIGHWAY 97 EAST OF PINE PASS

Figure 2 shows a location map of the area of Highway 97 east of Pine Pass.

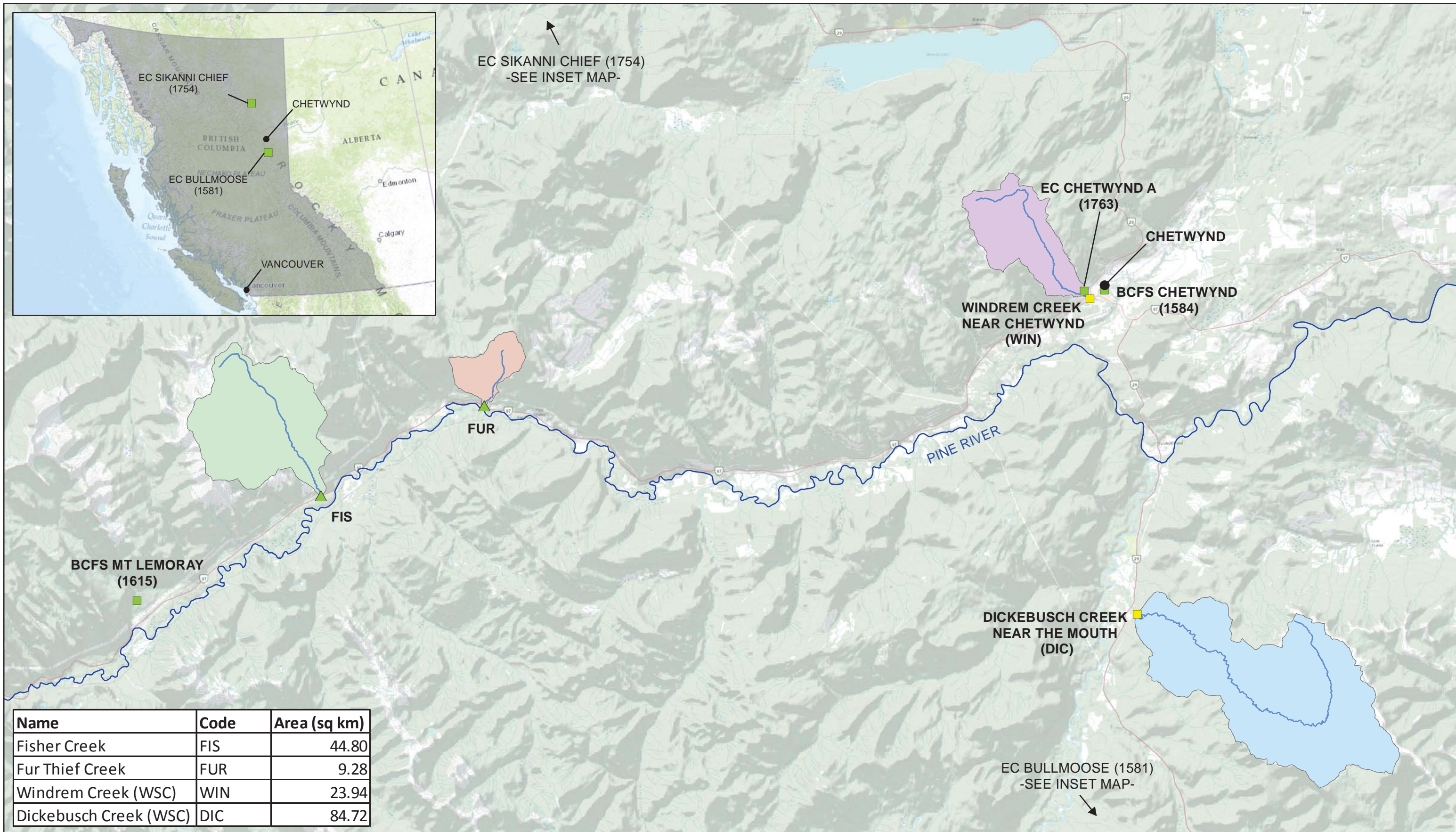
2.3.1 THE OBSERVED HISTORICAL CLIMATE RECORD

The historic dataset for Highway 97 east of Pine Pass utilizes amalgamated data from the following Environment Canada climate stations for years containing at least 90% complete data. The amalgamated record contains a total of 34 years with 5 years excluded due to data gaps (1997, 2002, 2006, 2008, and 2009):

- Environment Canada (EC) *Chetwynd Airport 1181508* (Chetwynd A), elevation 609.6 metres (Figure 2)
 - Period of record: 1982-2011. Incomplete daily data for most years (precipitation and temperature used) with intermittent hourly data available for summer periods.
- EC *Chetwynd BCFS 1181509* (Chetwynd BCFS), elevation 659.9 metres, a decommissioned climate station approximately 1.5 km north-northeast of Chetwynd A (Figure 2)
 - Period of record: 1973-1982. Incomplete daily data for most years (precipitation and temperature used) with intermittent hourly data available for some summer periods.

2.3.2 HISTORICAL OBSERVATIONS OF CLIMATE VS. GCM SIMULATIONS AND FUTURE PROJECTIONS

Figure 3 shows the period-averaged annual mean temperature and precipitation simulated by each GCM run, for three time periods: 1) the historical period, 2) the mid-21st-century (2040-2069), and 3) the late-21st-century (2070-2100). Also shown are the means from the observed historical record (solid black circle). The agreement between the three GCMs for the simulated historical period (all three lines meet at about the same point for period 1951-2000) is most certainly the result of their statistical downscaling by the BCSD technique (the last step in their downscaling) which, by construct, forces their agreement with the historical climatological values in the ANUSPLIN dataset (see Murdock et al., 2013). It appears likely that the ANUSPLIN dataset differs from the Chetwynd station observations and that would be the explanation for the difference in Figure 3 between the annual means at the station and those of the GCMs for 2051-2000. We don't know whether Chetwynd A or Chetwynd BCFC were included in the observational dataset that served as a basis for ANUSPLIN.



Name	Code	Area (sq km)
Fisher Creek	FIS	44.80
Fur Thief Creek	FUR	9.28
Windrem Creek (WSC)	WIN	23.94
Dickebusch Creek (WSC)	DIC	84.72


 Ministry of Transportation and Infrastructure

 northwest hydraulic consultants

- Hydrometric Station
- Climate Stations
- ▲ Key Sites
- Streams

DATA SOURCES:
 BACKGROUND - ESRI WORLD TOPO MAP
 WATERSHEDS AND STREAMS - FWA
 HYDROMETRIC STATIONS - WATER SURVEY OF CANADA
 CLIMATE STATIONS - ENVIRONMENT CANADA

SCALE - 1:200,000

 N

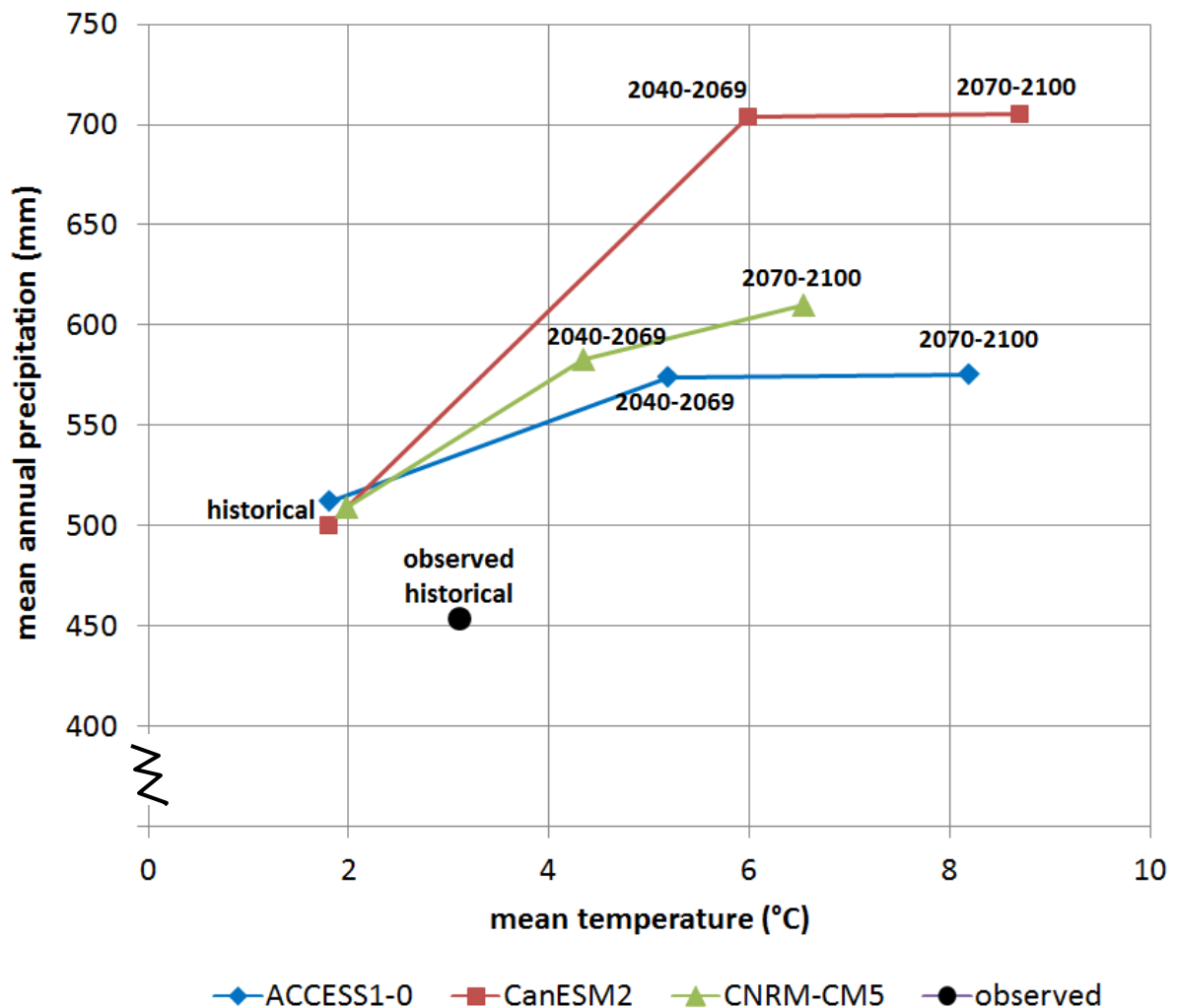
Coordinate System: NAD 1983 UTM ZONE 10N
 Units: METERS

Job: 300314 Date: 26-MAR-2014

CCEVA - ENGINEERING ANALYSIS REPORT
 HIGHWAY 97 EAST OF PINE PASS WATERSHED AND CLIMATE STATION LOCATIONS
FIGURE 2

All three GCM runs project large increases in mean annual temperature at this location, a warming of between 4.5°C and nearly 7°C by the end of the century (Figure 3). In the case of CanESM2, warming is projected to occur rapidly, reaching 4°C by mid-century. All three GCM runs also project increases in mean annual precipitation, in the case of CanESM2 by as much as 40%. Analysis of seasonal changes was outside the scope of this study.

Figure 3. Mean temperature and annual precipitation for the observed historical record and GCM hindcasts and projections for Highway 97 east of Pine Pass



The projected future changes in mean annual precipitation seen in Figure 3 are in part due to changes in the mean intensity of precipitation on wet days, and in part to changes in the mean number of wet days per year. Figure 4 shows the projected values of mean intensity and number of wet days. The area of the rectangles shown gives the mean annual precipitation. The simulated historical mean annual precipitation is higher than the station observations because the lower mean

precipitation intensity and the larger number of wet days of the grid cell (compared to the point station) do not balance each-other out (refer to the discussion in Section 2.2).

All three GCM runs project rises in mean precipitation intensity on wet days, and two of them project increases in the mean number of wet days per year (Figure 4). The ACCESS1-0 run projects a small decline in wet day occurrence.

The distribution of daily precipitation for the observed historical record, and the historical simulations and future projections from each GCM are shown in Figure 5.

Figure 4. Observed and GCM-simulated mean number of wet days per year and mean precipitation intensity on wet days for Highway 97 east of Pine Pass; the area of the rectangles shown gives the mean annual precipitation.

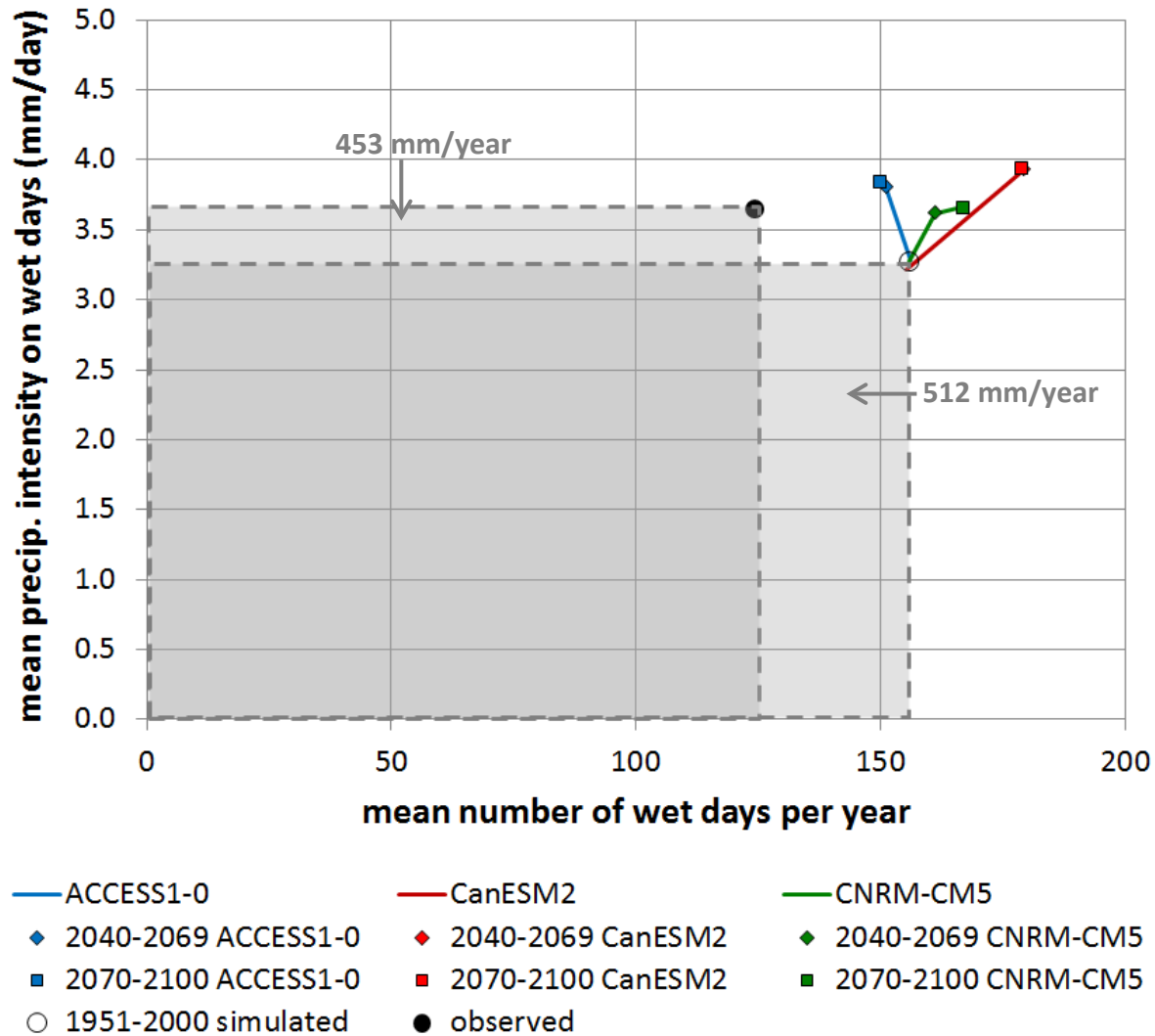


Figure 5. Probability of non-exceedance plots for daily precipitation at Highway 97 east of Pine Pass (showing observed, GCM hindcasted, and GCM projected)

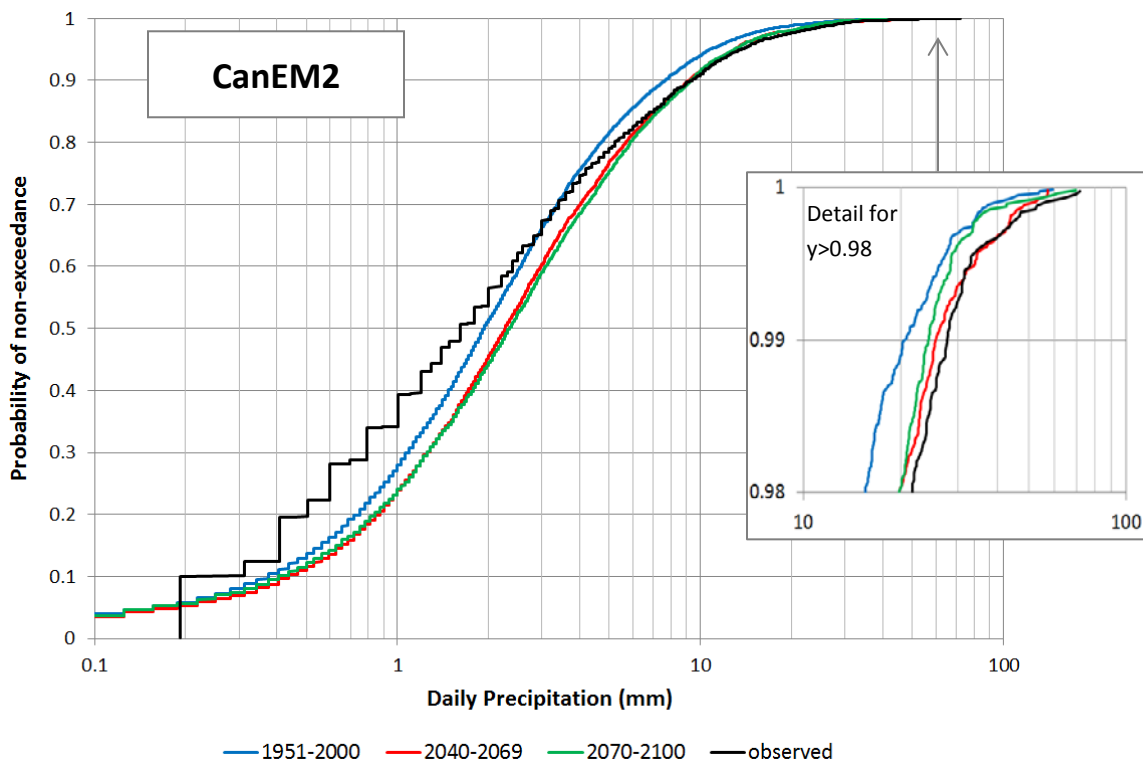
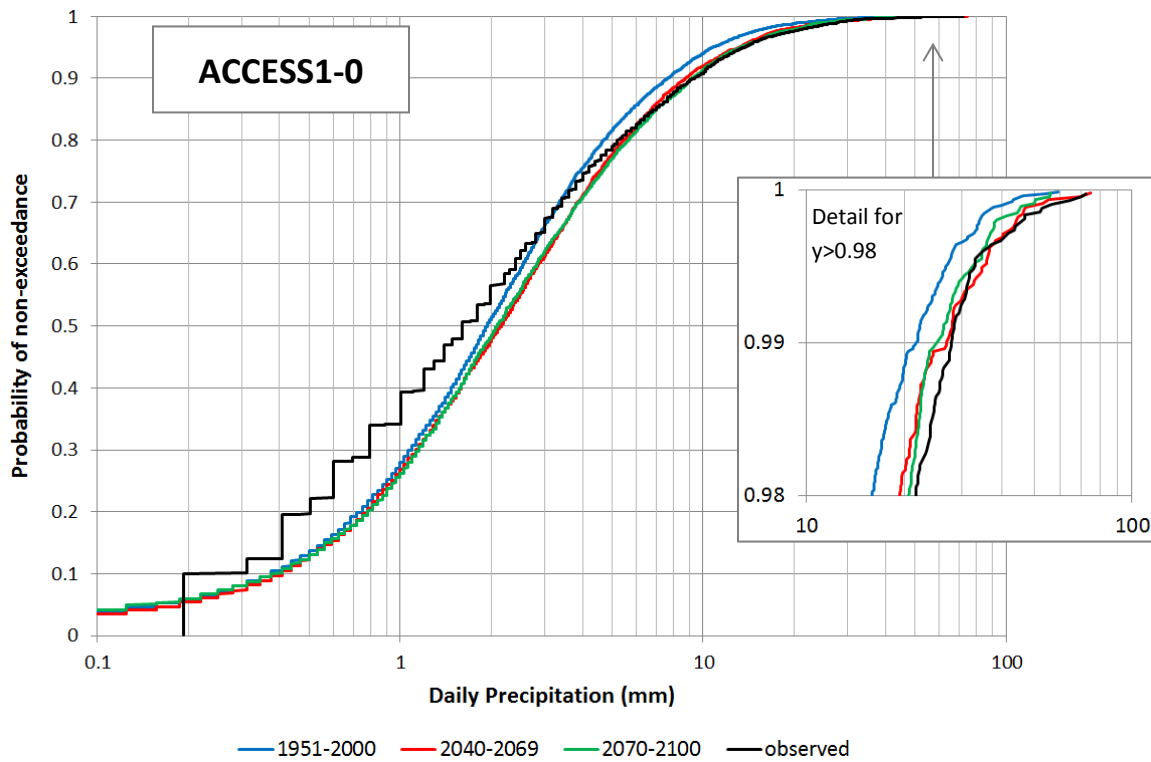
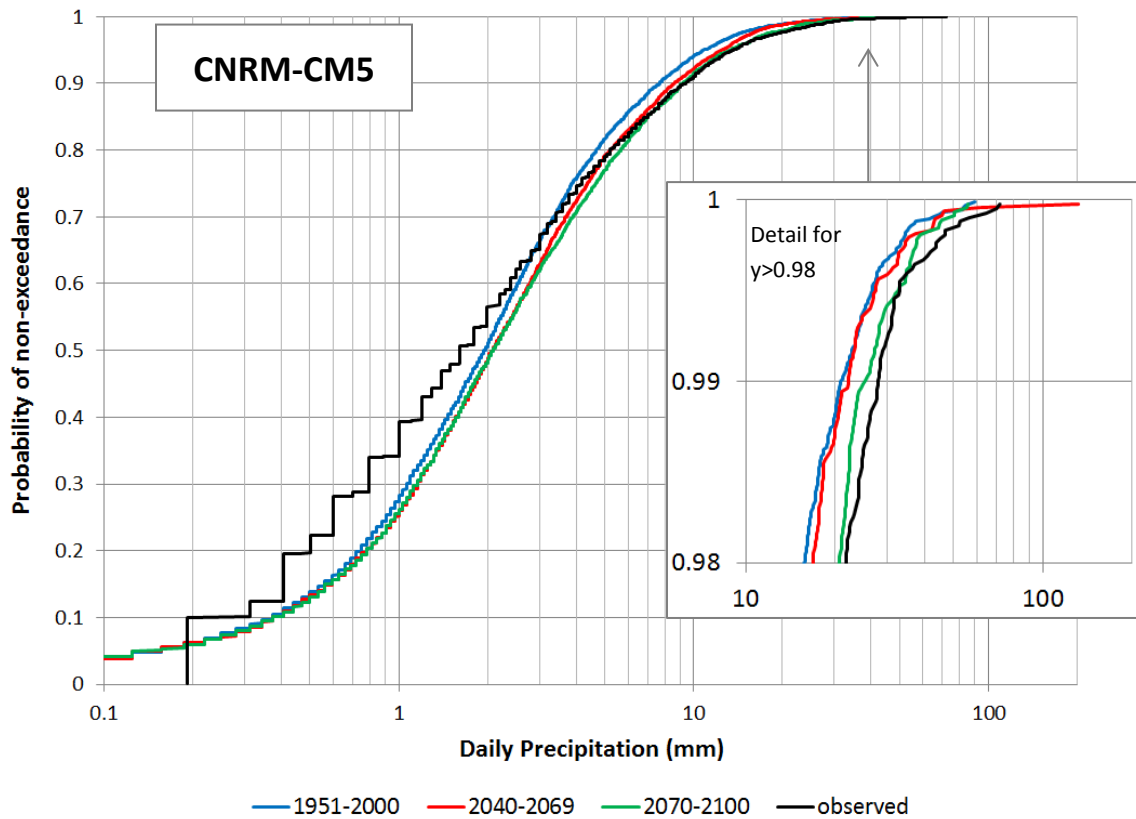


Figure 5 (cont'd). Probability of non-exceedance plots for daily precipitation at Highway 97 east of Pine Pass (showing observed, GCM hindcasted, and GCM projected)



As shown in Figure 6, the length of wet periods (defined as uninterrupted sequences of days receiving precipitation) simulated for the historical period has a distribution quite similar to observations, for all three GCM runs; the largest differences being for CanESM2. Only relatively small changes are projected for the 21st century.

Since the simulations have more wet days per year than the station observations, but their wet periods are similar in length, then it must be the case that the dry simulated periods tend to be shorter than the station dry periods. This can be seen in Figure 7. This figure also shows that future projected changes in dry period duration are small.

Figure 6. Non-exceedance probability for the duration of a wet period at Highway 97 east of Pine Pass

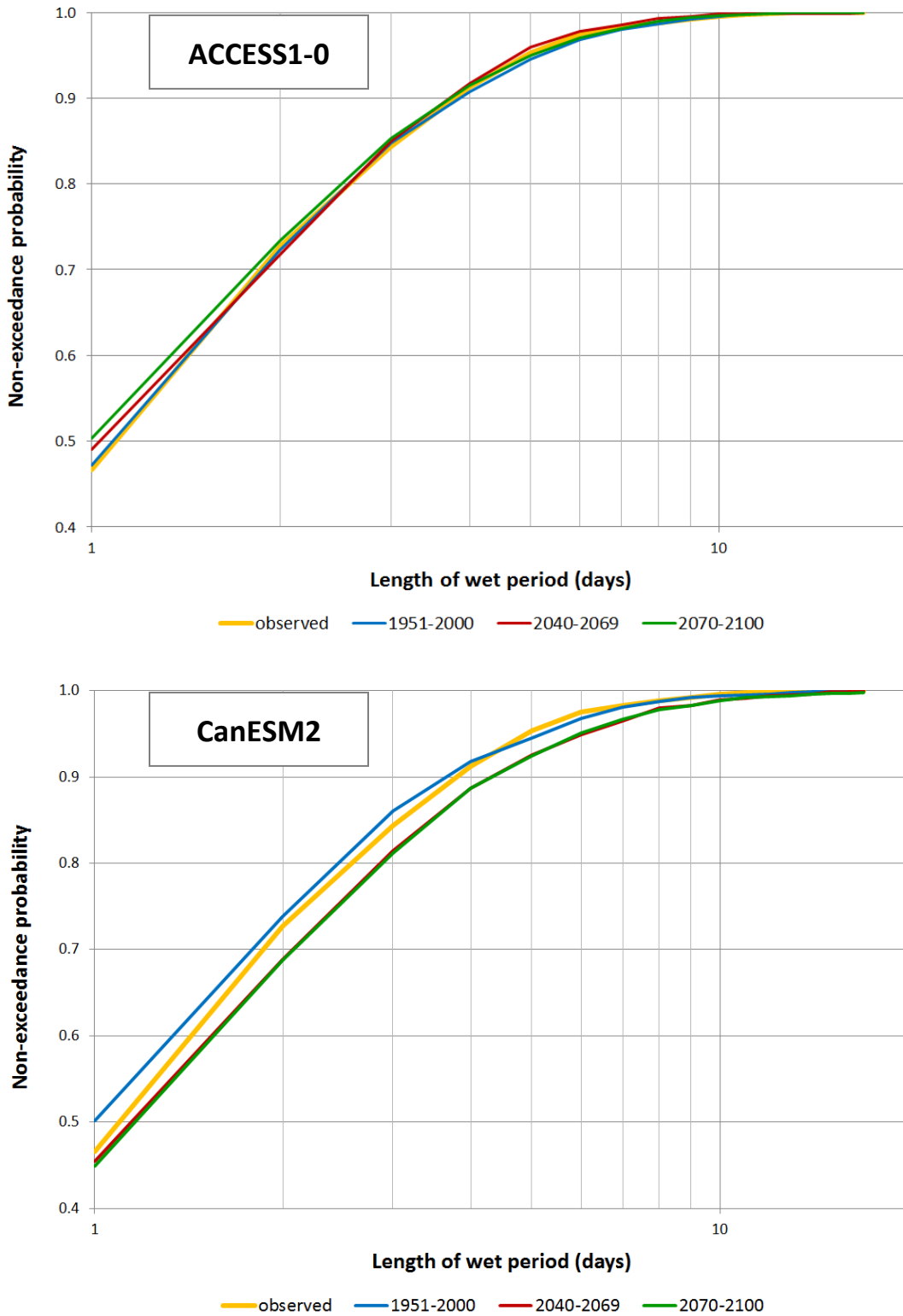


Figure 6 (cont'd). Non-exceedance probability for the duration of a wet period at Highway 97 east of Pine Pass

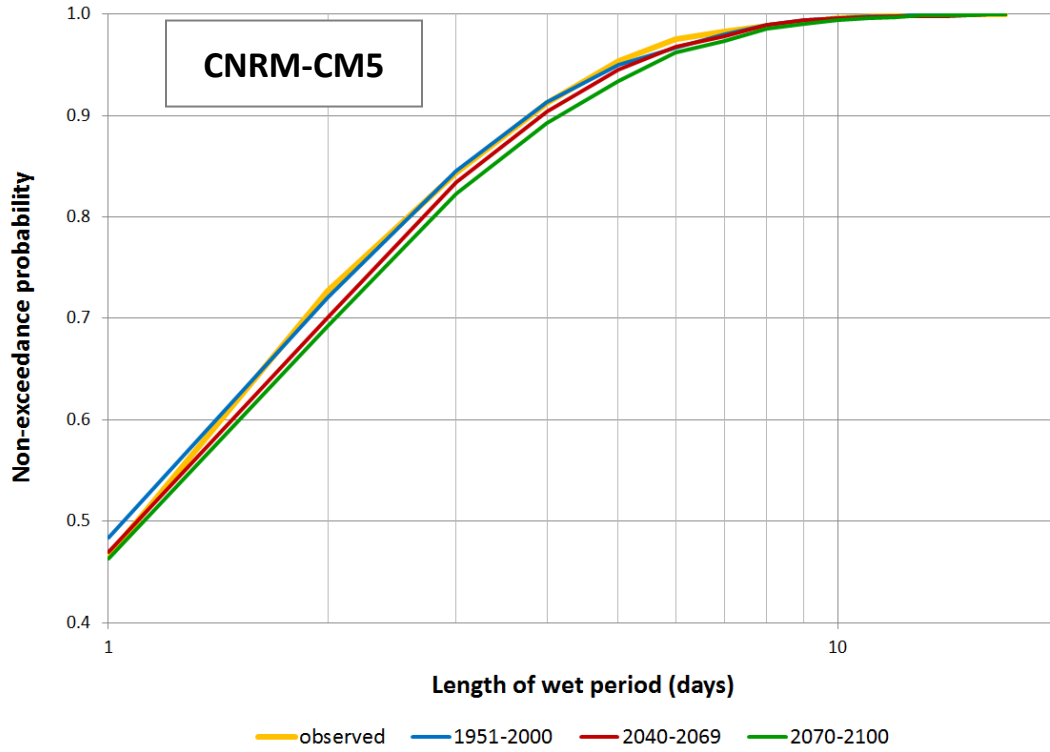


Figure 7. Non-exceedance probability of the duration of a dry period at Highway 97 east of Pine Pass

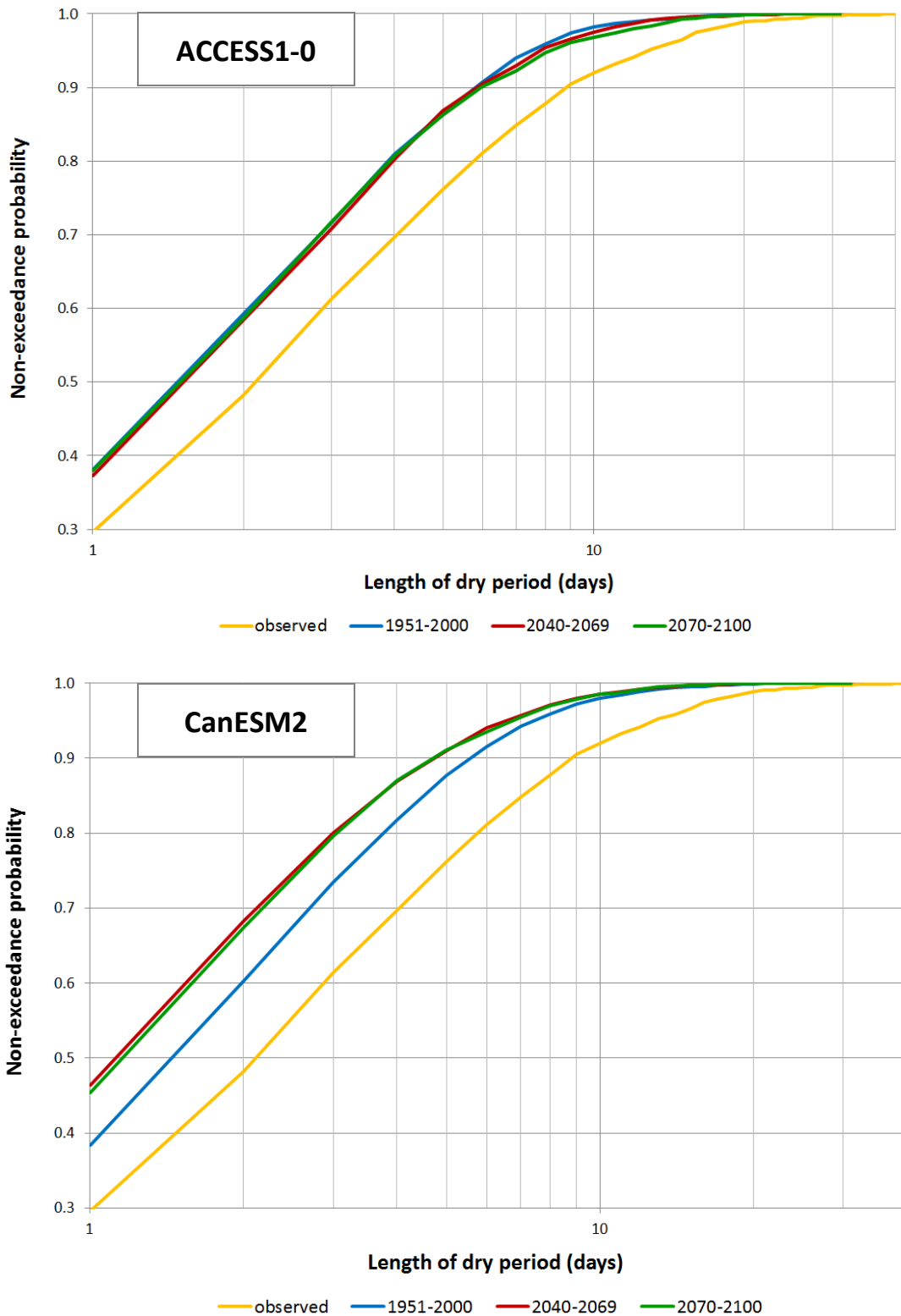
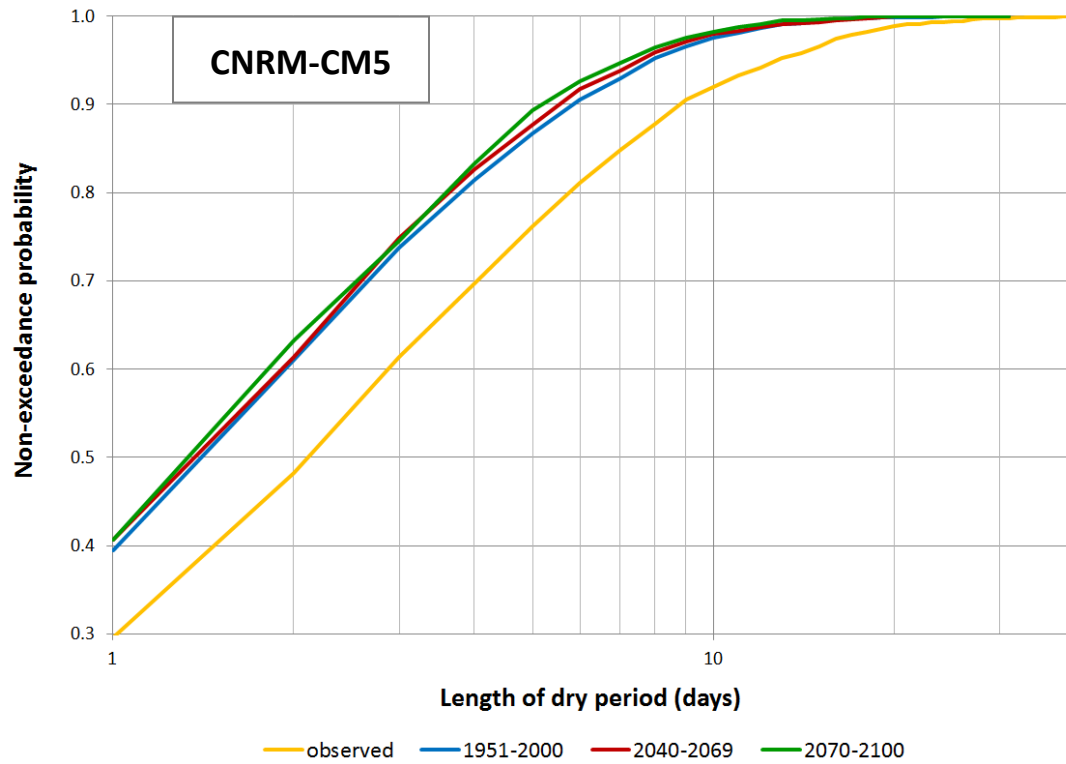


Figure 7 (cont'd). Non-exceedance probability of the duration of a dry period at Highway 97 east of Pine Pass



Important to this study is the occurrence of multiple-day precipitation events. Figure 8 shows the percentiles of total precipitation accumulated over different periods from 1 day through 30 days. For all three GCMs there appears an overall tendency for the projected rate of increase in the 10th percentile to be slightly faster than that of the 50th percentile, and for the rate of increase of the 50th percentile to be slightly faster than that of the 90th percentile, up until mid-century. After mid-century, only the CNRM-CM5 run projects a further increase in the 90th percentile through the late century. CNRM-CM5 does not project increases in the 50th percentile from mid-century to late-century, yet projects increases in the 90th percentile during that same period.

Figure 8. Simulated historical and projected precipitation totals over multiple-day periods at Highway 97 east of Pine Pass

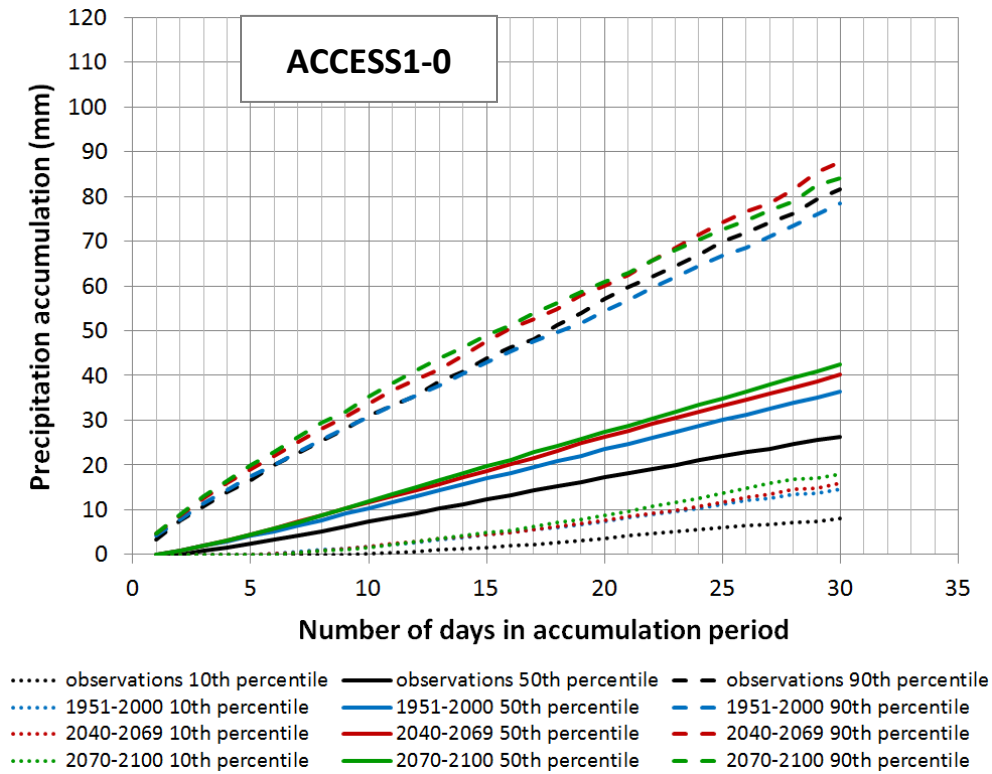
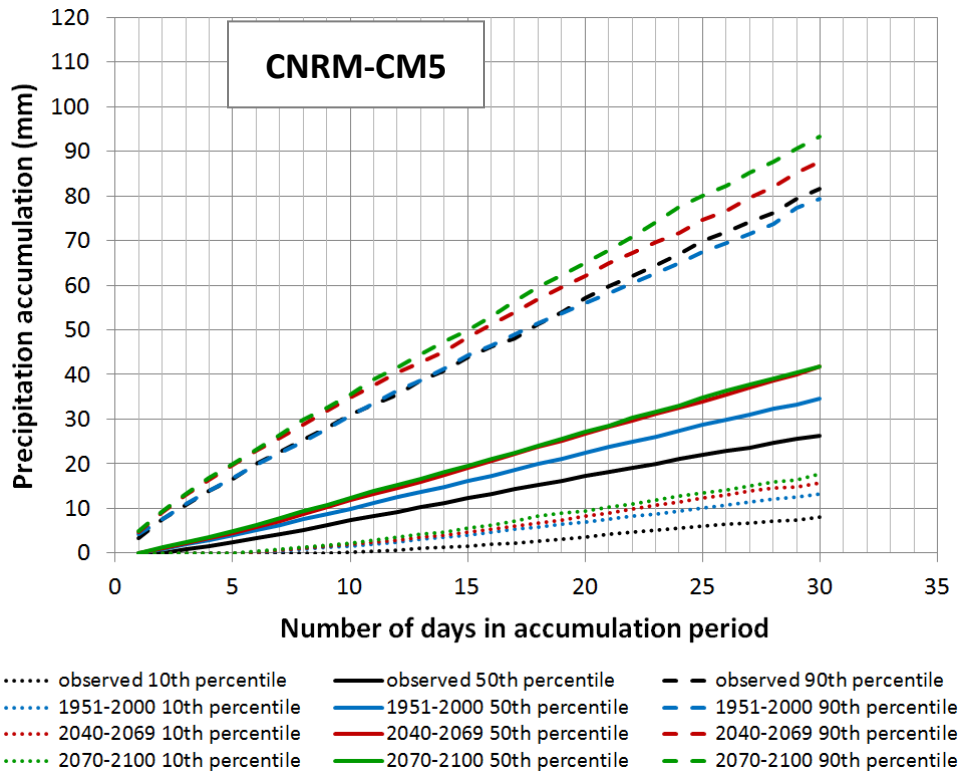
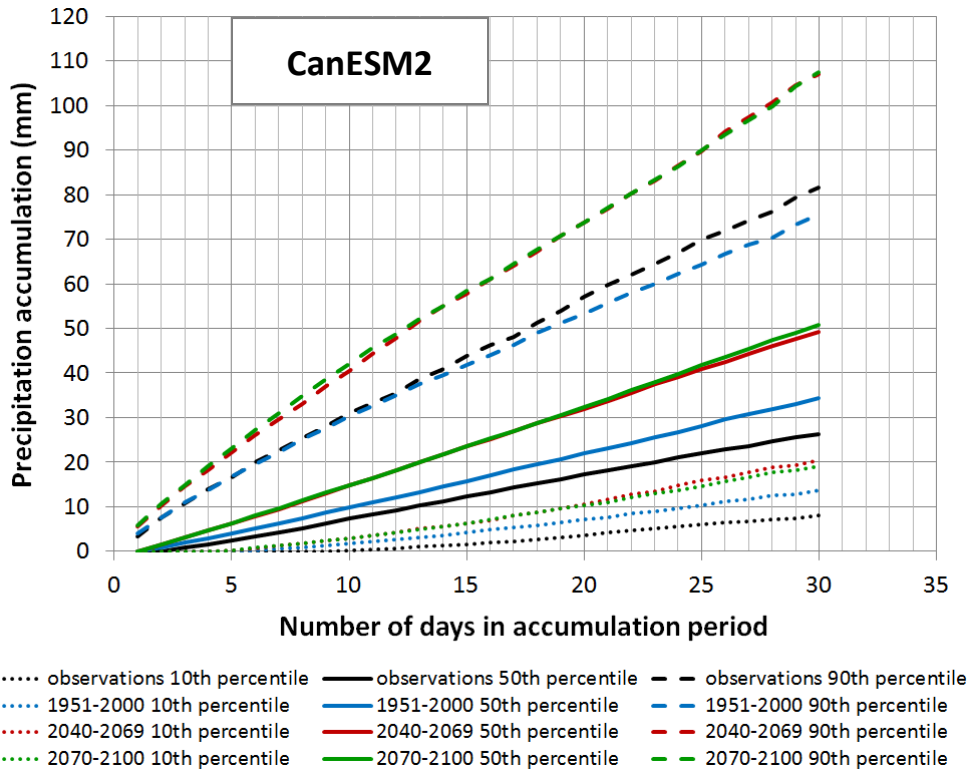


Figure 8 (Cont'd). Simulated historical and projected precipitation totals over multiple-day periods at Highway 97 east of Pine Pass

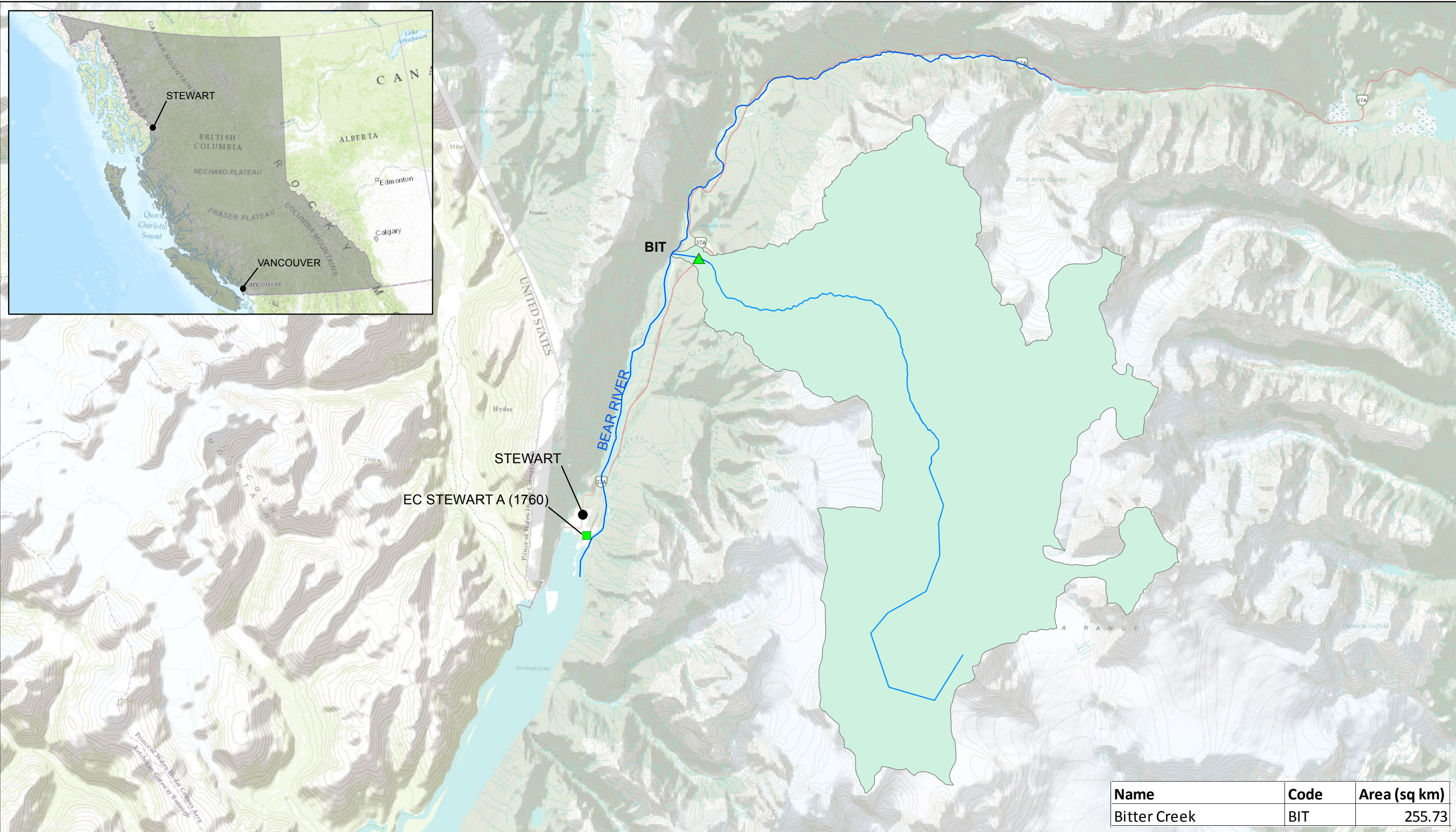


2.4 HIGHWAY 37A NEAR STEWART

A location map for the area of Highway 37A near Stewart, BC is shown in Figure 9. Figures 10 through 13 tell a story that is in many respects similar to that presented for Fisher Creek in the previous section. This time, however, all three GCM runs project increases from mid-century to late-century in precipitation mean annual totals. In the case of Fisher Creek such increases were mostly limited to the period leading up to mid-century.

The ACCESS1-0 run does not project significant changes in the 50th percentile of precipitation, yet projects increases in the 90th percentile, to mid-century and further on to late-century (Figure 13). The CanESM2 run projects the largest future increases in the 90th percentile of precipitation.

The observed historical record for Highway 37A near Stewart is the daily record at Environment Canada Station 1067742 (Stewart Airport), which covers the period from 1974-2012.



Name	Code	Area (sq km)
Bitter Creek	BIT	255.73

BRITISH COLUMBIA
The Best Place on Earth

Ministry of Transportation and Infrastructure

nhc
northwest hydraulic consultants

- Climate Stations
- ▲ Key Sites
- Streams

DATA SOURCES:
BACKGROUND - ESRI WORLD TOPO MAP
WATERSHEDS AND STREAMS - FWA

SCALE - 1:150,000

0 1 2 3 4 5 6 KM

N

Coordinate System: NAD 1983 UTM ZONE 9N
Units: METERS

Job: 300314 Date: 17-MAR-2014

CCEVA - ENGINEERING ANALYSIS REPORT
HIGHWAY 37A NEAR STEWART, BC
BITTER CREEK WATERSHED AND CLIMATE STATION LOCATIONS

FIGURE 9

Figure 10. Mean temperature and annual precipitation for the observed historical record and GCM hindcasts and projections for Highway 37A near Stewart

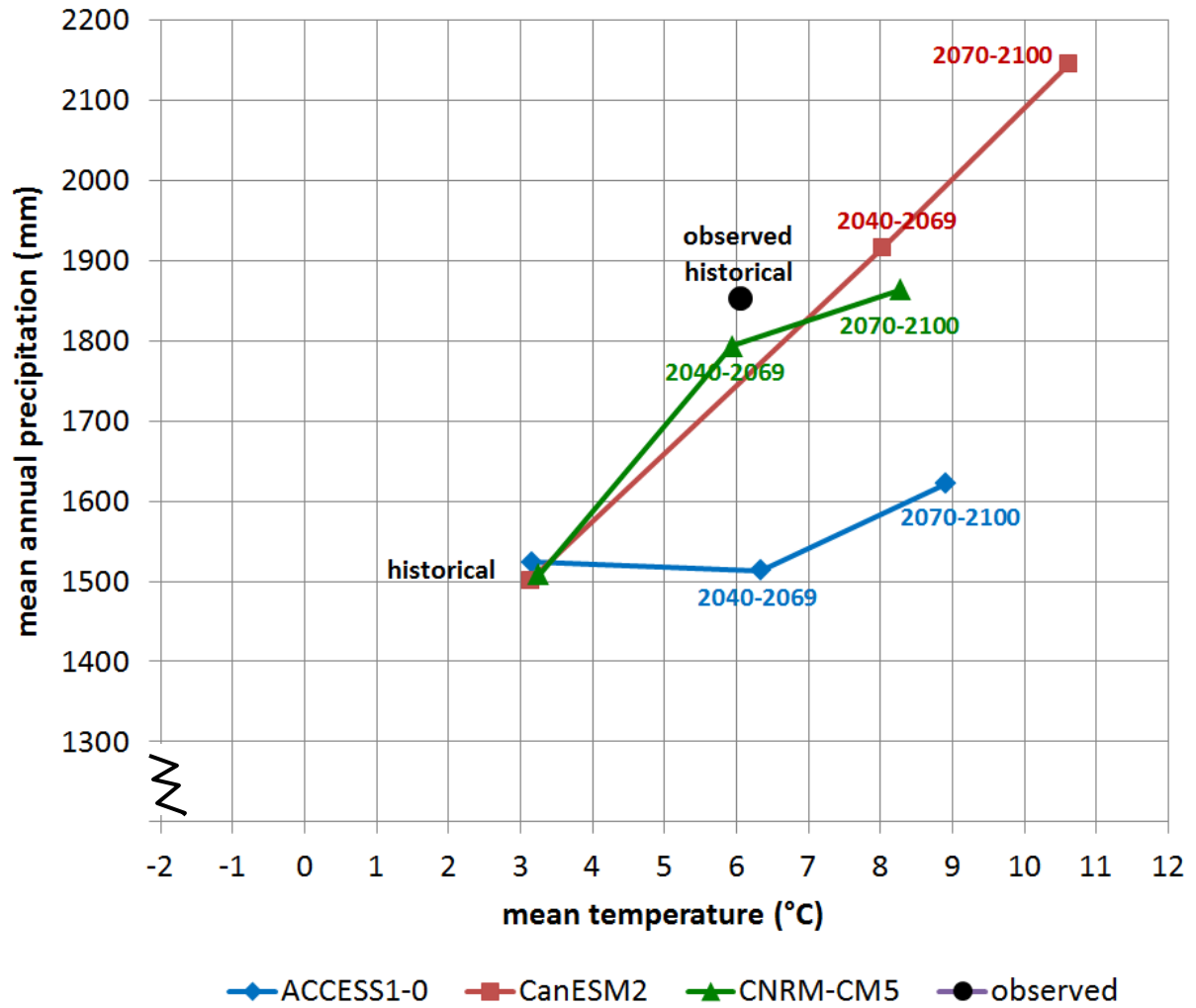


Figure 11. Observed and GCM-simulated mean number of wet days per year and mean precipitation intensity on wet days for Highway 37A near Stewart; the area of the rectangles shown gives the mean annual precipitation.

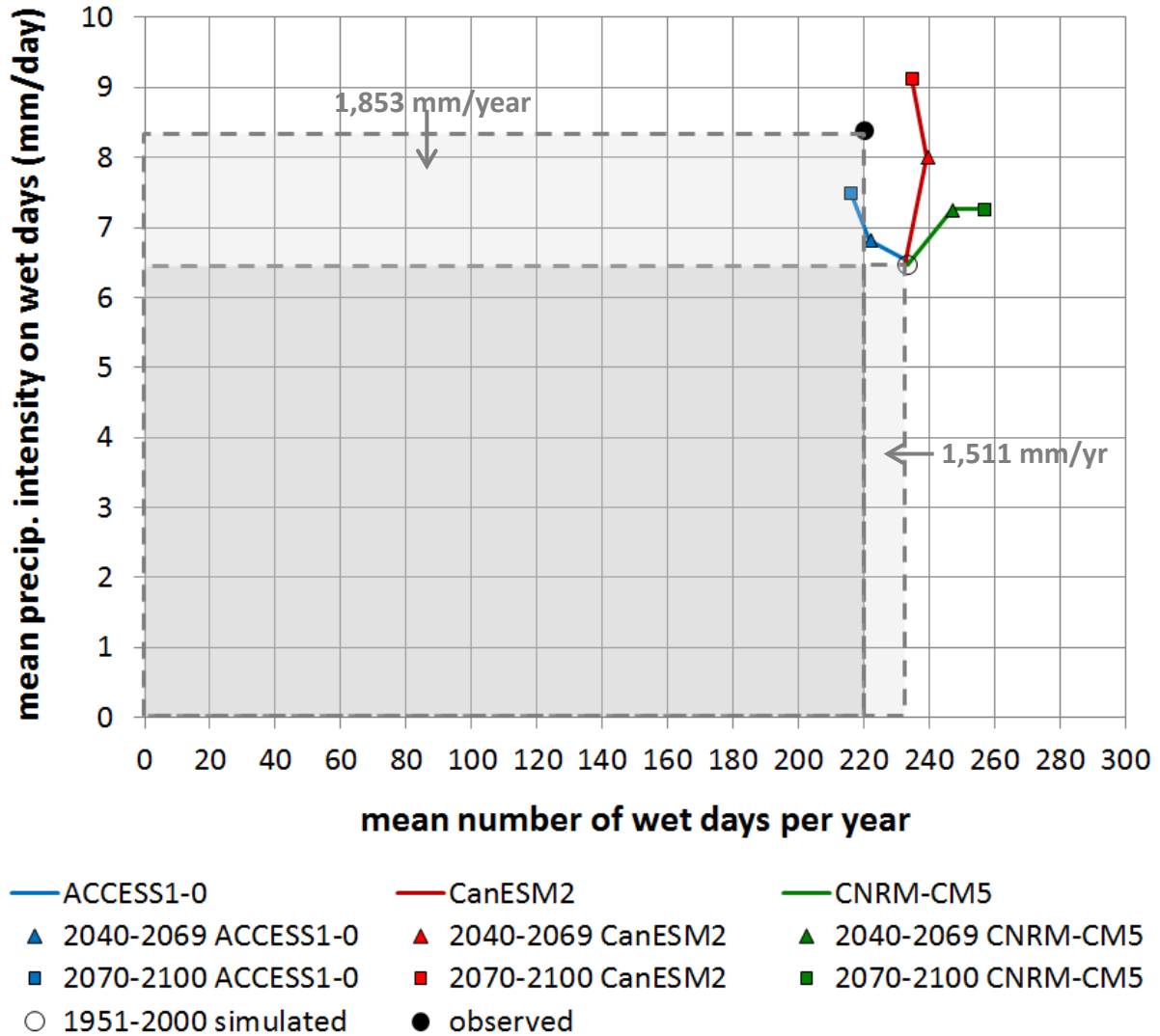


Figure 12. Probability of non-exceedance plots for daily precipitation at Highway 37A near Stewart (showing observed, GCM hindcasted and GCM projected)

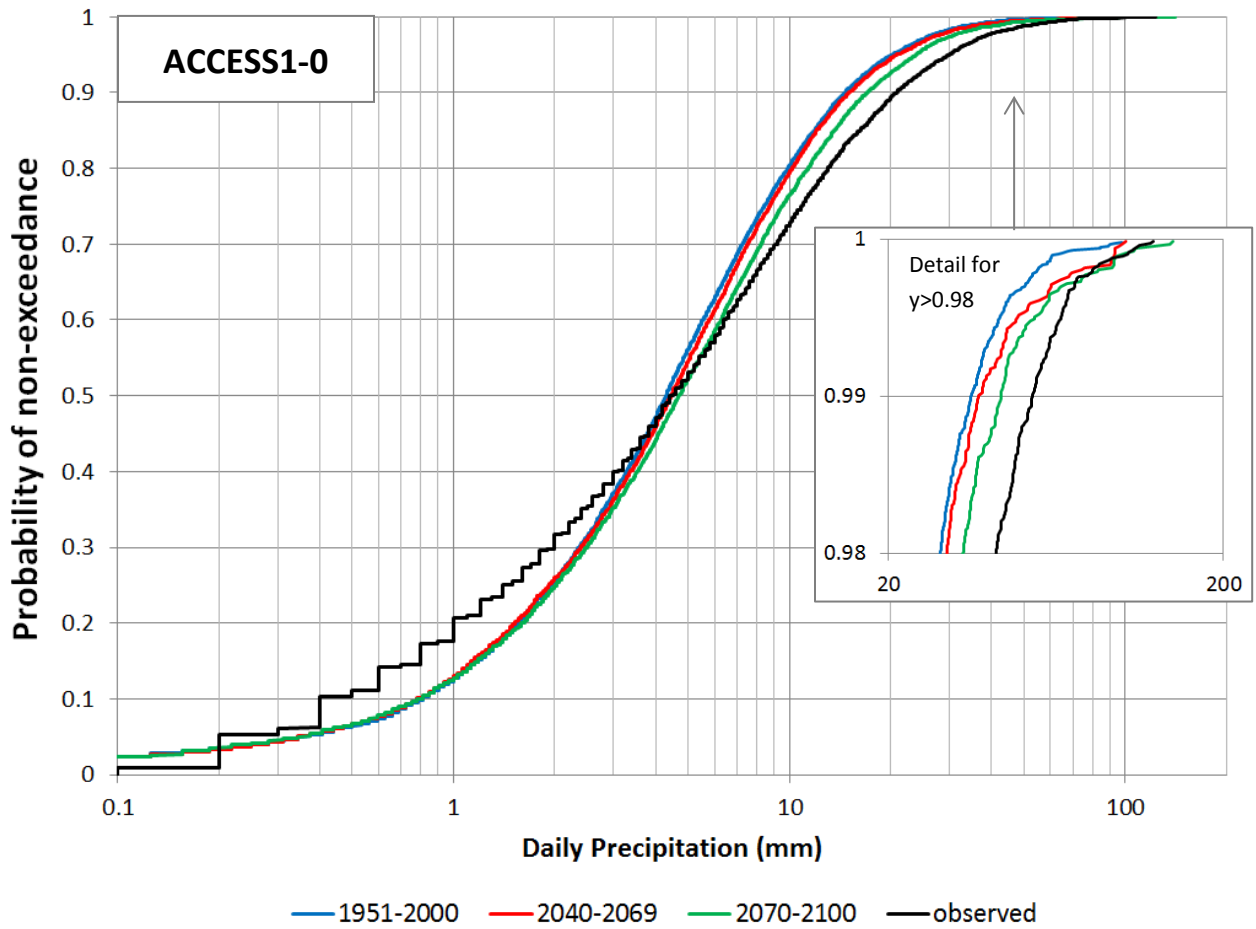


Figure 12 (cont'd). Probability of non-exceedance plots for daily precipitation at Highway 37A near Stewart (showing observed, GCM hindcasted and GCM projected)

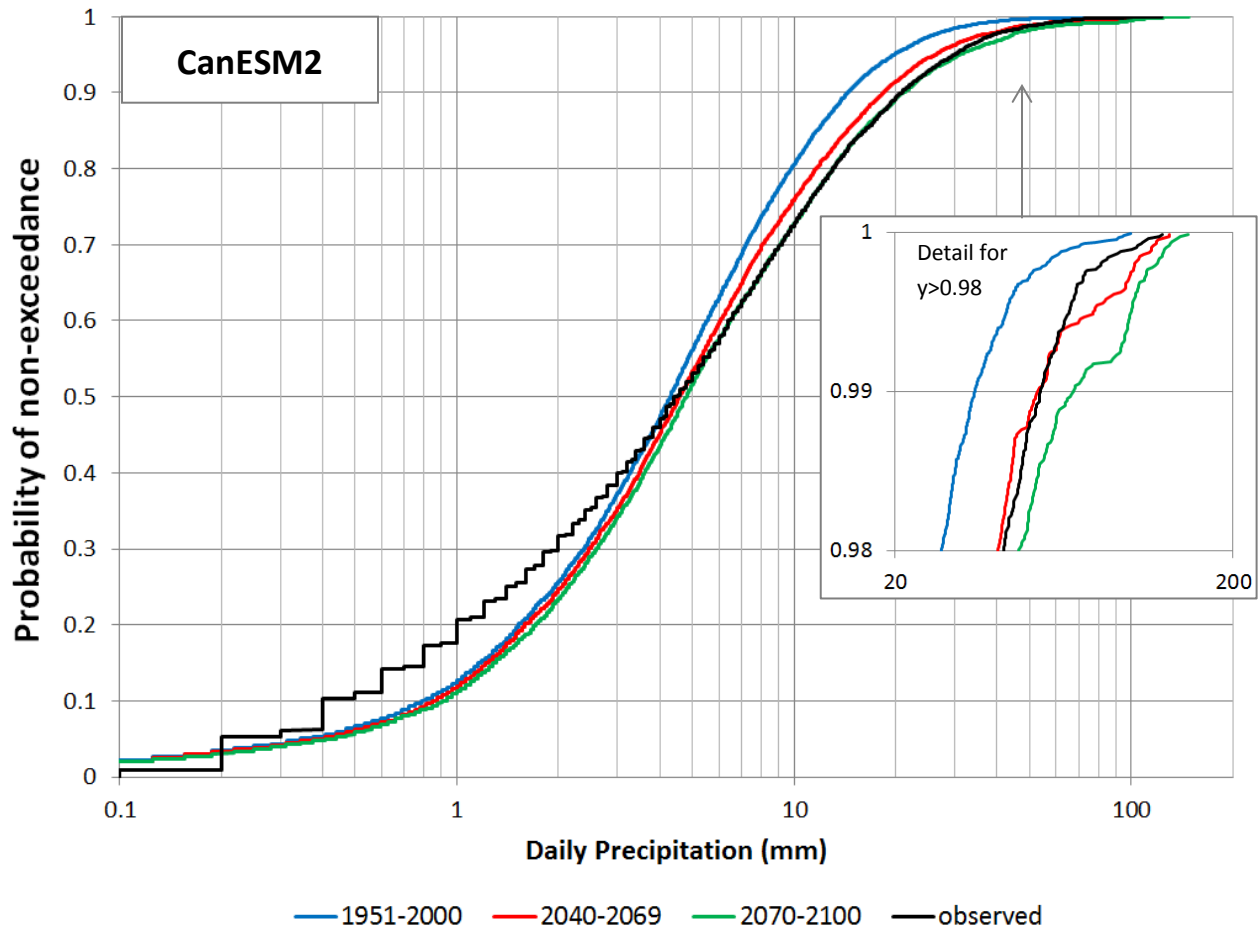


Figure 12 (cont'd). Probability of non-exceedance plots for daily precipitation at Highway 37A near Stewart (showing observed, GCM hindcasted and GCM projected)

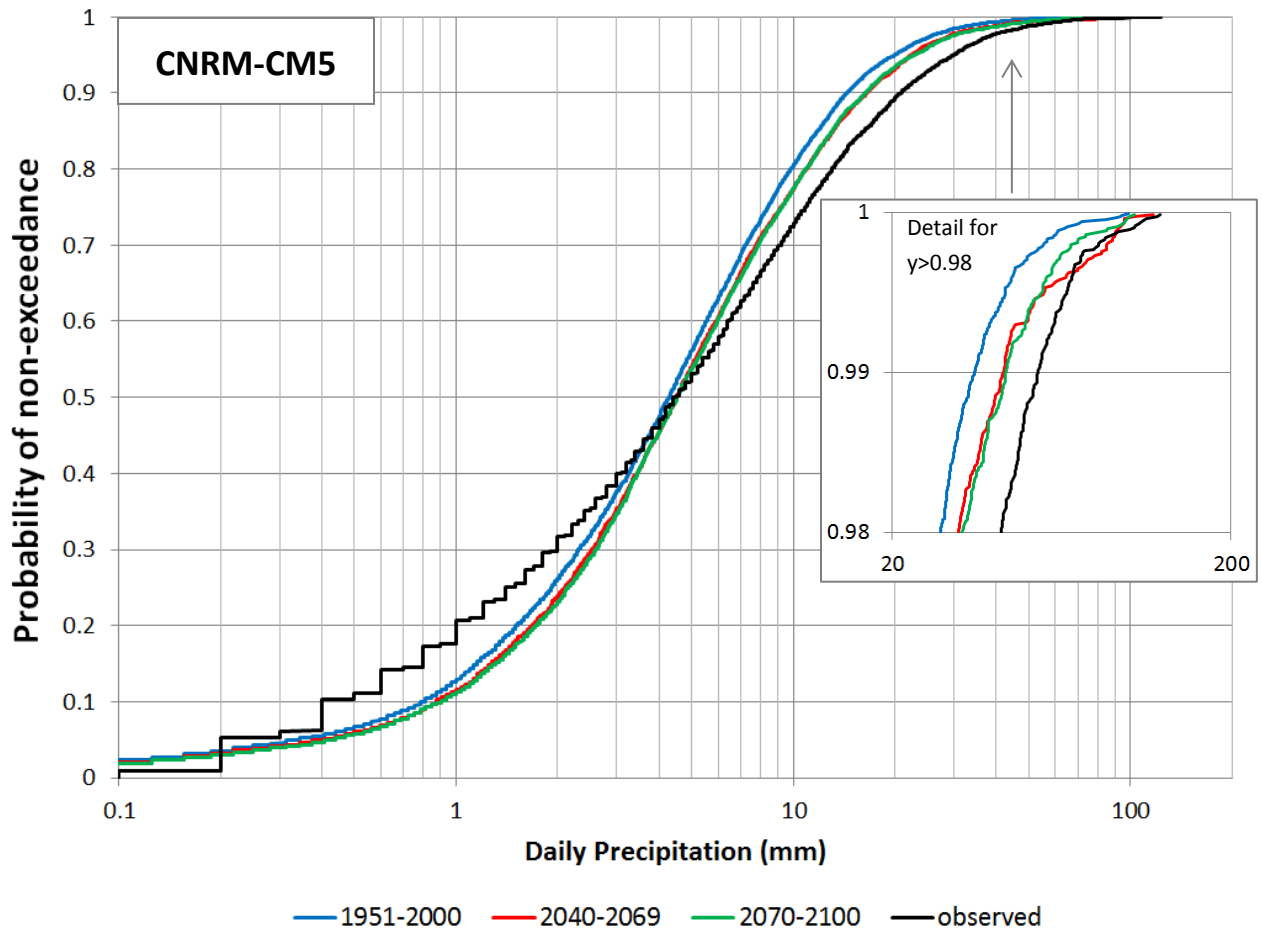


Figure 13. Simulated historical and projected precipitation totals over multiple-day periods for Highway 37A near Stewart

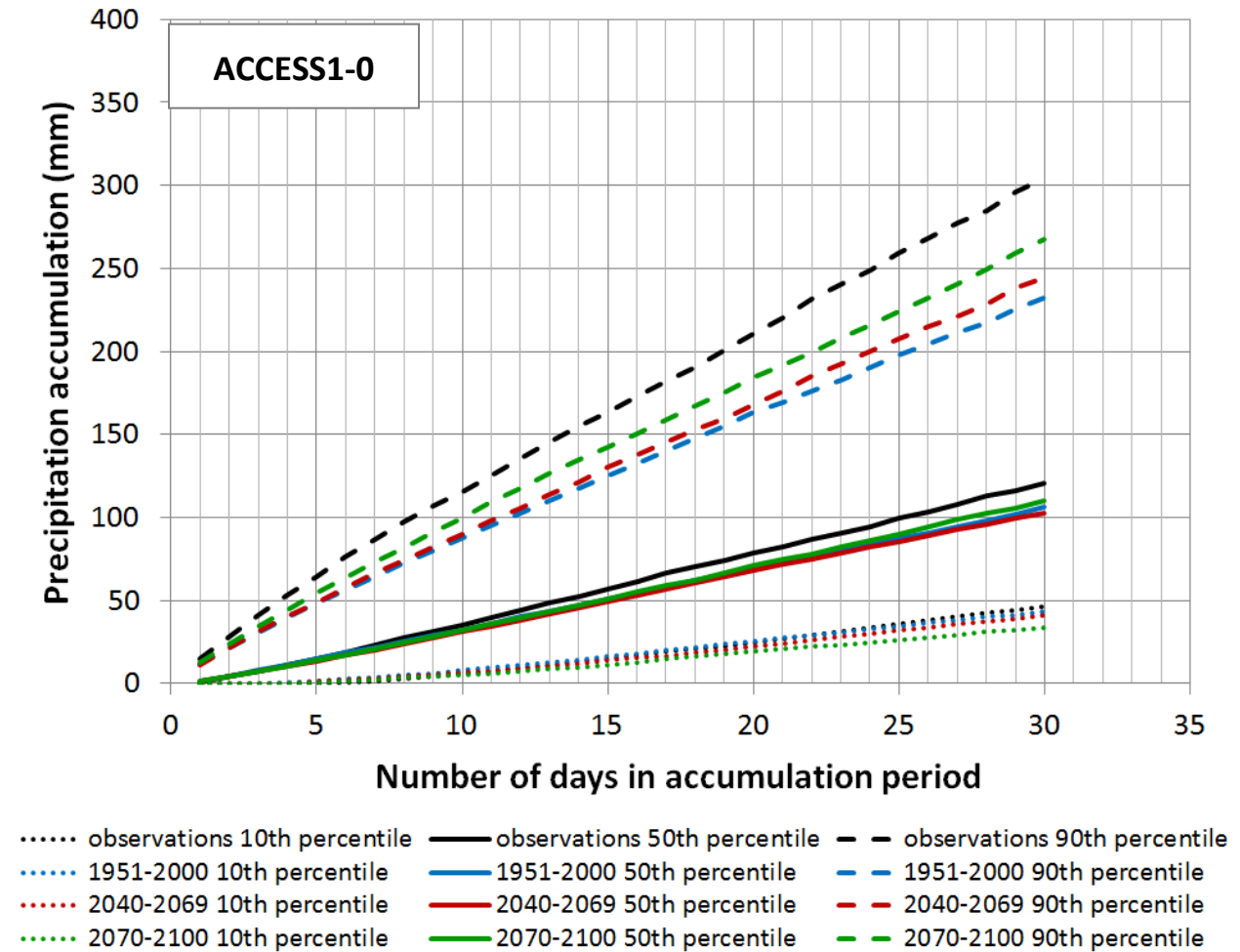


Figure 13 (cont'd). Simulated historical and projected precipitation totals over multiple-day periods for Highway 37A near Stewart

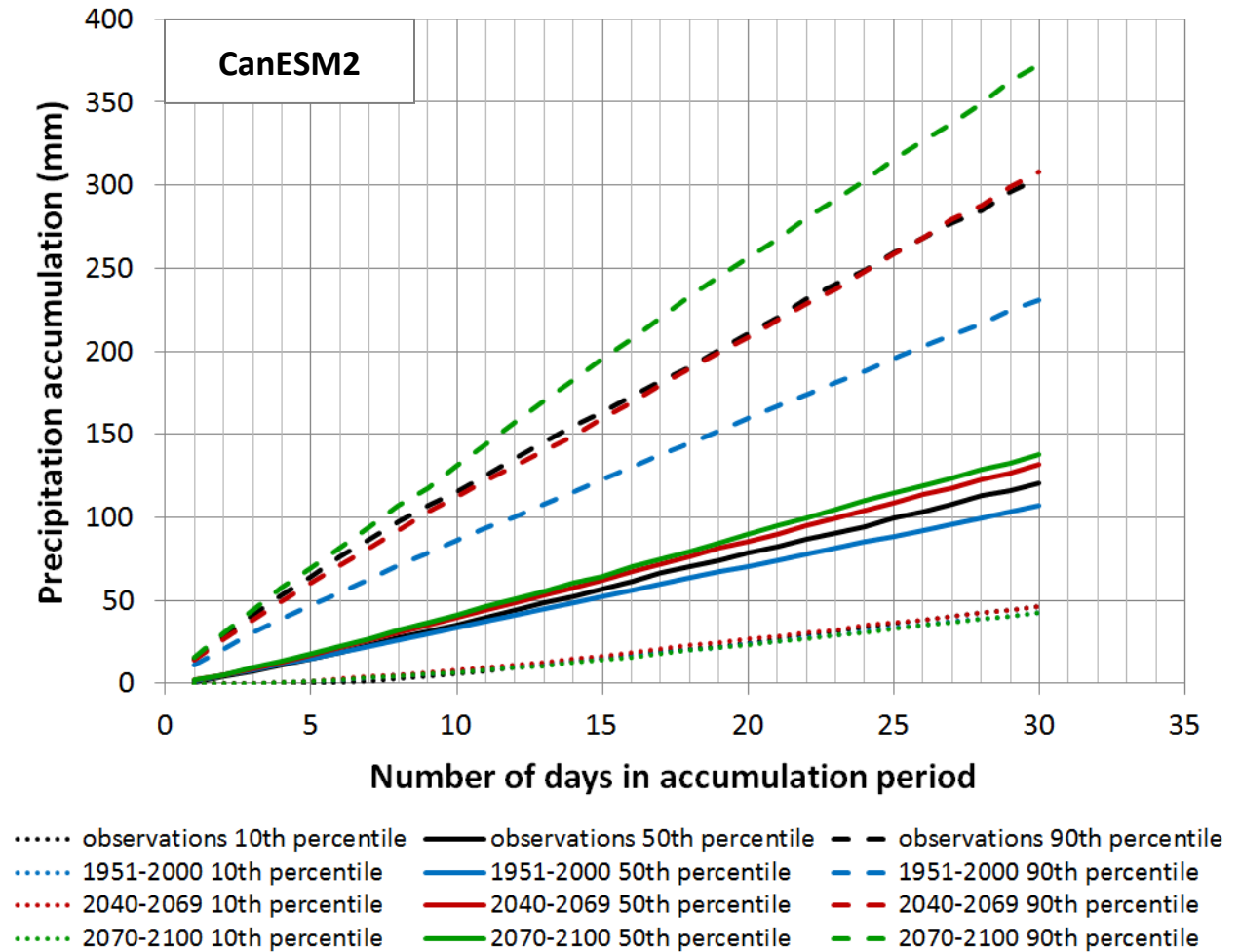
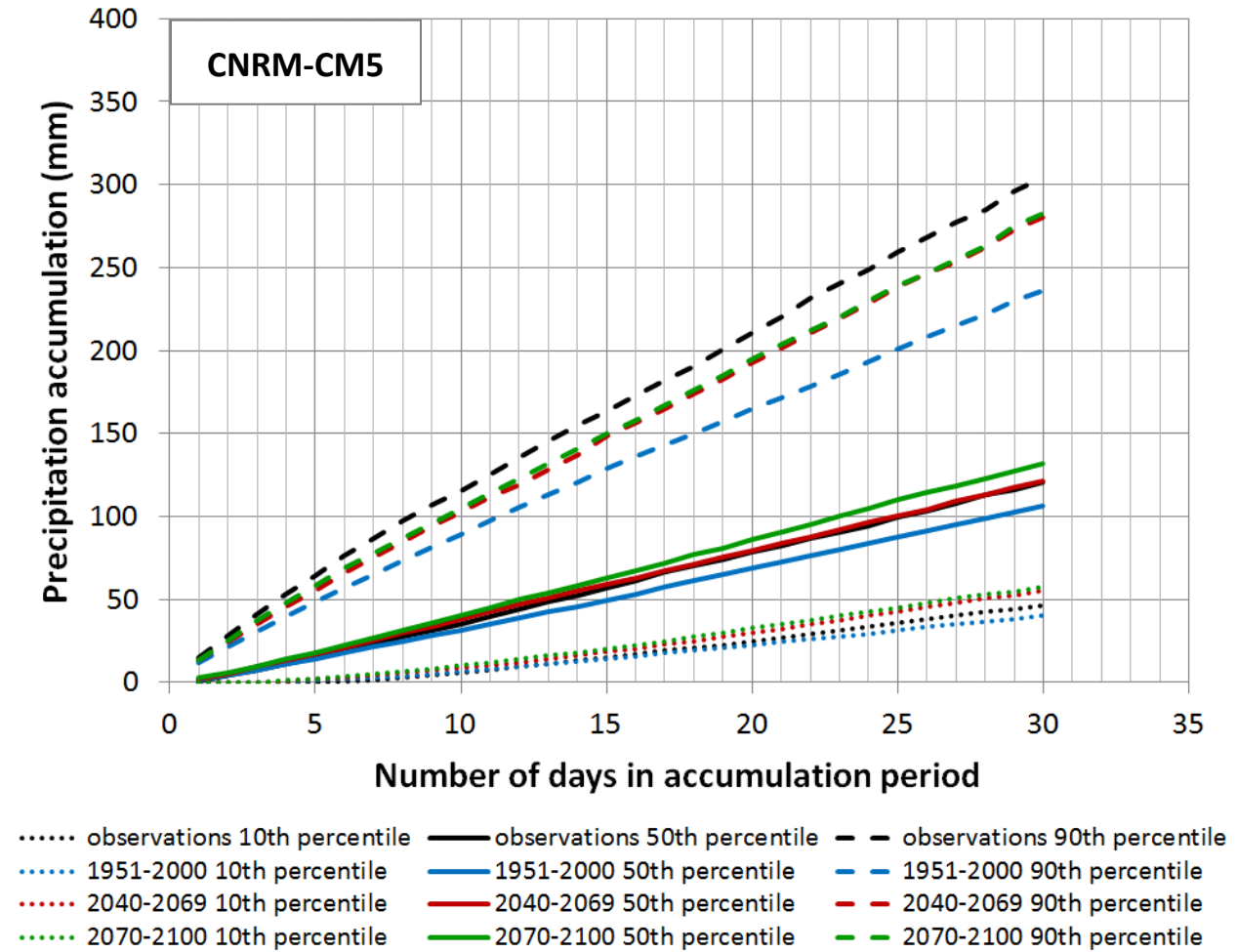


Figure 13 (cont'd). Simulated historical and projected precipitation totals over multiple-day periods for Highway 37A near Stewart



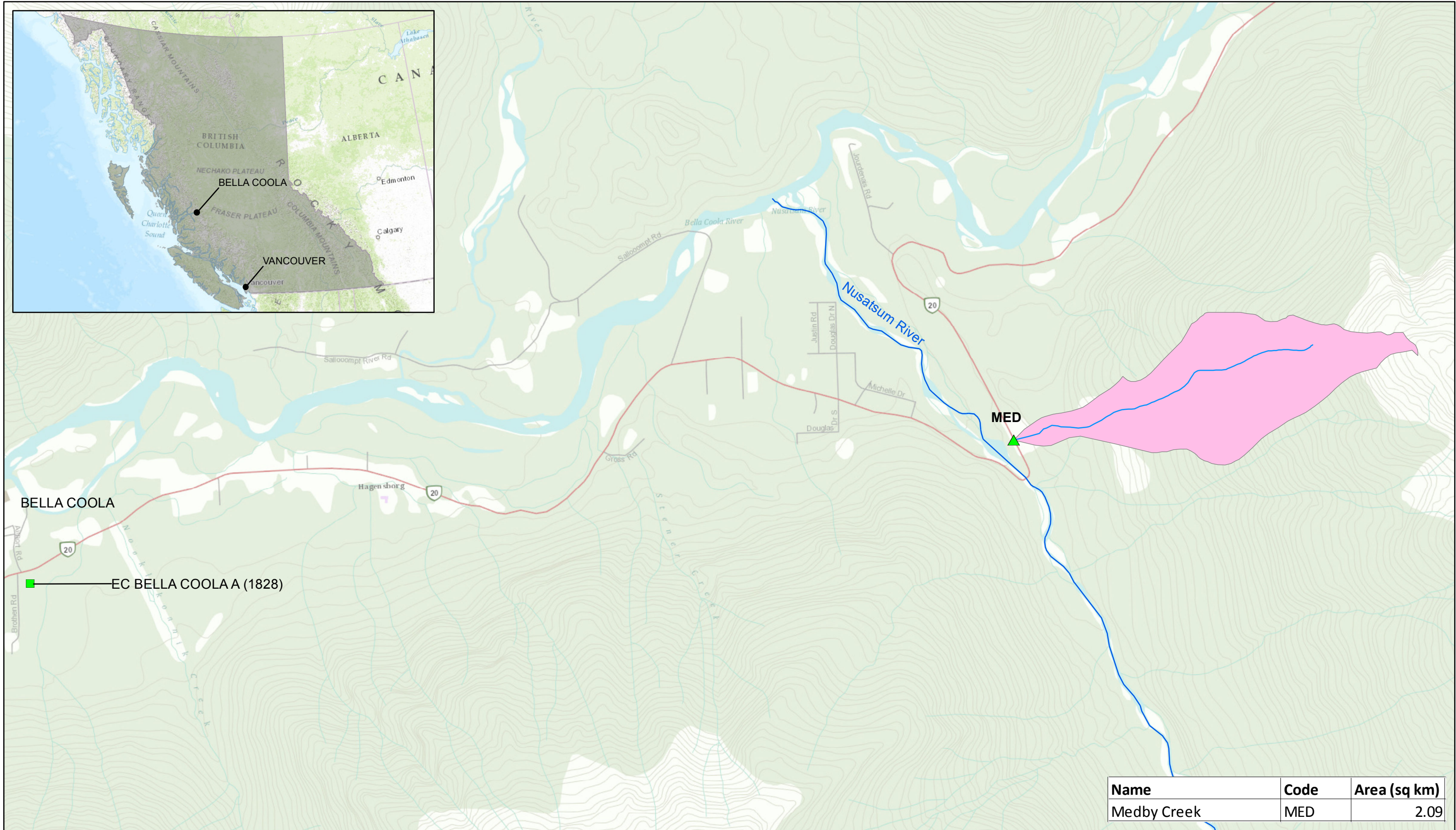
2.5 HIGHWAY 20 NEAR BELLA COOLA

A location map for Highway 20 near Bella Coola is shown in Figure 14.

Figure 15 and Figure 16 summarize the observations-based, historical GCM simulations, and GCM projections for different time horizons, for mean annual temperature and precipitation, average number of wet days in a year, and mean precipitation intensity on wet days. The observed mean annual precipitation is more than double that for Fisher Creek. The observed mean average temperature is 8.5°C. The downscaling procedure – which is based on the ANUSPLIN climatological data set (see Murdock et al., 2013), assigned a lower temperature to this grid cell, about 4.5°C (Figure 15).

Projections by all three GCM runs are for intense future warming, up to 6.5°C by late century for CanESM2 (Figure 15). All three GCM runs project increases in mean precipitation intensity (Figure 16 and Figure 17). This intensification pertains mostly to the high quantiles of precipitation (we looked at the 90th percentile of precipitation intensity) rather than to median (50th percentile) or low intensity precipitation (10th percentile), as can be seen in Figure 17 and Figure 18. For two of the GCM runs (Can-ESM2 and CNRM-CM5), the 10th percentile of precipitation is projected to decrease, while the 90th percentile increases and the median changes little (Figure 18).

For two GCM runs (ACCESS1-0 and Can-ESM2), the 90th percentile of daily precipitation increases faster in the projections than the 50th percentile (Figure 18). In the case of Can-ESM2, the 50th percentile of precipitation is projected to increase by 15% by late century, while the 90th percentile is projected to increase by 39%.



Name	Code	Area (sq km)
Medby Creek	MED	2.09

BRITISH COLUMBIA
The Best Place on Earth

Ministry of Transportation and Infrastructure

nhc
northwest hydraulic consultants

- Climate Stations
- ▲ Key Sites
- Streams

DATA SOURCES:
BACKGROUND - ESRI WORLD TOPO MAP
WATERSHEDS AND STREAMS - FWA

SCALE - 1:30,000

0 0.5 1 Kilometers

Coordinate System: NAD 1983 UTM ZONE 9N
Units: METERS

Job: 300314 Date: 17-MAR-2014

CCEVA - ENGINEERING ANALYSIS REPORT
HIGHWAY 20 NEAR HAGENSBORG, BC
MEDBYCREEK WATERSHED AND CLIMATE STATION LOCATIONS

FIGURE 14

Figure 15. Mean temperature and annual precipitation for the observed historical record and GCM hindcasts and projections for Highway 20 near Bella Coola.

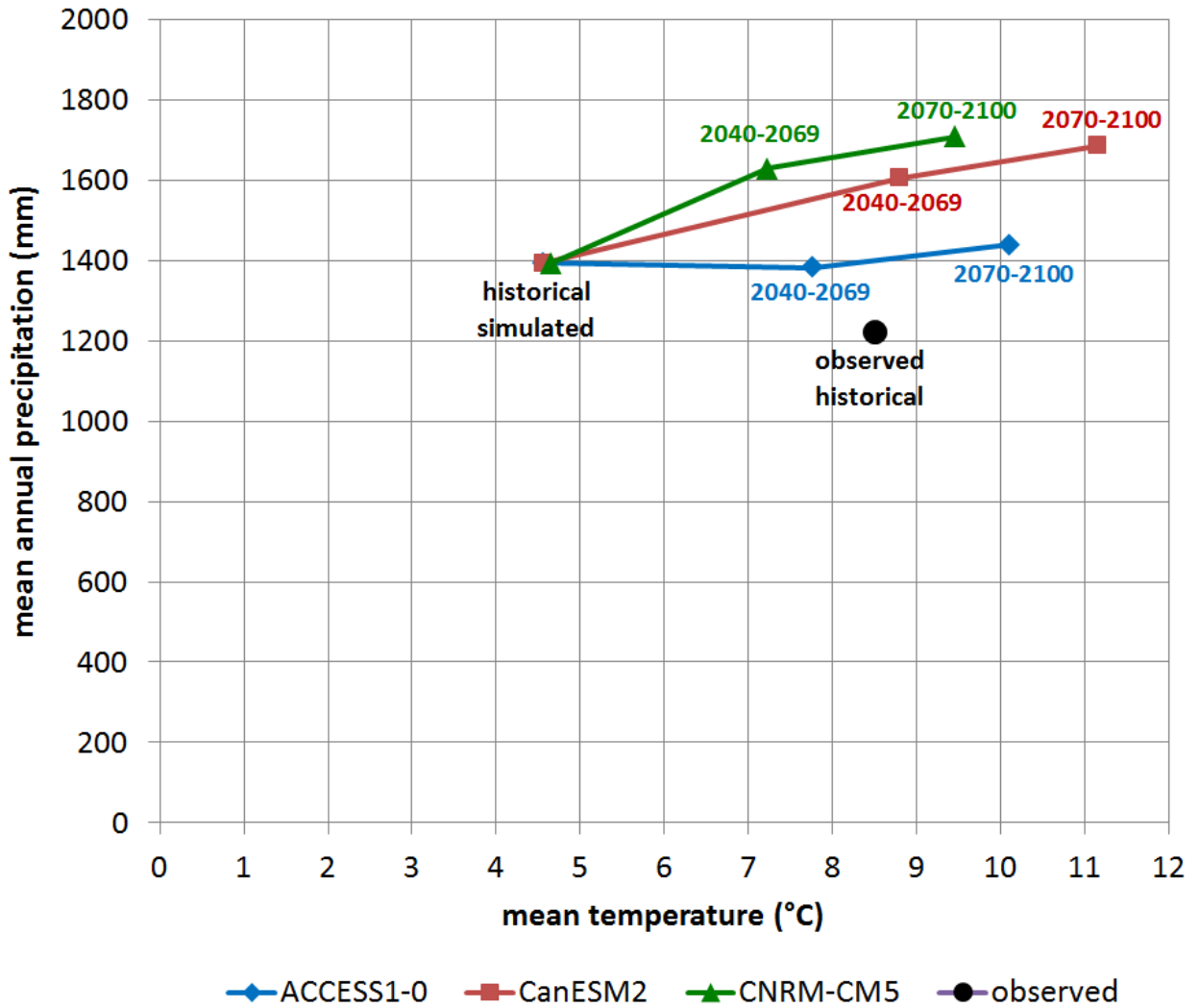


Figure 16. Observed and GCM-simulated mean number of wet days per year and mean precipitation intensity on wet days, for Highway 20 near Bella Coola.

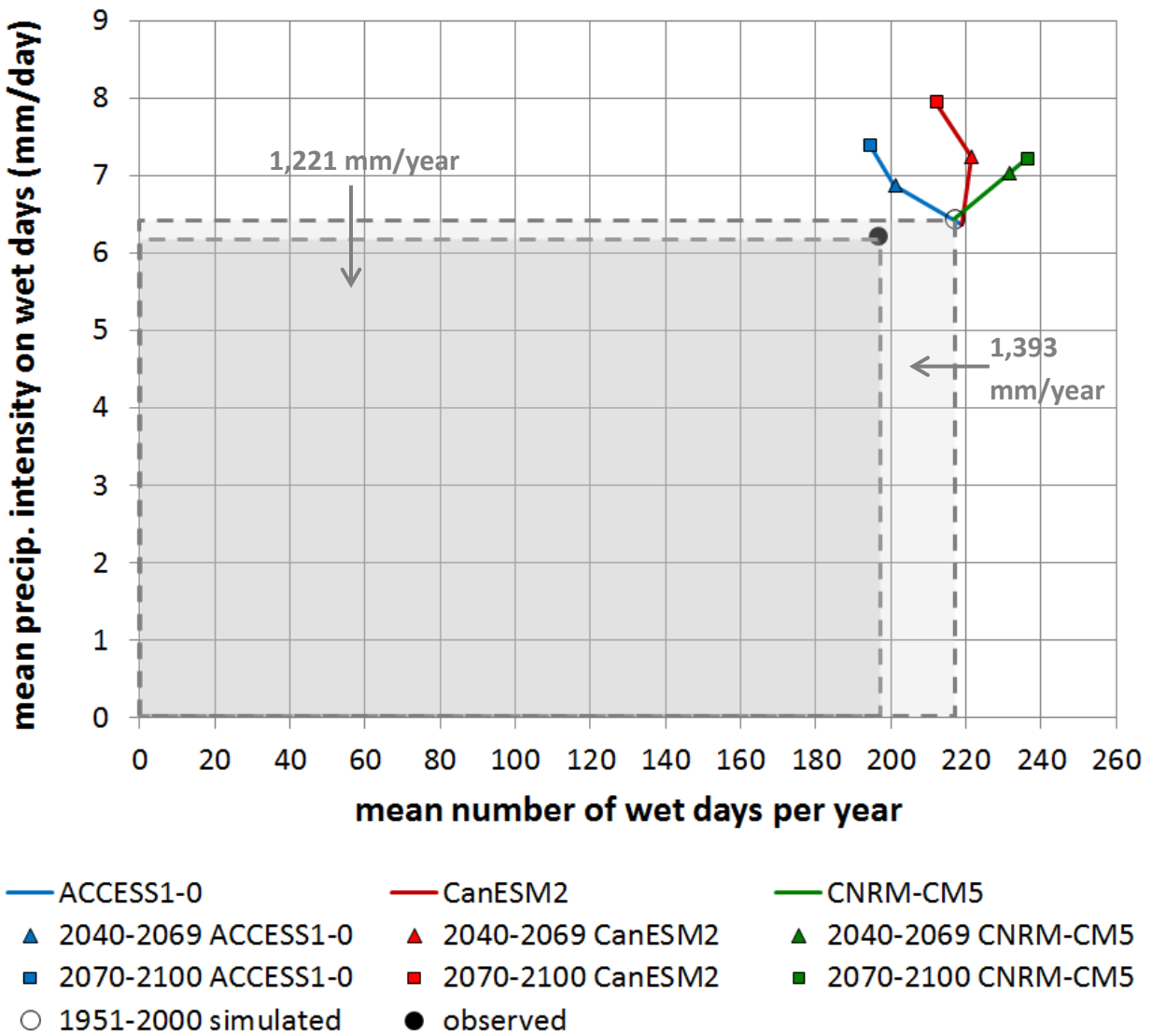


Figure 17. Probability of non-exceedance plots for daily precipitation at Highway 20 near Bella Coola, showing observed, GCM hindcasted and GCM projected.

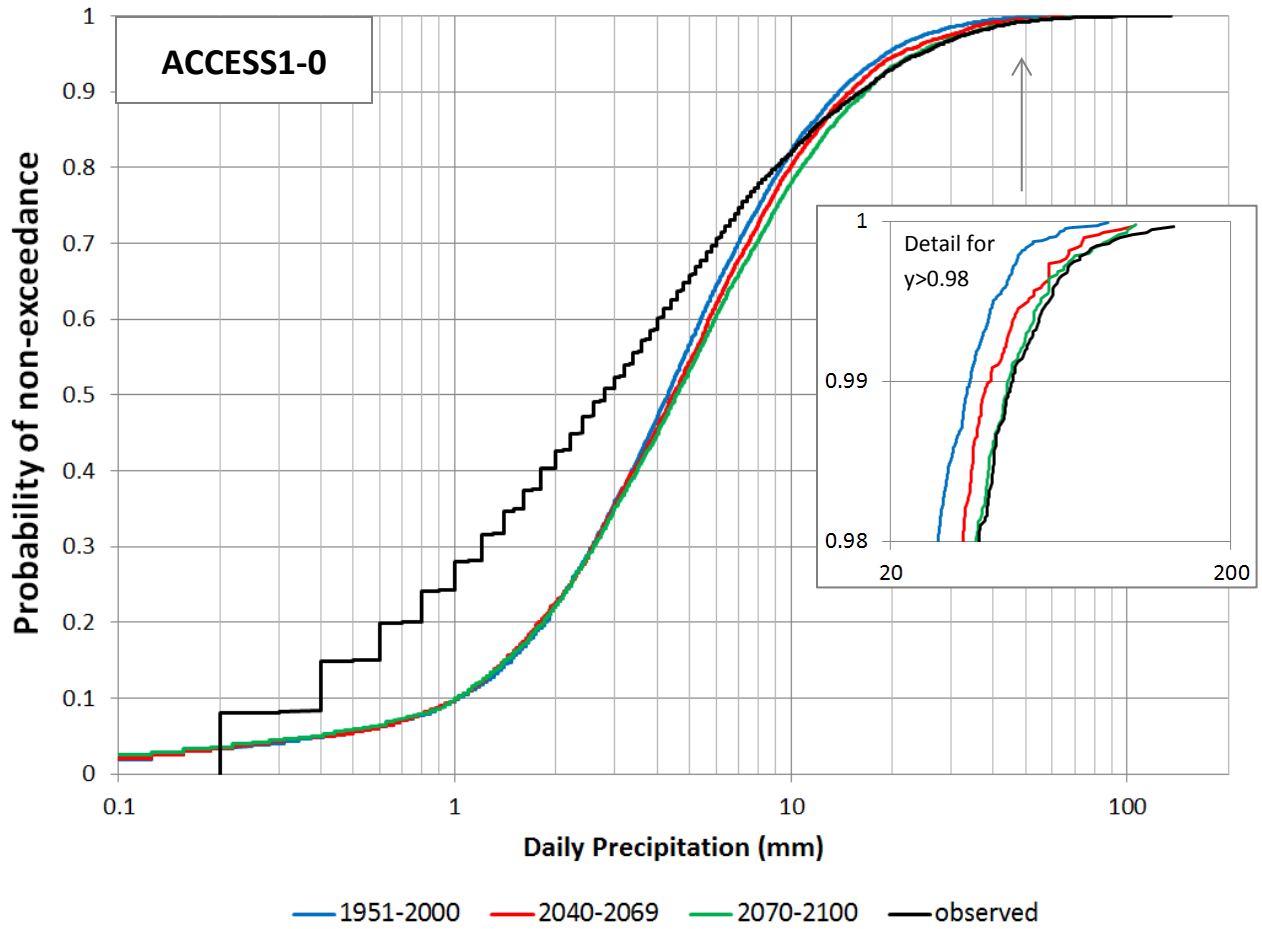


Figure 17 (cont'd). Probability of non-exceedance plots for daily precipitation at Highway 20 near Bella Coola, showing observed, GCM hindcasted and GCM projected.

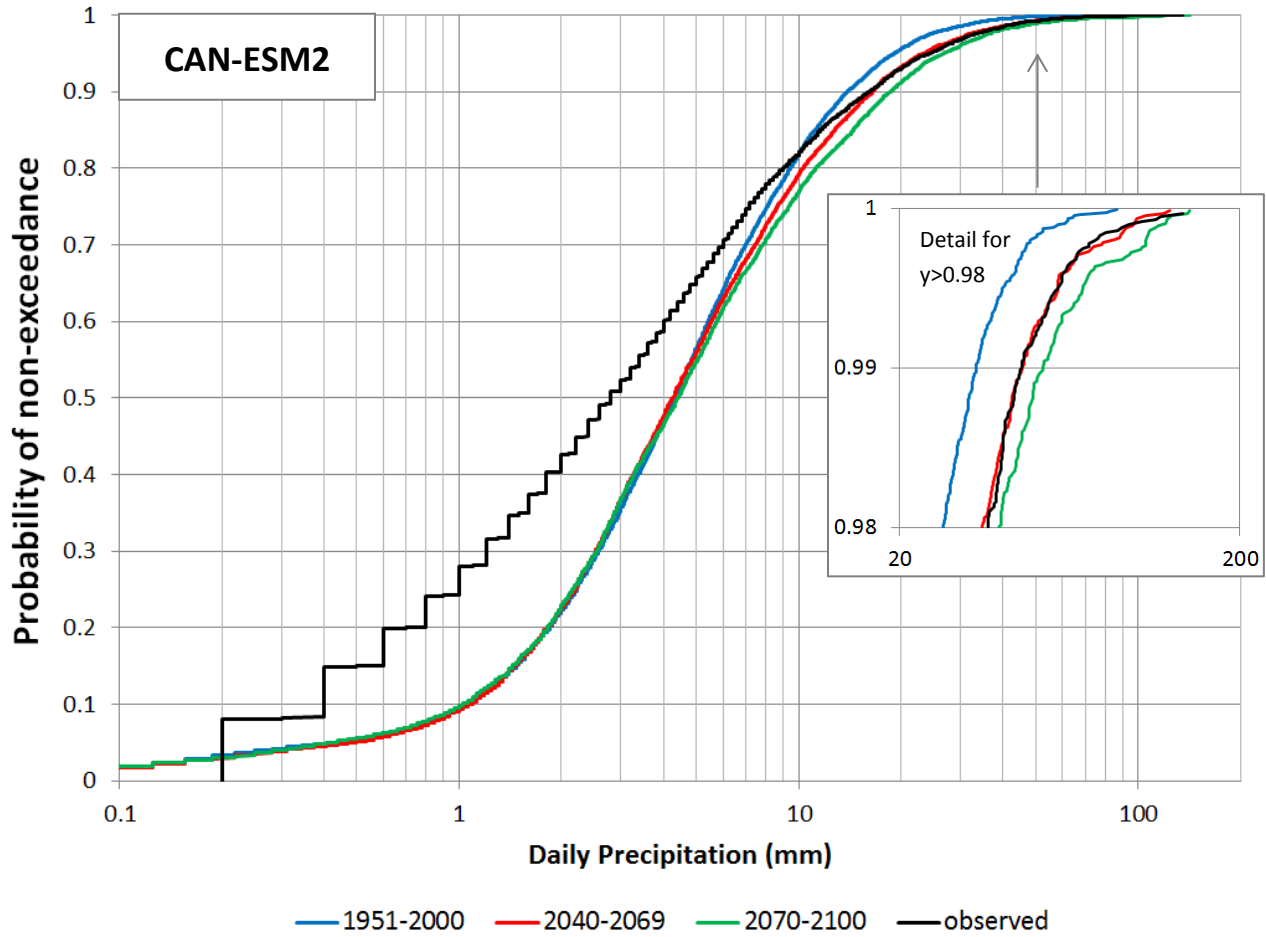


Figure 17 (cont'd). Probability of non-exceedance plots for daily precipitation at Highway 20 near Bella Coola, showing observed, GCM hindcasted and GCM projected.

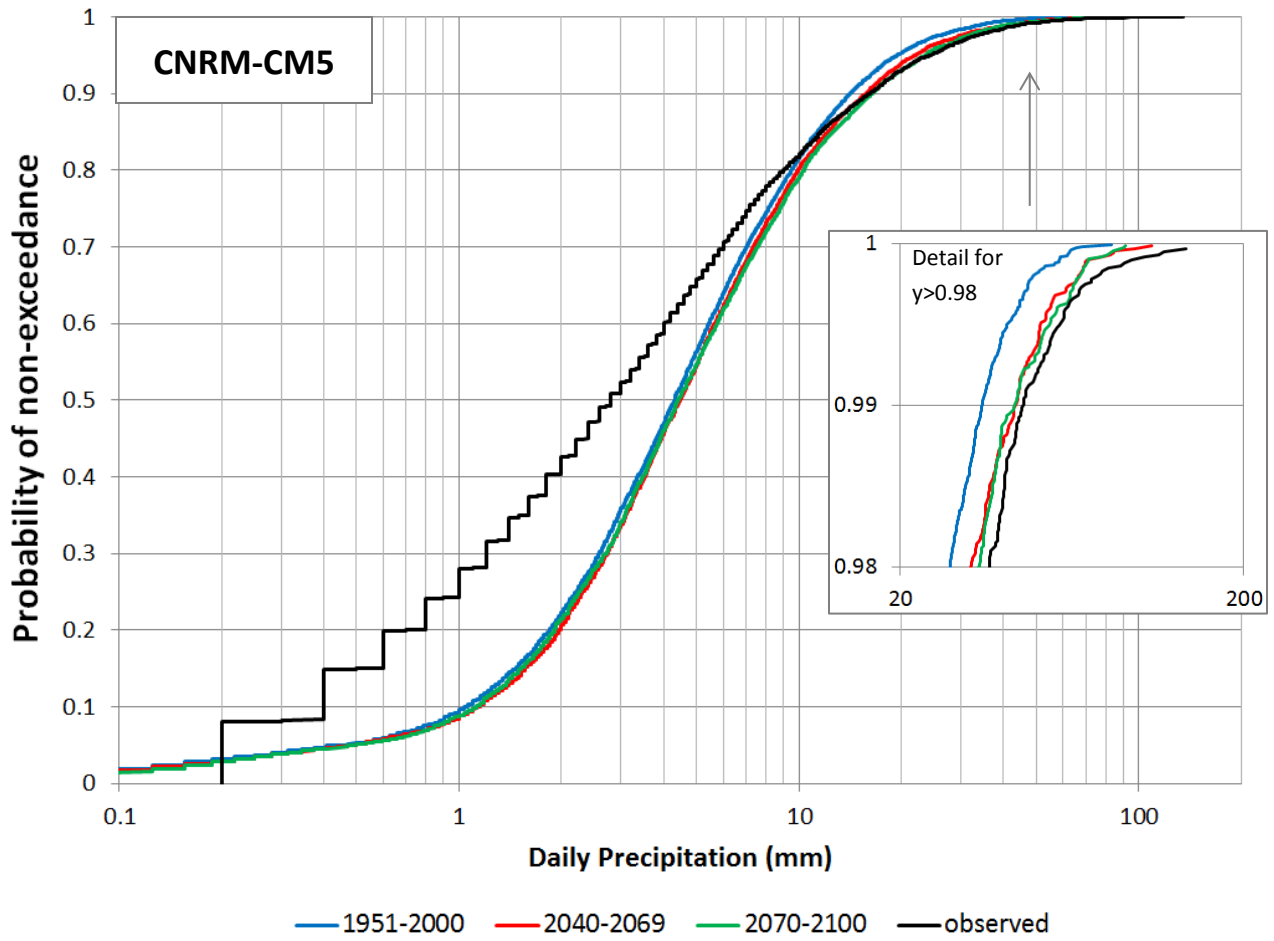


Figure 18. Simulated historical and projected precipitation totals for different accumulation periods for Highway 20 near Bella Coola.

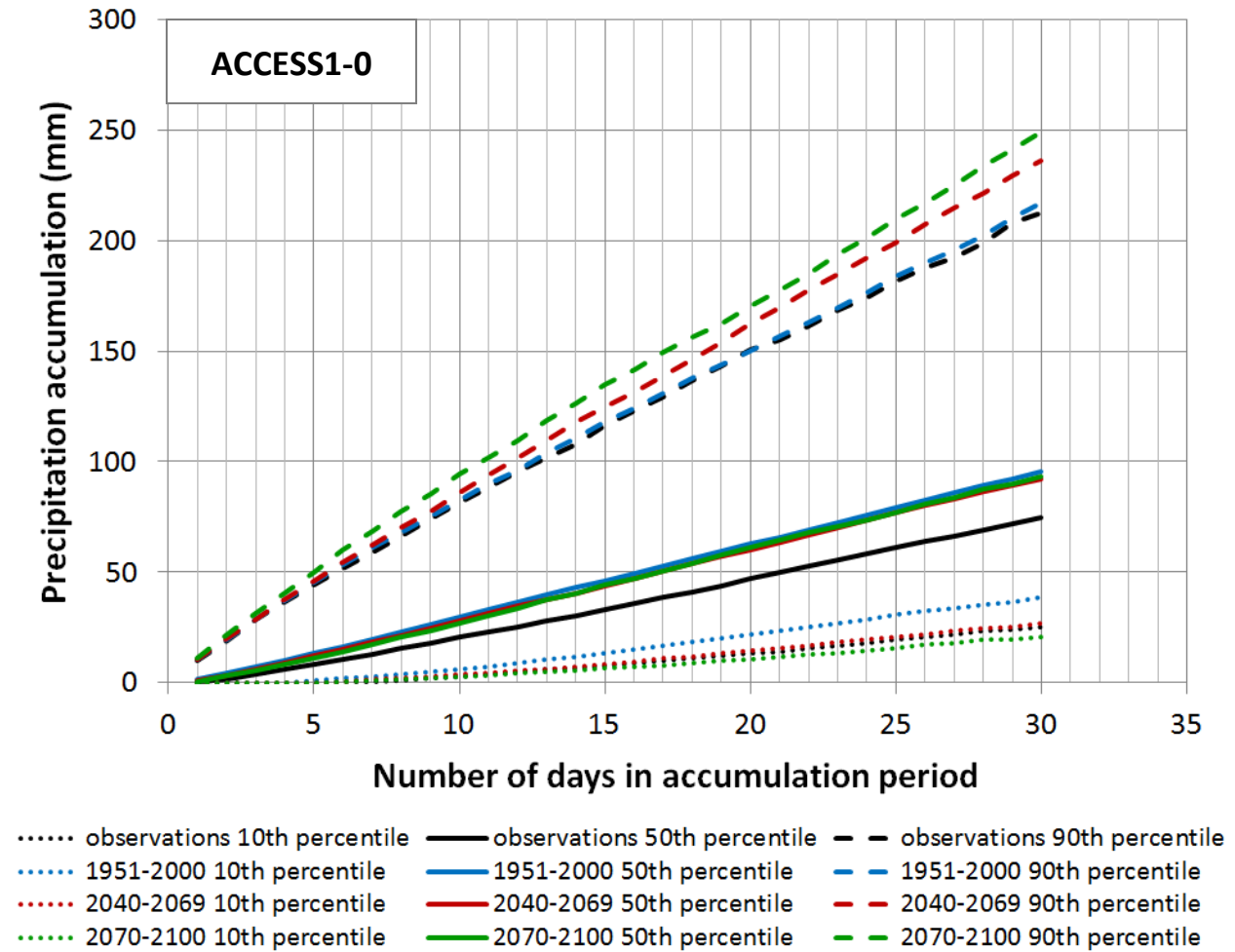


Figure 18 (cont'd). Simulated historical and projected precipitation totals for different accumulation periods for Highway 20 near Bella Coola.

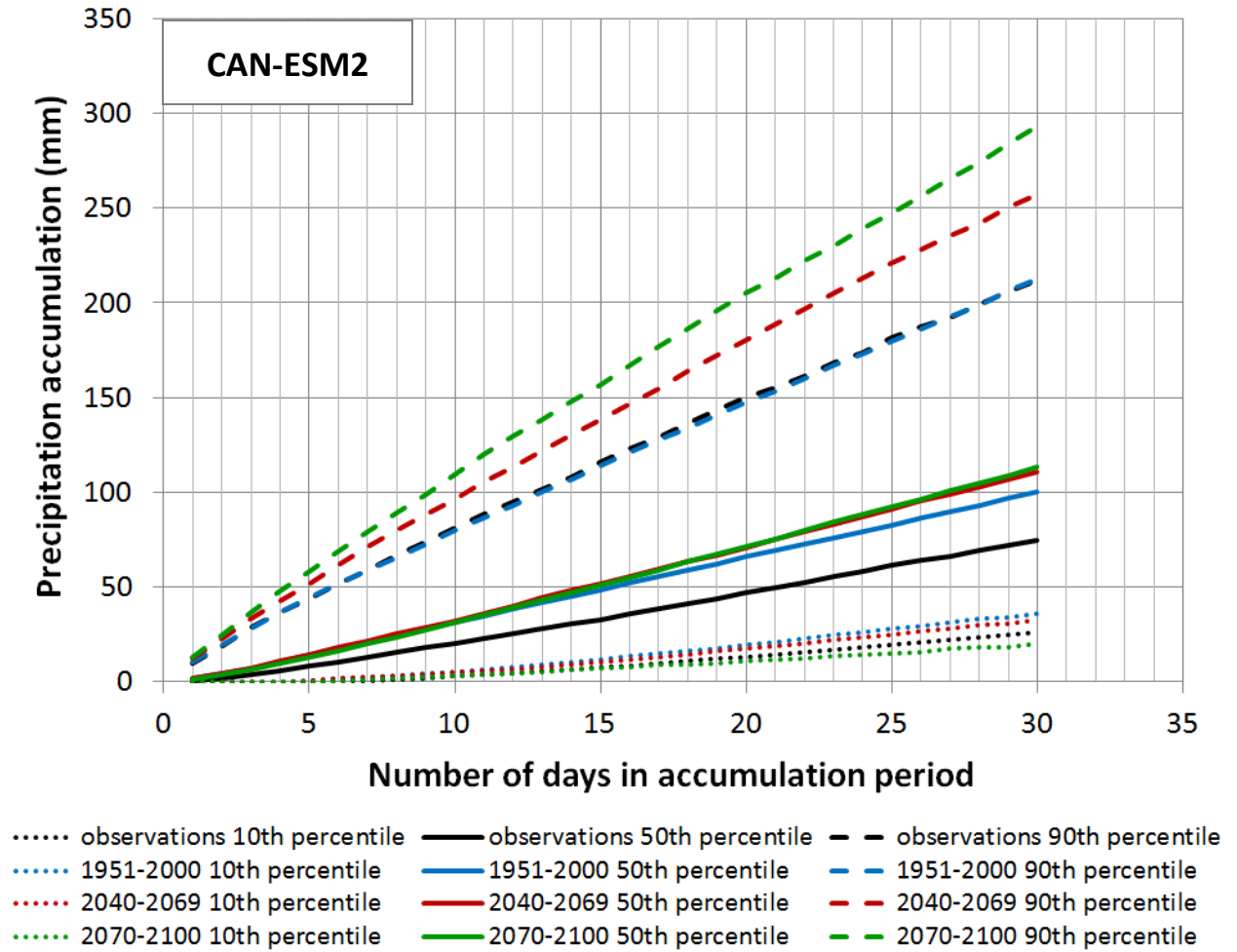
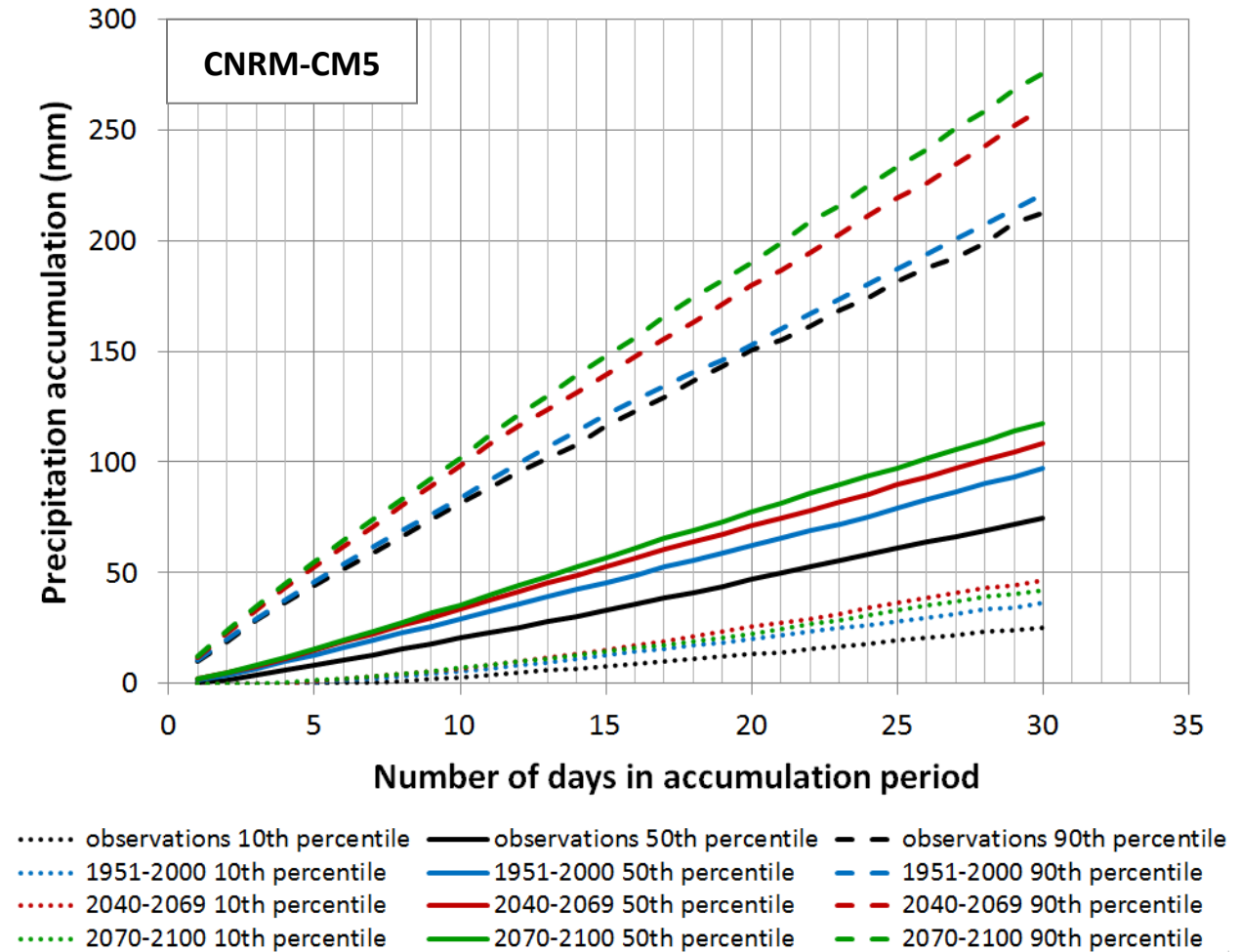


Figure 18 (cont'd). Simulated historical and projected precipitation totals for different accumulation periods for Highway 20 near Bella Coola.



2.6 HYDROLOGIC MODELLING OF STREAMFLOW IN FISHER CREEK

2.6.1 OVERVIEW OF THE HEC-HMS MODEL

Hydrologic modelling has been used to simulate streamflow on Fisher Creek at the Highway 97 Bridge. The objective is to estimate the percent increase in the 200-year maximum hourly flow for the two future climate periods (2050-2069 and 2070-2099) relative to the historic period (1973-2010).

The US Army Corps of Engineers' Hydrologic Engineering Center Hydrologic Modeling System (HEC-HMS, Version 3.5) software (USACE, 2010) was used for hydrologic modelling. Details on the development, calibration, and testing of the model are provided in Appendix B.

A total of 34 complete years of climate data were available from Chetwynd A and Chetwynd BCFS over the period 1973-2011 and were amalgamated for hydrologic simulations, with five years excluded due to data gaps (1997, 2002, 2006, 2008, and 2009) (refer to Section 2.3.1). The first year (1973) was a model warm-up and was not included in subsequent analyses. Historic years 1974-2011 correspond to simulation years 1974-2006 due to the requirement of having sequential years of input to the model (see annual maxima of hourly discharge at the Fisher Creek Bridge location provided in Table 4 and note that the large outlier for the CNRM-CM5 climate projection for the period 2040-2069 is in bold type).

Precipitation and temperature input data for future period simulations have been developed by altering the historic records of those data sets to match the statistics of GCM projections. In total, three climate scenarios were examined for each climate period (providing a total of six future climate simulations) based on the GCMs considered (ACCESS1, CANESM2, and CNRM-CM5).

2.6.2 LIMITATIONS OF THE MODELLING

The Fisher Creek HEC-HMS model has a high level of uncertainty because there is no observed streamflow data with which to calibrate it. The parameters of the Fisher Creek model have been assigned based on limited calibration of a HEC-HMS model for Windrem Creek in nearby Chetwynd, BC, for which there are observations of streamflow (NHC, 2013). Model simulations have been driven by climate inputs (precipitation and air temperature) from the two EC climate stations (Chetwynd A and Chetwynd BCFS approximately 45 kilometres east of the watershed, refer to Appendix B). A discussion of the development, calibration and testing of the Windrem Creek Model is provided in Appendix B. In the following sections, the Windrem Creek model will be referred to as the 'Proxy Model'.

The historic and future model simulations do not account for land use changes such as development for human habitation, forest harvesting, forest fires, or insect infestations etc. The Fisher Creek watershed has been modelled as fully forested, but forest harvesting has occurred in the past and will likely continue in the future. Land use changes like those mentioned above may increase maximum annual flow (Alila et al., 2009; Kuras et al., 2012) above what is currently predicted by model simulations.

A sensitivity analysis of simulated streamflow to the two most sensitive model parameters (precipitation gradient and time of concentration) has been provided in Section 2.6.7.

2.6.3 MODELLING APPROACH

Ideally, hourly climate data would be used to calibrate the HEC-HMS model to hourly streamflow for the entire period simulations. The ideal study watershed would contain at least two climate stations positioned at a low and high elevation so that adequate estimates of temperature and precipitation gradient could be determined. Accounting for the spatial and temporal variability of these inputs is of particular importance for proper simulation of convective summer rain storms, which cause the largest peak flows in Pine Pass tributaries like Fisher Creek. The ideal watershed would also have one or more snow courses to account for winter and pre-freshet snowpack snow water equivalents (SWE). In reality, the available climate and snow course data for the region is intermittent and sparse. There are only a few meteorological (MET) stations and one snow course station within 50 km of Fisher Creek and all of the MET stations are at low elevations.

Since annual peak flows are of particular interest particular focus has been paid to simulating the hydrometeorological and basin processes and interactions that contribute to high flows.

An overview of the model processes, methods and computational types used in HEC-HMS are provided below. The methods are described in the following sections, with a more detailed description of the development, calibration, and testing of the Proxy Model in Appendix B.

Snow Accumulation and Ablation Model

HEC-HMS incorporates an improved temperature index method adapted from USACE's Streamflow Synthesis and Reservoir Regulation (SSARR) hydrologic model, which tracks antecedent temperatures and the state of the snowpack to predict snowmelt yield in a more realistic manner. This is accomplished via the model's Antecedent Temperature Index algorithm. During the winter, the model's Cold Content parameter represents the "heat deficit" in the snowpack. As temperatures rise or liquid water is added to the snowpack, the cold content is reduced and the antecedent temperature index is used to calculate melt from the snowpack. With these state variables, the model can track whether or not a snowpack is ripe and ready to melt or if it is cold and would require substantial heat input before melting. While HEC-HMS does not explicitly distinguish

between open and forested areas, this is one of the factors implicitly expressed in the melt rate coefficient.

Table 2. Summary of selected model processes

Model process	Method	Computational type
Input precipitation	Point location	Elevation-area
Input temperature	Point location	Elevation
Snowmelt	Temperature index	Elevation-area
Canopy	Simple	Lumped by sub-basin
Surface	Simple	Lumped by sub-basin
Evaporation	Monthly average	Lumped by sub-basin
Soil/Loss	Soil Moisture Accounting	Parameters lumped by sub-basin
Hydrograph Transform	Clark Unit Hydrograph	Time of concentration and storage coefficient
Base flow	Linear Reservoir	Lumped by sub-basin

Basin Loss Method

Soil moisture accounting (SMA) has been selected as the basin loss method in HEC-HMS. The soil moisture accounting method represents the soil column using multiple layers and allows for continuous (rather than event-based) hydrologic simulation. The hydrologic response of the near-surface, interflow, and groundwater zones can be analyzed separately with SMA.

Each layer of the model – canopy, surface, soil profile, and groundwater – is represented by a storage depth. Precipitation first fills the canopy storage (foliage) and then falls to surface storage (small depressions on the ground).

Within the soil and groundwater layers, water moves at a rate proportional to the saturation fraction of the underlying layer. Soil profile storage (the first layer), is made up of an “upper zone” and “tension storage”. Upper zone storage represents dynamic storage in the soil profile. It can infiltrate to the groundwater layer below and is the first portion of the soil profile storage to be lost to evapotranspiration. Tension storage represents the volume of water that can be held in the soil against gravity drainage. It is the first portion of the soil profile storage to be filled, and can only be lost to evapotranspiration.

The groundwater layers receive input from the layer above and lose storage either via percolation or through outflow. Outflow from the groundwater layers is represented by a linear reservoir process that is then routed to the base flow module of HEC-HMS. The base flow module can introduce additional linear reservoirs if additional lag or more attenuation of groundwater flows is needed.

Soils in the Fisher Creek and Proxy Model are assumed to originate from morainal parent material, with values of field capacity and porosity adopted from prior modelling efforts at the Upper Penticton Creek Watershed Experiment (Thyer et al., 2004, p.7). The selected ratio of field capacity to porosity was held constant (0.58) during model calibration.

Hydrograph Transform Method

The Clark Unit Hydrograph transform method has been selected to explicitly represent variations in surface runoff travel time across the modelled watersheds. The Clark unit hydrograph is a synthetic unit hydrograph method. A time versus area curve is used to develop the translation hydrograph resulting from a burst of precipitation. The resulting translation hydrograph is routed through a linear reservoir to account for storage attenuation effects across the watershed. The time of concentration defines the maximum travel time of runoff within the watershed, while the storage coefficient accounts for storage effects in the linear reservoir. The storage coefficient is estimated as 0.4 based on calibration and testing of the Proxy Model (Appendix B).

The time of concentration has been determined by first calculating the unit hydrograph lag time. Lag time is approximately the time difference between the center of mass of rainfall and the center of mass of runoff. Lag time is a function of physical basin characteristics and has been determined using GIS and Equation 1 (after Equation 1 in USBR, 1987):

$$L_g = C \left(\frac{LL_{ca}}{S^{0.5}} \right)^N \quad (1)$$

where:

L_g = unit hydrograph lag time, in hours

N = a constant, analyses of unit hydrograph data, have led to the conclusion that the exponent N should be 0.33, regardless of the location of the drainage basin.

C = a constant, additional analyses of unit hydrograph data, have led investigators to conclude that C should be 26 times the average Manning's n value representing the hydraulic characteristics of the drainage network.

L = the length of the longest watercourse from the point of concentration to the boundary of the drainage basin, in miles. The point of concentration is the location on the watercourse where a hydrograph is desired,

L_{ca} = the length along the longest watercourse from the point of concentration to a point opposite the centroid of the drainage basin, in miles, and

S = the overall slope of the longest watercourse (along L), in feet per mile

The average value of Manning’s roughness coefficient (used to determine the constant ‘C’) was determined to be 0.06 from calibration of the Proxy Model. The lag time for Fisher Creek from Equation 1 is then 1.8 hrs. Time of concentration is taken as lag time divided by 0.6 (USDA-SCS, 1972) and thus has a value of 3 hrs for the Fisher Creek.

Evapotranspiration

Evapotranspiration is defined as a monthly average within the Fisher Creek Model using measurements from the Upper Penticton Creek Watershed Experiment (Pike et al., 2010, p.149), which is expected to have similar evapotranspiration rates as the Pine tributary watersheds. Measurements are based on average daily evaporation of intercepted water, tree transpiration, and below-canopy evaporation (transpiration from the understory and trees less than 3 m tall, plus evaporation from the soil surface).

2.6.4 SIMULATIONS USING THE FISHER CREEK MODEL

The calibrated parameters from the Proxy Model were used in the Fisher Creek Model with the exception of the hydrograph transform (changed to 3 hours), watershed area (changed from 24 km² to 44.8 km²), and elevation-area distributions. Watershed characteristics for Windrem (Proxy) and Fisher are provided in Table 3 below.

Table 3. Watershed characteristics for Windrem Creek (Proxy) and Fisher Creek.

Watershed	Drainage Area (km ²)	Mean Elevation (m)	Min Elevation (m)	Max Elevation (m)	Waterbody	Aspect	Hydrologic Zone (Obedkoff, 2000, 2003)
Windrem (Proxy)	24.1	980	630	1340	0.0%	SE	Southern Rocky Mountain Foothills
Fisher	44.8	1251	664	1900	0.4%	SE	Southern Rocky Mountain Foothills

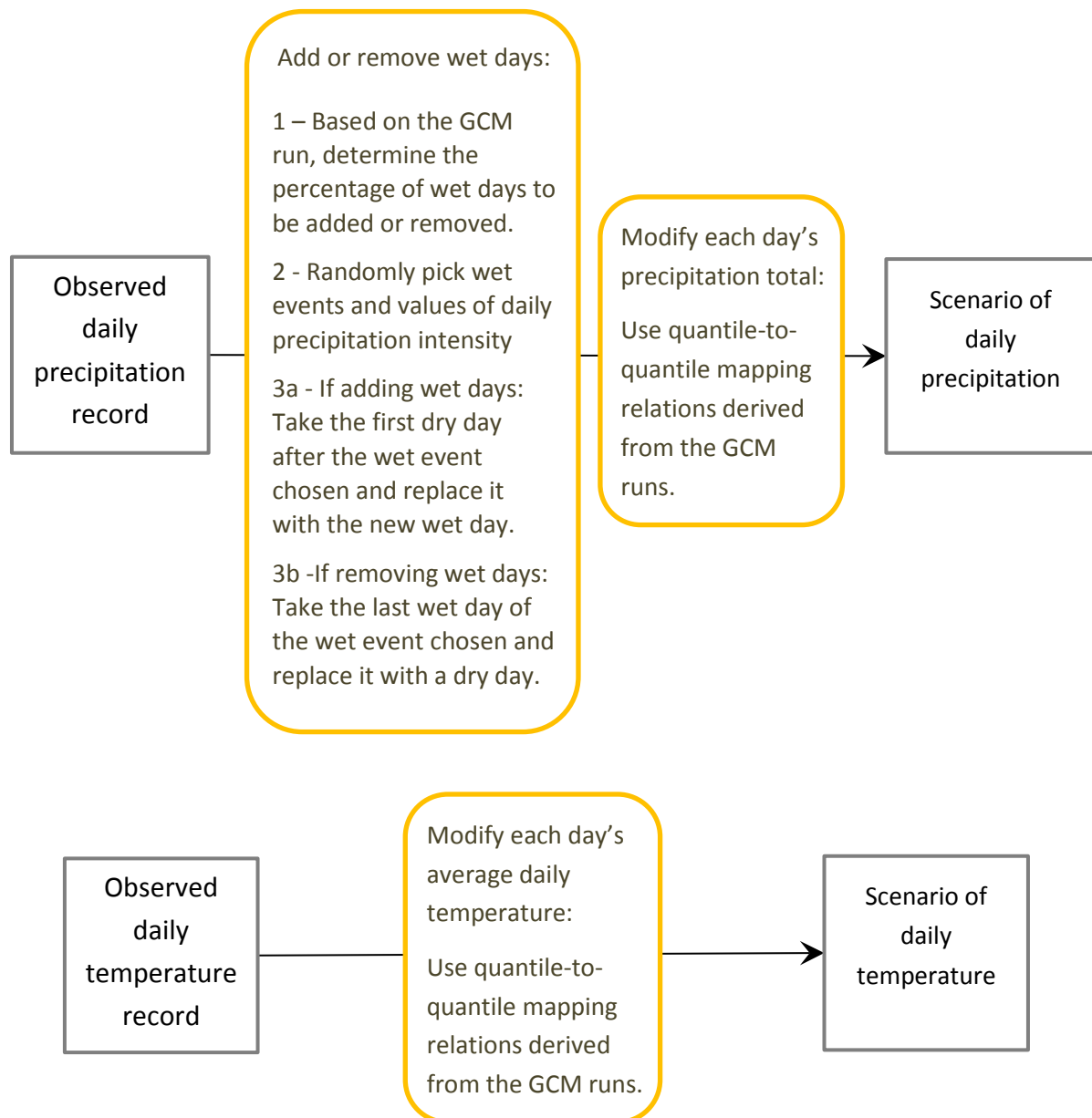
The Fisher Creek model is used to simulate streamflow using the 34 year record of historic climate data (from the period 1973-2011) and two (2), 34-year records of future climate data developed from GCM projections (described below in Section 2.6.5).

2.6.5 DEVELOPMENT OF FUTURE CLIMATE DATA FOR INPUT TO THE FISHER CREEK MODEL

The three downscaled GCM climate simulations provided by PCIC served as the basis for development of future climate scenarios to simulate with the Fisher Creek Hydrologic Model. The underlying statistical analyses and methodological details are provided in Appendix A.

The diagram in Figure 17 summarizes our procedure for creating future climate scenario time series. For each climate scenario, the observed precipitation record was modified so that its mean annual number of wet days increased or decreased by the same percentage as simulated by the GCM run (see description of steps in the figure). The resulting daily record was then subjected to daily quantile-to-quantile mapping so as to modify the daily values of precipitation intensity in the same manner as seen in the GCM simulations, i.e., when comparing future projections to the GCM's historical simulations. Daily quantile mapping was also used to modify the daily mean temperature to reflect the future changes projected by the GCM simulations.

Figure 19. Summary of the procedure used for creating time series of daily precipitation and temperature for future climate scenarios



2.6.6 FISHER CREEK MODEL RESULTS

The Fisher Creek watershed hydrologic model simulation inputs (temperature and precipitation) and outputs (SWE and discharge) are provided in graphical form for the seven climate scenarios (historic climate record and six future climate projections) over the following pages.

Figure 20. Fisher Creek watershed hydrologic model simulation inputs (temperature and precipitation) and outputs (SWE and discharge) for the historic climate record.

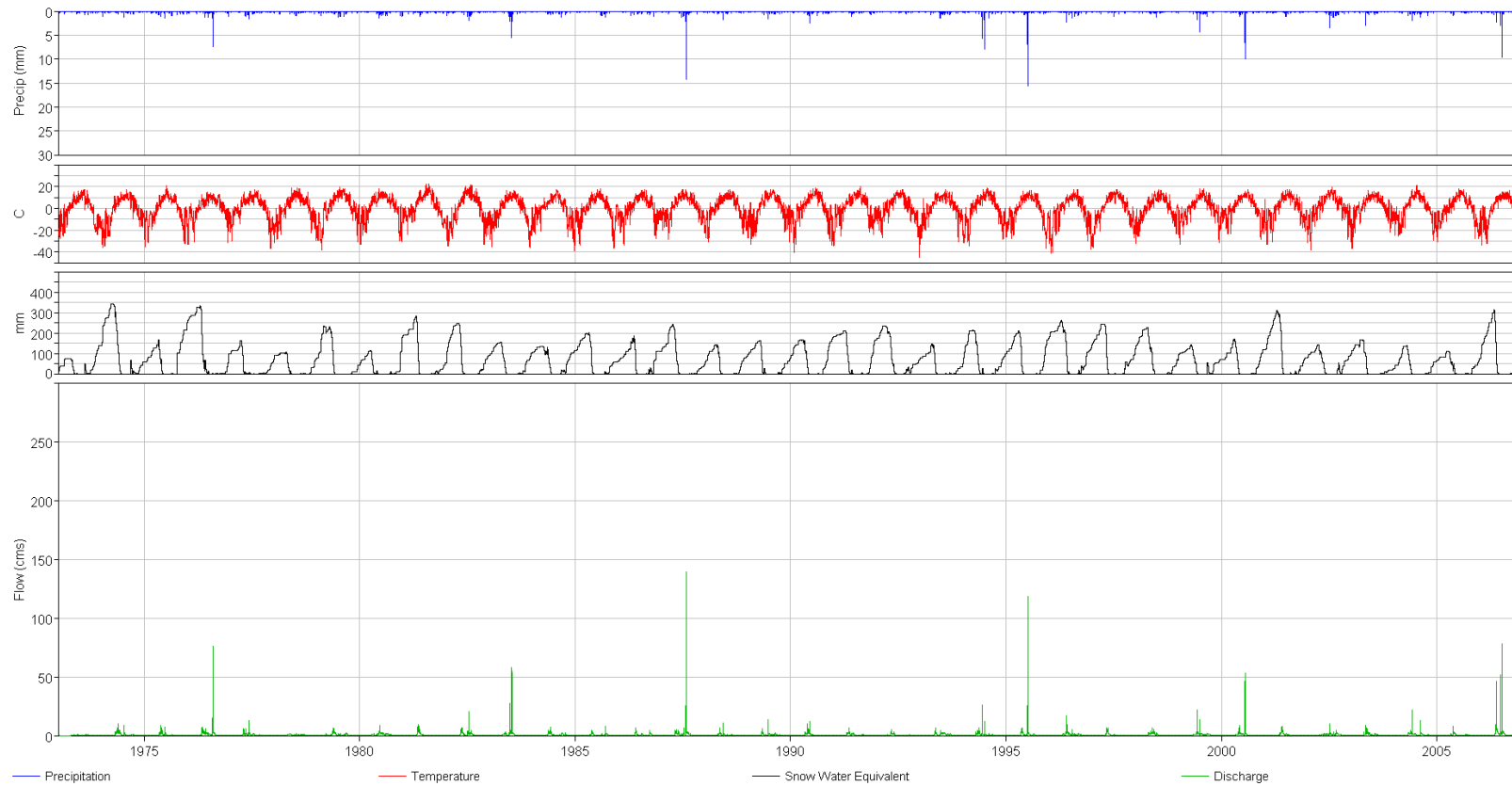


Figure 21. Fisher Creek watershed hydrologic model simulation inputs (temperature and precipitation) and outputs (SWE and discharge) for the ACCESS1 2040-2069 climate scenario.

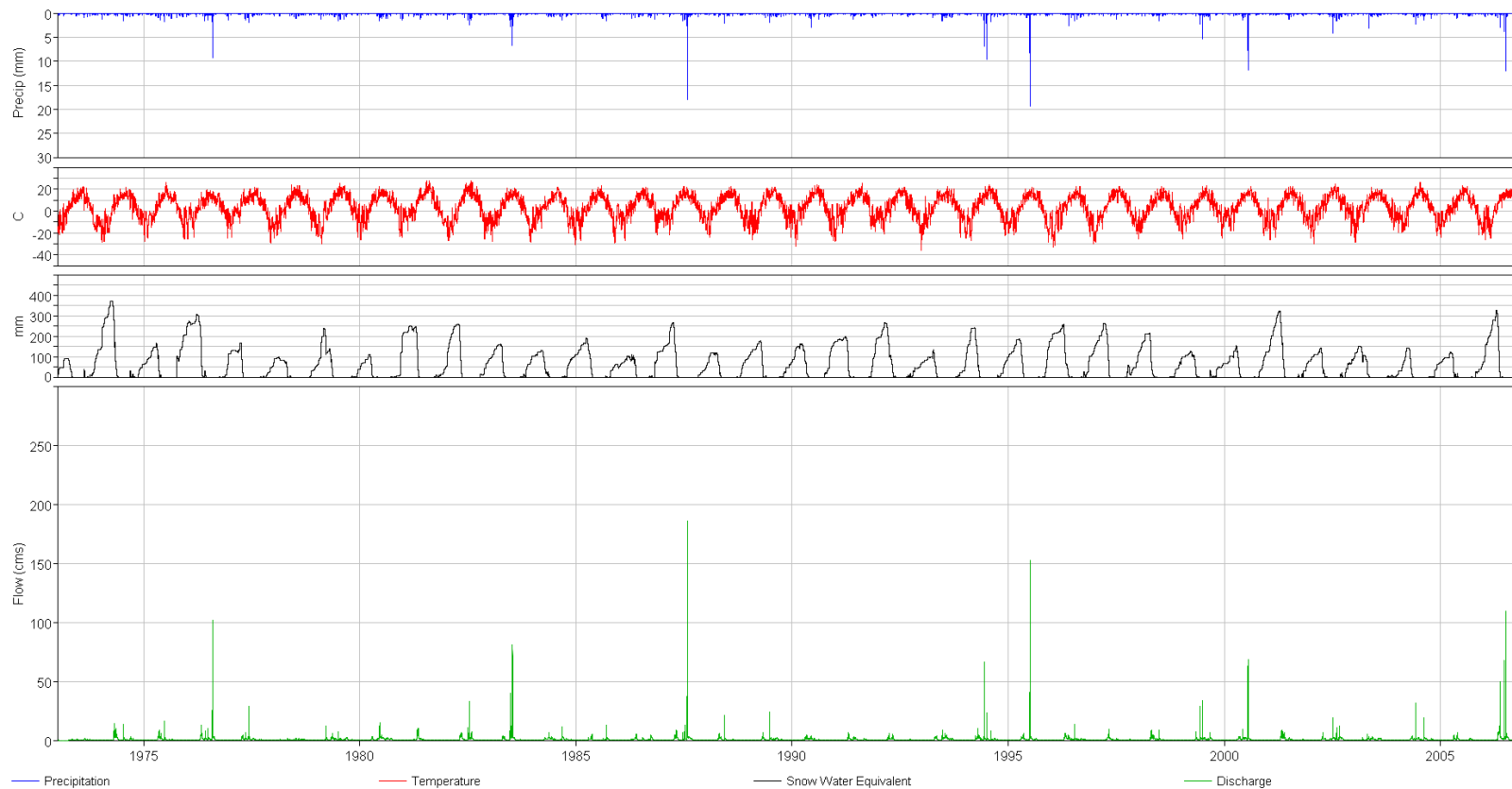


Figure 22. Fisher Creek watershed hydrologic model simulation inputs (temperature and precipitation) and outputs (SWE and discharge) for the ACCESS1 2070-2100 climate scenario.

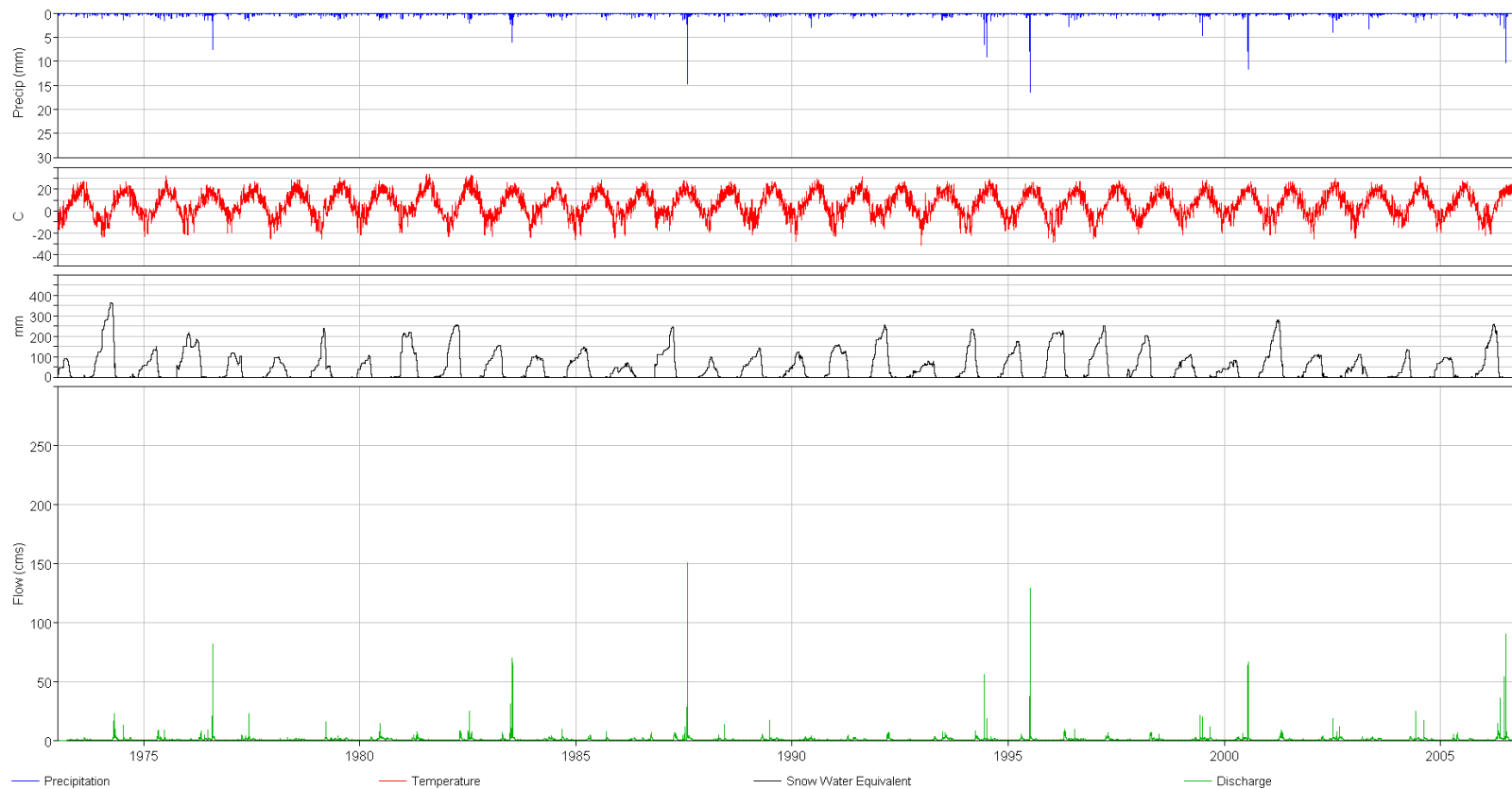


Figure 23. Fisher Creek watershed hydrologic model simulation inputs (temperature and precipitation) and outputs (SWE and discharge) for the CanESM2 2040-2069 climate scenario.

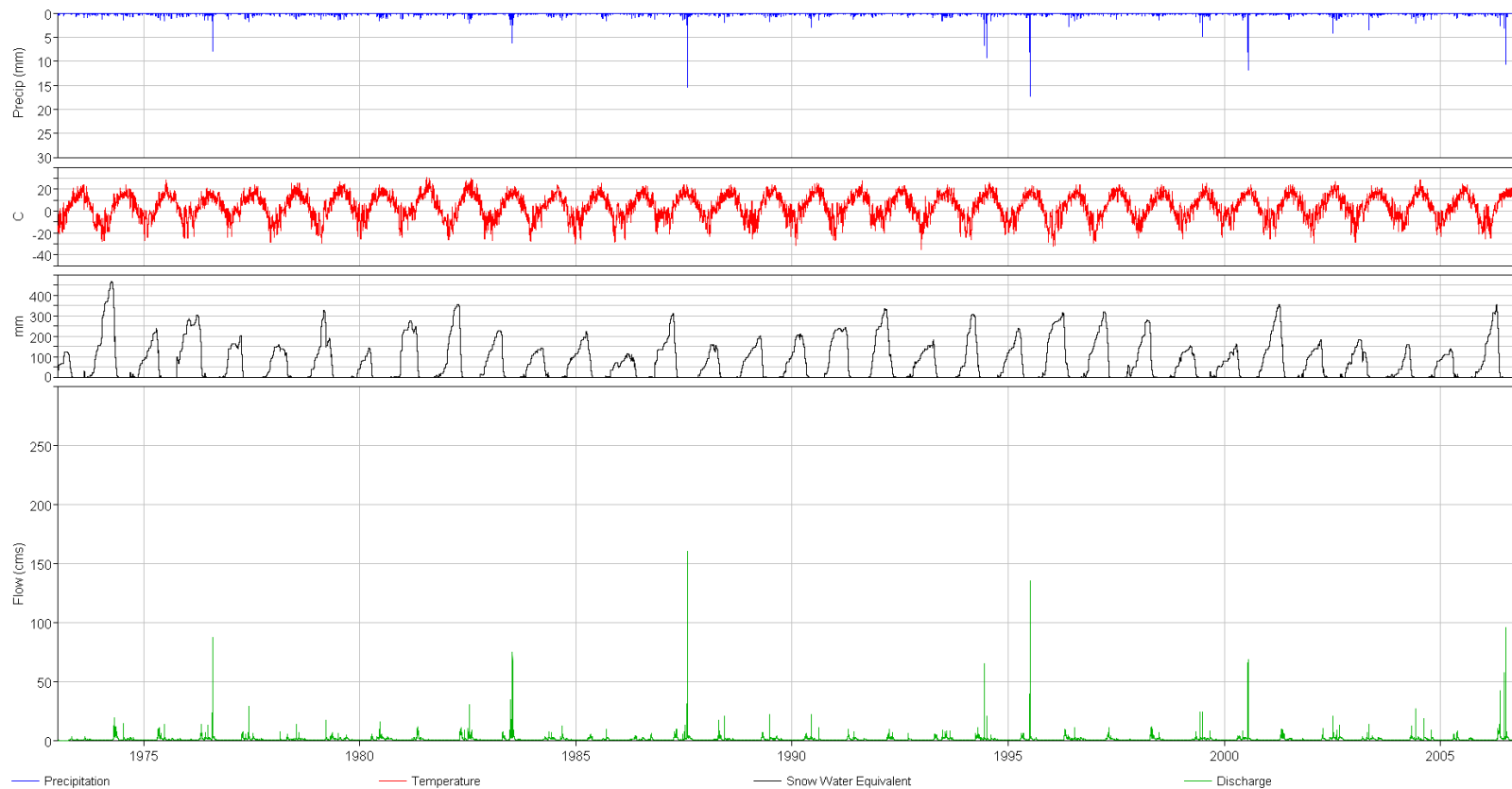


Figure 24. Fisher Creek watershed hydrologic model simulation inputs (temperature and precipitation) and outputs (SWE and discharge) for the CanESM2 2070-2100 climate scenario.

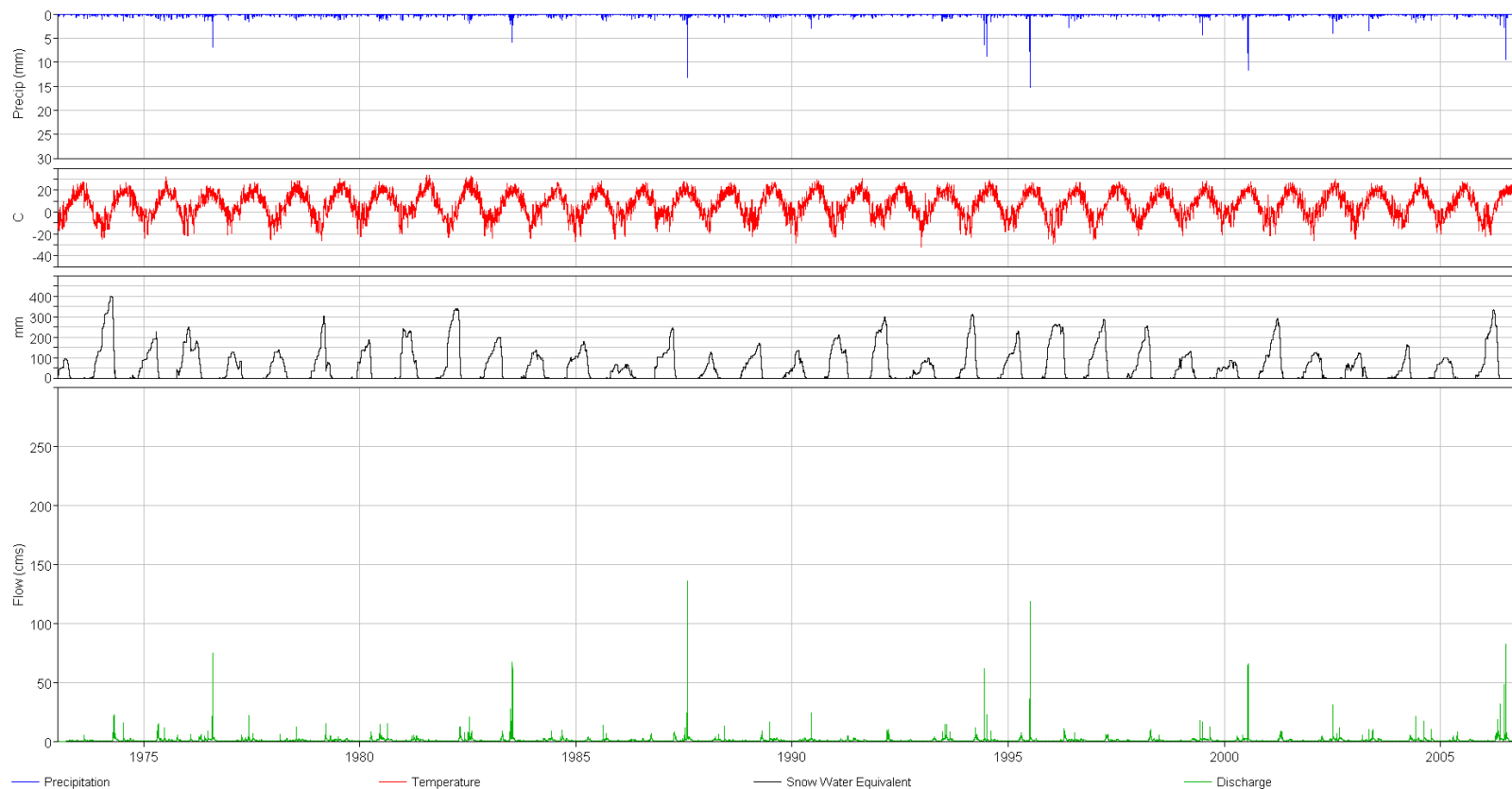


Figure 25. Fisher Creek watershed hydrologic model simulation inputs (temperature and precipitation) and outputs (SWE and discharge) for the CNRM-CM5 2040-2069 climate scenario.

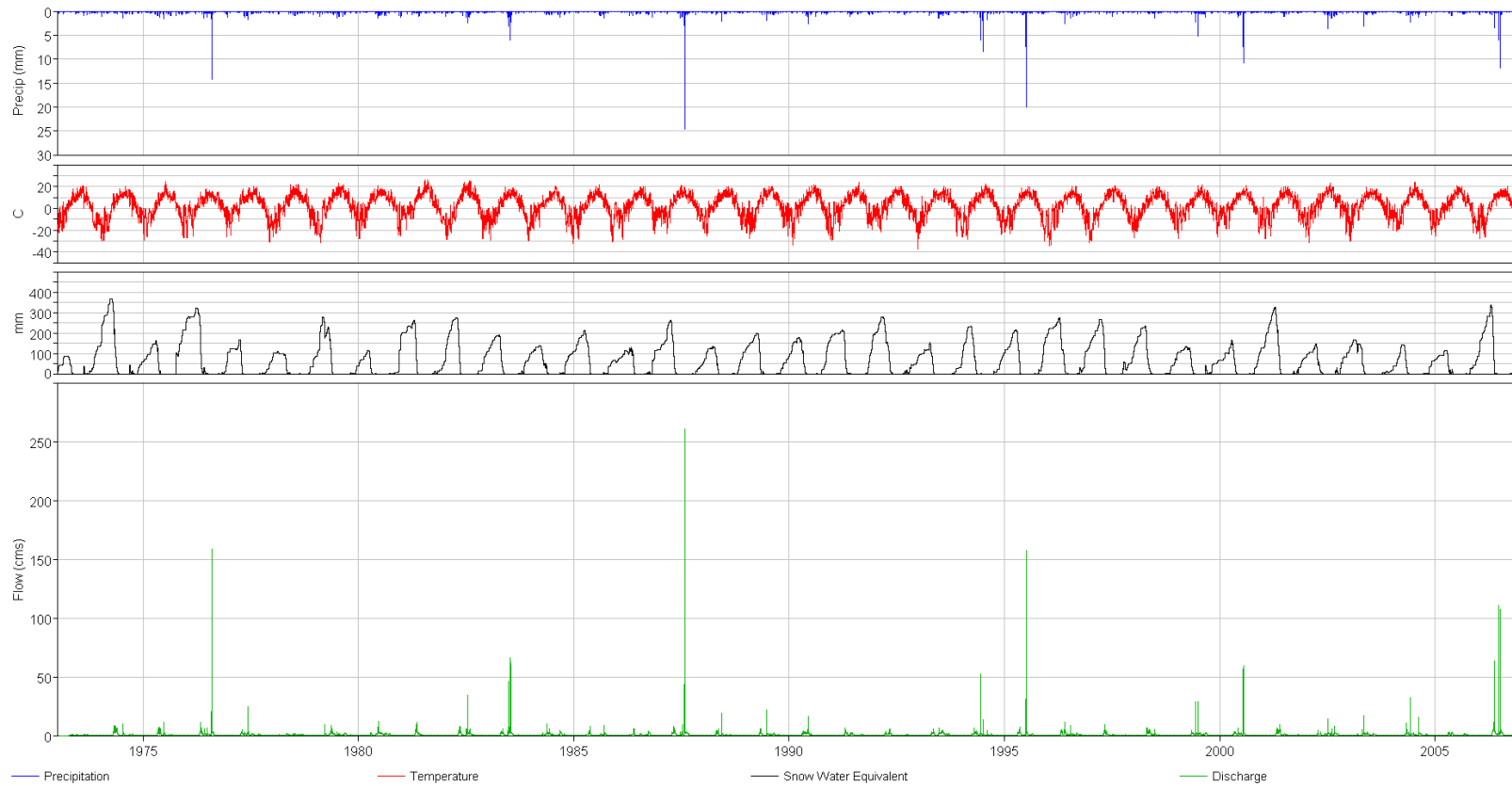
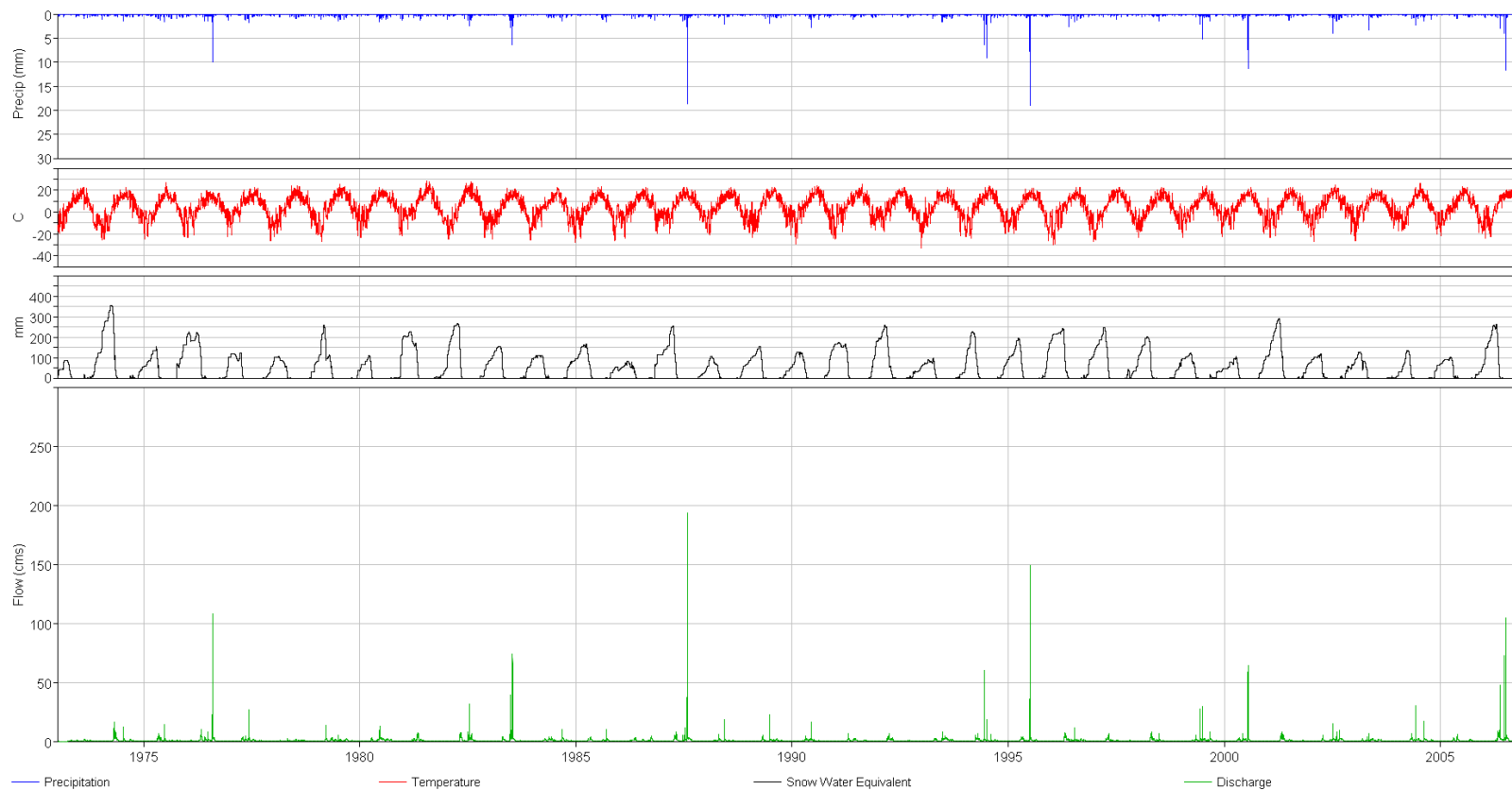


Figure 26. Fisher Creek watershed hydrologic model simulation inputs (temperature and precipitation) and outputs (SWE and discharge) for the CNRM-CM5 2070-2100 climate scenario.



Annual maxima of hourly discharge at the Fisher Creek Bridge location are provided in Table 4. Note, the large outlier for the CNRM-CM5 climate projection for the period 2040-2069 (simulation and historic years 1987), in bold in Table 4.

Table 4. Annual peak hourly discharges (m³/s) at Fisher Creek Bridge from the seven scenario simulations (historic climate and six future climate projections).

Historic Year	Simulation Year	Historic	ACCESS1 2040- 2069	ACCESS1 2070- 2100	CanESM2 2040- 2069	CanESM2 2070- 2100	CNRM-CM5 2040- 2069	CNRM-CM5 2070- 2100
1974	1974	10.4	13.9	22.8	19.2	22.9	10.4	16.3
1975	1975	8.8	16.5	9.0	13.2	15.0	11.6	14.0
1976	1976	76.0	101.5	81.4	87.5	74.6	158.8	108.0
1977	1977	12.5	28.9	22.8	28.6	21.9	24.6	26.4
1978	1978	1.8	1.7	2.4	13.5	12.4	1.7	2.8
1979	1979	6.5	12.3	15.6	17.4	14.7	9.5	13.8
1980	1980	9.0	14.9	14.0	15.5	15.1	12.1	12.9
1981	1981	9.4	10.2	7.2	11.3	5.3	11.1	7.5
1982	1982	20.6	33.0	24.4	30.0	20.3	34.4	31.8
1983	1983	58.1	80.7	69.9	74.8	67.0	66.6	73.7
1984	1984	7.5	11.1	9.2	12.1	9.1	10.0	10.1
1985	1985	7.9	12.5	7.4	9.7	13.8	8.9	9.8
1986	1986	6.6	5.0	6.4	5.9	6.6	6.1	4.5
1987	1987	139.3	186.0	150.2	160.0	135.6	260.5	193.5
1988	1988	10.6	20.9	13.4	20.4	12.6	18.8	18.5
1989	1989	13.7	24.0	17.3	21.8	16.3	21.7	22.6
1990	1990	12.4	4.6	3.6	22.0	23.7	16.6	16.5
1991	1991	6.9	6.7	4.8	9.7	4.9	6.4	6.8
1992	1992	5.1	6.0	6.8	9.5	10.0	5.9	6.4
1993	1993	6.4	8.8	7.4	8.7	14.1	6.3	7.9
1994	1994	26.0	66.6	55.9	64.7	61.7	52.4	59.8
1995	1995	118.6	152.6	128.7	135.3	118.4	157.0	149.0
1996	1996	17.2	13.7	9.2	11.1	11.0	11.8	11.2
1998	1997	6.5	9.4	6.6	10.5	6.0	9.1	6.4
1999	1998	6.4	8.6	6.8	11.2	10.2	6.6	7.8
2000	1999	21.8	33.4	21.3	23.9	17.7	28.8	29.5
2001	2000	53.2	68.7	66.0	68.2	65.5	59.5	63.9
2003	2001	8.2	8.7	8.6	9.7	8.7	9.4	8.3
2004	2002	9.8	18.8	18.2	20.6	30.7	14.0	15.1
2005	2003	8.7	5.0	2.9	13.6	10.3	16.8	6.3
2007	2004	21.9	31.8	24.4	26.9	20.9	32.3	30.4
2010	2005	8.0	6.4	6.9	8.3	8.2	3.4	5.8
2011	2006	77.8	109.6	89.9	95.5	82.4	110.6	104.7

2.6.7 ANALYSES OF HISTORICAL AND FUTURE MAXIMUM HOURLY FLOW IN FISHER CREEK

Frequency Analysis

Annual maxima have been extracted from the seven scenario simulations (historic climate and six future climate projections) of continuous hourly discharge at the Fisher Creek Bridge location and flood frequency analysis carried out to determine the 200-year return period hourly maximum flow for each scenario. Trends were not apparent in the annual peak flow datasets.

Similar to observed datasets in the region, two distinct populations are apparent in the simulated annual maximum hourly flow series, whereby annual flood events are predominantly driven by snowmelt or rainfall. Fitting peak flow frequency curves by conventional means (i.e. with a mathematical function) produces poor results, and a graphical fitting method was used to provide consistency in the estimation of the 200-year return period hourly peak flow (USACE, 1994). While this method is subjective, operationally, the graphical method is not inferior to other methods since the range of uncertainty caused by sampling variability is always large (Benson, 1968). Frequency analysis fits are provided in Appendix C.

Table 5 provides a summary of estimates of the 200-year return period hourly peak flow, based on the simulations of the historic climate and future climate projections (with changes relative to the simulated historic baseline).

There is a large outlier in the annual peak hourly discharge dataset for the CNRM-CM5 climate scenario for the period 2040-2069 (bold value in Table 4). This outlier has large leverage on the estimate of the 200-year return period hourly peak flow (Figure C6, Appendix C), which results in a large % change in comparison to the historic baseline (in bold in Table 5). This is due to an exceptionally high daily precipitation value present in the CNRM-CM5 climate scenario (details in Appendix A). To assess the sensitivity of both the climate scenario and hydrologic simulations to the high daily precipitation value, an additional estimate of the 200-year hourly peak flow has been provided based on simulations that exclude the high precipitation value in the development of the CNRM-CM5 climate scenario (in parentheses in Table 5). The estimate of the 200-year hourly peak flow is substantially reduced, and reduces both the range and mean change of this value for the mid-century period (2040-2069). The frequency analysis fit for this additional simulation is provided in Appendix D. These large differences make it apparent that this assessment would benefit from simulation of additional climate projections to provide a better sampling of projected climate impacts.

Table 5. Estimates of 200-year hourly peak flow at Fisher Creek Bridge based on simulations of historic climate and future climate projections, with changes relative to the observed historic baseline. Values in parentheses are from simulation with an alternate CNRM-CM5 climate scenario, developed by exclusion of an exceptionally high daily precipitation value (details in Appendix A).

Scenario	Mean Annual Precipitation (mm)	Change Relative to Historic	Mean Temperature Over Period (°C)	Change Relative to Historic	200-year Hourly Peak Flow (m ³ /s)	Change Relative to Historic
Historic Record	453.1		3.1		190	
ACCESS1-0 2040-2069	520.8	15%	6.5	110%	245	29%
ACCESS1-0 2070-2100	521.2	15%	9.5	206%	200	5%
CanESM2 2040-2069	619.3	37%	7.3	135%	210	11%
CanESM2 2070-2100	616.7	36%	10.1	226%	180	-5%
CNRM-CM5 2040-2069	520.8	15%	5.5	77%	340 (195)	79% (3%)
CNRM-CM5 2070-2100	538.9	19%	7.6	145%	250	32%
Period	Range of Change Relative to Historic		Range of Change Relative to Historic		Range of Change Relative to Historic	Mean Change Relative to Historic
2040-2069	+67.6 to +166.2 mm		+2.3 to +4.2 °C		11% to 79% (3% to 29%)	39% (14%)
2070-2100	+68 to +163.5 mm		+4.5 to +7.0 °C		-5% to 32%	11%

The changes in the 200-year return period hourly peak flows for the ACCESS1-0 and CanESM2 scenarios relative to the historic record (far right column in Table 5), are slightly higher (3% higher for all 4 scenarios) than the changes in the historic extreme daily precipitation value (72 mm) that would be derived from the quantile to quantile plots relating daily downscaled ACCESS1-0 and CanESM2 simulated precipitation for the historic period versus the two future periods (Figures 6 and 11, respectively in Appendix A). This appears to imply a direct relation between the extreme precipitation events in the climate scenarios, and the estimate of the 200-year return period hourly peak flow based on the hydrologic model simulated streamflow. Put another way, this implies a near one to one rainfall-runoff relation over a threshold return period event, where incremental

changes in precipitation are equivalent to changes in the resultant peak discharge. This may be due to one or a combination of the following:

- The presence of this process in the limited sample size of extreme events that the Proxy Model was calibrated to, which may be particular to the calibration watershed (Windrem).
- The Proxy Model is oversimplified in its representation of the watershed; for example, it does not include forest harvesting and roads, which can alter internal catchment processes with varying effects on watershed response to extreme events (Alila et al., 2009; Kuras et al., 2012).
- The changes to the sub-daily precipitation distributions for input to the hydrologic model are equivalent to the changes in the daily precipitation, since information to imply otherwise does not exist.
- Extrapolation in the peak flow frequency analysis to the 200-year event is based on an even smaller subset of the simulated peak flow time series.

The changes in the 200-year return period hourly peak flows for the CNRM-CM5 scenario relative to the historic record, are different (-21% and -4% for the 2040-2069 and 2070-2100 periods, respectively) than the changes in the historic extreme daily precipitation value that would be derived from the quantile to quantile precipitation plots (Figure 16 in Appendix A). While this could imply a higher threshold above which the watershed response changes, this may also be due, in part, to the uncertainty in the fit of the extreme daily precipitation event (Figure 16 in Appendix A).

It is crucial to note that the apparent one to one rainfall-runoff relation cannot be generalized for other watersheds, as the relation between changes in precipitation and change in the 200-year peak flow event is not always direct and depends on a multitude of factors and processes.

The simulated mean change in the 200-year event for the mid-century period (2040-2069) is higher than the 10% increase that is currently recommended by APEGBC (2012) to account for the potential impacts of climate change, while the mean change for latter part of century (2070-2100) is close to this value (Table 5). NHC has been in discussions with PCIC regarding the decrease for the latter part of the century in comparison to mid-century period and the following explanations have been put forth:

- The decrease may be due to the natural variability within climate models or an anomaly in GCMs selected.
- Projected precipitation changes between 2040-2069 and 2070-2100 are negligible, so the smaller projected 200-year peak flow for the latter period appears to have something to do with the larger temperature projections for the end of the century as compared to mid-century.

- Increasing precipitation may result in increasing snow storage and freshet magnitude, but increasing temperatures also tend to reduce snow accumulation and reduce the amount of snow runoff available for freshet events. However, annual snowmelt peak flows are the smaller contingent of the Fisher Creek peak flow regime so such changes are not expected to have a direct effect on the 200-year event, which is mainly determined by rainfall peaks.
- Evaporation in the HEC-HMS model is prescribed (monthly average), and while this parameter is not affected directly, dryer antecedent conditions can exist due to increasing soil moisture deficits between the typical spring/summer snowmelt freshet peaks and summer rainfall peaks.

A future assessment may be undertaken, examining the changes to the dominant processes generating annual peak flows in the future climate simulations, with the historic climate simulation as a baseline reference. It's possible that snowpacks melt earlier in the spring/summer and/or there is less snow accumulation due to higher temperatures, which would both result in higher soil moisture deficits later in the summer, which could potentially reduce rainfall peaks.

Other Sensitivity Analyses conducted on the HEC-HMS model output

It is important to note that while model simulations did not incorporate any changes to land-use and forest cover (e.g. logging or pine beetle outbreaks) over the simulation period, the greatest source of error is from the lack of spatial and temporal meteorological data.

The average annual precipitation gradient is expected to be a satisfactory representation of winter precipitation gradients, but a poor representation of gradients occurring during convective summer storms. Gradients for the latter are highly variable both spatially and temporally, and a lack of spatial data in the study area does not allow for simulations to account for this variability. Thus the application of a constant gradient is expected to result in discrepancies between actual and simulated precipitation intensities, spatial distributions, and total precipitation over the basin for convective summer storms. Over a long enough simulation period, however, a rough approximation of the peak flow regime for each watershed considered may be achievable since the integrated response at the watershed outlet (in terms of annual peak flows) to precipitation inputs in the watershed would be expected to overestimate flows for some events, while underestimating flows for other events. The Fisher Creek model's sensitivity to the average annual precipitation gradient has been assessed, using an upper limit of 130.1% (equivalent to the original 86.7% multiplied by a factor of 1.5) and a lower limit of 43.4% (equivalent to the original 86.7% multiplied by a factor of 0.5) as shown in Table 6. While the 200-year hourly peak flow changes relative to the simulated historic baseline have changed, the relative ranking of the 200-year hourly peak flows for the three climate projections (from highest to lowest: CNRM-CM5, ACCESS1, CanESM2) have not changed for the two periods (2040-2069 and 2070-2100), nor has the trend of smaller projected 200-year peak flows for the latter period.

As previously mentioned, the time of concentration employed for the Fisher Creek watershed is derived from the calibration watershed (Windrem), based on the average Manning’s n value (representing the hydraulic characteristics of the drainage network) determined from the observed lag time for the latter for the largest event on record (1987). The Fisher Creek model’s sensitivity to the time of concentration has been assessed, using an expected upper limit of the average Manning’s n value (0.1), which has a corresponding time of concentration of approximately 5 hours (Table 6). Similar to the results of the sensitivity analysis for the precipitation gradient, the relative ranking and trend in the GCM projection simulations are maintained, but the 200-year hourly peak flow changes (relative to the simulated historic baseline) are greater for both the mid and latter part of the century (greater by 2-9% for the six scenarios in comparison to Table 5; not shown in Table 6).

Frequency analysis fits for the sensitivity analysis are provided in Appendix D.

Table 6. Fisher Creek HEC-HMS Model sensitivity to adjustment of precipitation gradient and time of concentration

Scenario	200-year hourly peak flow (m ³ /s, QMH) and variance caused by adjustment of the following parameters				
	Precipitation Gradient (Base Value = 86.7 %)			Time of Concentration (Base Value = 3.00)	
	Upper Limit (UL) Tested 130.1%	Lower Limit (LL) Tested 43.4%	QMH Variance from baseline (UL/LL)	Upper Limit (UL) Tested 4.94	QMH Variance from baseline (UL)
Historic Record	230	140	21.1% / -26.3%	140	-26.3%
ACCESS1-0 2040-2069	290	190	18.4% / -22.4%	190	-22.4%
ACCESS1-0 2070-2100	230	150	15% / -25%	150	-25%
CanESM2 2040-2069	245	160	16.7% / -23.8%	160	-23.8%
CanESM2 2070-2100	210	135	16.7% / -25%	135	-25%
CNRM- CM5 2040- 2069	400	270	17.6% / -20.6%	260	-23.5%
CNRM- CM5 2070- 2100	300	195	20% / -22%	190	-24%

2.7 CLIMATE CHANGE IMPACTS TO FUTURE STREAMFLOW AT OTHER LOCATIONS

NHC has made inferences as to expected impact of climate change on streamflow at Fur Thief, Bitter and Medby Creeks based on the assessed impact of projected climate change on streamflow at Fisher Creek and on the climate change projections for mean annual precipitation and mean temperature for the Bella Coola and Stewart regions. These inferred impacts on streamflow will be used in the Vulnerability Analysis described in Part II.

2.7.1 FUR THIEF CREEK CULVERT AT HIGHWAY 97 EAST OF PINE PASS

For Fur Thief Creek the impact of project climate change on streamflow should be similar to that at Fisher Creek given the close proximity of the two watersheds. Therefore, we'll assume the following percentage increases in flow at Fur Thief for each GCM/ time period combination:

Table 7. Estimated increase in 200-year maximum hourly flow at Fur Thief Creek.

Scenario	Change Relative to Historic
Historic Record	--
ACCESS1-0 2040-2069	29%
ACCESS1-0 2070-2100	5%
CanESM2 2040-2069	11%
CanESM2 2070-2100	-5%
CNRM-CM5 2040-2069	79%
CNRM-CM5 2070-2100	32%

2.7.2 BITTER CREEK BRIDGE NO. 0554 AT HIGHWAY 37A NEAR STEWART

Bitter Creek is located in Highway 37A near Stewart (Figure 9). The GCM projections for change in mean annual precipitation near Stewart varied from those predicted for the area of Highway 97 east of Pine Pass (compare Figures 3 and 10). Projections for rise in mean annual temperature was roughly the same for the two areas. Table 8 summarizes the differences in GCM projections for the two areas, using the simulated historic climate as a baseline¹.

¹ As noted the percentage (%) changes in precipitation and changes in temperature (°C) shown in Table 8 (and Table 10 following) are based on the use of simulated historic climate as a baseline. The differences vary from those shown previously in Table 5 (for Fisher Creek) because those values used the observed historical data as a baseline.

Table 8. Comparison of GCM Projections for the areas of Highway 97 east of Pine Pass and Highway 37A near Stewart (from Figures 3 and 10)

GCM Run	Projected Change in mean annual precip (%)		Projected Change in mean temperature (°C)	
	Highway 97 east of Pine Pass	Highway 37A near Stewart	Highway 97 east of Pine Pass	Highway 37A near Stewart
ACCESS1-0 2040-2069	+12%	-1%	+3.4	+3.2
ACCESS1-0 2070-2100	+13%	+6%	+6.4	+5.8
CanESM2 2040-2069	+41%	+28%	+4.2	+4.9
CanESM2 2070-2100	+41%	+43%	+6.9	+7.5
CNRM-CM5 2040-2069	+14%	+19%	+2.4	+2.7
CNRM-CM5 2070-2100	+20%	+24%	+4.6	+5.0

Projected changes in mean annual precipitation are lower at Highway 37A near Stewart than at Highway 97 for the ACCESS1-0 scenarios and CanESM2 2040-2069 and slightly higher for CanESM2 2070-2100 and both CNRM-CM5 scenarios.

In a mountainous coastal area like Stewart extreme floods have historically been more apt to be caused by rain falling on snow. Therefore, for scenarios in which relatively large changes in mean temperature are projected the effect may be that the 200-year magnitude actually decreases because there is presumably less chance of having snow on the ground during a rainfall event. For scenarios in which relatively small changes in mean temperature are projected the effect may be that the 200-year magnitude increases because there is more chance of cold weather (producing snow fall) being immediately followed by warmer weather (producing rain fall on top of the snow cover). Taking this all into account we'll assume the percentage increases in 200-year flow at Bitter Creek shown in Table 9.

Table 9. Estimated increase in 200-year maximum hourly flow at Bitter Creek.

Scenario	Change Relative to Historic
Historic Record	--
ACCESS1-0 2040-2069	10%
ACCESS1-0 2070-2100	2%
CanESM2 2040-2069	6%
CanESM2 2070-2100	-5%
CNRM-CM5 2040-2069	85%
CNRM-CM5 2070-2100	30%

2.7.3 MEDBY CREEK CULVERTS AT HIGHWAY 20 NEAR BELLA COOLA

Medby Creek is located on Highway 20 near Bella Coola (Figure 14). The GCM projections for change in mean annual precipitation near Bella Coola varied from those predicted for the area of Highway 97 east of Pine Pass (compare Figures 3 and 15). Projections for rise in mean annual temperature was roughly the same for the two areas. Table 10 summarizes the differences in GCM projections for the two areas.

Table 10. Comparison of GCM Projections for the areas of Highway 97 east of Pine Pass and Highway 20 near Bella Coola (from Figures 3 and 15)

GCM Run	Projected Change in mean annual precip (%)		Projected Change in mean temperature (°C)	
	Highway 97 east of Pine Pass	Highway 20 near Bella Coola	Highway 97 east of Pine Pass	Highway 20 near Bella Coola
ACCESS1 2040-2069	+12%	-1%	+3.4	+3.2
ACCESS1 2070-2100	+13%	+3%	+6.4	+5.6
CanESM2 2040-2069	+41%	+15%	+4.2	+4.2
CanESM2 2070-2100	+41%	+21%	+6.9	+6.6
CNRM-CM5 2040-2069	+14%	+17%	+2.4	+2.6
CNRM-CM5 2070-2100	+20%	+22%	+4.6	+4.8

Projected changes in mean annual precipitation are lower at Highway 20 near Bella Coola than at Highway 97 for the ACCESS1-0 and CanESM2 scenarios and are higher for both CNRM-CM5 scenarios.

Bella Coola is a mountainous coastal area and like Stewart extreme floods have historically been more apt to be caused by rain falling on snow. Therefore projected mean temperature variations will have a similar effect at Bella Coola as they did for Stewart (Section 2.7.2). We'll assume the percentage increases in 200-year flow at Medby shown in Table 11.

Table 11. Estimated increase in 200-year maximum hourly flow at Medby Creek.

Scenario	Change Relative to Historic
Historic Record	--
ACCESS1 2040-2069	10%
ACCESS1 2070-2100	2%
CanESM2 2040-2069	6%
CanESM2 2070-2100	-8%
CNRM-CM5 2040-2069	90%
CNRM-CM5 2070-2100	35%

3 PART II - VULNERABILITY ANALYSIS

Previous climate impact assessments by MOTI have defined vulnerability as the ratio of total discharge load (m^3/s) at a stream crossing structure to total discharge capacity (m^3/s). Total design discharge load (L_T) is defined as the summation of the existing design discharge estimate (L_E); the Climate Load (L_C), or increase in design discharge expected as a result of climate change (Sections 2.5 and 2.6 of this report); and other anticipated changes in design discharge load (L_O):

$$L_T = L_E + L_C + L_O \quad (2)$$

The last term, L_O provides allowances for increased runoff due to ground cover changes caused by logging, forest fires, human development, insect infestation etc.

Total discharge capacity (C_T) is defined as the summation of existing discharge capacity (C_E); the allowance for increased capacity due to future climate change (C_M), if applicable; and other capacity changes (C_A) such as loss of effective flow area due to anticipated aggradation:

$$C_T = C_E + C_M + C_A \quad (3)$$

For bridge structures existing capacity (C_E) is the discharge that produces a water surface elevation that is the full freeboard depth (1.5 m) below the minimum soffit elevation. For culverts, existing capacity is the discharge that produces a headwater elevation equal to the inlet crown elevation.

3.1 ESTIMATES OF TOTAL LOAD AND TOTAL CAPACITY AT SELECTED STRUCTURES

3.1.1 FISHER CREEK BRIDGE NO. 7110 AT HIGHWAY 97 EAST OF PINE PASS

Total Load

The design peak flow for Fisher Creek was determined using regional analysis (NHC 2013). Curves relating unit peak runoff to drainage area were developed based on flood frequency analysis of three nearby gauged streams (Dickebusch Creek, WSC 07FB004; Sukunka River above Chamberlain Creek, WSC 07FB007; and Sukunka River at the mouth, WSC 07FB006). Since Dickebusch Creek is closest in size to Fisher Creek, its 200-year peak discharge estimate had a dominant influence on the Fisher Creek estimate (the Sukunka gauges both had watershed sizes orders of magnitude larger than Fisher Creek). The 200-year peak discharge estimate for Fisher Creek is $207 m^3/s$; as an instantaneous peak discharge that agrees quite well with the baseline 200-year maximum hourly flow predicted by the Fisher Creek HEC-HMS model ($190 m^3/s$; Table 5)

The range of climate change load increase considered for Fisher Creek is -5 % to 79% of L_E as presented in Section 2.6.7 (Table 5). Additional loads due to future logging and forest fires amount to a further increase of up to 30% (Alila et al, 2009; Kuras et al, 2012) on L_E , which is considered a

reasonable upper limit to account for these effects. Assuming the full 30 % increase would be a worst case scenario. Studies have shown that it can take up to 7 to 10 years for recovery from a complete forest fire burn (as opposed to a canopy burn, for example). Logging related increases are most strongly influenced by the effect of logging road development and the way in which roads concentrate runoff, as opposed to effects of actually cutting down trees. Logging recovery times can therefore vary a great deal depending on the level and effectiveness of road deactivation measures.

Total Capacity

The existing discharge capacity (C_E) at Fisher Creek Bridge is approximately $10 \text{ m}^3/\text{s}$ based on channel conditions that existed following the 2011 flood. Its capacity is not expected to be reduced further during a major flood event, despite the potential for aggradation and debris accumulation, because scour will likely maintain at least a $10 \text{ m}^3/\text{s}$ flow rate.

3.1.2 FUR THIEF CREEK CULVERT AT HIGHWAY 97 EAST OF PINE PASS

Total Load

The design peak flow for Fur Thief Creek was determined using the same regional analysis as was used for Fisher Creek (NHC 2013). The 200-year peak discharge estimate for Fur Thief Creek is $46.3 \text{ m}^3/\text{s}$.

The range of climate change load increase considered for Fur Thief Creek is -5 % to 79% of L_E as discussed in Section 2.7.1. Additional loads due to future logging and forest fires amount to a further increase of up to 30% (Alila et al, 2009; Kuras et al, 2012).

Total Capacity

The existing discharge capacity (C_E) at Fur Thief Creek Culvert is approximately $8 \text{ m}^3/\text{s}$. Aggradation of sediment and debris during a single, major flood event is expected to fully block the undersized structure and reduce its capacity to zero.

3.1.3 BITTER CREEK BRIDGE 0554 AT HIGHWAY 37A NEAR STEWART

Total Load

The design peak flow for Bitter Creek was determined using regional analysis (NHC 2012). Flood frequency analysis was first used to determine peak flows for three predictor watersheds (Bear Creek, WSC 08DC006; More Creek, USGS 15024684; and Surprise Creek, WSC 08DA005) for a range of return periods. The Generalized Extreme Value (GEV) frequency distribution (method of weighted moments) provided the best fit to observed peak flows in the sample data sets. The peak flow estimates for the predictor watersheds were then scaled by area to the Bitter Creek Bridge using a scaling exponent of 0.75 (Eaton et al., 2002), where:

$$\text{Peak Flow Bitter Creek} = (\text{Peak Flow WSC}) * (\text{Area Bitter Creek}/\text{Area WSC}) 0.75 \quad (1)$$

The resulting 200-year peak flow estimate for Bitter Creek is 589 m³/s.

The range of climate change load increase considered for Bitter Creek is -5 % to 85% of L_E as discussed in Section 2.7.2.

Other load increases for Bitter Creek include a potential 25% increase relative to the 200-year flow accounting for a small glacial outburst flood coinciding with a 200-year peak flow and it is considered reasonable to assume that such an event would be coincident with the 200-year peak flow as long as glaciers remain in the watershed (NHC 2012). Larger outburst floods are possible but it may not be reasonable to assume they would be coincident with a 200-year peak flow. Additional loads due to future logging and forest fires amount to a further increase of up to 30% (Alila et al, 2009; Kuras et al, 2012).

Total Capacity

The existing discharge capacity (C_E) at the newly replaced Bitter Creek Bridge is equal to the estimated 200-year peak flow, 589 m³/s. There is no additional capacity to account for climate change (C_M). Aggradation of sediment over the life of the bridge (50 years), assuming it goes unchecked and unmaintained, could raise bed levels by 1.5 m and reduce the capacity to 150 m³/s.

3.1.4 MEDBY CREEK CULVERTS AT HIGHWAY 20 NEAR BELLA COOLA

Total Load

An estimate of the existing design (100-year peak) discharge at Medby Creek is made using the Rational Method approach. Medby Creek has a drainage area of approximately 2.1 km² (Figure 14)

The general form of the BC Rational Method Formula is as follows (Coulson, 1991):

$$Q_p = \frac{0.28CPA}{T_c} \quad (4)$$

where: Q_p is the peak instantaneous discharge in m³/s

C is a runoff coefficient

P is the total precipitation accumulated over T_c in mm

A is the drainage area in km², and

T_c is the time of concentration in hours

The base runoff coefficient, C, has been estimated at 0.85 from Table 1020A of the TAC Supplement (BC MOTI, 2007). The final 'C' used in Equation 4 is increased by 0.15 since the target return period exceeds 25-years and to account for a rain-on-snow contribution to the flood peak.

Time of concentration, T_c was estimated as 1.3 hrs using Figure 1020B in the TAC Supplement.

Estimates of 100-year precipitation were made using hourly data from Bella Coola BC Hydro Meteorological Station (Stn. No. 1060842 at 13 m elevation; data range 1970-1985)¹. A frequency analysis of annual maximum 1-hr and 2-hr rainfall at this station was carried out using available intensity and duration data for the station. Fitting a Gumbel distribution (Method of Moments) to the data and interpolating between the 1-hr and 2-hr intervals resulted in a 100-year, 1.3-hr rainfall total (P in Equation 4) of 23.2 mm.

Based on our estimates of all the variables, Equation 4 gives a 100-year peak discharge (design discharge, L_E) of 10.4 m³/s for Medby Creek.

The range of climate change load increase considered for Medby Creek is -8 % to 90% of L_E as discussed in Section 2.7.3. Additional loads due to future logging and forest fires amount to a further increase of up to 30% (Alila et al, 2009; Kuras et al, 2012).

Total Capacity

Existing capacity at Medby Creek has been estimated by developing a HEC-RAS model of the crossing. Channel geometry in the model is estimated from a sketch of the site prepared by Golder Associates (2012). The crossing consists of a 1,000 mm diameter CSP culvert and a 1,200 mm diameter CSP culvert, side by side. Modelling in HEC-RAS suggests the capacity is approximately 3.4 m³/s. Aggradation of sediment and debris during a single, major flood event is expected to fully block the undersized structure and reduce its capacity to zero.

3.2 VULNERABILITY AND CAPACITY DEFICIT AT THE SELECTED STRUCTURES

Table 12 summarizes the total load, total capacity, vulnerability and capacity deficit at all four structures.

¹ Note that the Environment Canada Station at Bella Coola Airport (EC 1060841) shown in Figure 14 could not be used for this analysis because it does not record hourly data.

Table 12. Vulnerability and Capacity Deficit at the selected structures

Structure	Range of Total load and its component parts ¹ (m ³ /s)				Total Capacity and its component parts ¹ (m ³ /s)				Vulnerability Range $V_R = L_T / C_T$	Capacity Deficit Range $C_D = L_T - C_T$ (m ³ /s)
	L_E	L_C^2	L_O^3	L_T	C_E^5	C_M	$C_A^{5,6}$	C_T		
Fisher Creek Bridge	207.0	-10.4 to 176	0 to 62.1	196.6 to 445.1	10.0	None	0.0	10	19.7 to 44.5	186.6 to 435.1
Fur Thief Culvert	46.3	-2.3 to 39.6	0.0 to 13.9	44.0 to 100.0	8.0	None	-8.0	0.0	Undefined (infinite)	44.0 to 100.0
Bitter Creek Bridge	589.0	-29.5 to 500.7	147.3 ⁴ to 324	706.8 to 1,413.7	589.0	None	-439.0	150	4.7 to 9.4	556.8 to 1.263.7
Medby Creek Culverts	10.4	-0.8 to 9.4	0 to 3.1	9.6 to 22.9	3.4	None	-3.4	0.0	Undefined (infinite)	9.6 to 22.9

Notes:

1. The load and capacity component definitions are as follows:
 - a. L_E = existing discharge load (design discharge estimate) in m³/s;
 - b. L_C = anticipated range of increase in load (discharge) due to climate change in m³/s;
 - c. L_O = other anticipated changes in load (discharge) due to things like logging, forest fire, insect infestations and human development;
 - d. C_E = existing discharge capacity in m³/s;
 - e. C_M = allowance for increased discharge capacity due to climate change in m³/s; note, none of the structures have such an allowance 'built-in' to their design;
 - f. C_A = other changes in discharge capacity (m³/s) due to things like loss of capacity due to sediment and debris aggradation at the structure.
2. Climate change load (L_C) is given as a modelled (Fisher Creek) or inferred (at other sites) range based on the range of future changes in precipitation and temperature as projected by the GCMs considered. The upper end of this range (79 % to 90% depending on the structure) reflects the presence of the high outlier of estimated maximum annual hourly discharge based on CNRM-CM5 mid-century climate projections; with the high outlier removed the upper end of the range would be 30 to 35%.
3. Other changes in load are presented as a range of 0 to 30 % of existing load; a 30 % increase is based on research by Alila et al (2009) and Kuras et al (2012) and is considered a reasonable upper limit to account for the effects of logging, forest fires, development etc. assuming that not all of these effects would be compounded.
4. The low end of the range for other loads at Bitter Creek represents the occurrence of a small glacial lake outburst flood coincident with the 200-year peak discharge, which is based on an assessment by NHC (2012); if future climate change eradicates glaciers in the watershed then this value would eventually reduce to zero.
5. Capacity is based on current MOTI design standards; at highway bridges this is the amount of flow that can pass through the bridge while still allowing 1.5 m of clearance from peak flood level to the minimum soffit level of the bridge; for culverts this is the amount of flow that can pass through the barrel with the headwater elevation equal to the upstream soffit (obvert) level of the culvert.
6. Other changes in capacity at the structures represent the tendency for sediment aggradation and debris accumulation to reduce or effectively eliminate the waterway opening area. For Fur Thief Creek and Medby Creek a single flood event can produce enough sediment and debris to completely block the existing, undersized culverts – regular maintenance would not be effective at reducing or eliminating this factor. At Bitter Creek, aggradation will build over time and reduce capacity more gradually – regular maintenance (channel dredging) could therefore reduce the effect of aggradation.
7. It should be noted that a lack of capacity is not the sole reason why structures fail; loss of erosion protection (e.g. rip rap) and the undermining and collapse of foundations can occur even when there is a surplus of flow capacity.

4 PART III - IMPACT OF RECENT EXTREME CLIMATE ON SELECTED STRUCTURES

Each of the four stream crossings introduced above experienced significant damage during recent, large flood events in 2010 or 2011, and in both years in some cases. In this section we review what those damages were and the role that extreme climate played in causing the damage.

4.1 FISHER CREEK BRIDGE NO. 7110 AT HIGHWAY 97 EAST OF PINE PASS

From mid-June to early July of 2011 the Peace District experienced a weather pattern of prolonged rainfall. One of the hardest hit areas was the Pine River Valley in the South Peace, in particular a 60 km length of Highway 97 west of Chetwynd, BC which includes the Fisher Creek Bridge crossing. The greatest rainfall amount occurred from June 23 to June 25. Hourly rainfall intensities during this period were not particularly high: at the Environment Canada weather station at Chetwynd, the highest hourly rainfall rate over the two day period was 6 mm/ hr; at the BC Forest Service weather station at Lemoray, BC (50 km west of Chetwynd), it was 8 mm/ hr. In both cases, the return period of the highest 1-hr rainfall intensity was well under 2-years. What made the June 2011 storm event so devastating was how long the rainfall lasted. For instance, 24-hour rainfall totals recorded at Chetwynd and Lemoray were 72 mm and 125 mm, respectively, and equaled or exceeded a 100-year return period at both locations – there is however considerable error in the estimate of return period given how short the climate records are.

The prolonged rainfall saturated hill slopes in every watershed inducing hundreds of separate landslides and debris flows in the mid- to upper watersheds of all the creeks resulting in historic volumes of sediment and wood debris being delivered to the Highway 97 crossings. Fisher Creek, like many of the other major crossings along the affected portion of Highway 97, is located on an alluvial fan. Prior to the flood, the stream channel has been flanked by low streambanks or levees. When the huge volumes of debris and sediment entered these fan reaches it was deposited in an ad-hoc fashion causing the banks to be overtopped and levees breached, generating even more debris and sediment and causing avulsions: the development of new stream channels across the alluvial fan.

The Fisher Creek Bridge is a two span bridge with an overall length of 18.3 m. It is dramatically undersized compared to the estimated 200-year design discharge with a capacity at minimum clearance level estimated to be about a 2-year flood. The bridge also has a central pier, which further reduces its effective capacity. During the 2011 flood the pier acted like a strainer trapping debris and sediment carried by the creek. Before long the bridge opening was completely blocked (Photo 1) and flow in the creek was diverted to the east and west alongside the highway. Flood waters eventually broke through the highway 100 m west of the bridge and directly behind both abutments. The bridge is supported on piles and the structure itself did not fail as a result of scour

associated with the flood. Farther upstream flood waters carried along new avulsion channels on the eastern portion of the fan by-passed the bridge entirely and flowed eastward along Highway 97.



Photo 1: Looking down at the Fisher Creek Bridge during the 2011 flood (June 25, 2011).

Because the flow in Fisher Creek was diverted in so many different directions during the 2011 flood it is impossible to estimate what the combined peak discharge may have been. Computer modelling of other creeks along Highway 97 with similarly sized watersheds suggests peak discharges ranged somewhere between a 25-year and 40-year return period.

In summary, the rainfall that spread across the South Peace in June 2011 was not remarkable for its intensity but for its duration. The duration of the rainfall induced hundreds of land and mudslides and elevated sediment and debris in the creeks to historic levels. On Fisher Creek, the sediment and debris overwhelmed the creek channel all along the length of its alluvial fan and caused the highway bridge to become blocked. It should be emphasized that the Fisher Creek Bridge would also have been severely damaged by a storm with shorter duration, more intense rainfall because the waterway opening is so small. The bridge deficiencies include its inability to pass sediment and debris and not just its lack of discharge capacity. Previous studies (NHC 2013) have recommended debris and sediment control on the Fisher Creek fan because even if the bridge has been large enough the upstream channel would still have been overwhelmed and avulsions would still have occurred and damaged the highway.

4.2 FUR THIEF CREEK CULVERT AT HIGHWAY 97 EAST OF PINE PASS

The Fur Thief Culvert is a 2.2 m diameter corrugated metal pipe. It was subjected to the same rainfall event as Fisher Creek Bridge – the two watersheds are separated by only a short distance. Fur Thief Culvert is also severely undersized and its discharge capacity to the culvert soffit is 8 m³/s, a fraction of the estimated design discharge 46.3 m³/s. During the 2011 flood a particularly large landside occurred in the mid- to upper elevations of the watershed. Debris and sediment from the slide travelled the entire length of the stream and accumulated upstream of Highway 97 causing the culvert to become blocked and the highway overtopped (Photo 2).



Photo 2: Looking down at the Fur Thief Culvert during the 2011 flood (June 25, 2011).

Again, due the accumulation of debris and spreading of flow over and alongside the highway it is impossible to say with any certainty what the peak discharge was during the 2011 flood. However, based on the size of the watershed (9.3 km²) and the measured short-duration rainfall intensities the peak discharge was probably in the range of 15 m³/s to 20 m³/s, which equates to a return period of 20 to 30 years.

Like Fisher Creek Bridge, the deficiencies at Fur Thief Creek Culvert include its inability to pass sediment and debris and not just its lack of discharge capacity. However, as was also the case at Fisher Creek the Fur Thief crossing would have been overwhelmed in 2011 even if the structure had been properly sized. The massive slide that occurred in the watershed appears to have been attributable to a failed stream crossing (probably a culvert) on a forestry road, and it would have caused significant destruction regardless.

4.3 BITTER CREEK BRIDGE 0554 AT HIGHWAY 37A NEAR STEWART

From September 5th to September 8th, 2011 a low pressure weather system in the Gulf of Alaska brought sustained, heavy rainfall to BC's mid and north Coast and the Bitter Creek watershed. Approximately 200 mm of rainfall was recorded at Stewart Airport over a 4-day period. An informal estimate of the maximum 24 hr rainfall during the event is 120 mm, which occurred between September 7th and September 8th (MOTI, 2011). The intensity of the rainfall was high at times but for the most part it was moderate but steady. The duration of the rainfall resulted in saturated slopes throughout the watershed and high inputs of sediment and debris to the stream. Retreating glaciers in the upper watershed have left a great deal of unconsolidated coarse sediments exposed and vulnerable to erosion. Sediment buildup in the lower reaches of the stream caused the river to shift and erode its banks, adding even more sediment and debris.

The former Bitter Creek Bridge had an overall length of 50.6 m and three spans of approximately equal length. The abutments were founded on spread footings perched above the stream on bridge end fill. The original drawings for the bridge showed the banks and fill slopes protected with 500 kg rip-rap extending 30 m upstream of the bridge and 20 m downstream. However in Photo 3, which was taken prior to the eventual washout of the bridge, it appears there was little if any of the original rip-rap remaining.



Photo 3: Looking down at Bitter Creek Bridge prior to the washout - flow is left to right (September, 2011).

A photo taken of emergency protection being placed at the bridges west abutment shortly before the washout (Photo 4) indicates the flood level as at or near the elevation of the abutment footing, or 0.5 m to 1 m below the soffit of the bridge. Computer modelling shows the discharge corresponding to this level would have been in the range of 250 m³/s to 300 m³/s. The bridge was originally designed to accommodate a discharge of 300 m³/s, the 200-year discharge as it was estimated in 1982. The present day estimate of the 200-year peak discharge is 589 m³/s and a discharge of 300 m³/s would equate to a return period of about 30 to 35 years in present day terms.

The Bitter Creek Bridge did not fail due a lack of flow capacity, strictly speaking. It failed as a result of the large sediment and debris loads in the creek and the fact that the bridge piers trapped most of the large debris causing sediment build-up and widening of the channel towards the west immediately upstream of the bridge. The erosion of the upstream west bank outflanked whatever rip-rap protection remained and eventually undermined the spread footing that supported the west abutment. The fact the abutment was supported on a perched spread footing did not cause the failure but it was certainly a contributing factor – had the abutment been on piles, the road may have washed out but the structure would have survived.



Photo 4: Emergency protection being placed at the west abutment of Bitter Creek Bridge shortly before the bridge was washed out (September, 2011).

4.4 MEDBY CREEK CULVERTS AT HIGHWAY 20 NEAR BELLA COOLA

A rainfall event struck BC's mid-coast on September 24th and 25th, 2010 and caused widespread flooding throughout the Bella Coola Valley. Approximately 240 mm of rain reportedly fell in a 36

hour period and the maximum 24-hr rainfall was 193 mm at the Environment Canada climate station at Bella Coola Airport (Ball 2010). It has been suggested that the Bella Coola River experienced a 100-year flood as a result of the storm.

Very small watersheds like Medby Creek (2 km²) probably experienced discharges that were well under a 100-year event. However, the sediment and small debris produced as a result of the rainfall plugged all of the small culverts like those at Medby Creek causing Highway 20 to be overtopped at such locations. Based on NHC's assessment of the flood hydrology at Medby Creek the former culverts were substantially undersized and the new culverts remain so. The original culverts may have been undersized because there was a lower standard used for the design flood return period. The reason they are still undersized is likely because the focus during the flood response phase was to re-establish pre-existing conditions. Later, during the flood recovery phase (when some structures may have been upgraded), more attention was probably paid to major infrastructure like highway bridge crossings as opposed to small culverts like those at Medby Creek. Had the culvert(s) been properly sized to match the dimensions of the anticipated flood channel (i.e. according to geomorphic principles rather than being sized to a headwater-to-depth HW/D ratio of 1.0 per the TAC Supplement) and outfitted with a protective headwall, the crossing would probably not have sustained much if any damage during the 2010 flood.

4.5 SUMMARY

Table 13. Summary of extreme climate event rainfall and estimated flows at the four structures

Site	Watershed Size km ²	Event Rainfall Intensity mm (duration, hrs)	Return Period of Rainfall (estimated) yrs (duration, hrs)	Streamflow at Site (estimated) m ³ /s	Return Period of Streamflow (estimated) m ³ /s
Fisher Creek	44.8	4.3 (24) ¹ 5.6 (4)	100 (24) ⁴ 10 (4)	--	1: 25-40 ⁷
Fur Thief Creek	9.3	4.3 (24) ¹ 6.0 (2)	100 (24) ⁴ 2 (2)	15 – 20	1: 20-30 ⁷
Bitter Creek	276	5 (24) ²	20 (24) ⁵	275	20 ⁸
Medby Creek	2	8.0 (24) ³ 12.2 (1)	> 100 (24) ⁶ 25 (1)	--	25 ⁹

Notes:

1. Rainfall intensities for Fisher Creek and Fur Thief Creek (Highway 97) are averaged from the hourly records at EC Chetwynd and the BC Forest Service (BCFS) Station at Lemoray, located less than 10 km west of the creeks.
2. Rainfall intensities for Bitter Creek (Highway 37A) is based on a 24-hr estimate of total rainfall (Sept. 7 – 8, 2011) (BC MoTI, 2011)
3. Rainfall intensities for Medby Creek (Highway 20) are taken from Ball (2010).
4. Based on update (to 2011) of the IDF Curves for EC Chetwynd and BCFC Lemoray
5. Based on the IDF Curve (up to 2005) for EC Stewart A
6. Based on the IDF Curve (up to 2005) for EC Bella Coola A
7. No flow has been estimate at Fisher Creek; the estimated range of return periods is based on flow estimates for other similar size streams along Highway 97
8. No flow has been estimate at Fur Thief Creek; the estimated range of return periods is based on flow estimates for other similar size streams along Highway 97
9. Based on regional flood frequency analysis conducted by NHC (2012).

5 PART IV - COMMENTARY ON CURRENT PRACTICE AND BEST PRACTICE FOR THE FUTURE

5.1 CURRENT PRACTICE IN HYDROTECHNICAL DESIGN OF STREAM CROSSINGS

5.1.1 HYDROLOGIC ANALYSIS

Practicing engineers must use available climate and streamflow data to predict peak flows at stream crossings if data is not available for a site. The assumptions are that the data is random, independent, stationary, homogeneous, and representative of a site if used as a proxy, although it is recognized that this is often not the case. Adjusting for potential issues and accounting for uncertainty can be time consuming and is often not done due to cost. The effects of climate change will be another significant factor to account for, but it may take years of observations to see the effects in the data due to the natural variability of flood events. Notwithstanding the effects of climate change, there is a high degree of statistical variability in flood frequency analysis due to selection of the statistical method, lack of peak flow data (short records, data gaps or no data), data accuracy and quality. Adding the effects of climate change to the analysis greatly amplifies the variability of the results as illustrated by the current study.

Hydrological analysis is an important step but it is just one aspect of bridge and culvert waterway design. Depending on the site, current practice for estimating design discharge can include simple empirical methods (such as the Rational Method), single station or regional flood frequency analysis, and hydrologic modelling. Selecting one of these (or other available) statistical methods plus giving due consideration to the assessment and processing of the input data as noted above provides the hydrological context that then feeds into the following hydrotechnical design discussion.

5.1.2 HYDRAULIC DESIGN

Hydrotechnical design of bridges and culverts has evolved over the past few decades. Early designs for larger bridges were done by MOTI staff and/or consultants using the RTAC publication Guide to Bridge Hydraulics as a reference. Climate and hydrologic data was very sparse or non-existent. Bridge design in more remote areas of the province may have relied on local knowledge of the streams and installations were often done by bridge crews so there was less than a rigorous accounting of hydrotechnical aspects. Locations along Highway 97, such as Fisher Creek which had no available drawings and an opening that was somewhat undersized, may have been an example of this approach to design.

More recently MOTI has strengthened the approach used in hydrotechnical design by tying the process more closely to the Canadian Highway Bridge design Code (CAN/CSA-S6-06) and ultimately to the Guide to Bridge Hydraulics (TAC, 2004). The methodology is being promoted on MOTI's

website and is the current state of professional practice in BC for MOTI projects. The six principal steps in the MOTI methodology are as follows:

1. Background research, data acquisition and preliminary concepts
2. Site Inspection
3. Hydrological Estimation and Morphological Assessment
4. Hydraulic design of waterway opening
5. Scour evaluation and channel control works
6. Sensitivity Analysis

This methodology has been in use throughout Canada since the first edition of the Guide to Bridge Hydraulics was published in 1973. The current edition is a required reference in the Canadian Highway Bridge design Code and the BC Supplement to the Bridge Code. If the methodology is followed by a professional with suitable experience and qualifications, the result will be a robust bridge waterway opening design that suits the stream morphology at the proposed location.

5.2 BEST PRACTICE FOR THE FUTURE

5.2.1 HYDROLOGIC ANALYSIS

Future hydrologic analyses for bridge and culvert design, both in general and in the context of climate change, would be improved by the following means:

- Updating of regional peak flow analyses for the province
- Updating of rainfall intensity duration frequency (IDF) curves for the province, with an account for the potential impacts of climate change where possible
- When conducting hydrologic analyses, give consideration to the potential impacts of climate change specific to a region and/or watershed as applicable, as opposed to sole factor of safety increases; this would be accomplished both qualitatively (describing potential changes in processes, such as receding glaciers) and quantitatively
- Continued and enhanced monitoring of streamflow and climate throughout Canada with long term commitments of support from federal and provincial agencies; the potential for success in this venture could be improved through the establishment of inter-agency and private sector partnerships or legislated requirements

- Carrying out hydrologic analyses using more than one method (e.g. regional analysis, estimates from a proxy watershed, hydrologic modelling, rational method) to assess the convergence/divergence of estimates
- Better accounting of uncertainty in all methods of analysis

5.2.2 HYDRAULIC DESIGN

Effective bridge and culvert hydrotechnical design ultimately comes down to sizing the waterway opening and ensuring the opening can safely convey the water, sediment and debris that will pass through it. A waterway opening that is consistent with the natural channel characteristics and the local stream channel morphology is a critical component of a good design. Following the procedures in the Guide to Bridge Hydraulics and adopting MOTI's standards for flood clearance will result in a robust waterway opening design that should accommodate future climate change. For properly designed bridges a flood 5 to 15% greater than the design flood generally would be passed through the opening without failure of the structure. In most cases this slight increase in design discharge would have a relatively minor effect on water levels, channel width, and design velocity – the key variables in hydraulic design. However, the relationships between discharge and these variables is site specific and would be left to the designer to quantify using sensitivity analysis.

A technique used by hydraulic engineers is sensitivity analysis where all quantities that have a significant influence on results are increased or decreased to check the effect on the proposed design. Climate change is currently being quantified in terms of changes to precipitation and streamflow. Checking the sensitivity of the design discharge through the waterway opening is recommended to quantify the effects of flows higher than design flows occurring at the bridge site.

In the USA, for bridge scour evaluation, the FHWA uses a 1:100-year flood for design but requires that bridge foundations be checked against a 1:500-year flood (often about a 25% increase) which is considered a super flood. For comparison, using MoT's 1:200-year design flood standard, a sensitivity check of the 1:250-year and 1:500-year event would result in an increase of about 5% and 15% respectively of the design discharge. This sensitivity would be in the range of many climate change predictions.

This in effect builds in an allowance for climate change which will in most cases be adequate for the life of the bridge or culvert (50 to 75 years). This sensitivity approach coupled with sound hydrotechnical design that meets current standards will create robust waterway openings (bridge and culvert) with the capacity to accommodate climate change. The trade-off is that a portion of the freeboard buffer is now being allocated to a climate change component. This is discussed in more detail in the section 'Recommendations for Future Study'. As an example, the recent proposed Fisher Creek waterway opening design used this technique and a 20% increase in design discharge showed resiliency of the protection works, and an infringement into the freeboard of only 0.24m (20% was chosen by the designer based on local conditions).

Due to the uncertainty and variability of the climate change projections looking so far into the future, we suggest a classic approach to looking at the data: elimination of the high and low outliers and taking the average. The following Table shows the results.

Table 14. Summary of future changes in design discharge at the four structures with low and high estimates (CanESM2 late century and CNRM-CM5 mid-century) removed.

Scenario	Design Discharge Change Relative to Historic High & Low Outliers Removed (%)			
	Fisher Creek	Fur Thief Creek	Bitter Creek	Medby Creek
ACCESS1-0 2040-2069	29	29	10	10
ACCESS1-0 2070-2100	5	5	2	2
CanESM2 2040-2069	11	11	6	6
CanESM2 2070-2100	-	-	-	-
CNRM-CM5 2040-2069	-	-	-	-
CNRM-CM5 2070-2100	32	32	30	35
Average	19	19	12	13

The average of the bottom row in Table 14 is 16%. Increasing estimated design discharges today by some percentage to deal with future climate change appears to be overly conservative. In other words, if a design Q200 is say 100 m³/s based on current methodology, increasing it by 15% to 115 m³/s to account for climate change is not recommended because of the uncertainty with future projections. On the other hand, ensuring that a structure can accommodate an increase in discharge of 15% without significant damage is good engineering. The nature of flood damage is such that a flood 15 to 25% larger than design would cause incremental damage in the form of requiring maintenance to protection works, but quite likely the structure would not fail.

Our recommendation is that MoTI include a mandatory requirement for sensitivity checks at 5 and 15% greater than the design discharge for all structure designs. It should be noted that this does come with a cost as most engineers will round results upwards in light of a potential weakness in the design, for example, to the next size of riprap should velocities become too large as a result of the sensitivity check.

Studies done on bridge failures in the USA have shown that more than 50% of all failures are related to poor hydraulic design. This report has focused on streamflow but there are many other processes that can threaten BC's bridge and culvert infrastructure. The 100-year or 200-year stream flow is a relatively straight-forward and economical parameter to estimate using 'existing' data, as long as those making the predictions have a background in hydrology and are qualified to undertake such analysis. Detailed analyses to predict future streamflow (due to things like climate change) and other types of design events including those with extraordinary inputs of debris and sediment are much less straight-forward and perhaps uneconomical on a case by case basis. In planning for the future MOTI may need to focus on the following hydrotechnical issues:

- Use of clear spans over channels wherever possible, keeping piers (if they are necessary) on the periphery of channels;
- Larger culvert spans that match channel widths so that the structure has the highest possible capacity to transport debris and sediment; In NHC's opinion, use of the TAC supplement to size culverts on natural streams is inappropriate. The TAC supplement should only be used to size cross-drain culverts that carry runoff from the highway pavement.
- More focus on designing stable erosion control (like riprap) and better construction quality for things like riprap to help ensure that structures are better protected from lateral erosion when sediment and debris does build up; and acceptance of the fact that occasionally a major cleanout of the creek or river may be necessary in order to re-establish flow capacity. (some kind of agreement between MoT, MoE and DFO to ease the legislation around HADDs due to riprap construction and channel maintenance at bridges would go a long way to reducing the level of risk.)
- Coupling flow estimates with natural channel geometry to determine appropriate bridge and culvert opening widths;
- Installing debris control where it is practical to do so;
- Aligning new roadways to avoid the hazards associated with alluvial fans (a big issue in BC); this may mean more expenditure up front to avoid huge maintenance costs in future years.

5.3 RECOMMENDATIONS FOR FUTURE STUDIES

- An investigation into how the dominant processes generating annual peak flows in different areas of the Province (e.g. spring snowmelt, spring/ summer rainfall, fall/ winter rainfall, rain-on-snow etc.) may change in the future , with the historic climate simulation as a baseline reference.

- Investigate enhanced ways to characterize the effects of climate change on bridges and culverts rather than using precipitation and stream discharge. For example the use of changing water levels, channel widths or velocities would provide a better way of measuring the effects of climate change on structures.
- An observation from the recent MoT Yellowhead Climate Adaptation project was that we are anticipating a shift from freshet dominated flooding to a hybrid of precipitation and freshet flooding in some areas of the Province. Thus there is a need to study changes to the dominant processes generating annual peak flows in the future climate simulations, with the historic climate simulation as a baseline reference.
- The recommendations from this report suggest allocating part of the bridge or culvert freeboard allowance as a buffer for gradually increasing flows related to climate change. Freeboard has traditionally been used to accommodate the following: (i) uncertainty in predicting flows and water levels; (ii) ice and debris passage, and (iii) aggradation. As a suggestion, consider formally redefining the concept of 'clearance' at culverts and bridges, breaking it into components like: i) ice, debris passage, ii) aggradation allowance; iii) model sensitivity allowance (to account for potential errors in channel roughness, model boundary conditions, hydrological flow predictions, etc.) and iv) climate change allowance (to account for potential increases in flow).
- Up to date, comprehensive climate data is critical for hydrotechnical design yet these programs are constantly under scrutiny related to budget cuts. Water Survey of Canada hydrometric gauging stations and climate data from Environment Canada and other agencies provide the key inputs to bridge, culvert and roadway drainage design and their preservation should be supported wherever possible. An example of good use of this information is the MTO Intensity Duration Frequency (IDF) web tool; it uses the most current climate data which then automatically reflects changing climate patterns (if any) in a timely fashion.
- A simple graphical method for quantifying the effects of climate change on peak flows throughout the province. This could take the form of a map of the province with coefficients for adjusting peak flows. Such a map could be developed from simulations of projected climate data in well calibrated hydrologic models, unlike the Fisher Creek model used in this study, which is not well calibrated. A sensible starting point for such work would entail the screening of suitable watersheds in BC for the purposes of developing robust hydrologic models; particular attention would be paid to the availability of:

- ✓ gauged watersheds with long term records, making use of nested gauges;
- ✓ watersheds with nearby climate stations (both at higher and lower elevations in the watersheds to account for variable precipitation gradients and temperature lapse rates);
- ✓ watersheds with nearby snow course surveys or snow pillow data; and
- ✓ watersheds representing various flood-generating processes: (i) spring snowmelt; (ii) spring and summer rainfall; (iii) fall and winter rainfall and rain-on-snow; and (iv) hybrids or mixtures of the first three; and,
- ✓ watersheds that contain MOTI bridges and/ or culverts

6 REFERENCES

- Alila, Y., Kuras, P. K., Schnorbus, M., and Hudson, R. (2009). Forests and floods: A new paradigm sheds light on age-old controversies. *Water Resources Research*, 45(W08416), 24. doi:10.1029/2008WR007207.
- APEGBC (2012). Professional Practice Guidelines - Legislated Flood Assessments in a Changing Climate in BC (V1.1). 139 pp.
- Ball, J. (2010). High flow event – September 23 – September 30, 2010, Bella Coola Valley. Report prepared on behalf of the BC Ministry of Natural Resource Operations.
- BC MOTI, Nodelcorp, Government of Canada and PCIC. (2013). Climate Change Engineering Vulnerability Assessment of Three British Columbia Highway Segments (Rev 1).
- BC MOTI. (2011). Alaska-Stewart Highway flooding near Stewart, BC. Photo collage and description of the September 2011 event obtained via the internet at:
<http://www.flickr.com/photos/tranbc/sets/72157627493160347/>
- BC MOTI. 2007. BC Supplement to TAC Geometric Design Guide (2007 Ed.).
- BC MOTI. 1999. Highway Engineering Design Manual (S.1030 Hydraulics and Structures).
- Benson, M. (1968). Uniform flood-frequency estimating methods for federal agencies. *Water Resources Research*, 4(5), 891–908.
- Coles S. (2001) An introduction to statistical modeling of extreme values. Springer-Verlag, London, UK. 208 pp. WA273.6.C63 2001.
- Coulson, C.H. (editor) (1991). Manual of Operational Hydrology in British Columbia (2nd Edition). Ministry of Environment, Water Management Section, Hydrology Section.
- Eaton, B., M. Church, and D. Ham (2002), Scaling and regionalization of flood flows in British Columbia, Canada, *Hydrological Processes*, 16, 3245–3263.
- Golder Associates. 2012. Disaster Financial Assistance Arrangement (DFAA) Engineer Report for DFAA 1011-04 September 2010 Flood Event: Site 12 Hagensborg. Report prepared for MOTI.
- Hawkins, E., and Sutton, R. (2010) The potential to narrow uncertainty in projections of regional precipitation change. *Climate Dynamics* 37, 407–418. doi:10.1007/s00382-010-0810-6.
- Kundewicz, A.W., Kanae, S., Seneviratne, S.I., Handmer, J., Nicholls, N., Peduzzi, P., Mechler, R., Bouwer, L.M., Arnell, N., Mach, K., Muir-Wood, R., Brakenridge, G. R., Kron, W., Benito, G., Honda, Y., Takahashi, K., and Sherstyukov, B. (2013) Flood risk and climate change: global and

regional perspectives. *Hydrological Sciences Journal - Journal des Sciences Hydrologiques* 59(1): 1-28. DOI: 10.1080/02626667.2013.857411.

Kuras, P. K., Alila, Y., and Weiler, M. (2012). Forest harvesting effects on the magnitude and frequency of peak flows can increase with return period. *Water Resources Research*, 48(W01544), 19. doi:10.1029/2011WR010705.

Murdock, T. Q., Cannon, A. J., and Sobie, S. R. (2013) Downscaling extremes – a new set of climate change projections for Canada. Poster presented at the Fall Meeting of the American Geophysical Union, 12 December 2013, San Francisco, California.

NHC (2013). 2011 flood in the South Peace, Recovery Phase, Assessment of flood hydrology and sediment transport capacity for Highway 97 Tributaries to Pine River. BC Ministry of Transportation and Infrastructure, Engineering Branch, Victoria, BC. 34 pp.

NHC (2012). Highway 37 Bitter Creek Bridge; Hydraulic assessment and design parameters for bridge replacement. Report prepared for MMM Group Ltd., Vancouver, BC.

Obedkoff, W. (2000). Streamflow in the Omineca-Peace Region. British Columbia Ministry of Environment, Lands & Parks. 5 pp.

Obedkoff, W. (2003). Streamflow in the Lower Mainland and Vancouver Island, Aquatic Information Branch, Ministry of Sustainable Resource Management, Province of British Columbia. 186 pp.

Pike, R. G., Redding, T. E., Moore, R. D., Winkler, R. D., and Bladon, K. D. (2010). Compendium of forest hydrology and geomorphology in British Columbia, B.C. Ministry of Forests and Range, Forest Sciences Program, Victoria, B.C. and FORREX Forum for Research and Extension in Natural Resources, Kamloops, B.C. Land Management Handbook, 66. [online] Available from: www.for.gov.bc.ca/hfd/pubs/Docs/Lmh/Lmh66.htm.

Sillmann, J., Kharin, V. V., Zhang, X., Zwiers, F. W., and Bronaugh, D. (2013) Climate extremes indices in the CMIP5 multimodel ensemble: Part 1. Model evaluation in the present climate. *Journal of Geophysical Research Atmospheres* 118, 1716-1733, doi: 10.1002/jgrd.50203.

Transportation Association of Canada (TAC) (2004). *Guide to Bridge Hydraulics* (2nd Edition). Thomas Telford, London.

Thyer, M., Beckers, J., Spittlehouse, D., Alila, Y., and Winkler, R. (2004). Diagnosing a distributed hydrologic model for two high-elevation forested catchments based on detailed stand- and basin-scale data. *Water Resources Research*, 40, pp. 20. doi:10.1029/2003WR002414.

U.S. Army Corps of Engineers (USACE) (2010). *Hydrologic Modeling System HEC-HMS: User's Manual, Version 3.5*. [online] Available from: http://www.hec.usace.army.mil/software/hec-hms/documentation/HEC-HMS_Users_Manual_3.5.pdf.

United States Bureau of Reclamation (USBR) (1987). Design of Small Dams, A Water Resources Technical Publication, United States Department of the Interior. 3rd ed. U. S. Government Printing Office, Washington, D.C.

USACE (1994). Engineering and Design, Hydrologic Frequency Estimates (Regulation No. 1110-2-1450). U.S. Army Corps of Engineers, Washington, D.C. 7 pp.

USDA-SCS (1972). National Engineering Handbook. United States Department of Agriculture, Soil Conservation Service, Washington, D.C.

APPENDIX A

**DEVELOPMENT OF FUTURE CLIMATE SCENARIOS FOR FISHER CREEK'S HYDROLOGIC MODEL
(DETAILED WRITE-UP)**

**Engineering Analysis Report
Climate Change Engineering
Vulnerability Assessment of Three
British Columbia Highway Segments**

Final Report

Appendix A

BC Ministry of Transportation and Infrastructure
Engineering Branch
Victoria, BC

ATTN: Jim Barnes, Project Manager

March 28, 2014
300204

Table of Contents

1	Description of Methodology and Summary of the Climate Scenarios Constructed	6
2	Quantile-to-Quantile Relations Derived from the GCM Runs.....	13
2.1	ACCESS1-0 run1 for RCP8.5	13
2.2	CanESM2 run1 for RCP8.5	20
2.3	CNRM-CM5 run1 for RCP8.5.....	26
3	References	34

List of Tables

Table 1.	Parameter estimates for the generalized Pareto distribution (GPD) using the POT method and maximum likelihood, for the precipitation simulations from ACCESS1-0.....	14
Table 2.	Parameter estimates for the generalized Pareto distribution (GPD) using the POT method and maximum likelihood, for the precipitation simulations from CanESM2.....	20
Table 3.	Parameter estimates for the generalized Pareto distribution (GPD) using the POT method and maximum likelihood, for the precipitation simulations from CNRM-CM5.....	27

List of Figures

Figure 1.	Mean temperature and annual precipitation for the observed record (black dot) and for the three GCM hindcasts (marked “historical”) and projections for the mid-century and late-century periods.....	8
Figure 2.	Observed and GCM-simulated mean number of wet days per year and mean precipitation intensity on wet days for Highway 97 east of Pine Pass; the area of the rectangles shown gives the mean annual precipitation.....	9
Figure 3.	Summary of our procedure for creating future climate scenarios.....	10
Figure 4.	Mean temperature and annual precipitation for the observed record (black dot) and for the climate scenarios we created. Compare with Figure 1.....	11
Figure 5.	Our scenarios mean number of wet days per year, and mean precipitation intensity on wet days. Compare with Figure 2.	12
Figure 6.	Quantile to quantile plots relating daily downscaled ACCESS1-0-simulated precipitation for period 1 (x axis) to that for the mid-century period (y axis of the top panel) and the late-century period (y axis of the bottom panel).....	15
Figure 7.	Tenth, 50 th , and 90 th percentiles of precipitation accumulation for different aggregation periods, for our climate scenarios based on ACCESS1-0.	16
Figure 8.	Relationship between 50 th percentiles and 90 th percentiles of precipitation for different time horizons and for different aggregation periods (ranging from 1-day to 30-days), for our climate scenario based on ACCESS1-0.	17
Figure 9.	Quantile to quantile plots relating daily downscaled ACCESS0-1-simulated temperature for period 1 (x axis) to that for the mid-century period (y axis of the	

<p>top panel) and the late-century period (y axis of the bottom panel). The points align themselves along a polygonal line, and the equation for each segment is displayed.</p>	19
<p>Figure 10. Quantile to quantile plots relating daily downscaled CanESM2-simulated precipitation for period 1 (x axis) to that for the mid-century period (y axis of the top panel) and the late-century period (y axis of the bottom panel).</p>	21
<p>Figure 11. Tenth, 50th, and 90th percentiles of precipitation accumulation for different aggregation periods, for our climate scenarios based on CanESM2.....</p>	22
<p>Figure 12. Relationship between 50th percentiles and 90th percentiles of precipitation for different time horizons and for different aggregation periods (ranging from 1-day to 30-days), for our climate scenario based on CanESM2.....</p>	23
<p>Figure 13. Quantile to quantile plots relating daily downscaled CanESM2-simulated temperature for period 1 (x axis) to that for the mid-century period (y axis of the top panel) and the late-century period (y axis of the bottom panel). The points align themselves along a polygonal line, and the equation for each segment is displayed.</p>	25
<p>Figure 14. Quantile to quantile plots relating daily downscaled CNRM-CM5-simulated precipitation for period 1 (x axis) to that of a future period (y axis). The first two panels are alternative scenarios for the mid-century period: the first included all mid-century data points in fitting the extreme value distribution, the second having eliminated the highest GCM-simulated point (59, 131) before fitting the extreme value distribution.</p>	28
<p>Figure 15. Tenth, 50th, and 90th percentiles of precipitation accumulation for different aggregation periods, for our climate scenarios based on CNRM-CM5.</p>	30
<p>Figure 16. Relationship between 50th percentiles and 90th percentiles of precipitation for different time horizons and for different aggregation periods (ranging from 1-day to 30-days), for our climate scenario based on CNRM-CM5.....</p>	31
<p>Figure 17. Quantile to quantile plots relating daily downscaled CNRM-CM5-simulated temperature for period 1 (x axis) to that for the mid-century period (y axis of the top panel) and the late-century period (y axis of the bottom panel). The points align themselves along a polygonal line, and the equation for each segment is displayed.</p>	33

Appendix A: Development of Future Climate Scenarios for Fisher Creek's Hydrologic Model

In this appendix we present details on the methodology used for creation of the climate scenarios used for forcing the hydrologic model. In section 1 we describe the methodology and summarize the mean annual values that characterize the climate scenarios we created are summarized. In section 2, the quantile mapping technique is detailed and our development of specific quantile relations is presented.

1 DESCRIPTION OF METHODOLOGY AND SUMMARY OF THE CLIMATE SCENARIOS CONSTRUCTED

Figure 1 shows the mean temperature and annual precipitation for the observed record at Chetwynd meteorological station (black dot), and for the three GCM hindcasts (marked “historical”) and projections for the mid-century and late-century periods. The GCM results plotted are for the grid cell inside which the Chetwynd meteorological station is located. These GCM simulations had already been downscaled by PCIC and bias corrected.

The agreement between the three GCMs for the simulated historical period (all three lines meet at about the same point for period 1951-2000) is the result of their statistical downscaling by the BCSO technique (the last step in their downscaling) which, by construct, forces their agreement with the historical climatological values in the ANUSPLIN dataset (see Murdock et al., 2013). It appears likely that the ANUSPLIN values for this grid cell differs from the Chetwynd station observations and that would be the explanation for the difference in Figure 1 between the annual means at the station and those of the GCMs for 2051-2000. We don’t know whether Chetwynd A or Chetwynd BCFC were included in the observational dataset that served as a basis for ANUSPLIN.

For the future periods, the three GCM projections differ considerably, but in all three cases most of the precipitation changes are projected to occur by mid-century. Only CNRM-CM5 projects further increases in mean annual precipitation after mid-century, explained by an increase in the mean number of wet days per year (Figure 2). CanESM2 is the warmest and wettest of the three. ACCESS1-0 is almost as warm but is the least wet of the three. The projected rise in mean annual precipitation is the balance result of the projected changes in: a) mean precipitation intensity on wet days, and b) mean number of wet days per year. All three GCM runs project rises in mean precipitation intensity on wet days, and two of them project increases in the mean number of wet days per year (Figure 2). The ACCESS1-0 run projects a small decline in wet day occurrence.

In section 2.2 of the main report we reviewed the type of differences that can be expected between GCM simulations (for the area of a grid cell) versus meteorological station observations (which are essentially point values). These differences include lower mean and extreme intensity of daily precipitation, a larger number of wet days, and shorter mean duration of dry periods. These effects are seen in Figure 2. The area of the rectangles drawn on the figure gives the mean annual precipitation. In this case, the simulated historical mean annual precipitation is higher than the station observations because the lower mean precipitation intensity and the larger number of wet days of the grid cell (compared to the point station) do not balance each-other out (refer to the discussion in Section 2.2 in the main report).

GCM historical values and station values show many important differences, some of which are specific to their nature as area or point values, others which reflect limitations of the GCM formulation and spatial resolution, and still others which reflect limitations of the downscaling technique. Reliable simulation of precipitation processes remains perhaps the greatest challenge for GCMs.

The Fisher Creek Hydrologic Model had been partially calibrated against snow accumulation observations, using the same observational record from Chetwynd meteorological station, hence it was important to use the observational record as our base case. For this reason, and because of the differences reviewed above between the station observations and the GCM-simulated historical

climate, we constructed our climate scenarios by modifying the station's climate record according to the future changes in precipitation and temperature projected by the GCMs. Thus, the GCM-projected changes rather than the absolute values of their simulated variables, formed the basis for our climate scenarios that we used to run the Fisher Creek hydrologic model.

The diagram in Figure 3 summarizes our procedure for creating future climate scenarios. For each climate scenario, the observed precipitation record was modified so that its mean annual number of wet days increased or decreased by the same percentage as simulated by the GCM run (see description of steps in the figure). The resulting daily record was then subjected to daily quantile-to-quantile mapping so as to modify the daily values of precipitation intensity in the same manner as seen in the GCM simulations, i.e., when comparing future projections to the GCM's historical simulations. Daily quantile mapping was also used to modify the daily mean temperature, to reflect the future changes projected by the GCM simulations.

The resulting scenarios can be compared directly with the historical period, and so can the hydrologic simulations that use those scenarios. The basic characteristics of our climate scenarios are shown in Figures 4 and 5, which can be compared with Figures 1 and 2. The relative position of the three lines in Figure 5 differs somewhat from those in Figure 2. This is explained as follows. In the procedures numbered A.3a and A.3b in Figure 3, we randomly pick wet events from which to remove the last wet day (A.3a) or to which to add a wet day (A.3b). The random element of this procedure can alter, to a limited degree, the overall average precipitation intensity. ACCESS1-0 projects a decline in the average number of wet days in a year, while CanESM2 and CNRM-CM5 both project an increase in that variable. For the scenario based on ACCESS1-0, randomly selected wet events (an event is a sequence of wet days) had their last day replaced with a dry day. If by chance most wet days removed had below-average precipitation intensities, then the overall mean precipitation intensity of the scenario is artificially raised. This effect is likely to be of little or no consequence to the present study, where the focus is on flooding, hence on high-intensity precipitation or prolonged sequences of wet conditions.

Figure 1. Mean temperature and annual precipitation for the observed record (black dot) and for the three GCM hindcasts (marked “historical”) and projections for the mid-century and late-century periods.

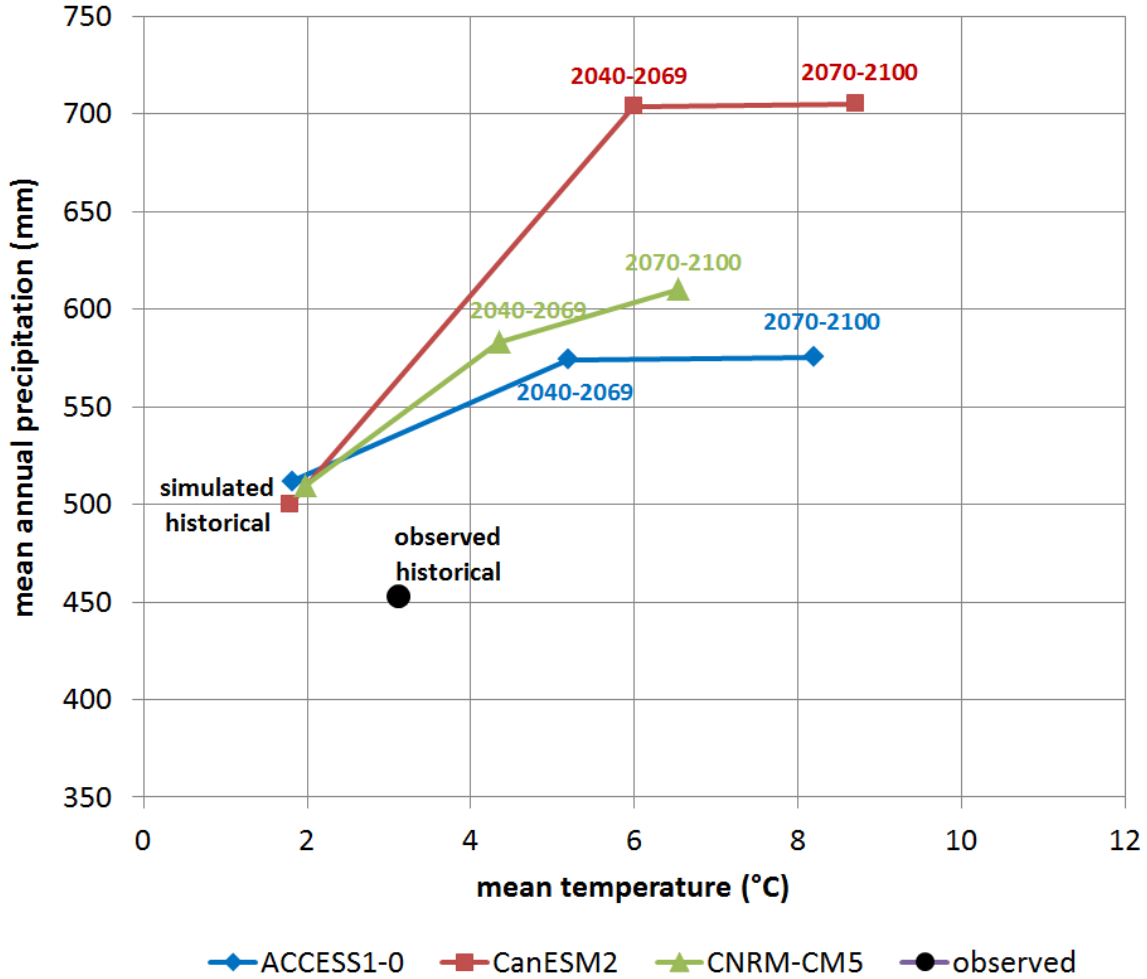


Figure 2. Observed and GCM-simulated mean number of wet days per year and mean precipitation intensity on wet days for Highway 97 east of Pine Pass; the area of the rectangles shown gives the mean annual precipitation.

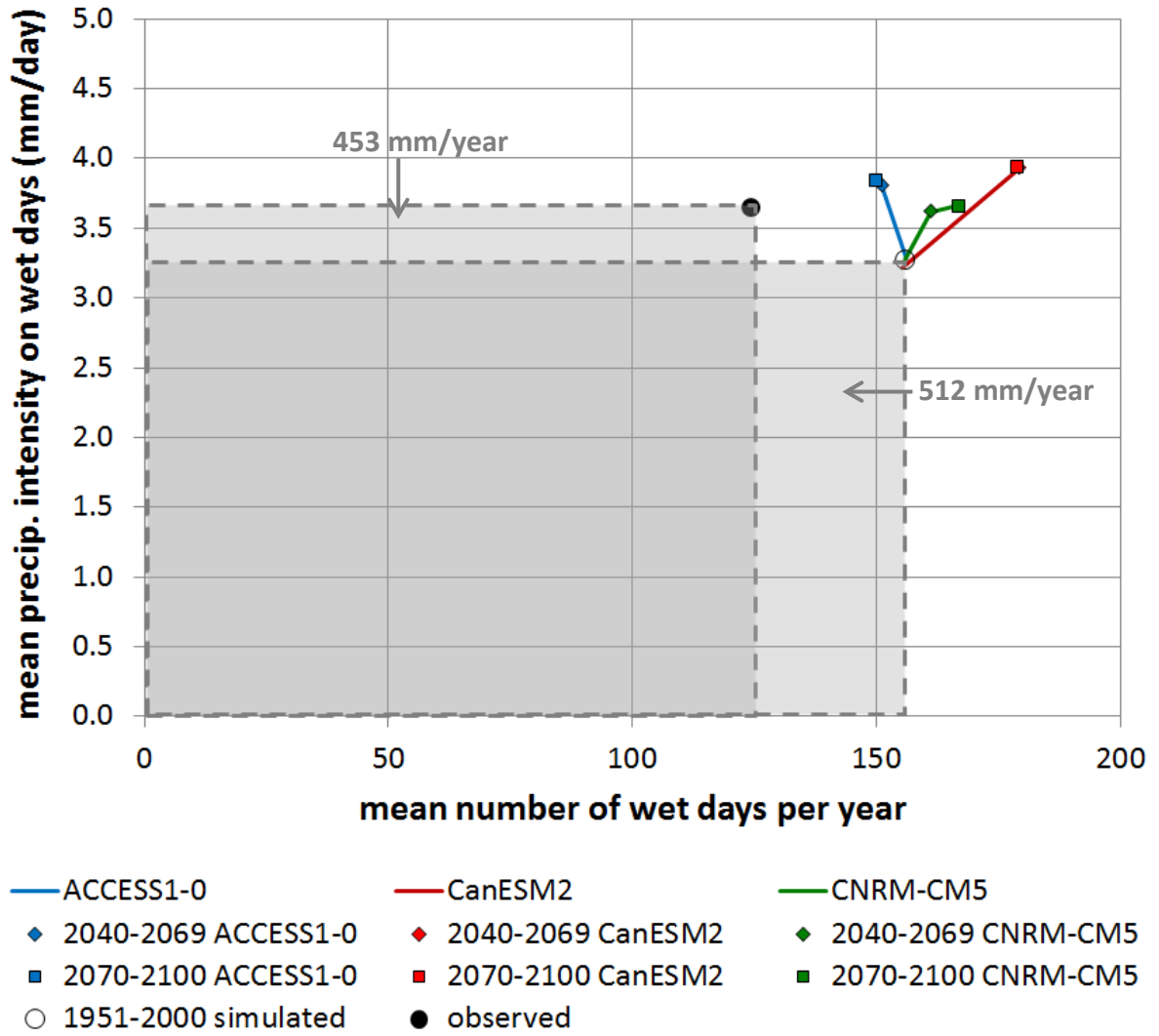


Figure 3. Summary of our procedure for creating future climate scenarios.

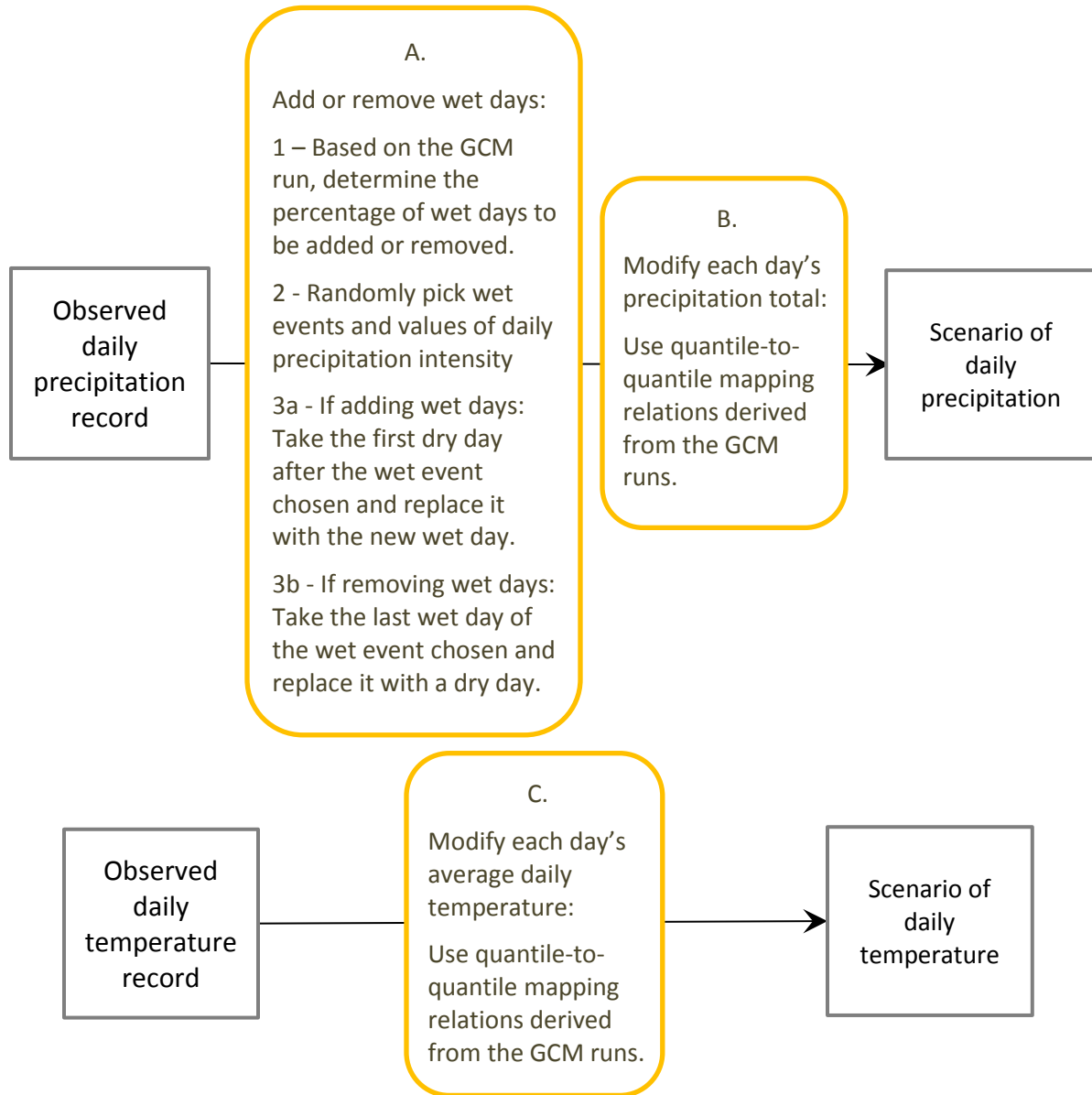


Figure 4. Mean temperature and annual precipitation for the observed record (black dot) and for the climate scenarios we created. Compare with Figure 1.

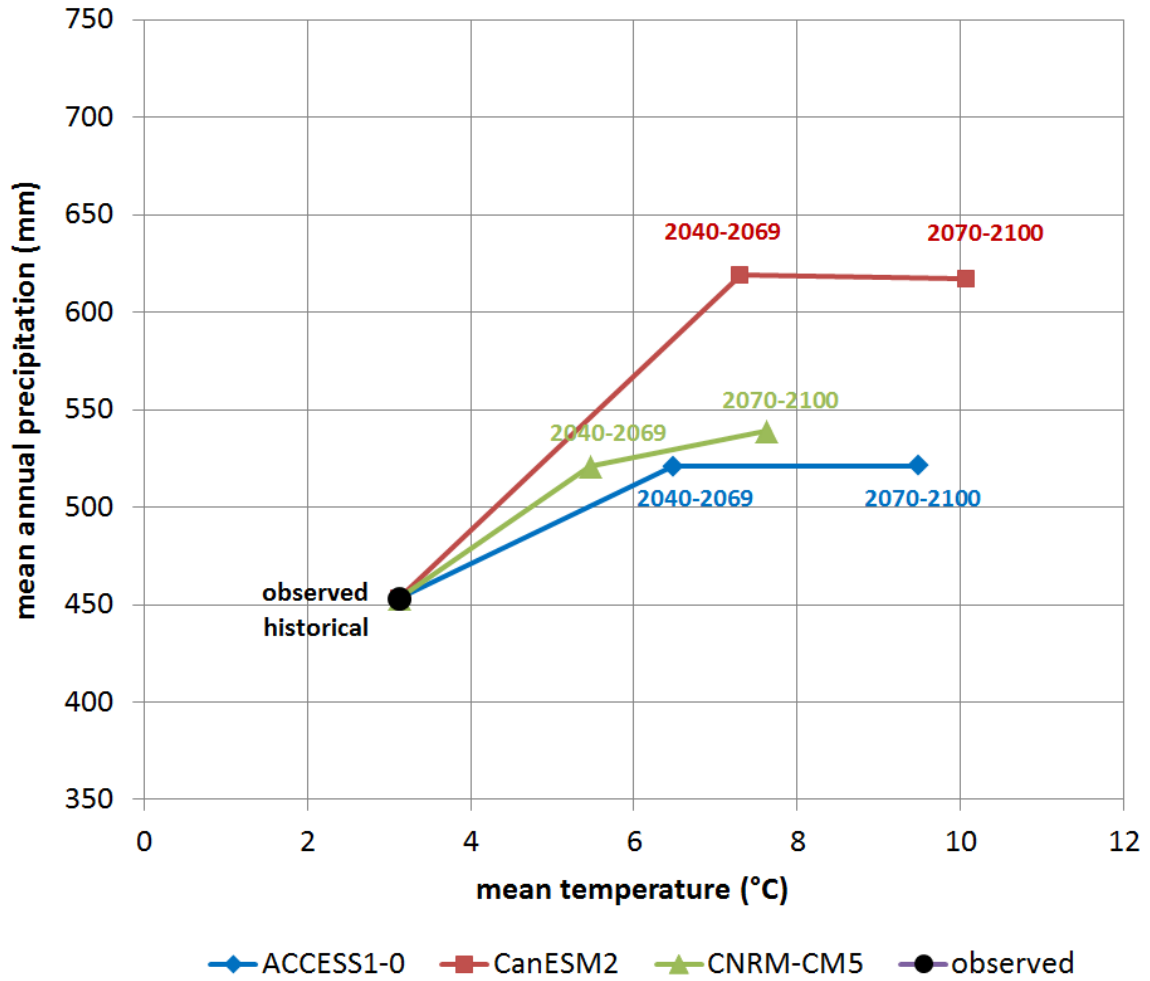
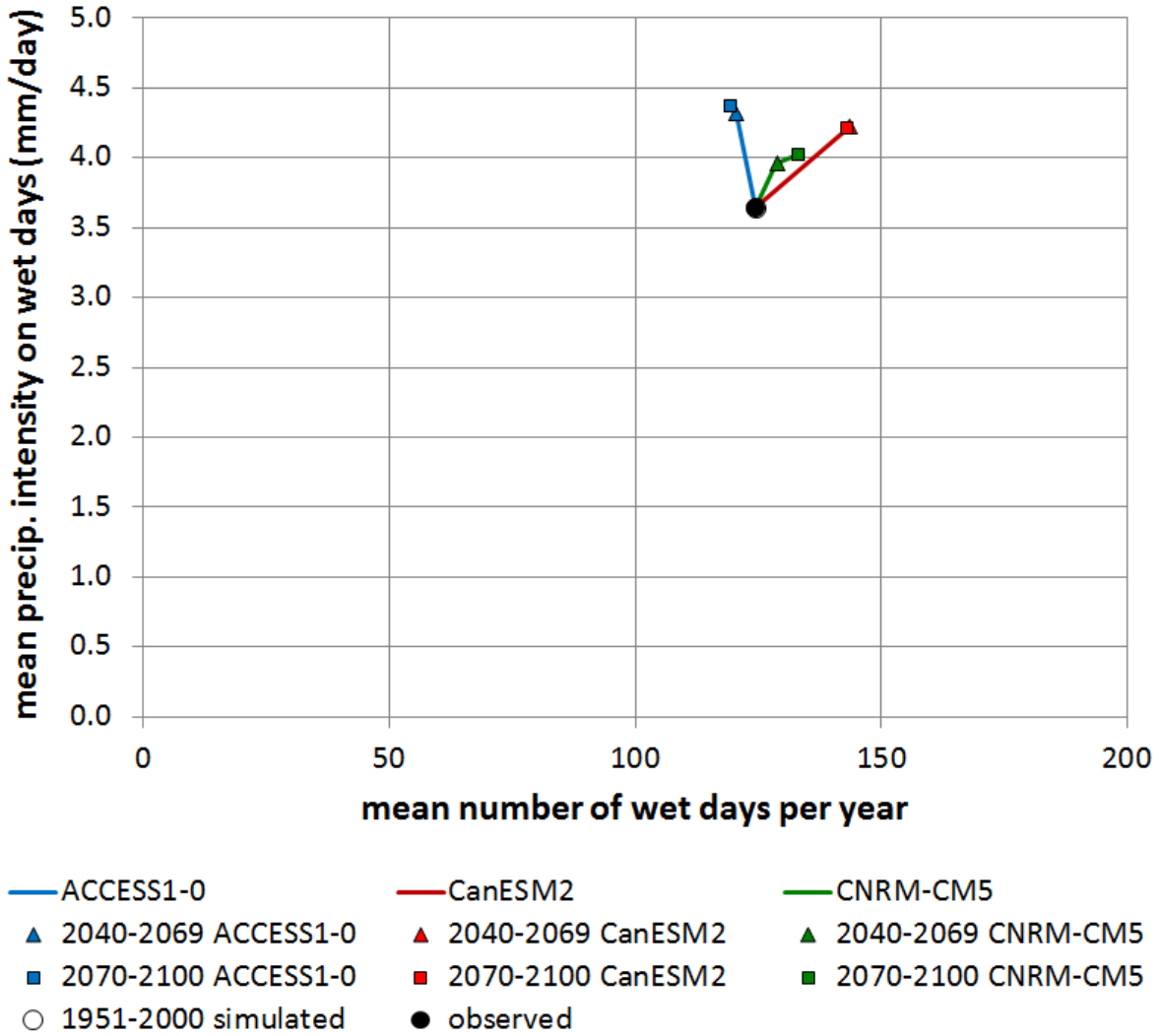


Figure 5. Our scenarios mean number of wet days per year, and mean precipitation intensity on wet days. Compare with Figure 2.



2 QUANTILE-TO-QUANTILE RELATIONS DERIVED FROM THE GCM RUNS

In this section we review the development of the quantile-to-quantile relations for daily precipitation intensity and daily average temperature that serve as basis for the construction of each climate scenario, as described in section 1.

Extreme events are rare by definition, hence are under-sampled with only 30 or 50 years of data. It is common practice in hydrology is to fit a generalized extreme value distribution (GEV) to the series of annual maxima, yielding estimates $\hat{\sigma}$ and $\hat{\xi}$ of the GEV parameters σ and ξ . This then allows an approximate analytical expression for the upper tail of the non-exceedance probability distribution. It has been shown (see Coles, 2001) that when a distribution's tail follows a GEV distribution, i.e., $(x|x > u)x \sim GEV$, then the amount by which x exceeds a high threshold u follows a Generalized Pareto distribution (GPD). The parameters of the GPD are the same as the GEV, σ and ξ . Scaling the exceedances values, we write, $\frac{x-u}{\sigma} \sim GPD$. This "peaks over threshold" (POT) method is increasingly adopted in hydrology, for it makes use of all events larger than a given threshold instead of being limited to the largest event in each year in the sample. By effectively using a larger data sample, the method reduces the uncertainty in the estimates $\hat{\sigma}$ and $\hat{\xi}$.

We follow the procedure outlined in Coles (2001) for selection of the threshold u and for parameter estimation using maximum likelihood (Coles, 2001, Eqn. 4.10 and following).

2.1 ACCESS1-0 RUN1 FOR RCP8.5

Our results for the ACCESS1-0 projections are reported in Table 1. For this GCM, we obtain that the most likely ξ value is $\hat{\xi} = 0$, which implies that the GPD reduces to an exponential distribution,

$$F(x) = 1 - e^{-\left(\frac{x-u}{\sigma}\right)} \quad \text{Equation 1}$$

Using indices 1, 2 and 3 to indicate the time period (see Table 1), we use eqn 1 to compare between corresponding quantiles from a future period and period 1, as follows,

$$1 - e^{-\left(\frac{x_2-u_2}{\sigma_2}\right)} = 1 - e^{-\left(\frac{x_1-u_1}{\sigma_1}\right)} \quad \text{Equation 2}$$

and

$$1 - e^{-\left(\frac{x_3-u_3}{\sigma_3}\right)} = 1 - e^{-\left(\frac{x_1-u_1}{\sigma_1}\right)} \quad \text{Equation 3}$$

Rearranging eqn 2 and 3 we can then express future quantiles as a linear function of the corresponding historical (period 1) quantiles, as follows,

$$x_2 = \frac{\sigma_2}{\sigma_1} x_1 + \left(u_2 - u_1 \frac{\sigma_2}{\sigma_1}\right) \quad \text{Equation 4}$$

and

$$x_3 = \frac{\sigma_3}{\sigma_1} x_1 + \left(u_3 - u_1 \frac{\sigma_3}{\sigma_1}\right) \quad \text{Equation 5}$$

Table 1. Parameter estimates for the generalized Pareto distribution (GPD) using the POT method and maximum likelihood, for the precipitation simulations from ACCESS1-0.

Time Period	Threshold u (mm)	Number of exceedances	$\hat{\sigma}$	$\hat{\xi}$
1. 1951-2000	18.0	112	8.31	0
2. 2040-2069	21.1	73	10.73	0
3. 2070-2100	21.8	75	7.99	0

Figure 6 compares the quantiles of daily precipitation for the future period (y axis) with their corresponding quantiles for the historical period (x axis), as simulated by ACCESS1-0. There are 999 dots in each figure panel, one for each of the 999 quantiles sampled: {0.001, 0.002, 0.003, ..., 0.999}. These are the empirical quantiles, i.e., those estimated directly by ranking the non-zero daily values simulated by the GCM and assigning to each one an estimated cumulative frequency equal to $(n - rank + 1)/(n + 1)$. This expression was chosen among many equally common possibilities, which would serve a similar function in this report.

The red line in each panel of Figure 6 indicates the quantile-to-quantile relationship for those daily precipitation values that exceed the threshold established in the POT. The red line is described by eqn 4 and 5, in which we inserted values from Table 1. The blue points, plotted using empirical rank, do not depart far from the red line. The black line in each panel of Figure 6 indicates a quantile-to-quantile relationship for precipitation values below the threshold $u_1 = 18 \text{ mm}$, and was obtained by linear regression. We used the red and black lines in Figure 6 to transform our 34-year observations-based daily precipitation record (x axis of the figure) into new, 34-year daily precipitation projection (y axis).

Compared to the base case (station observations), the future climate scenarios have different statistical distributions of precipitation, and the difference depends on which precipitation quantile is being considered. Figure 8 shows the 10th, 50th and 90th quantiles of precipitation, for different time periods of precipitation accumulation, from 1 day to 30 days. In the case of this GCM, the mid-century and late-century scenarios differ little. Figure 9 presents this information in a different way, and makes clear that the 90th percentile of precipitation is projected to rise faster than the 50th percentile (as per the multiplying constants in the regression equations on the figure panels).

Figure 6. Quantile to quantile plots relating daily downscaled ACCESS1-0-simulated precipitation for period 1 (x axis) to that for the mid-century period (y axis of the top panel) and the late-century period (y axis of the bottom panel).

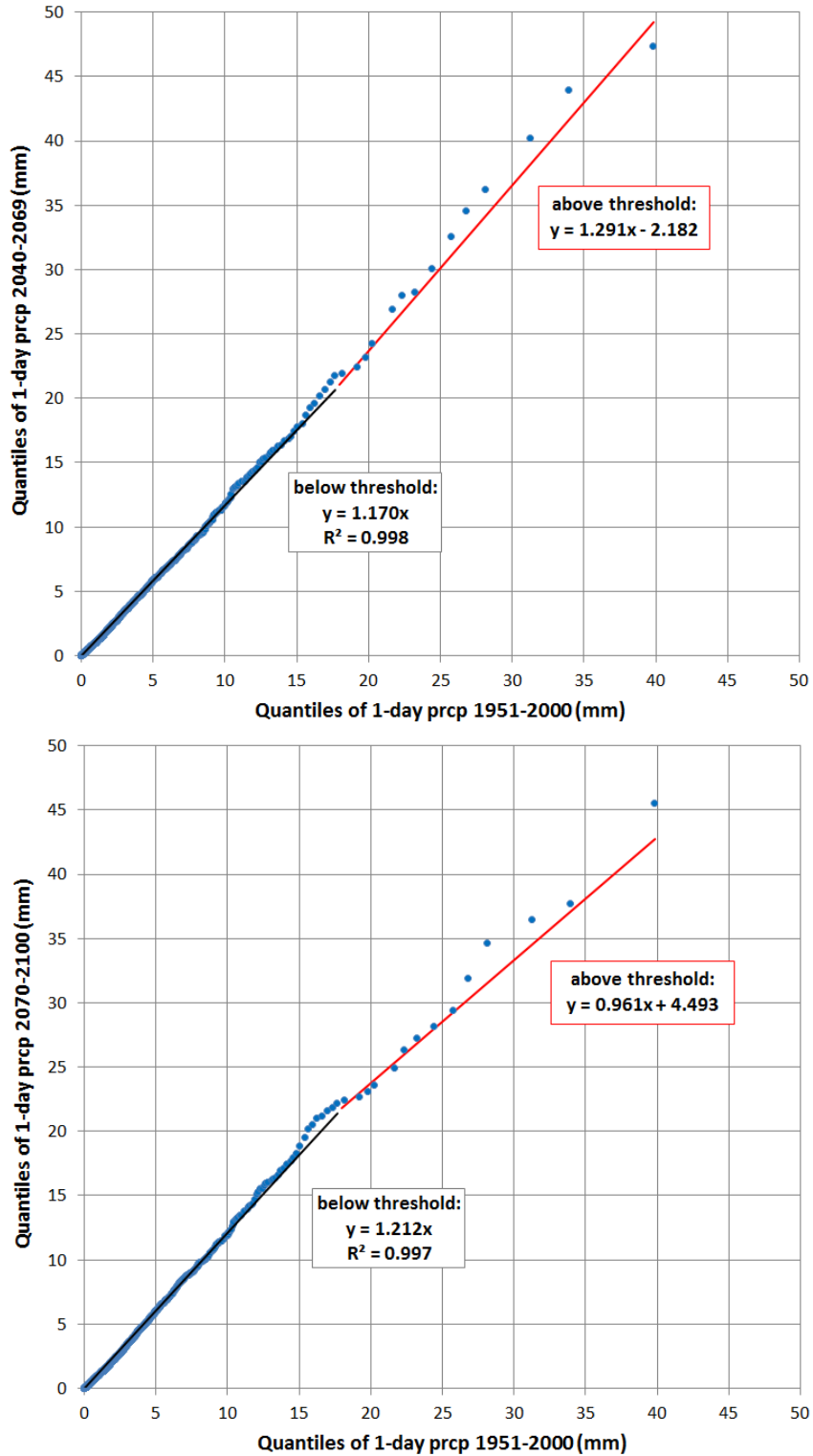


Figure 7. Tenth, 50th, and 90th percentiles of precipitation accumulation for different aggregation periods, for our climate scenarios based on ACCESS1-0.

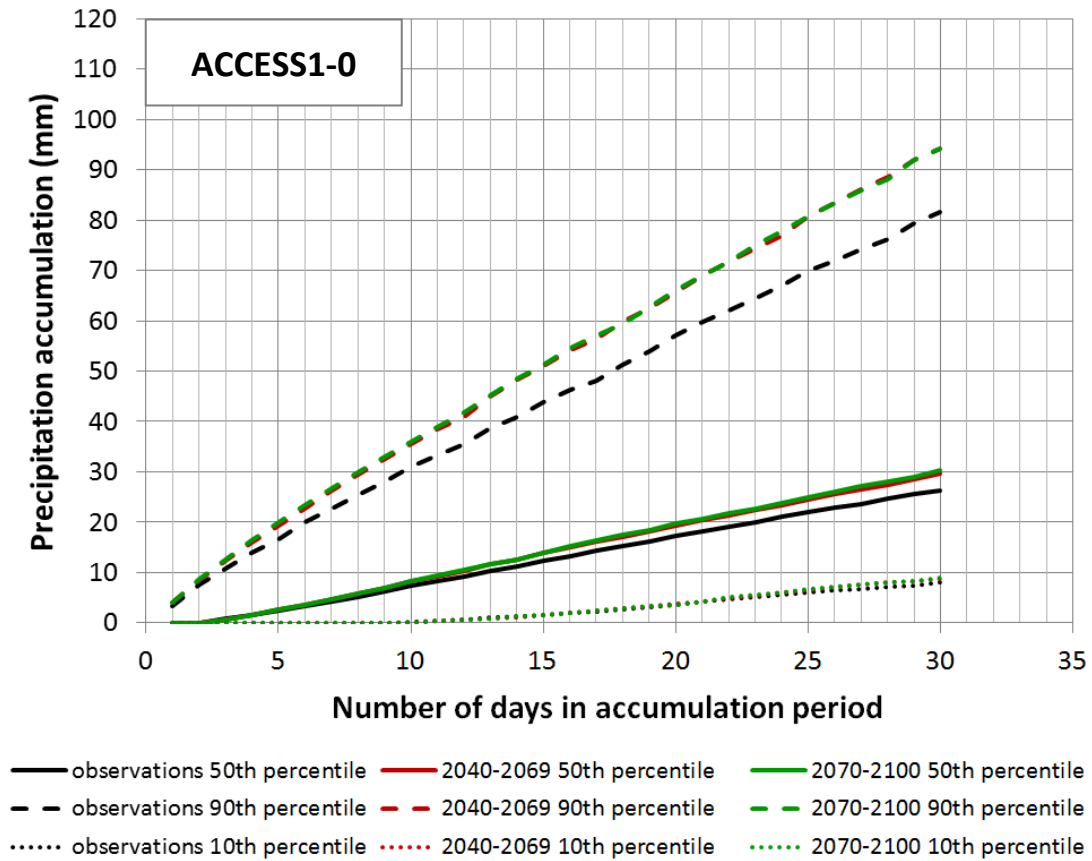
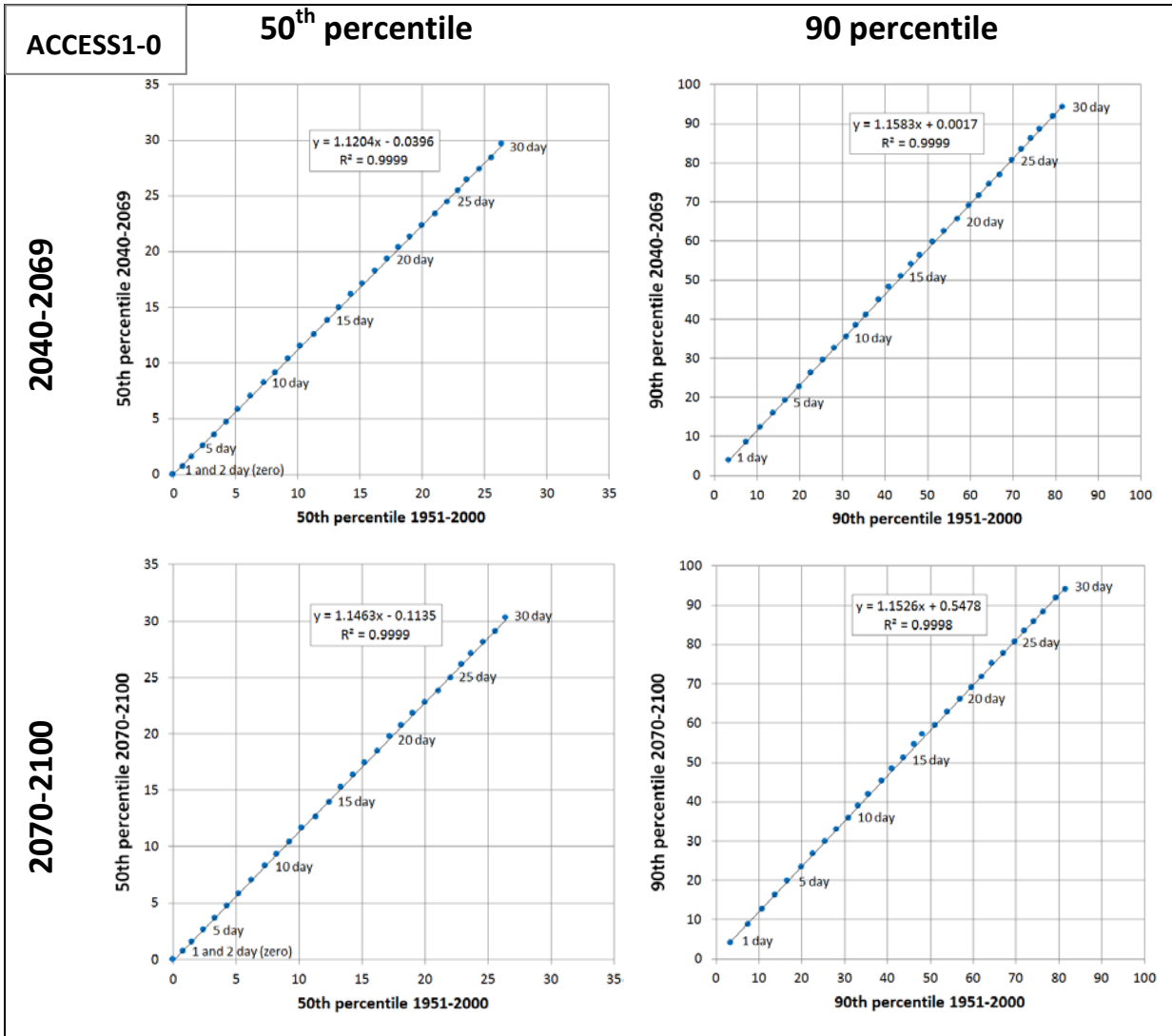


Figure 8. Relationship between 50th percentiles and 90th percentiles of precipitation for different time horizons and for different aggregation periods (ranging from 1-day to 30-days), for our climate scenario based on ACCESS1-0.

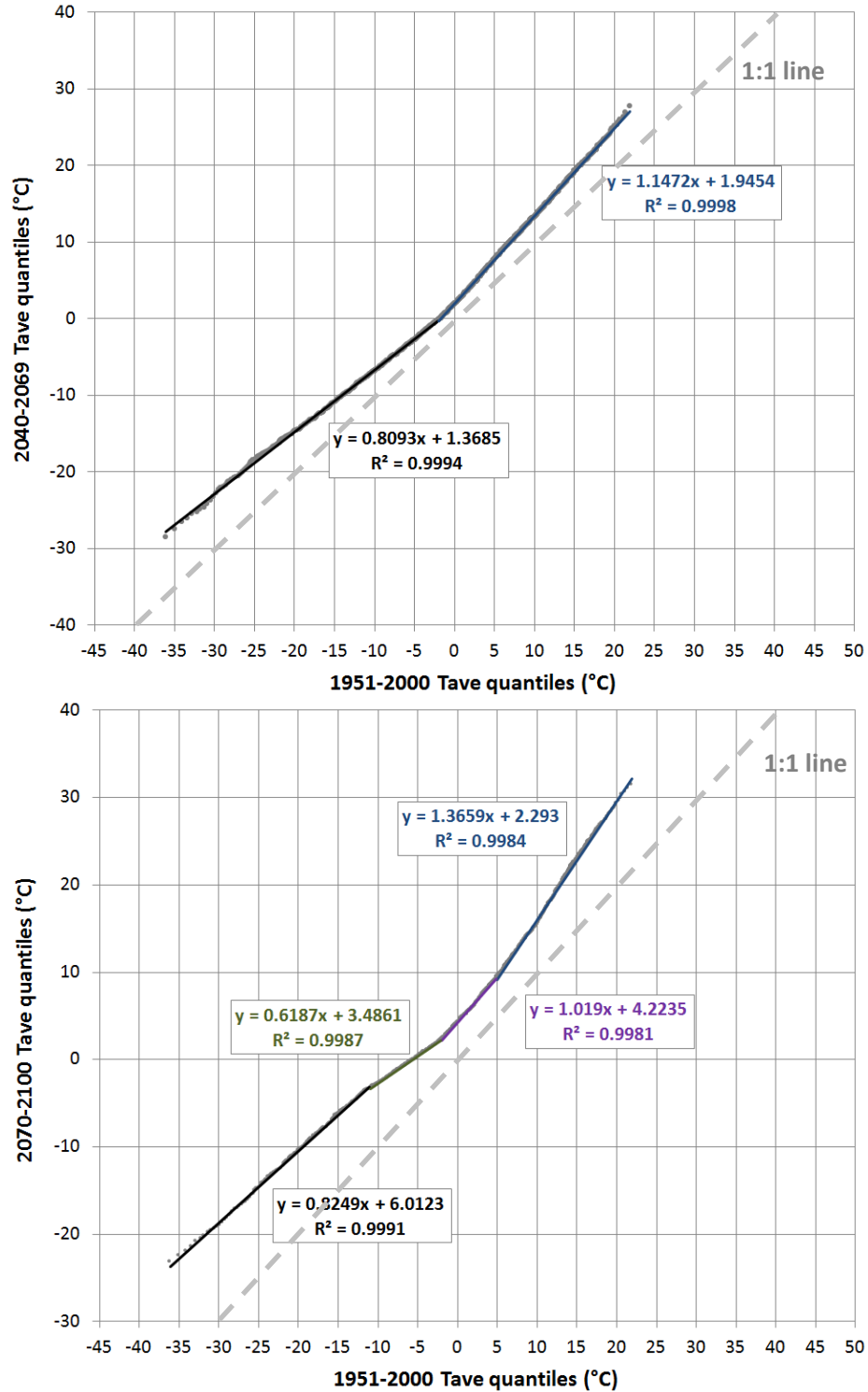


Temperature

The grey dots in Figure 9 (perhaps difficult to discern, given that they so closely align themselves along polygonal lines) indicate the quantiles of daily temperature for a future period (y axis) and their corresponding quantiles for period 1 (x axis), as simulated by the GCM. There are 999 dots in each figure panel, one for each of the 999 quantiles sampled: {0.001, 0.002, 0.003, ..., 0.999}. The empirical cumulative frequency is approximated by $(n - rank + 1)/(n + 1)$ for purposes of mapping quantiles against quantiles.

Linear regression was used to obtain the polygonal lines shown in the panels of Figure 9, where the resulting equations are displayed. These lines were used for transforming our 34-year observations-based daily temperature record (x axis) into new, 34-year daily temperature projection (y axis).

Figure 9. Quantile to quantile plots relating daily downscaled ACCESS0-1-simulated temperature for period 1 (x axis) to that for the mid-century period (y axis of the top panel) and the late-century period (y axis of the bottom panel). The points align themselves along a polygonal line, and the equation for each segment is displayed.



2.2 CANESM2 RUN1 FOR RCP8.5

Precipitation

The parameter estimates obtained by maximum likelihood are given in Table 3. Similar to ACCESS1-0, we have $\hat{\xi} = 0$ for all three time periods, and eqn 1 through eqn 5 apply. As we will see, the case of CNRM-CM5 is different because there we obtain $\hat{\xi} > 0$. The analysis for CanESM2 is similar to that for ACCESS1-0. Figures 10 through 13 are analogous to Figures 6 through 8. Contrary to the ACCESS1-0 scenario, in the CanESM2 scenario the 90th percentile of precipitation increases more slowly in the future than the 50th percentile (as per the multiplying constants in the regression equations of Figure 13).

Table 2. Parameter estimates for the generalized Pareto distribution (GPD) using the POT method and maximum likelihood, for the precipitation simulations from CanESM2.

Time Period	Threshold u (mm)	Number of exceedances	$\hat{\sigma}$	$\hat{\xi}$
1. 1951-2000	18.0	102	8.67	0
2. 2040-2069	22.0	91	8.94	0
3. 2070-2100	22.2	79	7.06	0

Figure 10. Quantile to quantile plots relating daily downscaled CanESM2-simulated precipitation for period 1 (x axis) to that for the mid-century period (y axis of the top panel) and the late-century period (y axis of the bottom panel).

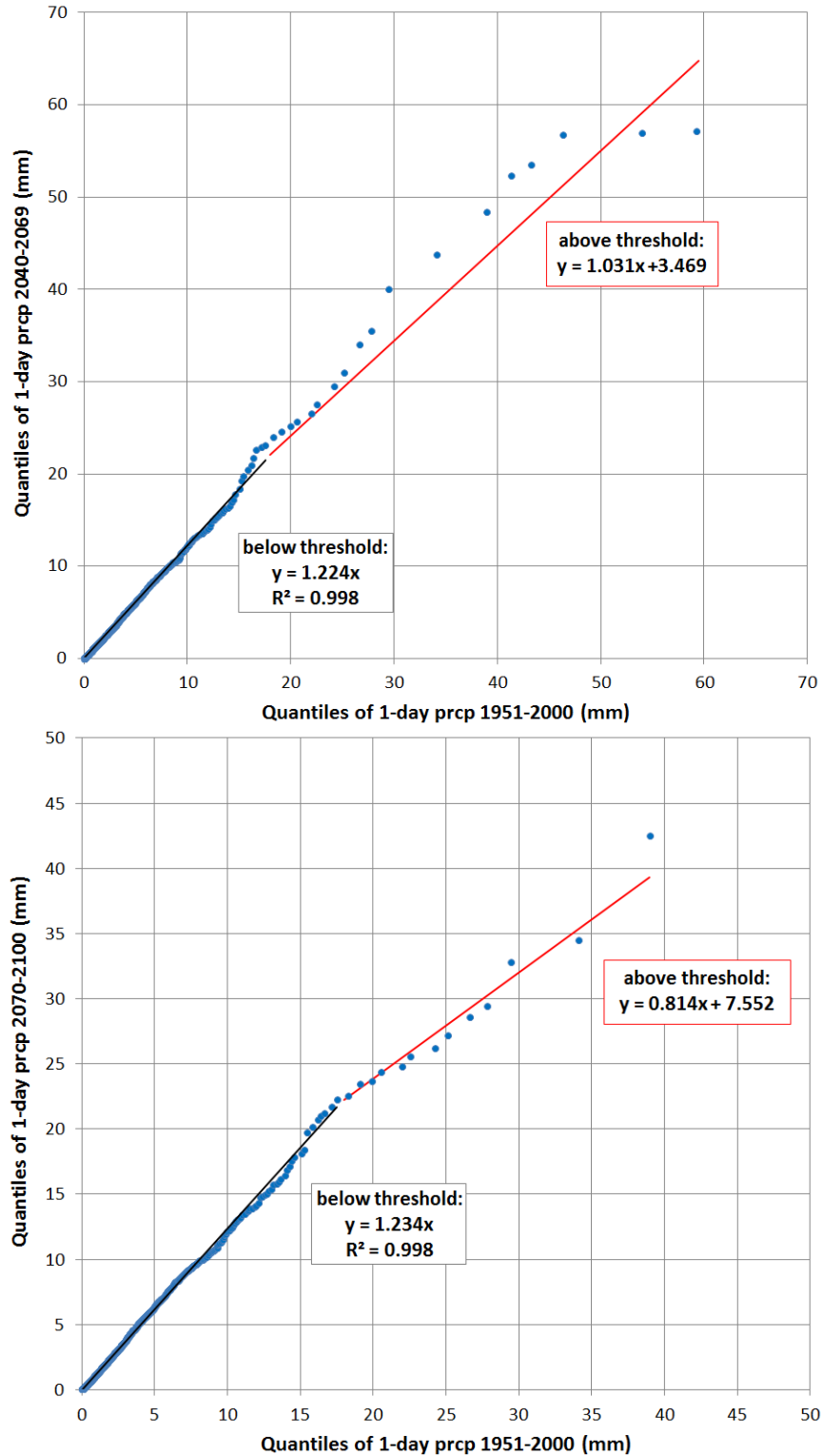


Figure 11. Tenth, 50th, and 90th percentiles of precipitation accumulation for different aggregation periods, for our climate scenarios based on CanESM2.

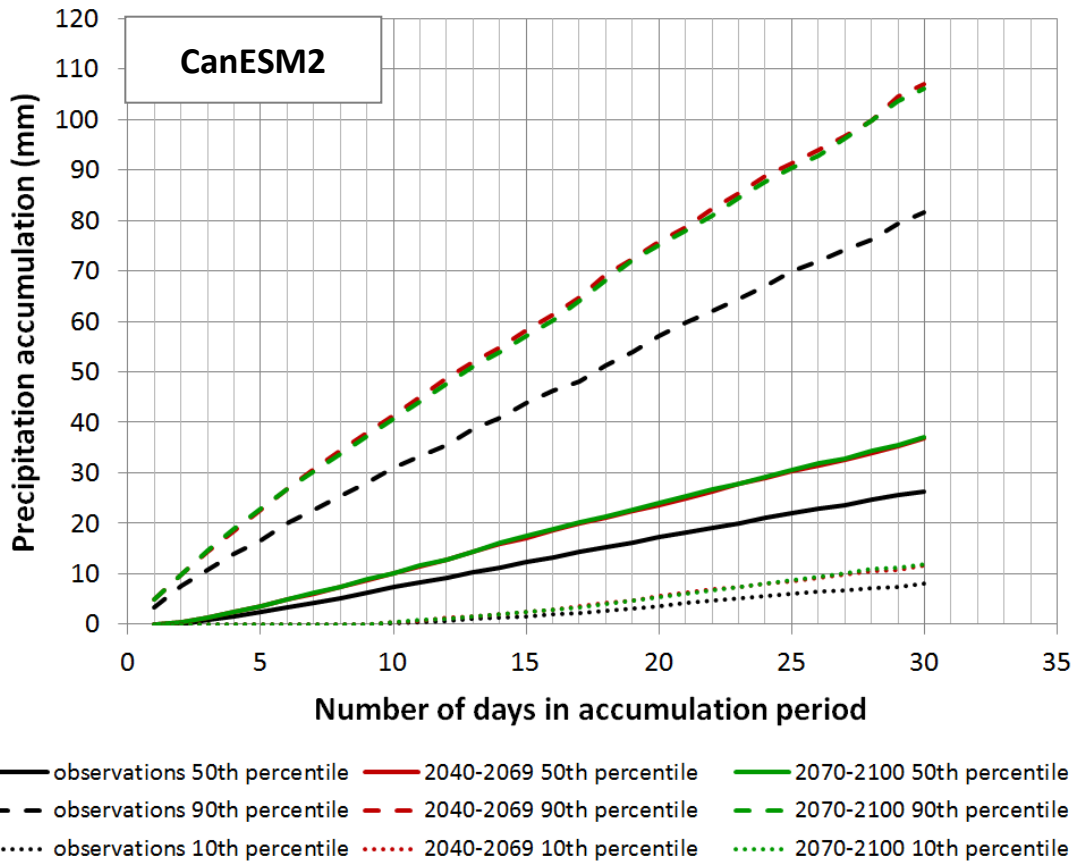
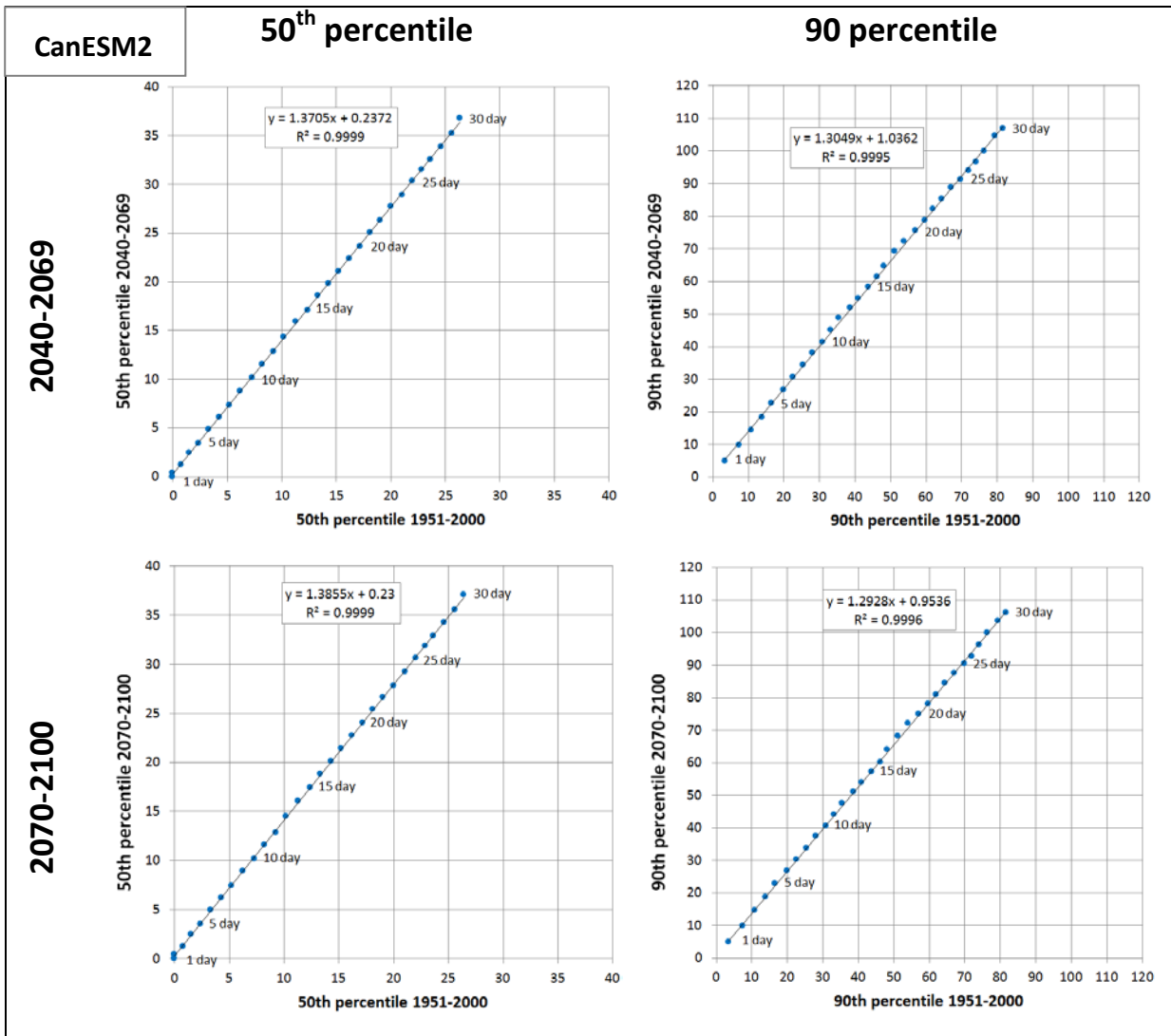


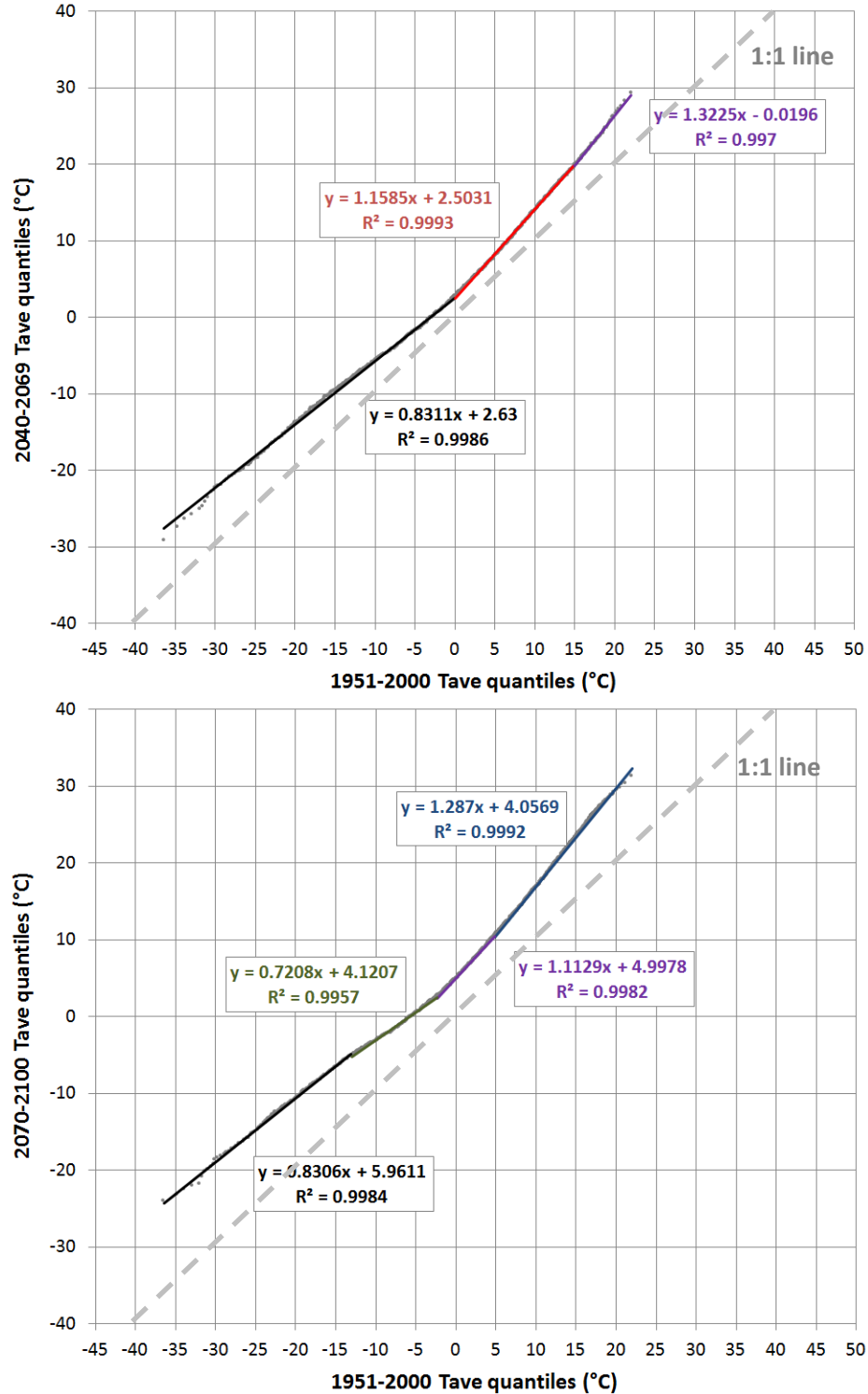
Figure 12. Relationship between 50th percentiles and 90th percentiles of precipitation for different time horizons and for different aggregation periods (ranging from 1-day to 30-days), for our climate scenario based on CanESM2.



Temperature

Figure 11 shows the temperature quantile mapping and is analogous to Figure 9. Linear regression was used to obtain the polygonal lines shown in the figure panels, where the resulting equations are displayed. These lines were used for transforming our 34-year observations-based daily temperature record (x axis) into new, 34-year daily temperature projection (y axis).

Figure 13. Quantile to quantile plots relating daily downscaled CanESM2-simulated temperature for period 1 (x axis) to that for the mid-century period (y axis of the top panel) and the late-century period (y axis of the bottom panel). The points align themselves along a polygonal line, and the equation for each segment is displayed.



2.3 CNRM-CM5 RUN1 FOR RCP8.5

Precipitation

One large daily precipitation value appears in the CNRM-CM5 mid-century projections, 131 mm, far higher than the maximum value of its historical simulations, 59 mm. The occurrence of this high value carries important implications to the extreme value analysis. In contrast with the other two GCM runs, where the most likely ξ parameter was zero, in this case the most likely ξ value is $\hat{\xi} = 0.28$ (Table 3). This implies strong concavity of the quantile mapping curve, the red line in Figure 14 (top panel), which in turn leads to a high value, 144.5 mm, in the scenario used to run the hydrologic model.

When the simulated high value of 131 mm is removed, and the extreme value analysis is repeated without it, we then obtain a most likely parameter value close to zero, $\hat{\xi} = 0.02$ (and $\hat{\sigma} = 8.03$). This case illustrates the volatile nature of parameter estimation in extreme value analysis, and the uncertainty associated with the estimates. The two scenarios (with and without including the high value) are clearly different, and large uncertainty is associated with either. This case illustrates one aspect of the large uncertainty associated with fitting extreme value distributions, especially when working from relatively small data samples.

For the late-century period CNRM-CM5 projections, the most likely ξ value is again distinct from zero, $\hat{\xi} = 0.07$ (Table 3). This results in a concave-upward curve in Figure 14 (bottom panel), but less marked than in the mid-century period.

For $\xi \neq 0$, the Generalized Pareto distribution is given by,

$$F(x) = 1 - \left(1 + \xi \cdot \left(\frac{x-u}{\sigma} \right) \right)^{-\frac{1}{\xi}} \quad \text{Equation 6}$$

Eqn 6 describes the distribution of daily precipitation above a high threshold u for the two future periods, where daily precipitation is denoted x_2 for the mid-century period, and x_3 for the late-century period. Quantile mapping from the historical period to a future period requires combining eqn 1 and eqn 6 for any given non-exceedance probability $F(x)$,

$$F(x_2) = F(x_1) \quad \text{Equation 7}$$

and

$$F(x_3) = F(x_1) \quad \text{Equation 8}$$

Expressing $F(x_2)$ and $F(x_3)$ by eqn 6 and $F(x_1)$ by eqn 1 (because $\hat{\xi}_1 = 0$), then eqn 7 and eqn 8 yield,

$$x_2 = \frac{\sigma_2}{\xi_2} \left[e^{\xi_2 \cdot \left(\frac{x_1 - u_1}{\sigma_1} \right)} - 1 \right] + u_2 \quad \text{Equation 9}$$

and

$$x_3 = \frac{\sigma_3}{\xi_3} \left[e^{\xi_3 \cdot \left(\frac{x_1 - u_1}{\sigma_1} \right)} - 1 \right] + u_3 \quad \text{Equation 10}$$

Eqn 9 and eqn 10, with the parameter values given in Table 3, describes the red lines in Figure 14. In that figure, quantiles {0.001, 0.002, ..., 0.999} are plotted, and in addition we plotted also the highest observations, i.e., quantiles above 0.999.

Table 3. Parameter estimates for the generalized Pareto distribution (GPD) using the POT method and maximum likelihood, for the precipitation simulations from CNRM-CM5.

Time Period	Threshold u (mm)	Number of exceedances	$\hat{\sigma}$	$\hat{\xi}$
1. 1951-2000	18.0	109	8.48	0
2a. 2040-2069	20.0	59	7.04	0.28
2b. 2040-2069 Removing the high outlier simulated precipitation value	20.0	58	8.03	0.02
3. 2070-2100	20.2	69	9.61	0.07

Figure 14. Quantile to quantile plots relating daily downscaled CNRM-CM5-simulated precipitation for period 1 (x axis) to that of a future period (y axis). The first two panels are alternative scenarios for the mid-century period: the first included all mid-century data points in fitting the extreme value distribution, the second having eliminated the highest GCM-simulated point (59, 131) before fitting the extreme value distribution.

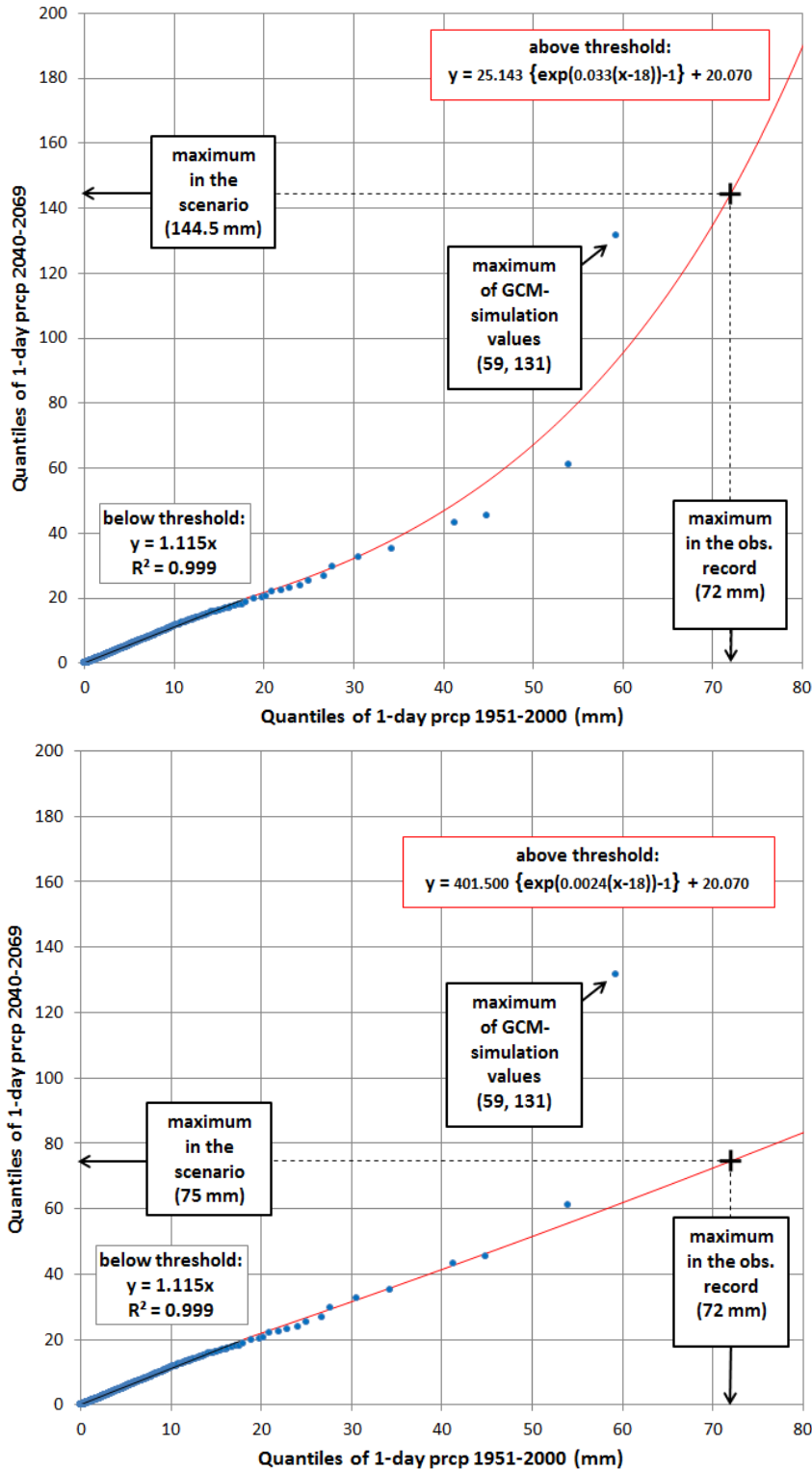


Figure 14 (Cont'd).

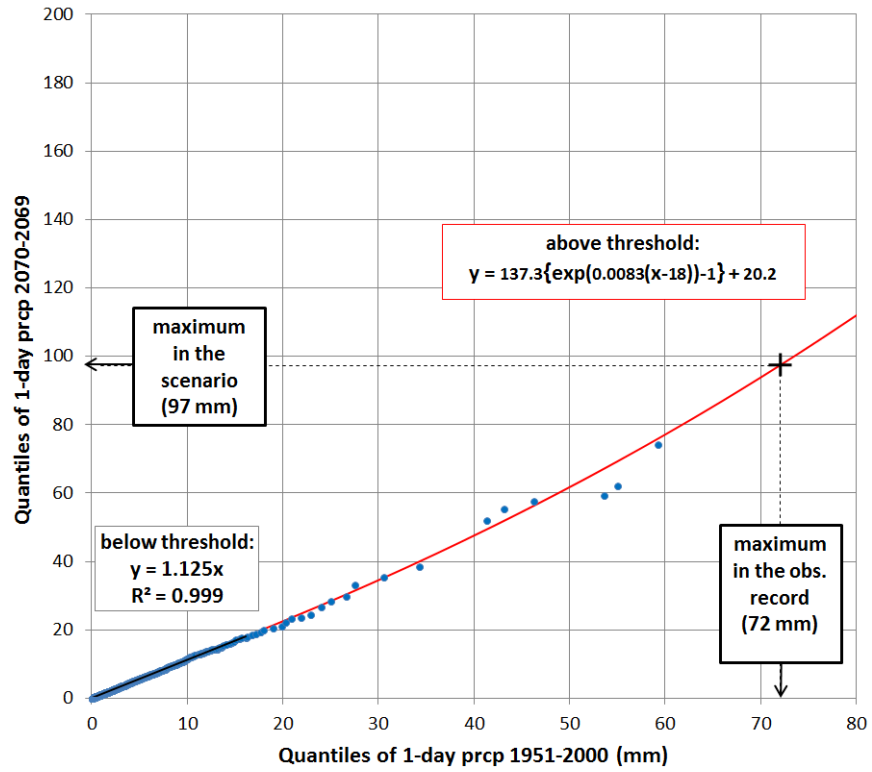


Figure 15. Tenth, 50th, and 90th percentiles of precipitation accumulation for different aggregation periods, for our climate scenarios based on CNRM-CM5.

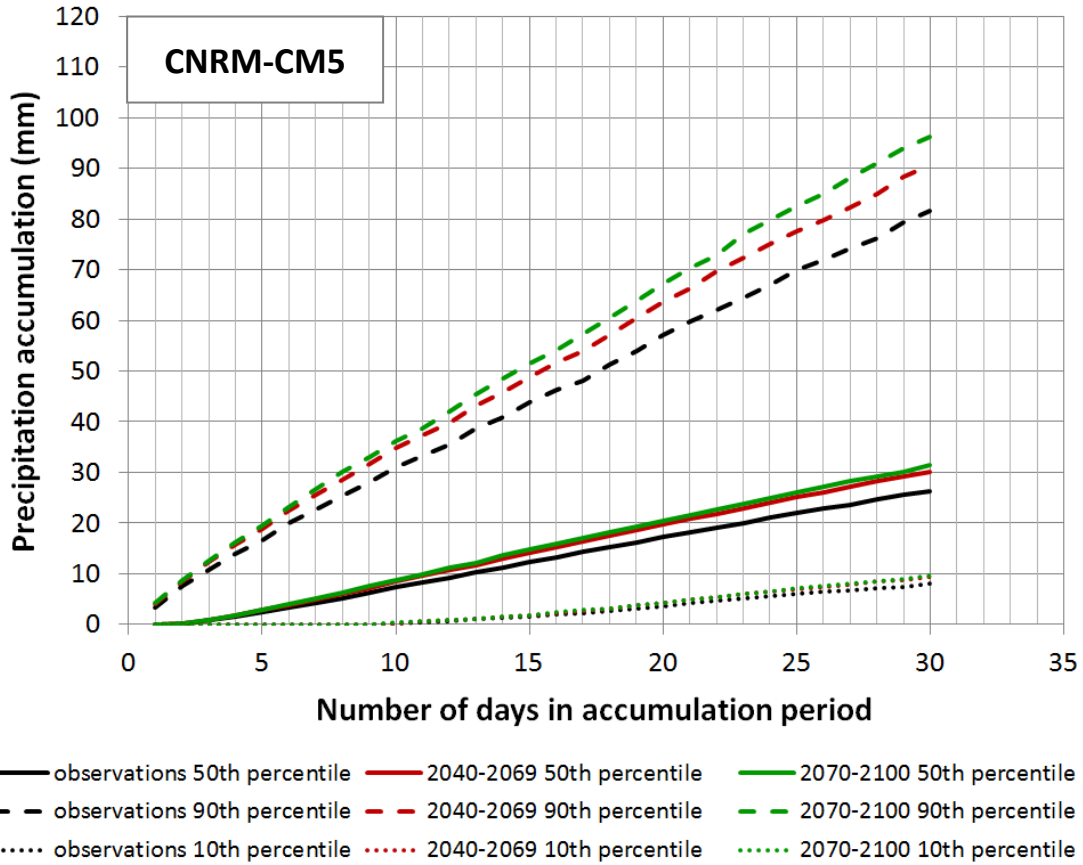
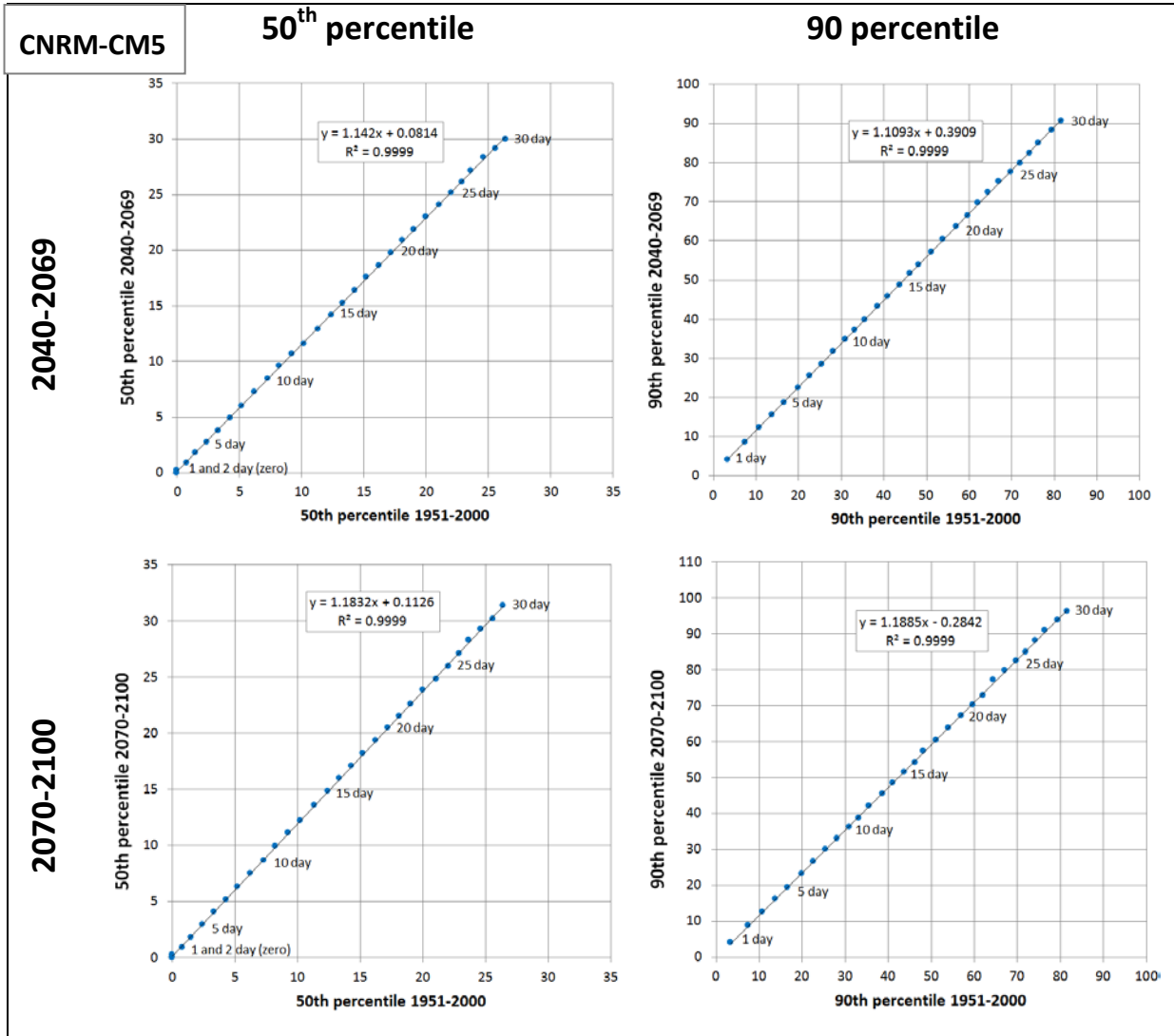


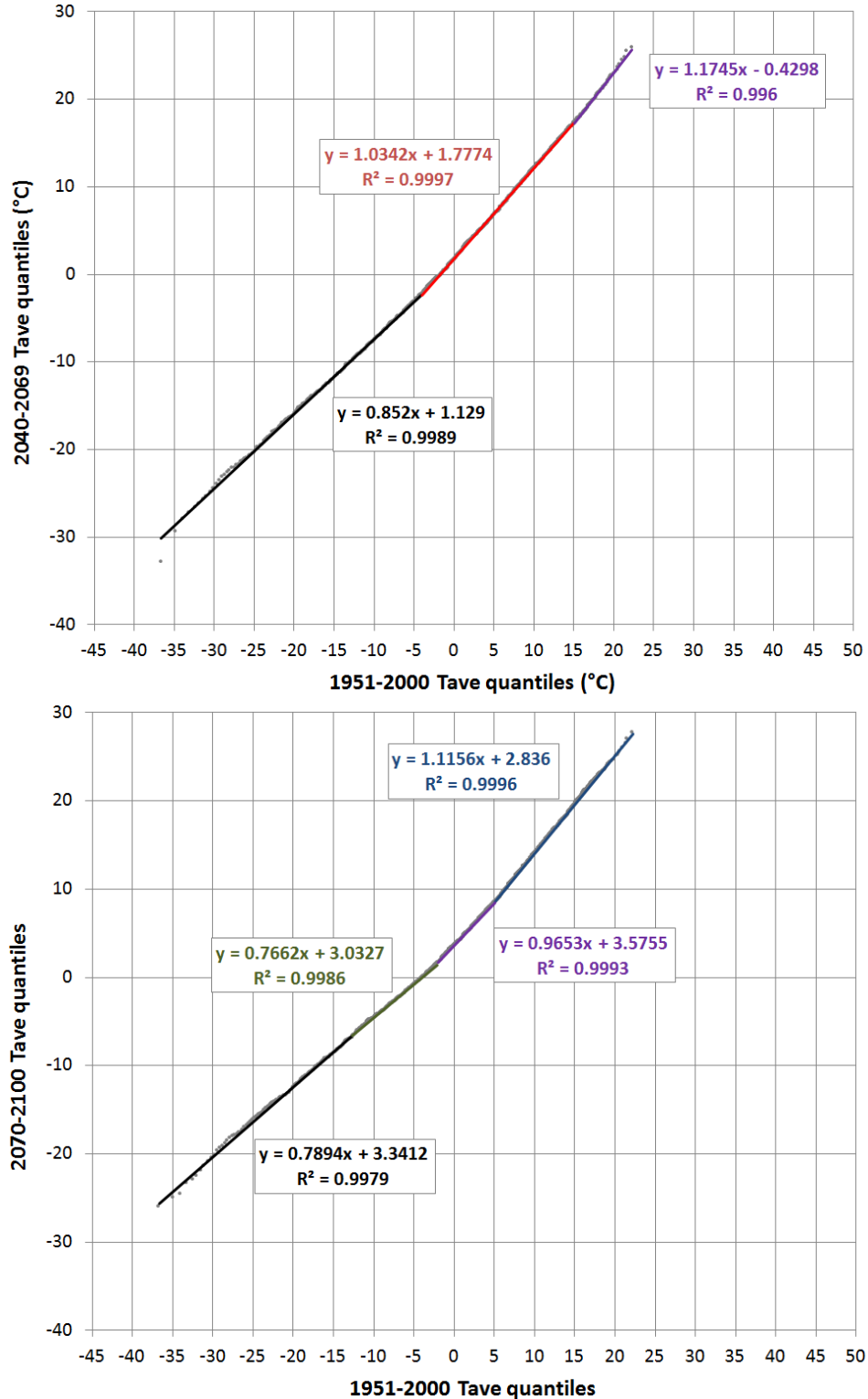
Figure 16. Relationship between 50th percentiles and 90th percentiles of precipitation for different time horizons and for different aggregation periods (ranging from 1-day to 30-days), for our climate scenario based on CNRM-CM5.



Temperature

Figure 17 shows the temperature quantile mapping. Linear regression was used to obtain the polygonal lines shown in the figure panels, where the resulting equations are displayed. These lines were used for transforming our 34-year observations-based daily temperature record (x axis) into new, 34-year daily temperature projection (y axis).

Figure 17. Quantile to quantile plots relating daily downscaled CNRM-CM5-simulated temperature for period 1 (x axis) to that for the mid-century period (y axis of the top panel) and the late-century period (y axis of the bottom panel). The points align themselves along a polygonal line, and the equation for each segment is displayed.



3 REFERENCES

Coles S. (2001) An introduction to statistical modeling of extreme values. Springer-Verlag, London, UK. 208 pp. WA273.6.C63 2001.

APPENDIX B

DEVELOPMENT, CALIBRATION AND TESTING OF THE PROXY (WINDREM CREEK) HEC-HMS MODEL

DEVELOPMENT, CALIBRATION, AND TESTING OF THE PROXY (WINDREM CREEK) MODEL

HEC-HMS was initially calibrated to the Windrem Creek watershed (Windrem), which flows into the town of Chetwynd from the north (Figure 1), and is situated approximately 45 kilometres east of the Fisher Creek watershed. Windrem has a south-east aspect and a drainage area of approximately 24 km². A majority of the watershed is forested based on the most recent Google Earth images (Dec 31, 2005), but forest harvesting appears to have occurred in the past. Windrem was selected since this is the only watershed in the study area with both a streamflow gauge, a nearby climate station (approximately 5 km from the Windrem watershed centroid as defined by the location of the streamflow gauge), and a snow course survey in the area (44 km northwest – not shown on Figure 1).

- Streamflow: Water Survey of Canada (WSC) *Windrem Creek near Chetwynd 07FB011* (WSC Windrem)
 - Period of record: 1986-1998. Manual gauge with seasonal data; daily data is intermittent or nonexistent for some years.
- Climate station: Environment Canada (EC) *Chetwynd Airport 1181508* (Chetwynd A), elevation 609.6 metres
 - Period of record: 1982-2011. Incomplete daily data for most years (precipitation and temperature used) with intermittent hourly data available for summer periods.
- Snow course survey: British Columbia Ministry of Forests, Lands and Natural Resource Operations (BCMFLNRO) *Bullhead Mountain 4A28* (Bullhead), elevation 798 metres
 - Period of record: 1984-2007. January to May monthly data; data is intermittent or nonexistent for some years.

For calibration purposes it was assumed that the manual data at WSC Windrem approximated the daily flow metric, and while there will be errors associated with this assumption, the manual data provides a reasonable representation of streamflow patterns in the watershed at the daily time step.

The model was first calibrated to SWE data at Bullhead and then to streamflow at WSC Windrem. SWE calibrations were quite successful given data limitations, and results are shown in Figure B1. for the 1986-1997 calibration periods – the observed and simulated SWE are shown in the third chart down from the top in Figure 1.

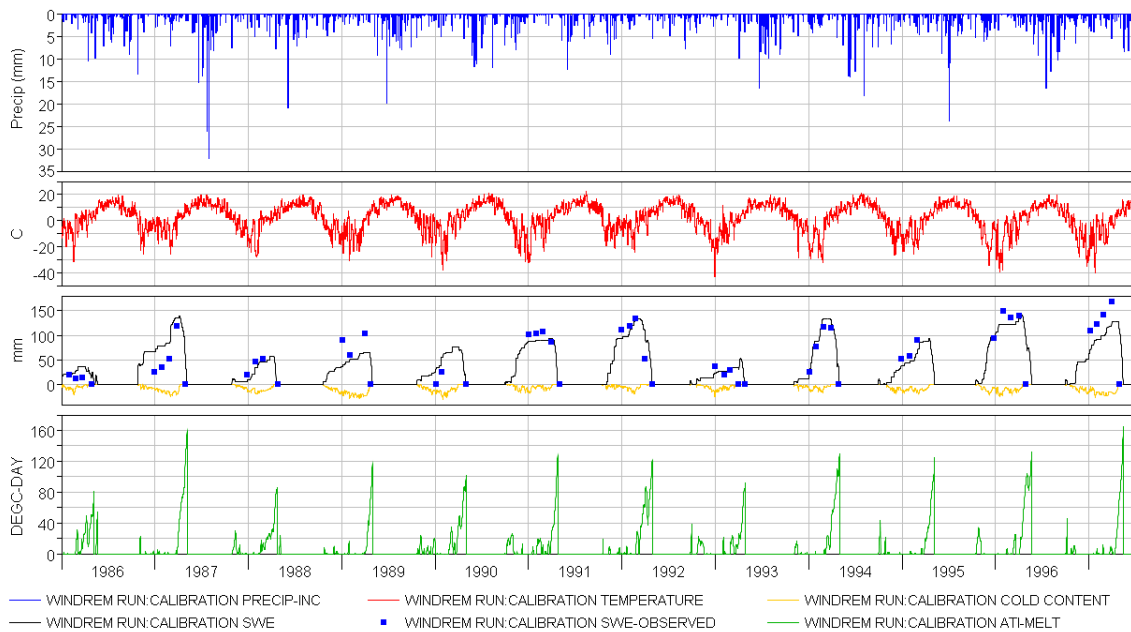


Figure B1. SWE calibration results at Windrem for the 1986-1997 calibration periods.

It was assumed that SWE at Windrem was similar to Bullhead at the model elevation band that corresponds to the elevation of the Bullhead snow course. Precipitation inputs were distributed over the watershed using area-elevation bands, with temperature similarly distributed using a temperature index model. A temperature lapse rate of 5.1 °C/km was assumed, while a simulation average precipitation gradient was computed (86.7% increase in precipitation per kilometre increase in elevation) based on an average annual difference between Chetwynd A and EC *Sikanni Chief 1187335* (Sikanni), which is at an elevation of 937 m. While this station is distant from the site (190 km north), other nearby EC stations lacked a significant elevation difference from Chetwynd or did not provide an acceptable representation of orographic effects combined with the predominant direction of movement of storms in the area. EC *Bullmoose 1181120*, for example, is close to the study site and at a sufficient elevation, but is situated in a rain shadow. Climate stations in the area that are not run by EC were not considered for this purpose due to short record lengths and/or lack of adequate quality assurance and quality control.

Once the model was calibrated to WSC Windrem, it was tested on the larger Dickebusch Creek watershed (Dickebusch) south of Chetwynd, which has an automatic continuous streamflow gauge:

- *WSC Dickebusch Creek near the Mouth 07FB004* (WSC Dickebusch)
 - Period of record: 1978-2010. Data is intermittent or nonexistent for some years, including annual peak instantaneous and daily flows; hourly flows are missing for most years.

Dickebusch has a north-east aspect and a drainage area of approximately 84 km². It is mostly forested but similar to Windrem, forest harvesting appears to have occurred in the past based on the most recent Google Earth images (Dec 31, 2005). Dickebusch was not as suitable as Windrem for the initial calibration since the watershed centroid (as defined by the location of the streamflow gauge) is approximately 23 km south-east of the Chetwynd A climate station, and storms in the larger watershed were not expected to be well represented by Chetwynd A due to the spatial and temporal variability of convective summer storms in this area. The availability of instantaneous peak flow data at the Dickebusch gauge, however, prompted testing of the calibrated Windrem model's peak flow parameters with observance of measured peak flow generation capacities at Dickebusch. Since the Windrem streamflow data are manual measurements, it is unlikely that measurements coincided with instantaneous peaks each year since these were recorded manually and only once each day. The calibrated model's peak flow parameters were modified to better simulate near instantaneous peaks (hourly metric) at both watersheds, by striking a balance between daily flow metrics at Windrem and Dickebusch with near instantaneous flows at Dickebusch for the largest storms on record when both watersheds had similar daily unit discharge values (discharge per unit area). Simulations were run with daily climate data during the winter period (since hourly data is not available) and hourly data for spring and summer rainfall storms when possible. Hourly data is preferred for spring and summer storms since it provides a better representation of high intensity rainfall inputs that may result in rapid (flashy) watershed response. Daily climate inputs are acceptable for the winter period since precipitation is predominantly in the form of snowfall.

The model was found to simulate plausible estimates of hourly annual peak flows at Windrem and Dickebusch for the years at each corresponding WSC gauge that overlapped with available climate data. A future assessment of the uncertainty in the rainfall-runoff modelling could include a comparison of the results of peak flow frequency analyses between simulated and observed datasets.

APPENDIX C

FISHER CREEK HEC-HMS MODEL: SIMULATED ANNUAL PEAK HOURLY DISCHARGE FREQUENCY ANALYSIS FITS

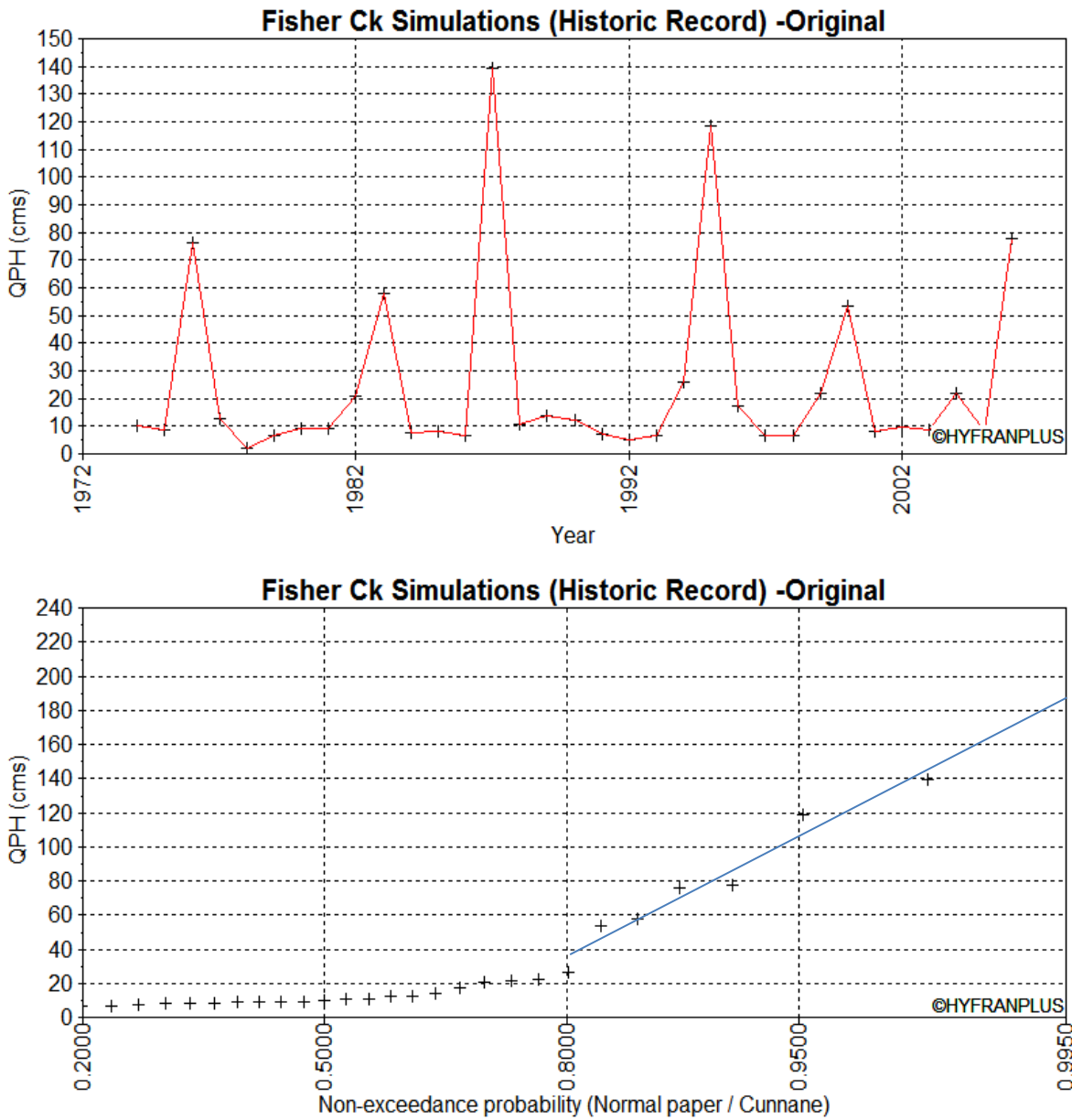


Figure C1. Simulated Fisher Creek Bridge annual hourly discharge maxima (top panel) and frequency analysis of the annual hourly discharge maxima (bottom panel) for the historic climate period.

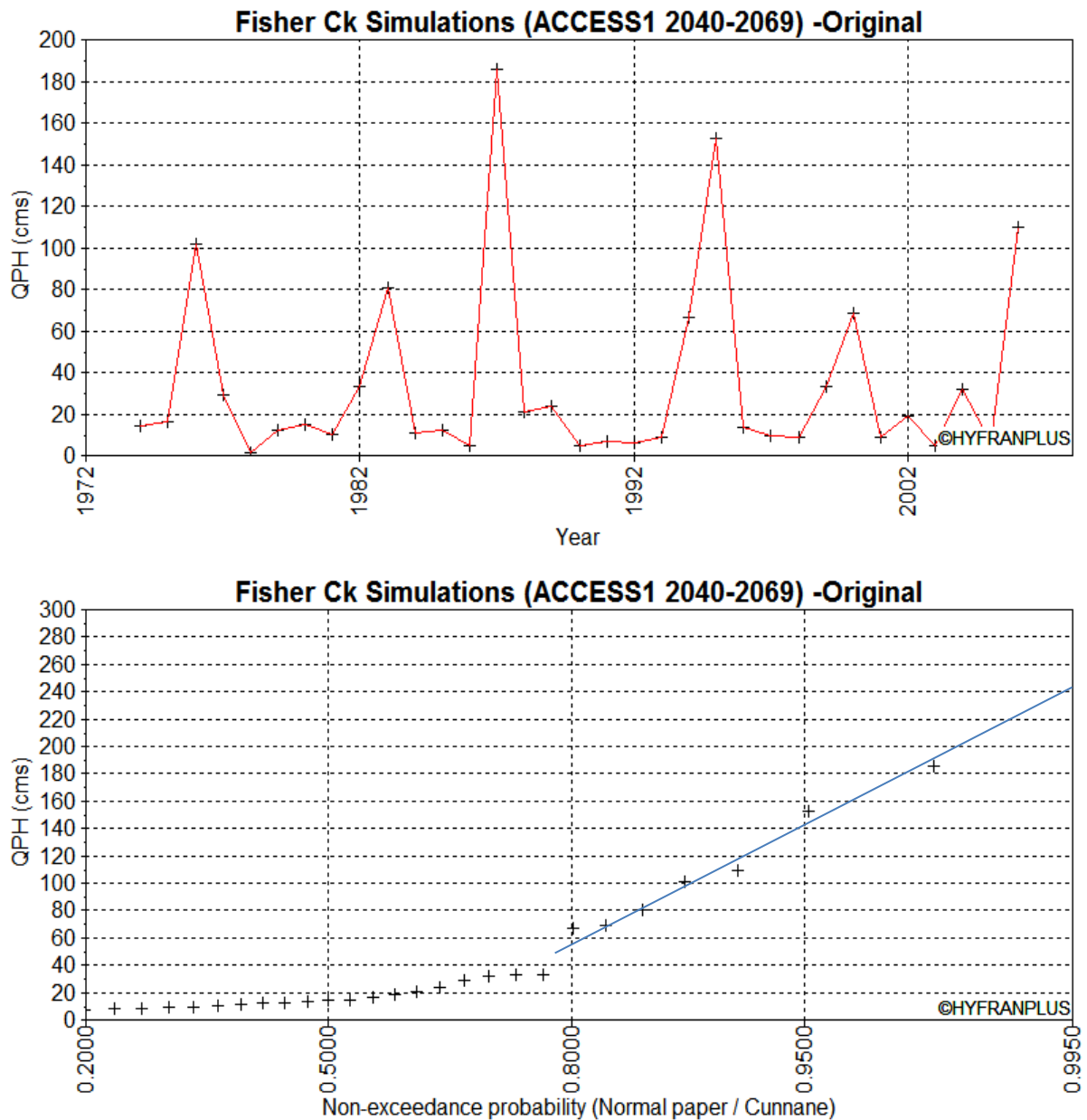


Figure C2. Simulated Fisher Creek Bridge annual hourly discharge maxima (top panel) and frequency analysis of the annual hourly discharge maxima (bottom panel) for the ACCESS1 climate projection for the period 2040-2069.

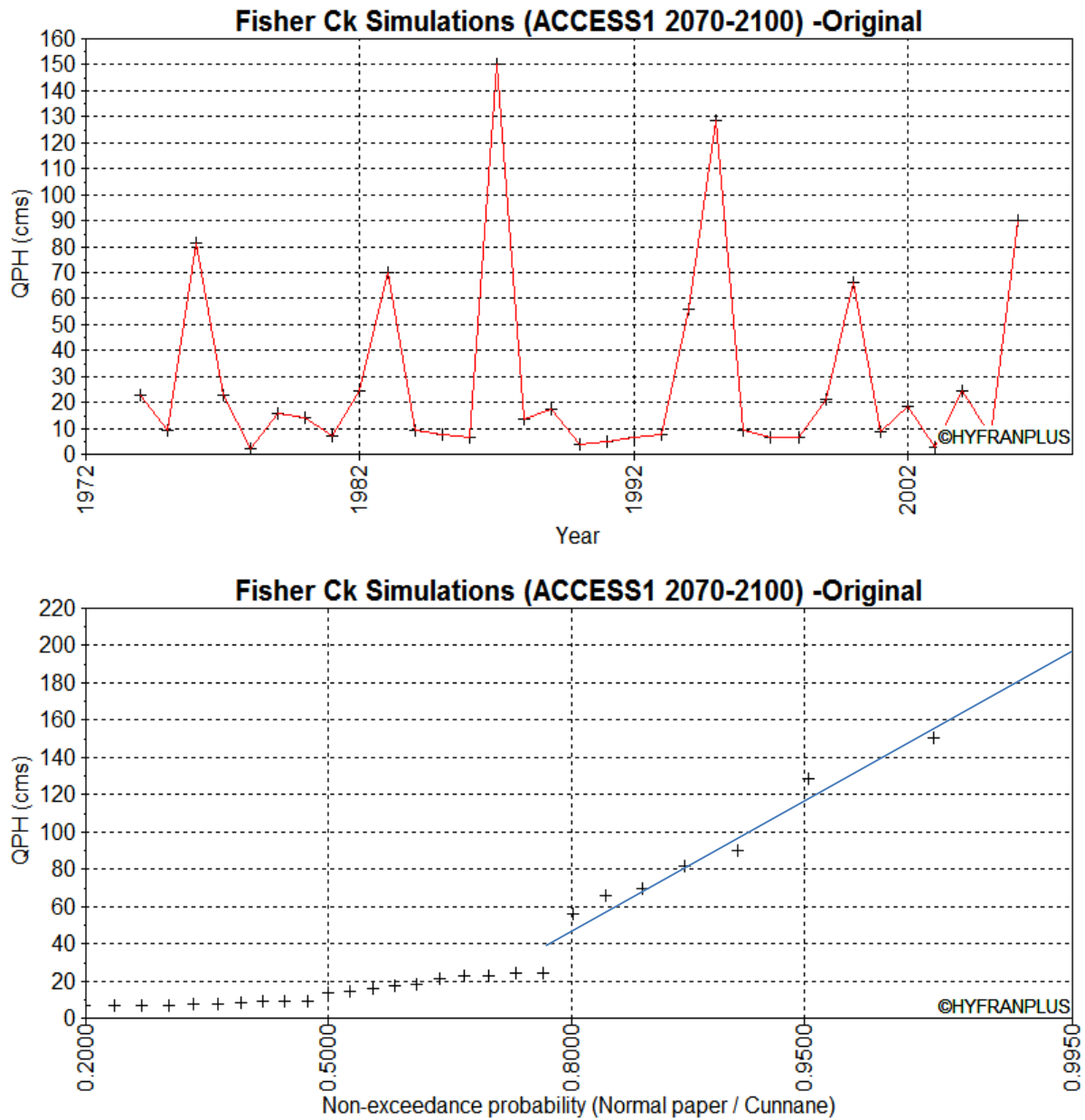


Figure C3. Simulated Fisher Creek Bridge annual hourly discharge maxima (top panel) and frequency analysis of the annual hourly discharge maxima (bottom panel) for the ACCESS1 climate projection for the period 2070-2100.

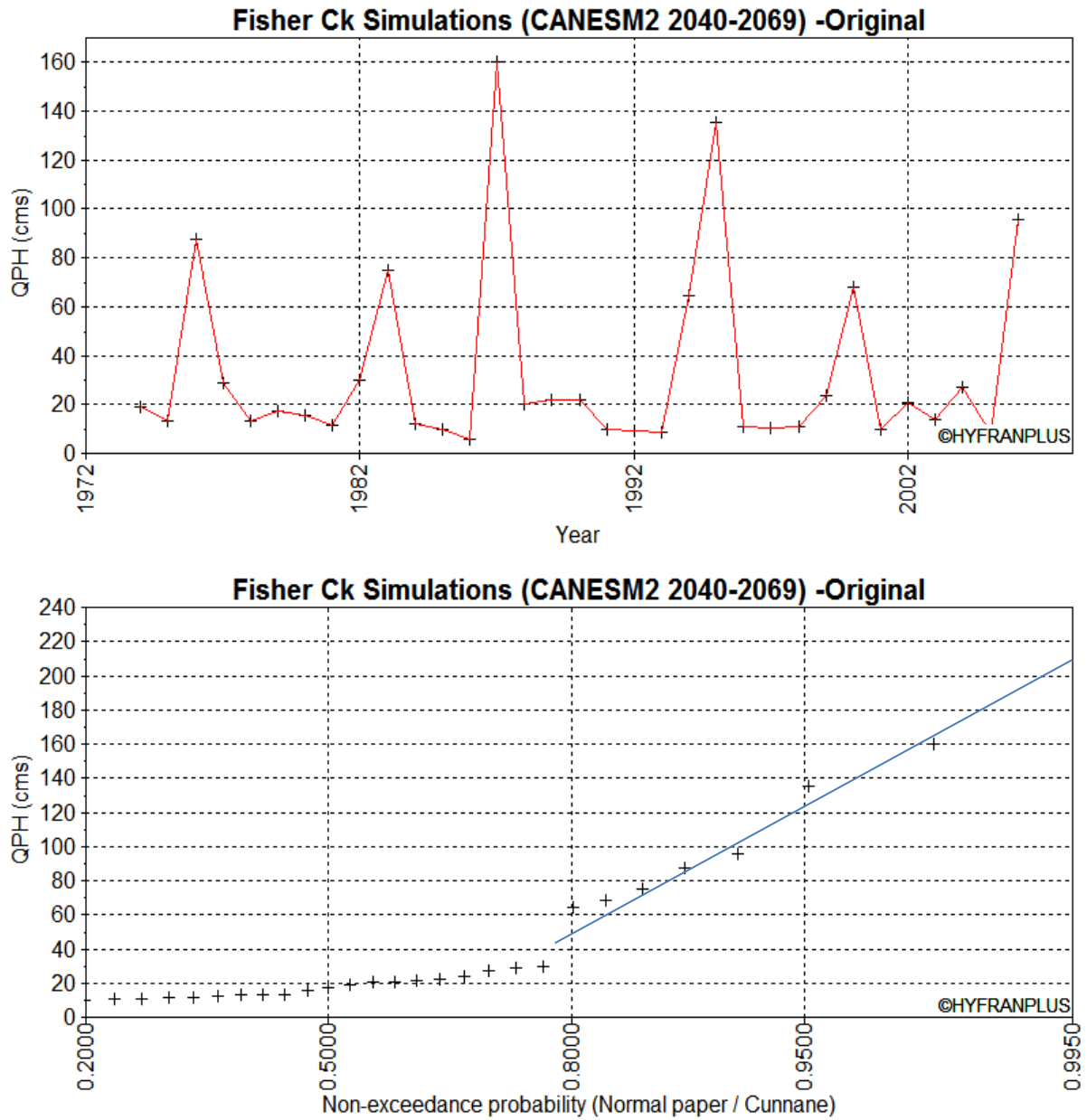


Figure C4. Simulated Fisher Creek Bridge annual hourly discharge maxima (top panel) and frequency analysis of the annual hourly discharge maxima (bottom panel) for the CanESM2 climate projection for the period 2040-2069.

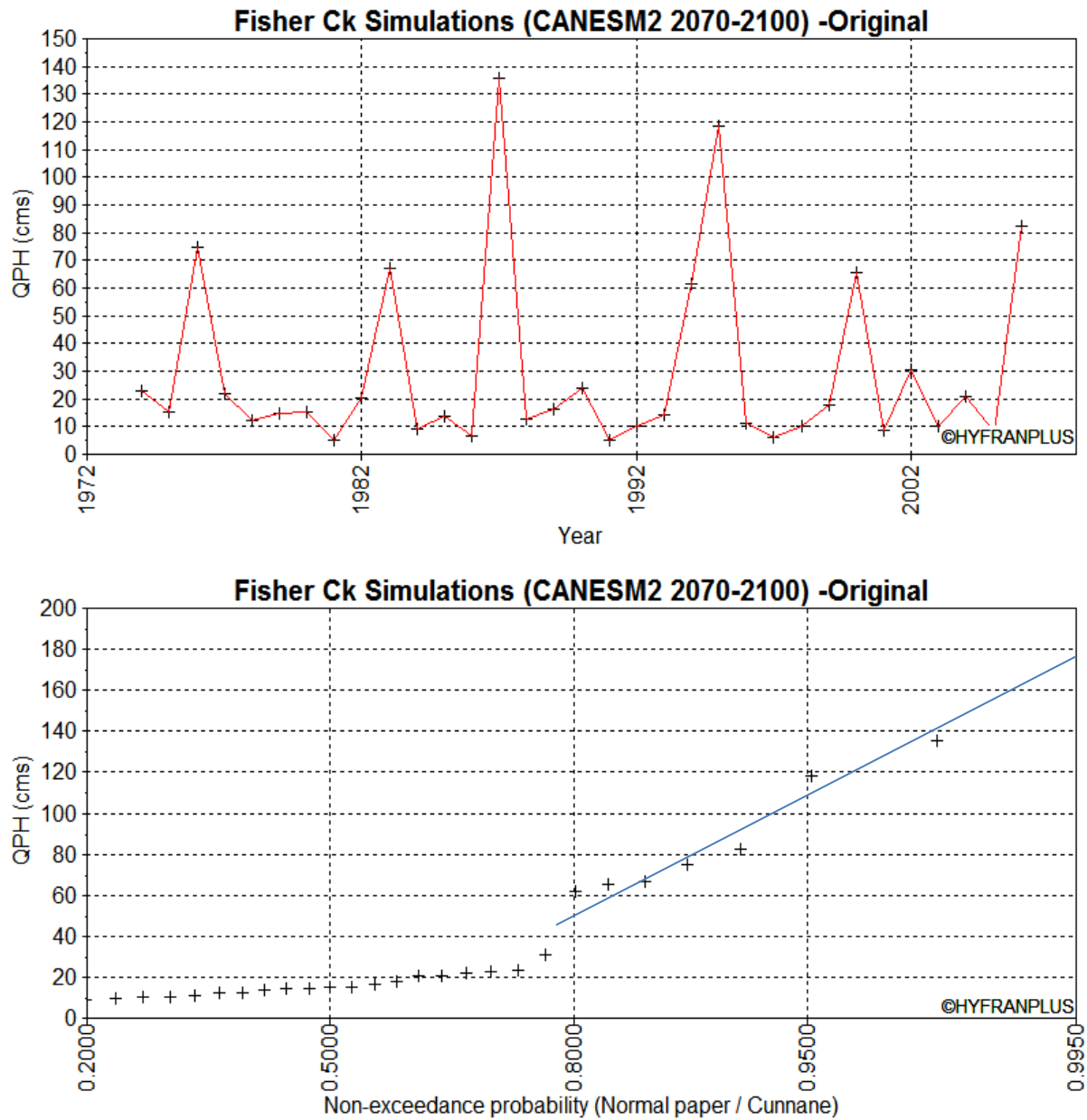


Figure C5. Simulated Fisher Creek Bridge annual hourly discharge maxima (top panel) and frequency analysis of the annual hourly discharge maxima (bottom panel) for the CanESM2 climate projection for the period 2070-2100.

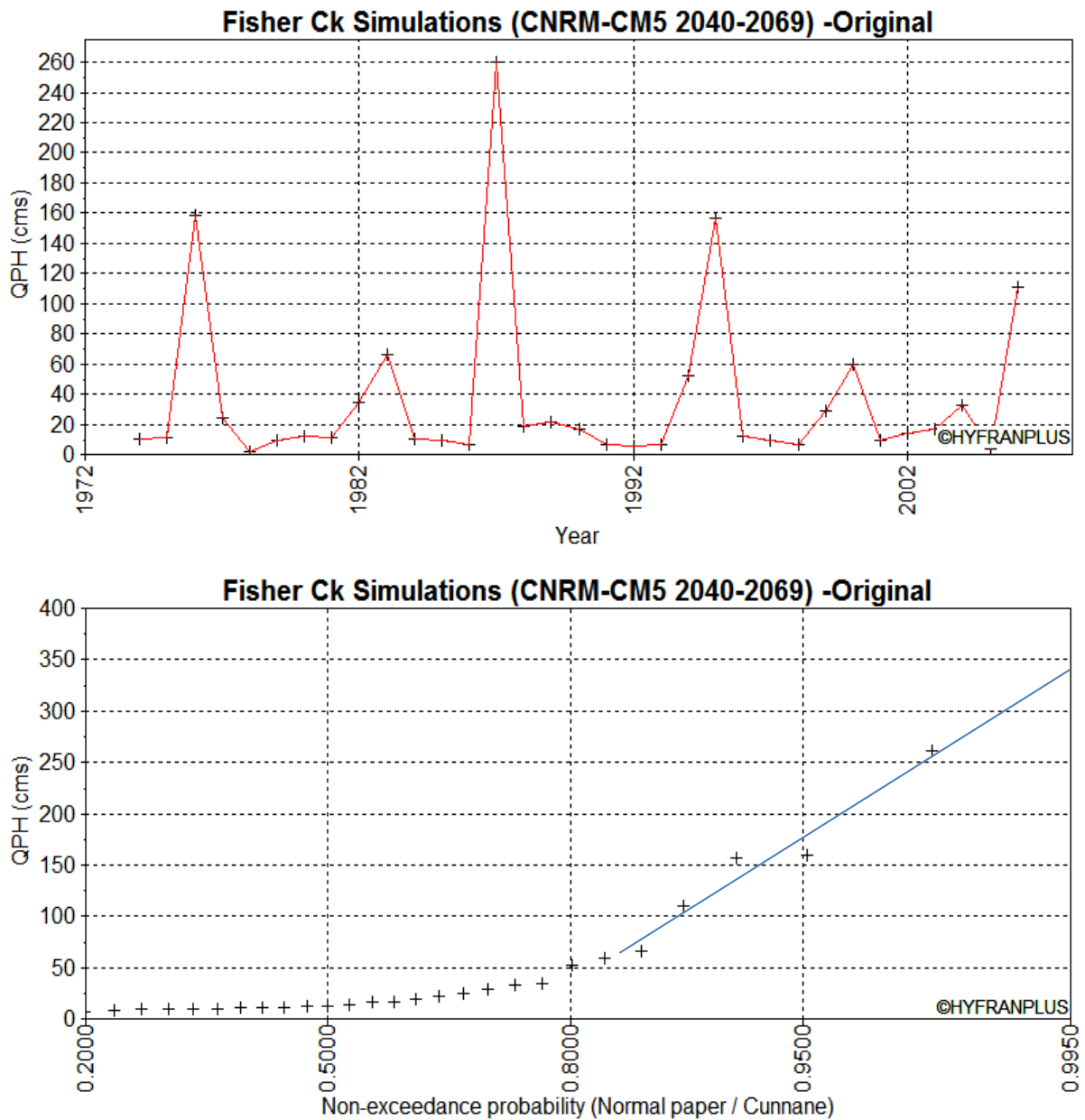


Figure C6. Simulated Fisher Creek Bridge annual hourly discharge maxima (top panel) and frequency analysis of the annual hourly discharge maxima (bottom panel) for the CNRM-CM5 climate projection for the period 2040-2069.

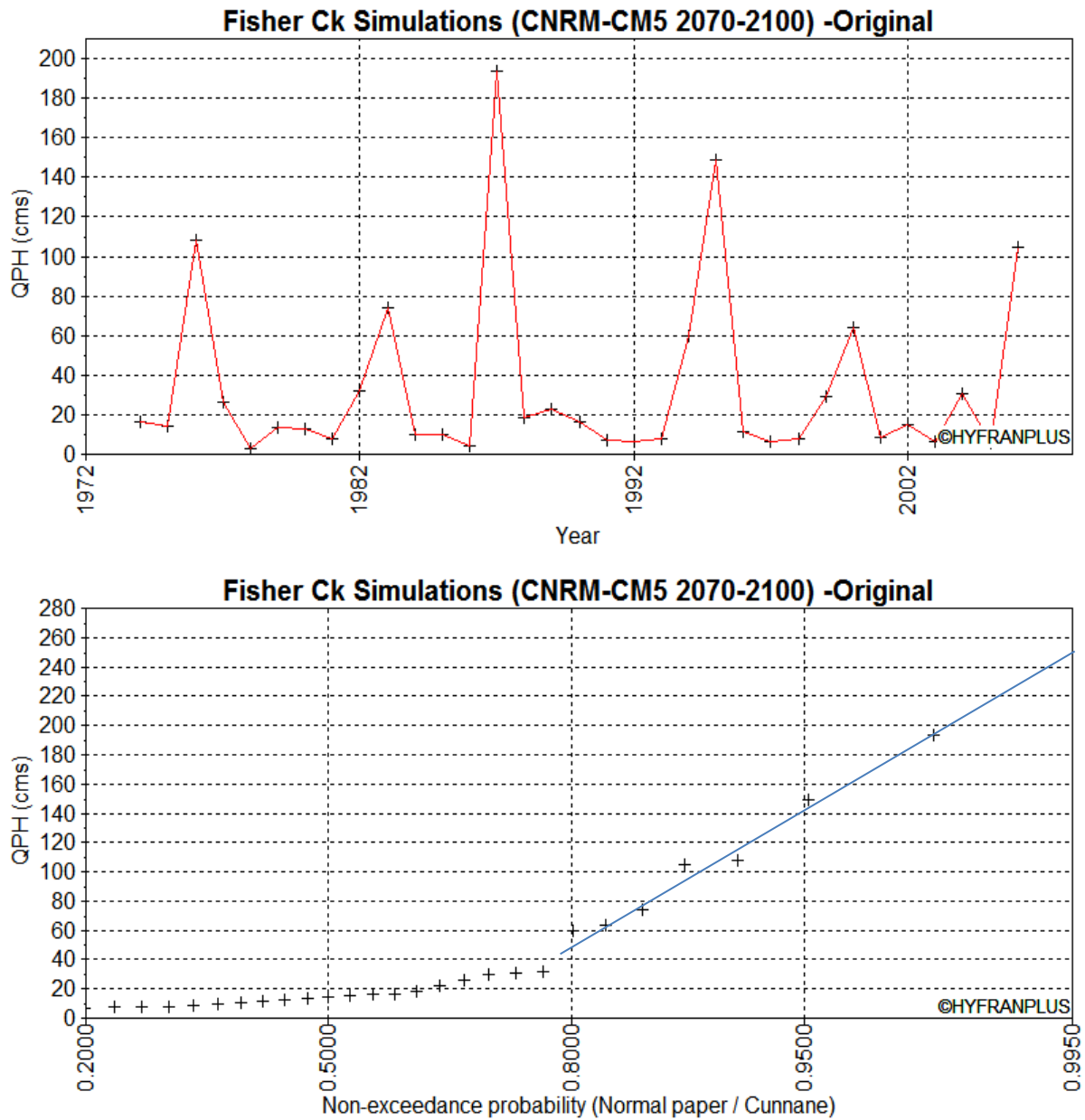


Figure C7. Simulated Fisher Creek Bridge annual hourly discharge maxima (top panel) and frequency analysis of the annual hourly discharge maxima (bottom panel) for the CNRM-CM5 climate projection for the period 2070-2100.

APPENDIX D

**SENSITIVITY ANALYSIS OF FISHER CREEK HEC-HMS MODEL: SIMULATED ANNUAL PEAK
HOURLY DISCHARGE FREQUENCY ANALYSIS FITS**

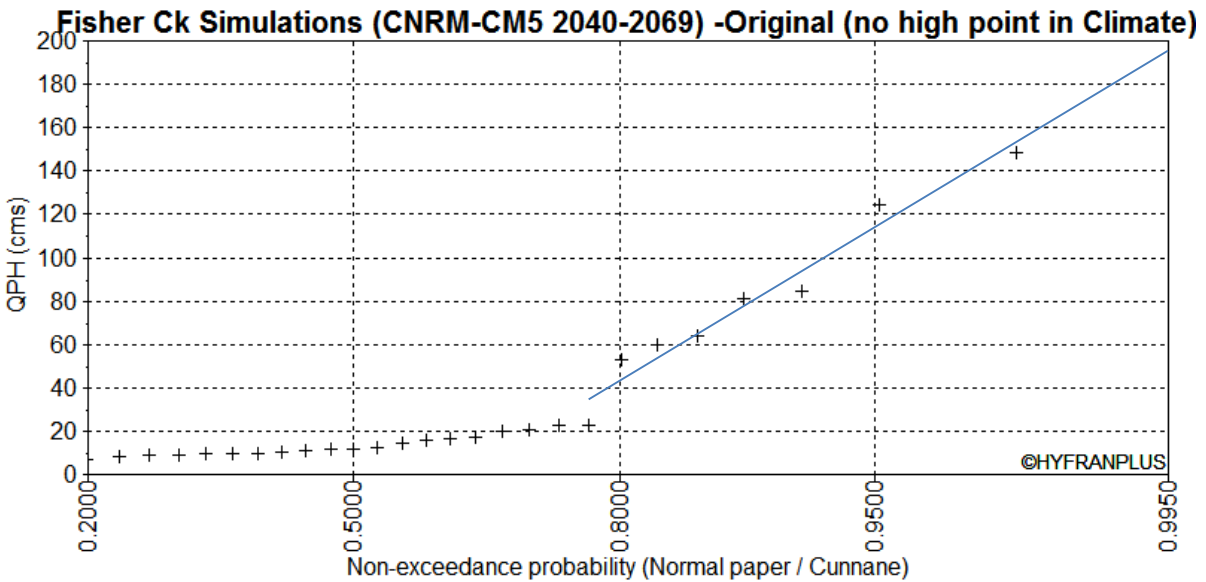
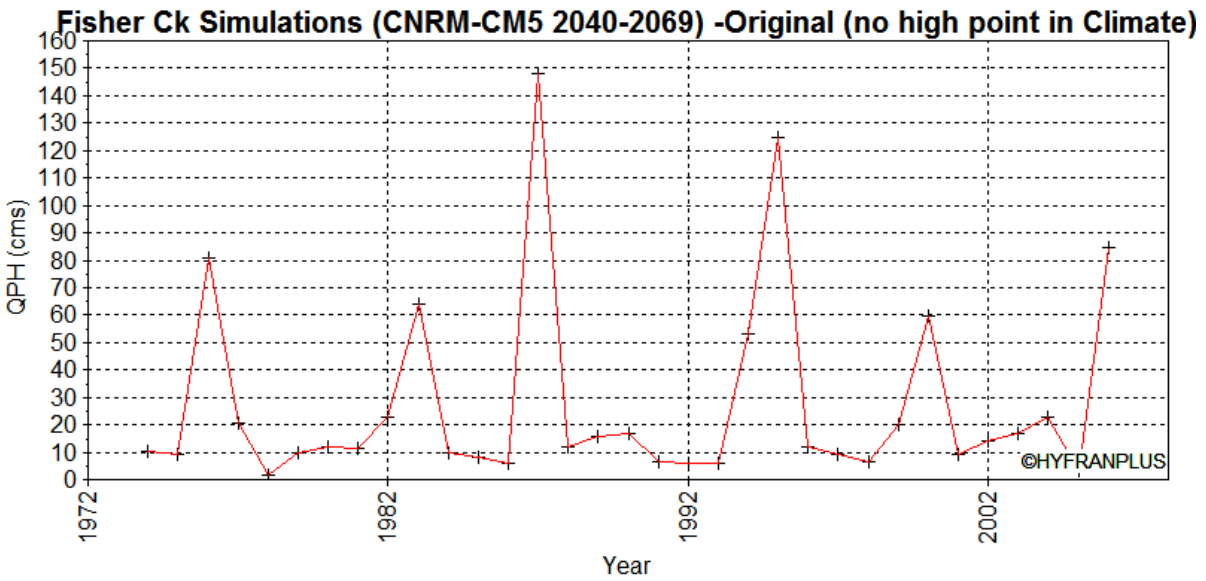


Figure D1. Sensitivity analysis: Fisher Creek HEC-HMS model simulation with an alternate CNRM-CM5 climate scenario, developed with the exclusion of an exceptionally high daily precipitation value (details in Appendix A); simulated Fisher Creek Bridge annual hourly discharge maxima (top panel) and frequency analysis of the annual hourly discharge maxima (bottom panel) for the historic climate period.

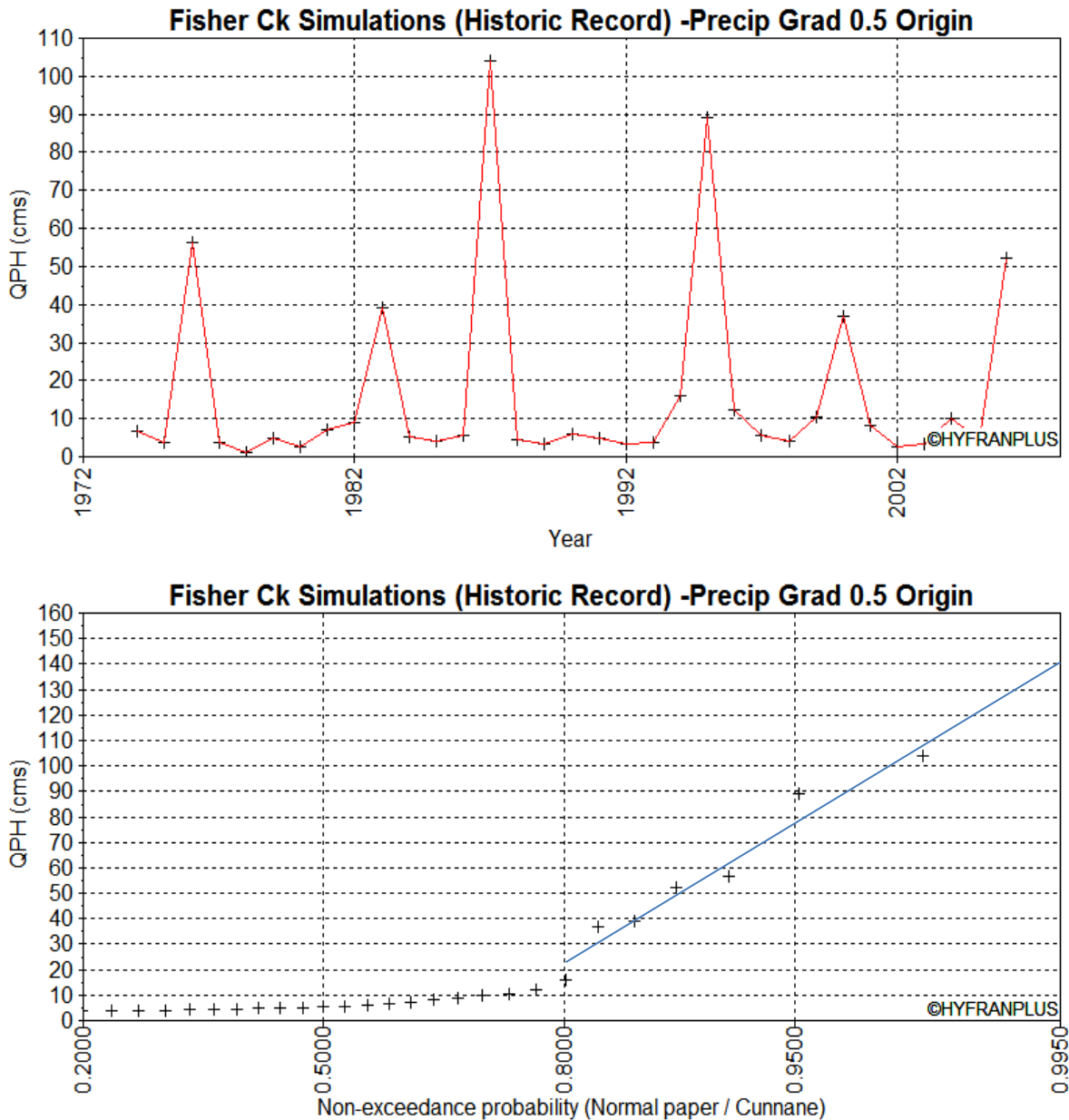


Figure D2. Sensitivity analysis: Fisher Creek HEC-HMS model precipitation gradient set to 50% of original value; simulated Fisher Creek Bridge annual hourly discharge maxima (top panel) and frequency analysis of the annual hourly discharge maxima (bottom panel) for the historic climate period.

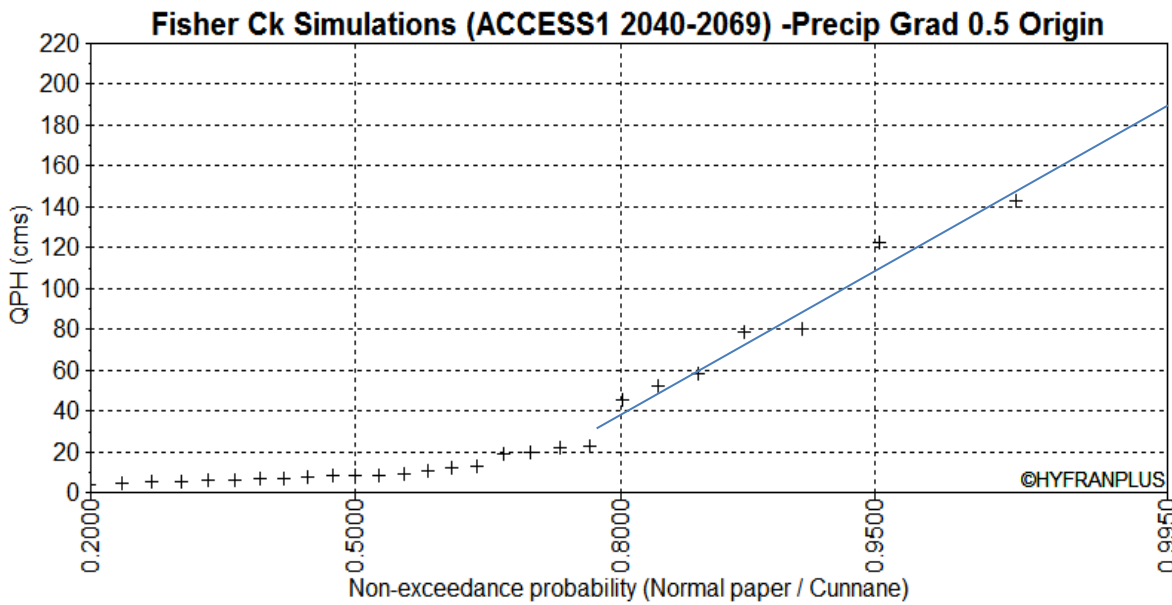
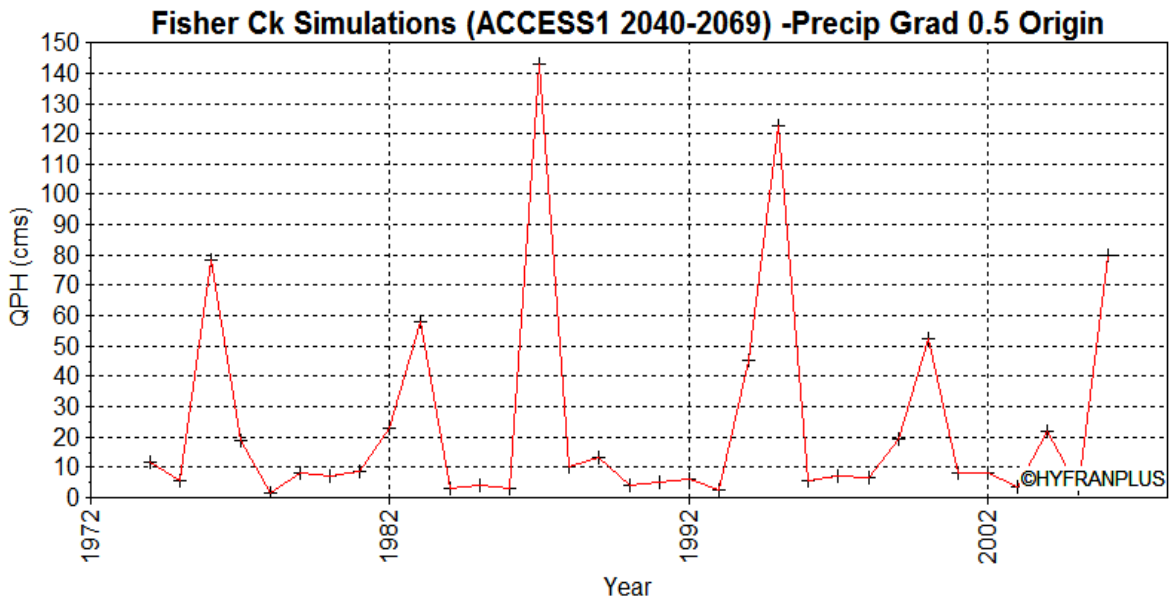


Figure D3. Sensitivity analysis: Fisher Creek HEC-HMS model precipitation gradient set to 50% of original value; simulated Fisher Creek Bridge annual hourly discharge maxima (top panel) and frequency analysis of the annual hourly discharge maxima (bottom panel) for the ACCESS1 climate projection for the period 2040-2069.

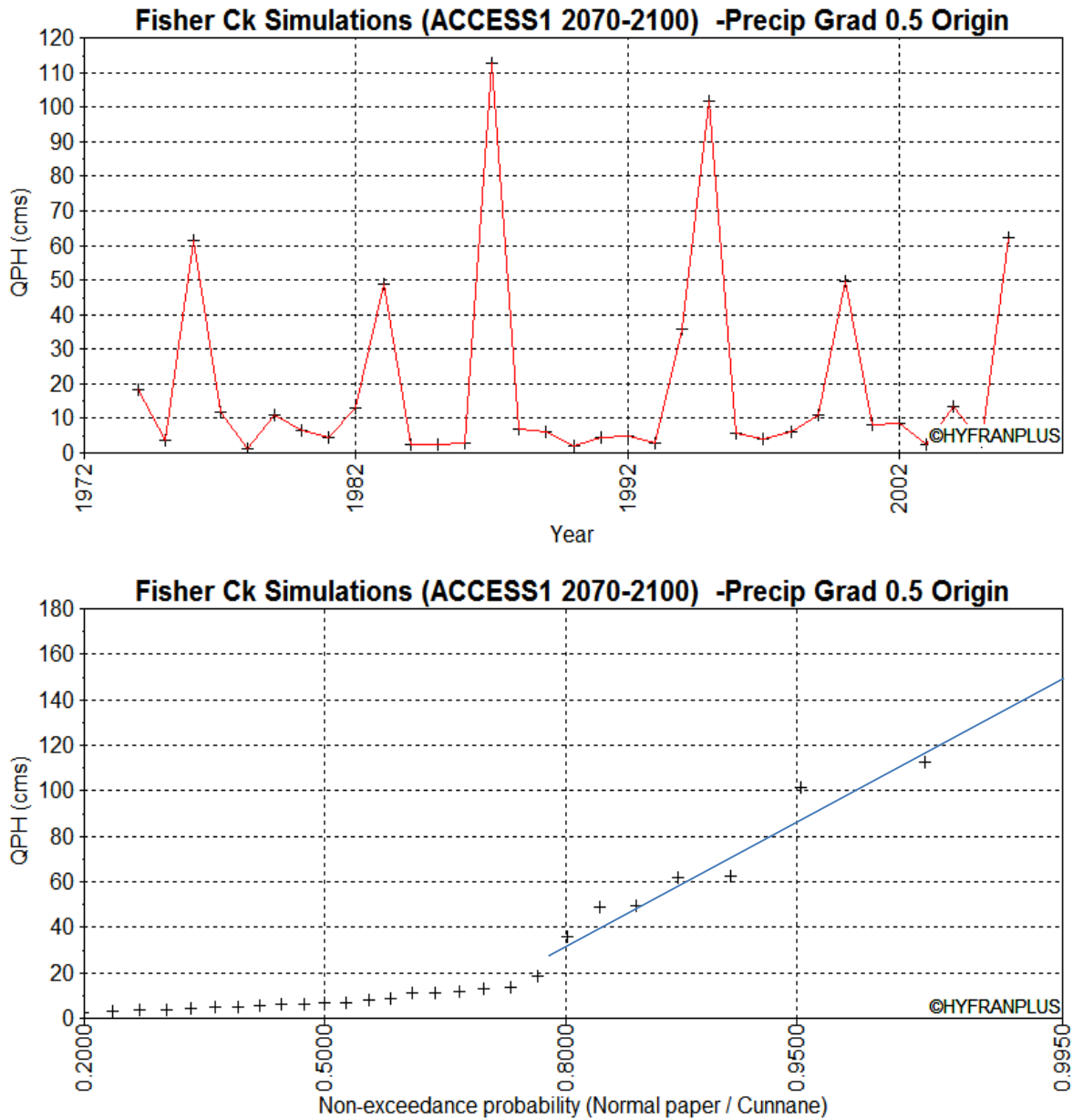


Figure D4. Sensitivity analysis: Fisher Creek HEC-HMS model precipitation gradient set to 50% of original value; simulated Fisher Creek Bridge annual hourly discharge maxima (top panel) and frequency analysis of the annual hourly discharge maxima (bottom panel) for the ACCESS1 climate projection for the period 2070-2100.

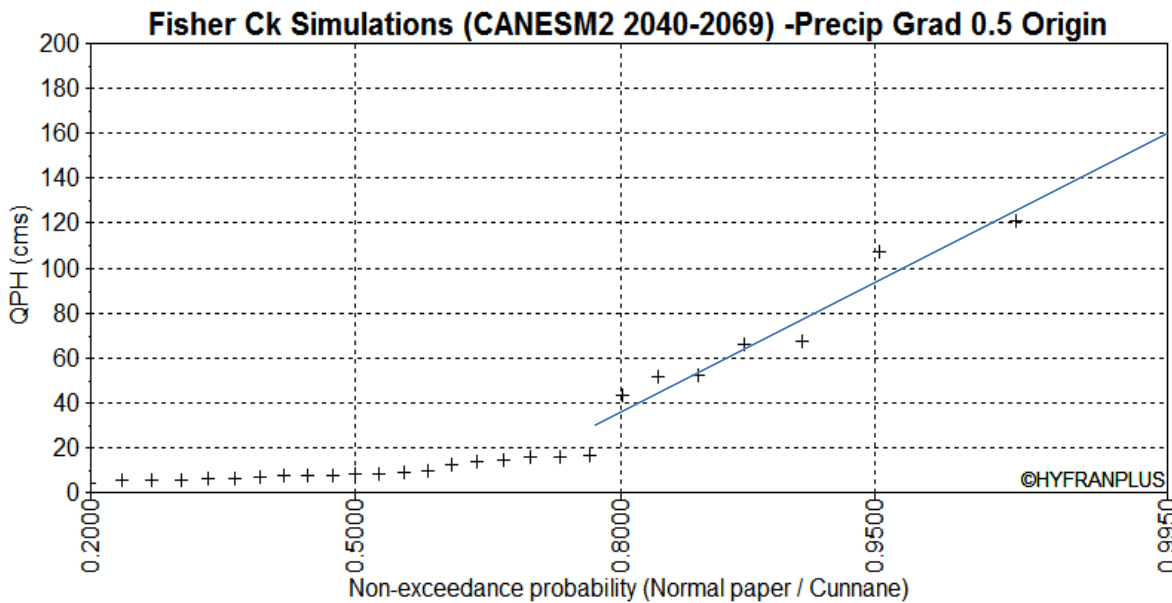
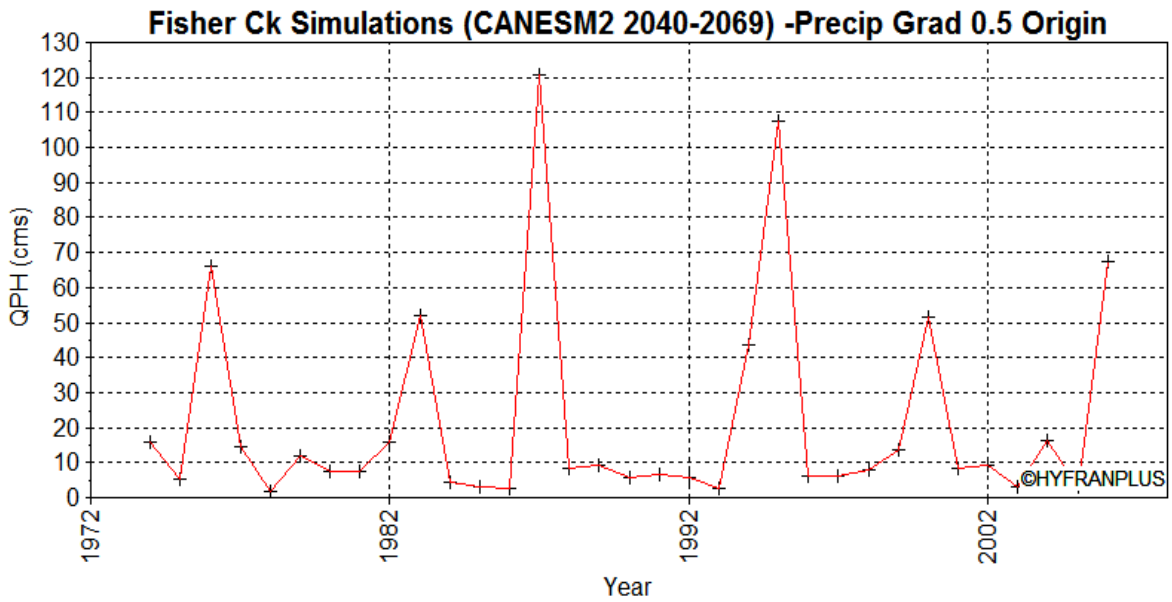


Figure D5. Sensitivity analysis: Fisher Creek HEC-HMS model precipitation gradient set to 50% of original value; simulated Fisher Creek Bridge annual hourly discharge maxima (top panel) and frequency analysis of the annual hourly discharge maxima (bottom panel) for the CanESM2 climate projection for the period 2040-2069.

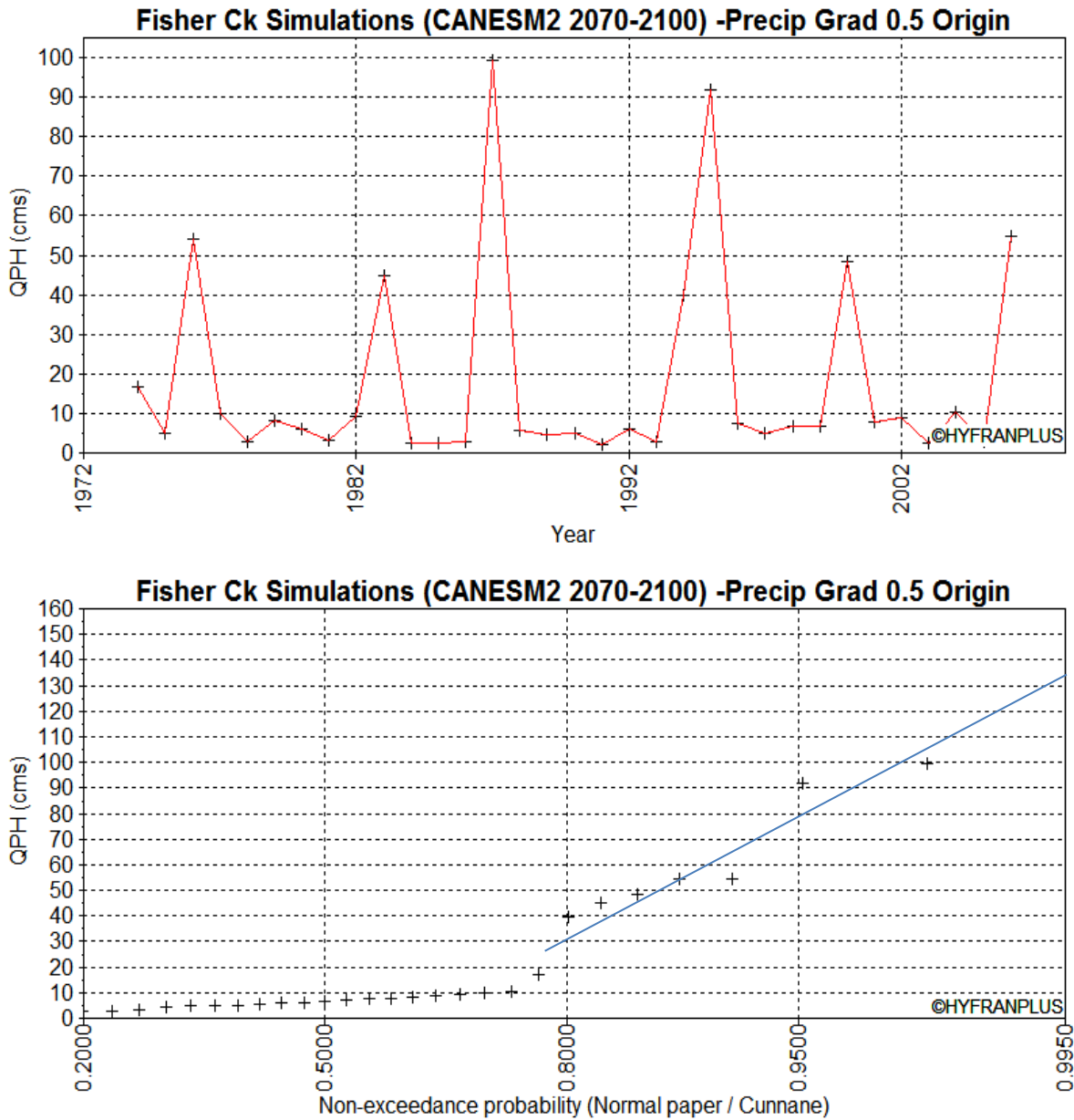


Figure D6. Sensitivity analysis: Fisher Creek HEC-HMS model precipitation gradient set to 50% of original value; simulated Fisher Creek Bridge annual hourly discharge maxima (top panel) and frequency analysis of the annual hourly discharge maxima (bottom panel) for the CanESM2 climate projection for the period 2070-2100.

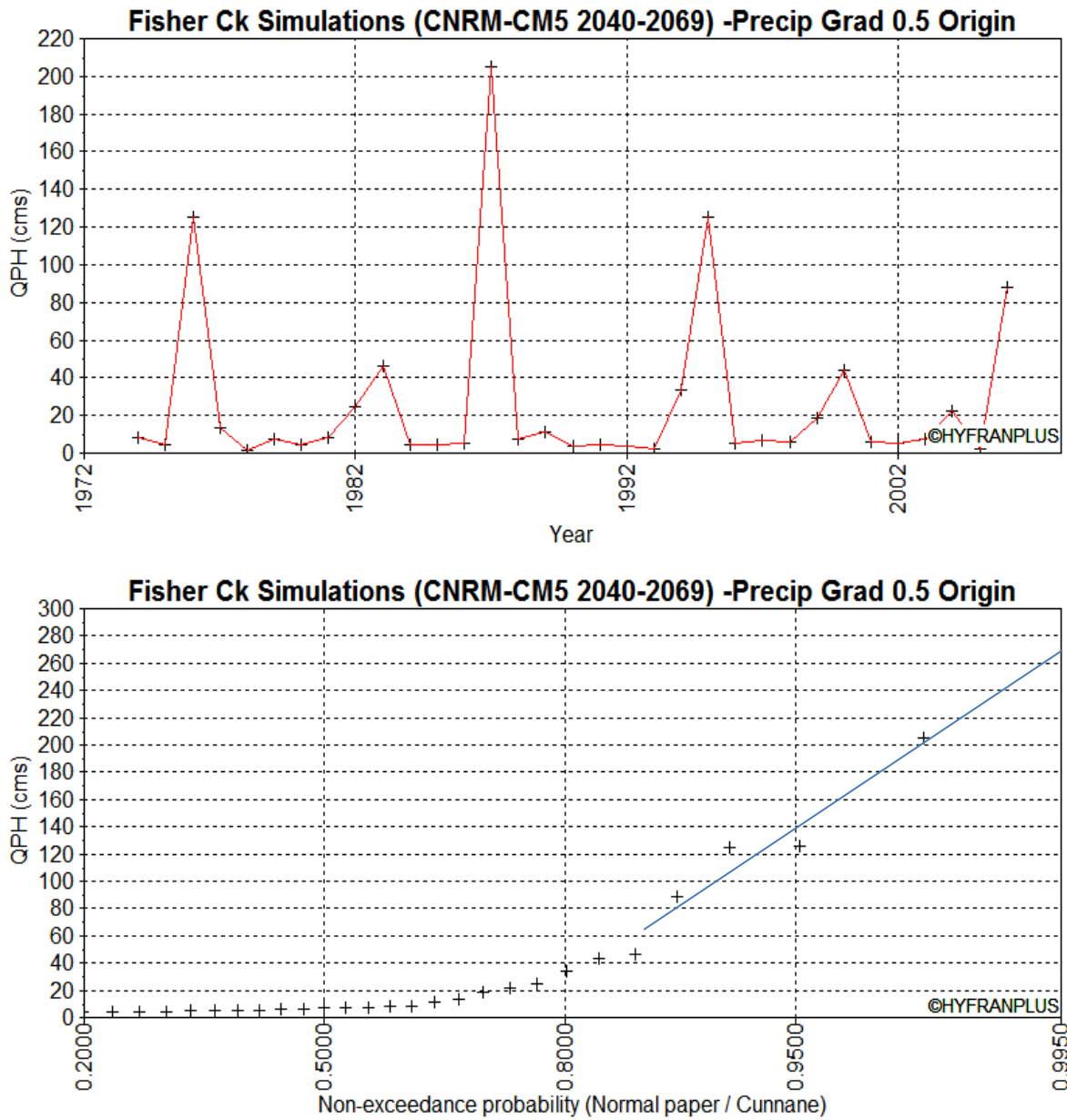


Figure D7. Sensitivity analysis: Fisher Creek HEC-HMS model precipitation gradient set to 50% of original value; simulated Fisher Creek Bridge annual hourly discharge maxima (top panel) and frequency analysis of the annual hourly discharge maxima (bottom panel) for the CNRM-CM5 climate projection for the period 2040-2069.

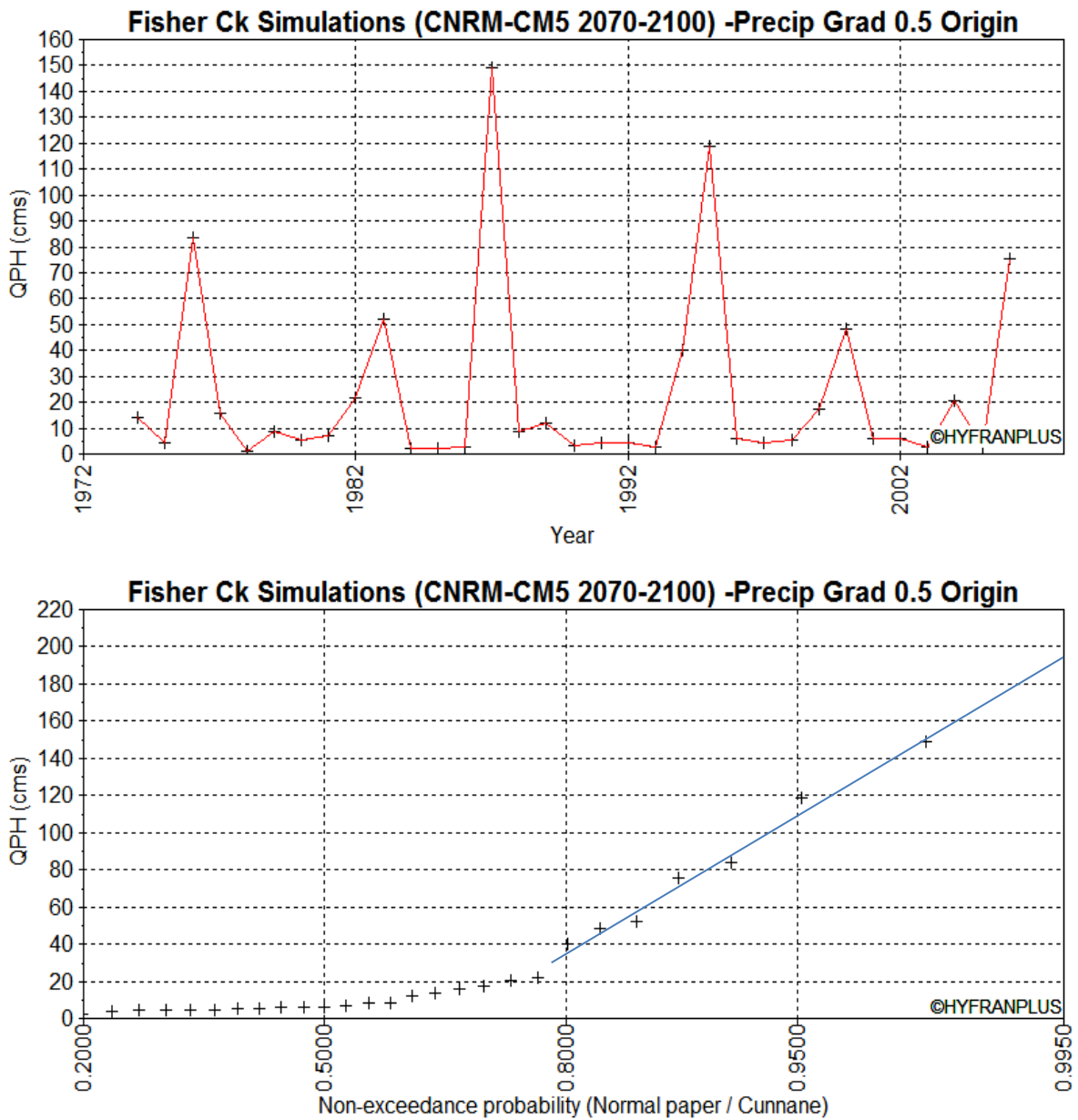


Figure D8. Sensitivity analysis: Fisher Creek HEC-HMS model precipitation gradient set to 50% of original value; simulated Fisher Creek Bridge annual hourly discharge maxima (top panel) and frequency analysis of the annual hourly discharge maxima (bottom panel) for the CNRM-CM5 climate projection for the period 2070-2100.

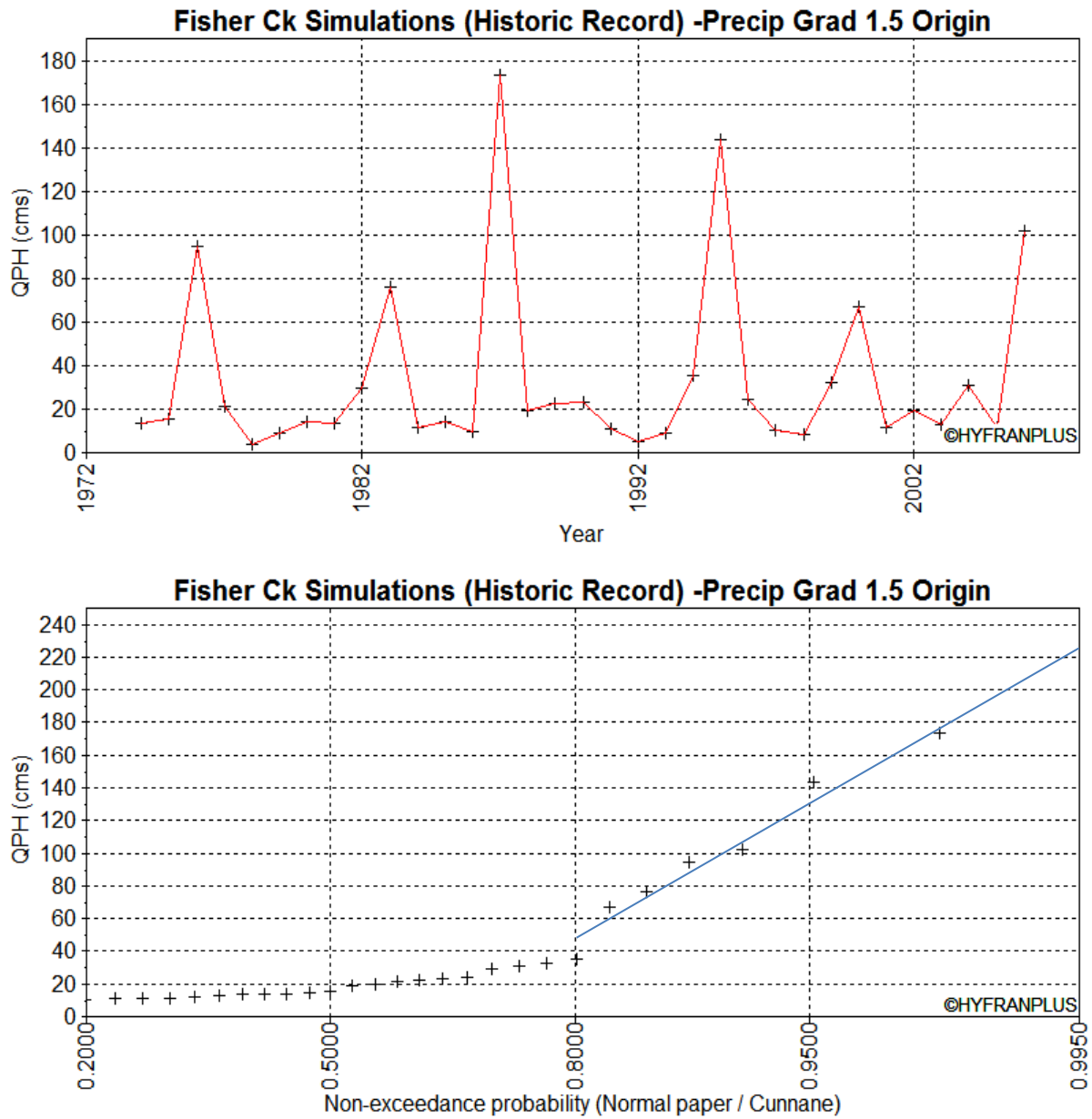


Figure D9. Sensitivity analysis: Fisher Creek HEC-HMS model precipitation gradient set to 150% of original value; simulated Fisher Creek Bridge annual hourly discharge maxima (top panel) and frequency analysis of the annual hourly discharge maxima (bottom panel) for the historic climate period.

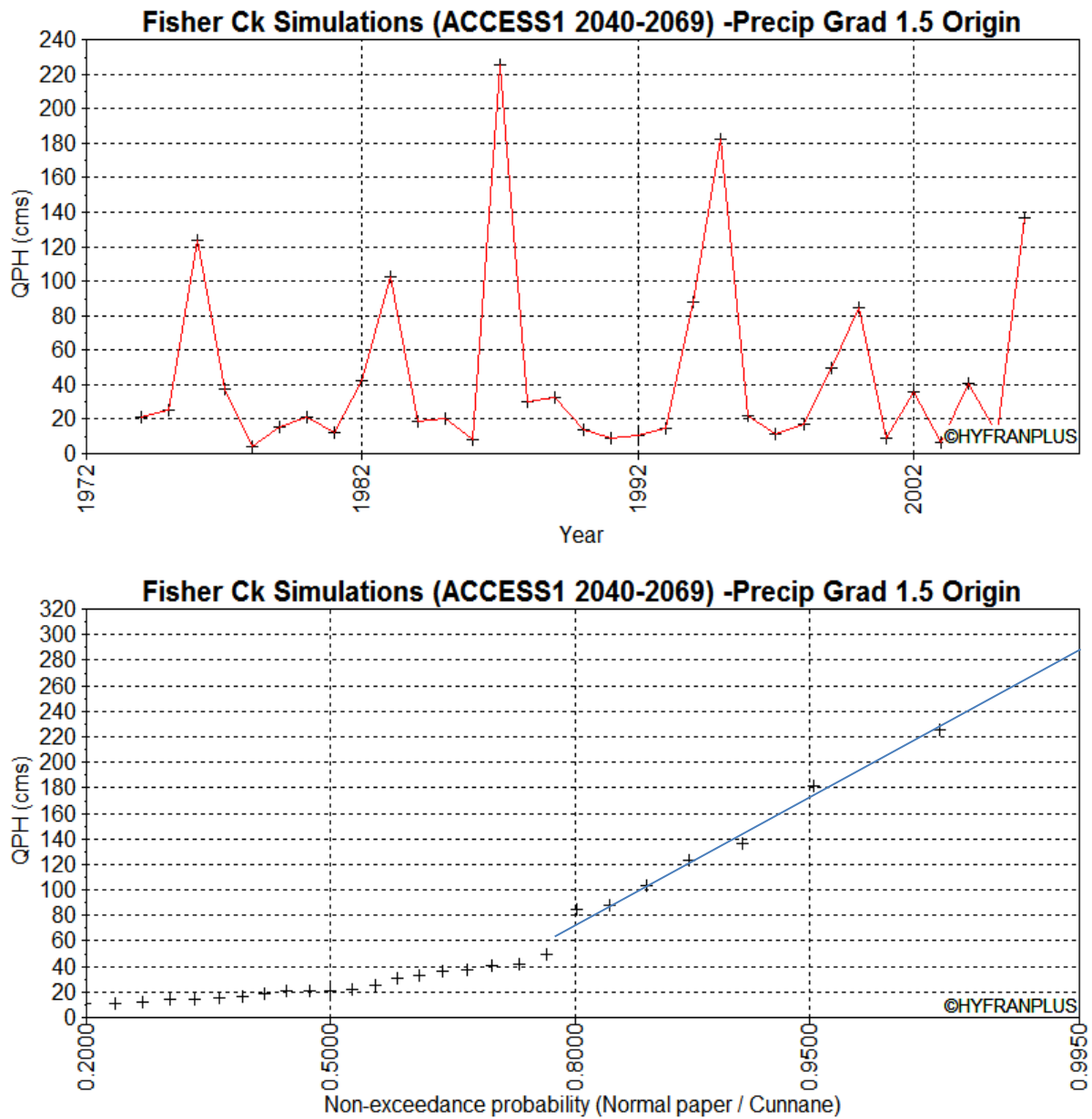


Figure D10. Sensitivity analysis: Fisher Creek HEC-HMS model precipitation gradient set to 150% of original value; simulated Fisher Creek Bridge annual hourly discharge maxima (top panel) and frequency analysis of the annual hourly discharge maxima (bottom panel) for the ACCESS1 climate projection for the period 2040-2069.

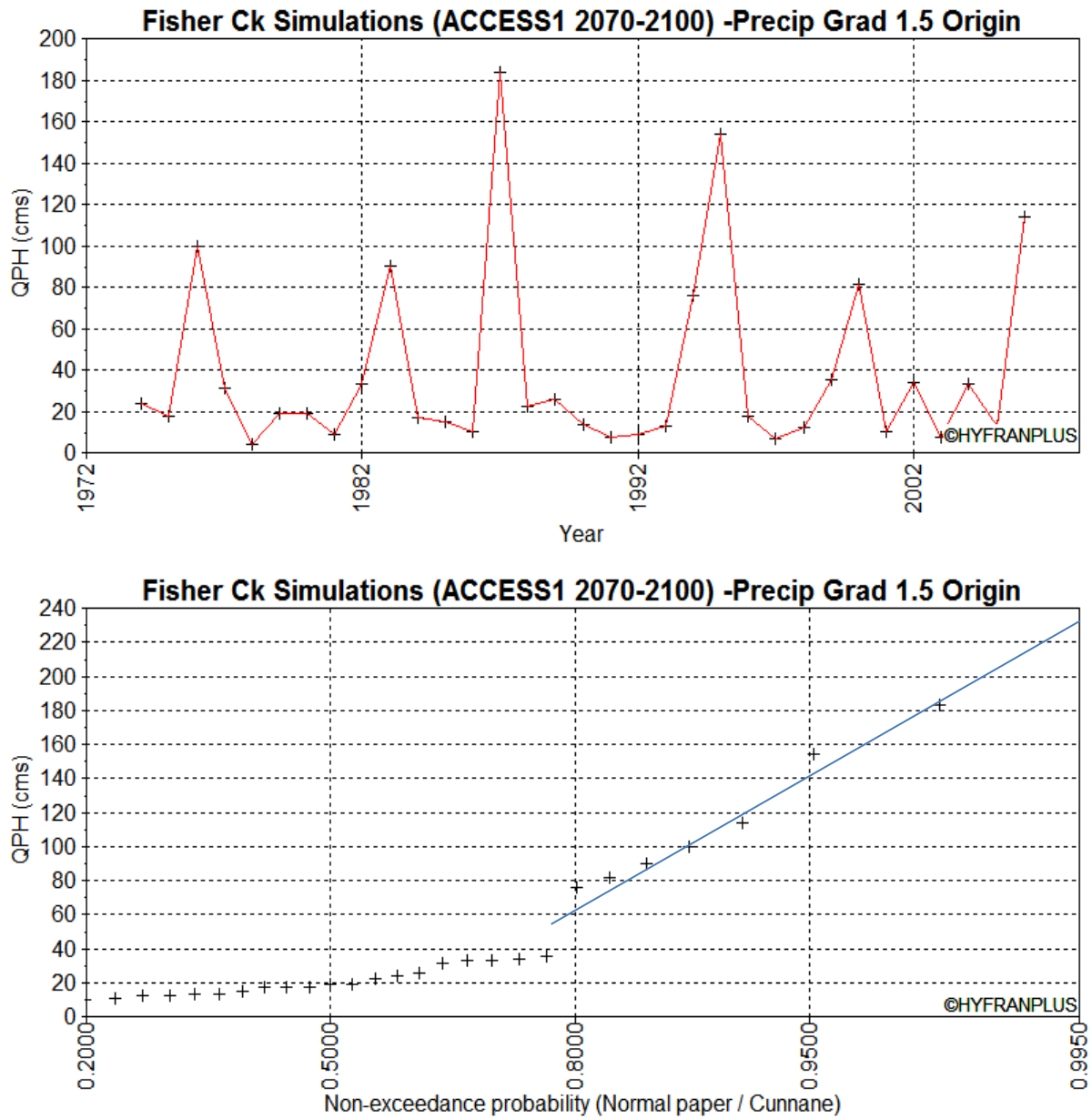


Figure D11. Sensitivity analysis: Fisher Creek HEC-HMS model precipitation gradient set to 150% of original value; simulated Fisher Creek Bridge annual hourly discharge maxima (top panel) and frequency analysis of the annual hourly discharge maxima (bottom panel) for the ACCESS1 climate projection for the period 2070-2100.

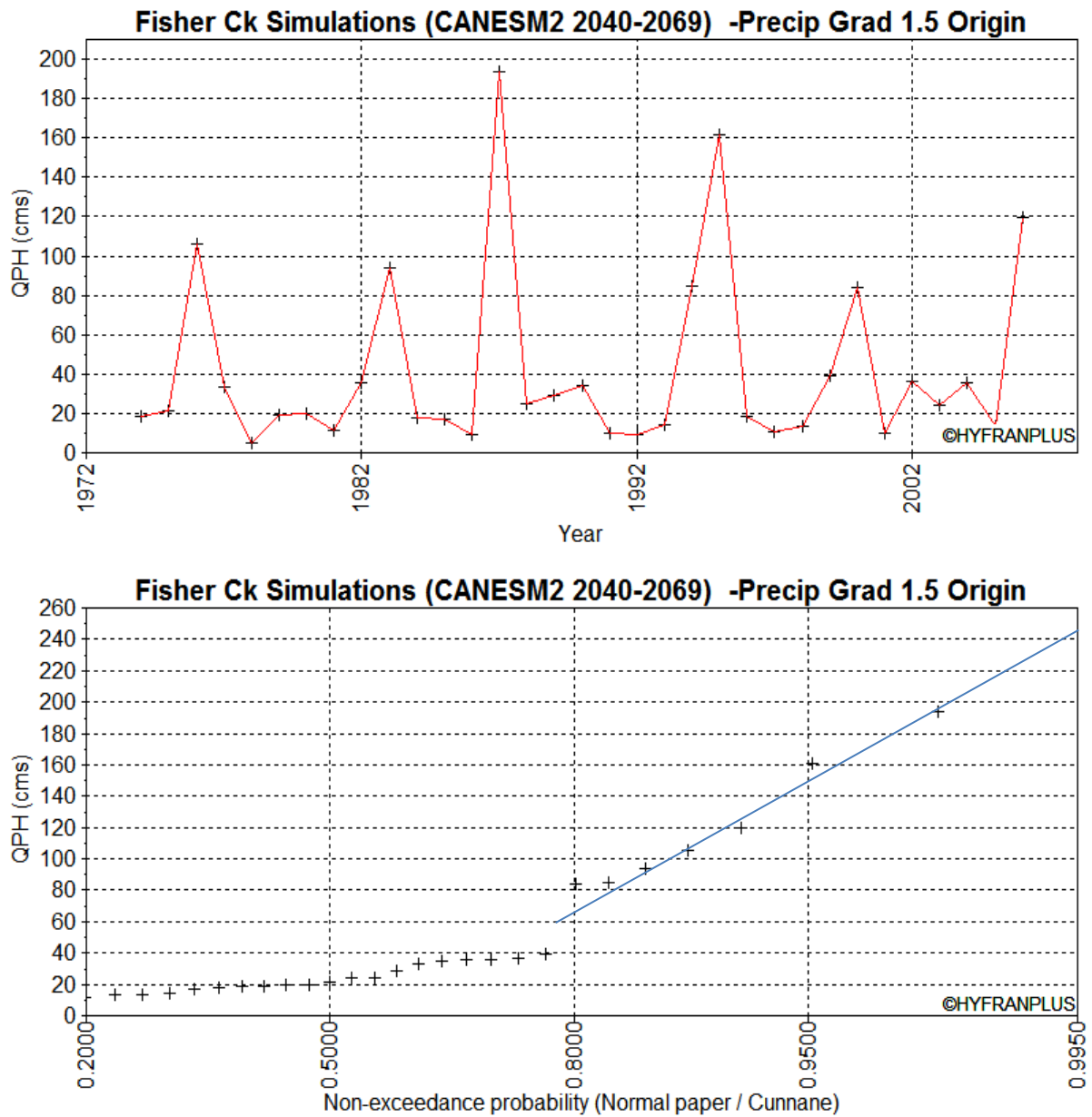


Figure D12. Sensitivity analysis: Fisher Creek HEC-HMS model precipitation gradient set to 150% of original value; simulated Fisher Creek Bridge annual hourly discharge maxima (top panel) and frequency analysis of the annual hourly discharge maxima (bottom panel) for the CanESM2 climate projection for the period 2040-2069.

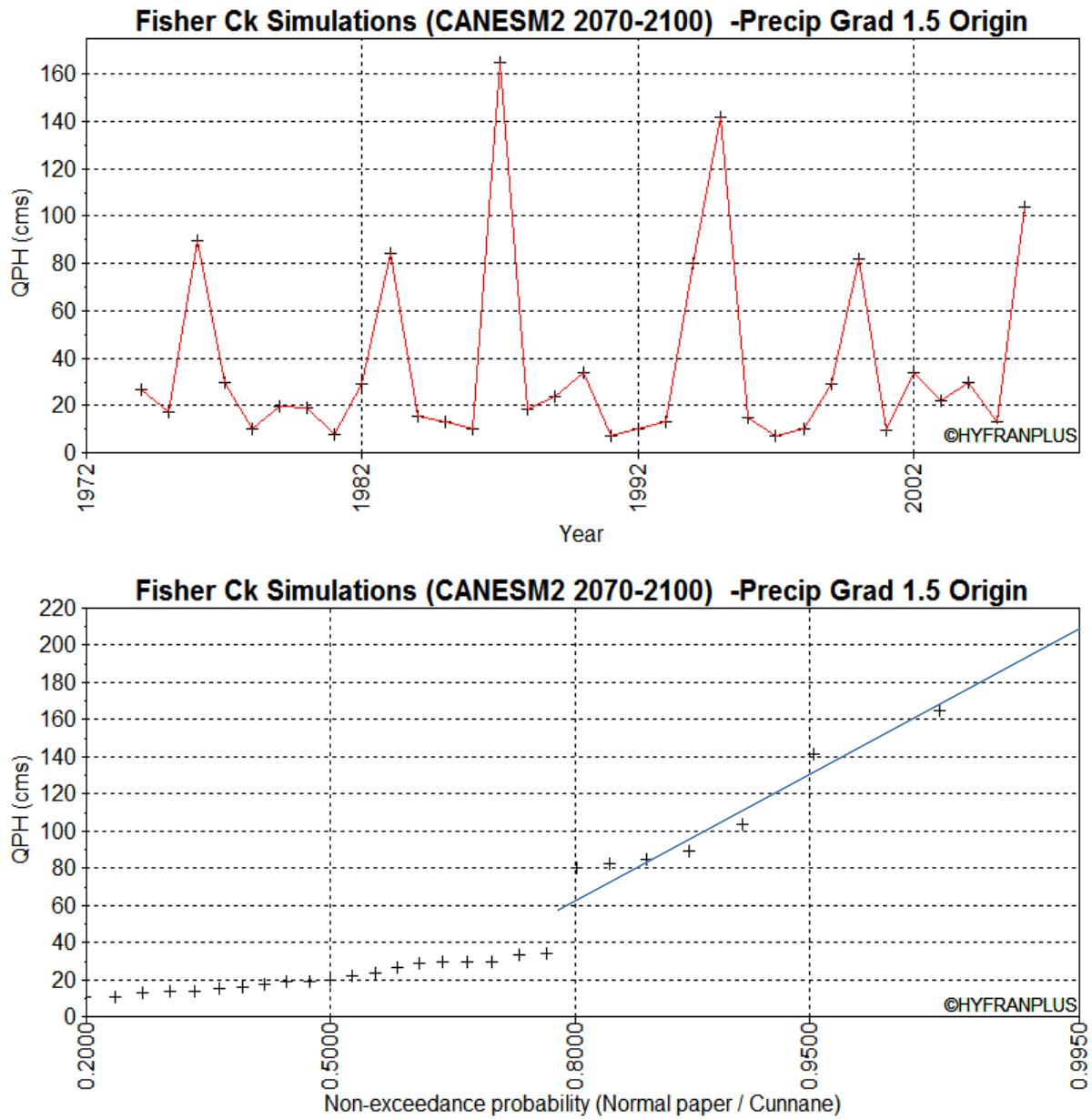


Figure D13. Sensitivity analysis: Fisher Creek HEC-HMS model precipitation gradient set to 150% of original value; simulated Fisher Creek Bridge annual hourly discharge maxima (top panel) and frequency analysis of the annual hourly discharge maxima (bottom panel) for the CanESM2 climate projection for the period 2070-2100.

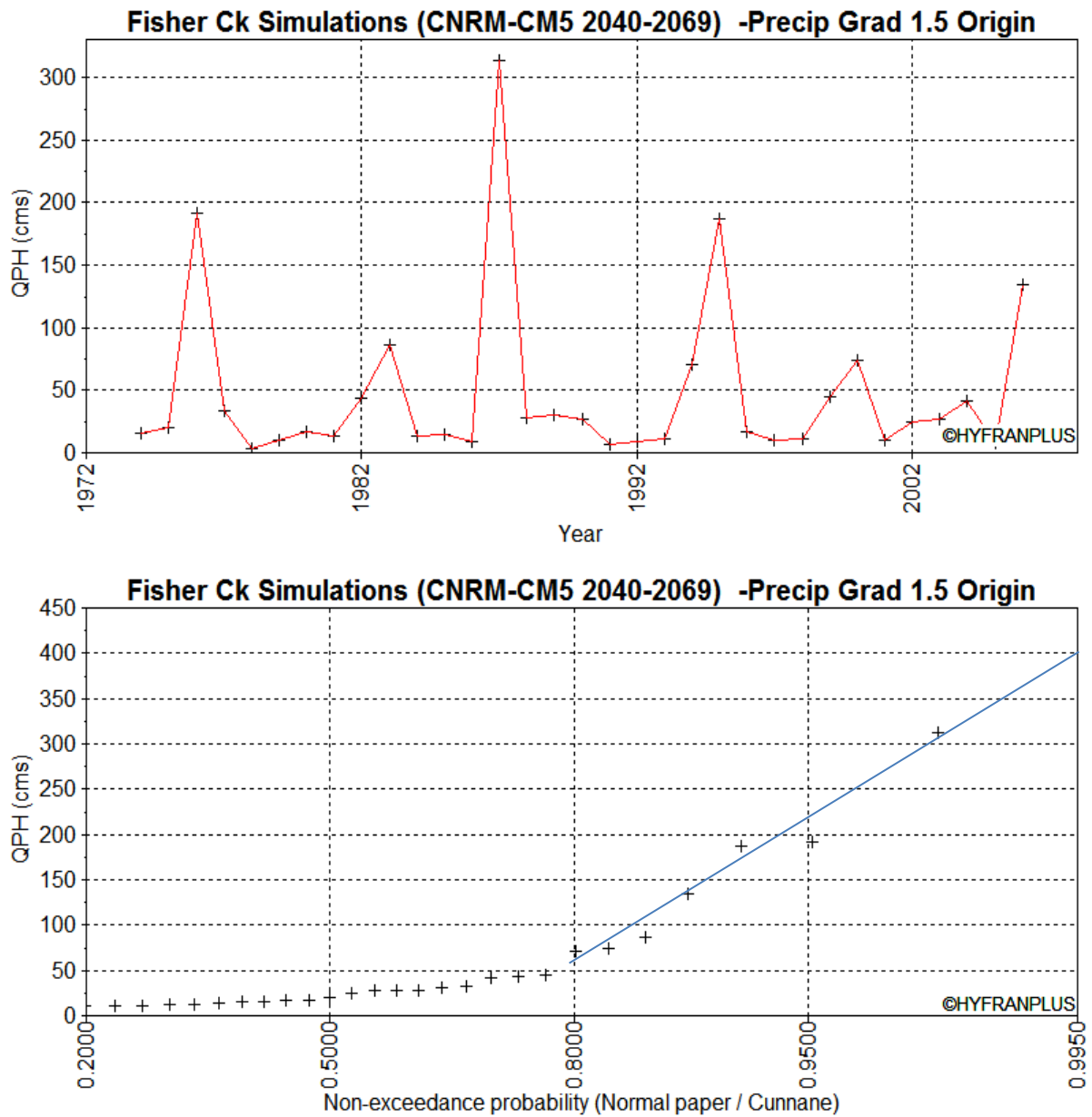


Figure D14. Sensitivity analysis: Fisher Creek HEC-HMS model precipitation gradient set to 150% of original value; simulated Fisher Creek Bridge annual hourly discharge maxima (top panel) and frequency analysis of the annual hourly discharge maxima (bottom panel) for the CNRM-CM5 climate projection for the period 2040-2069.

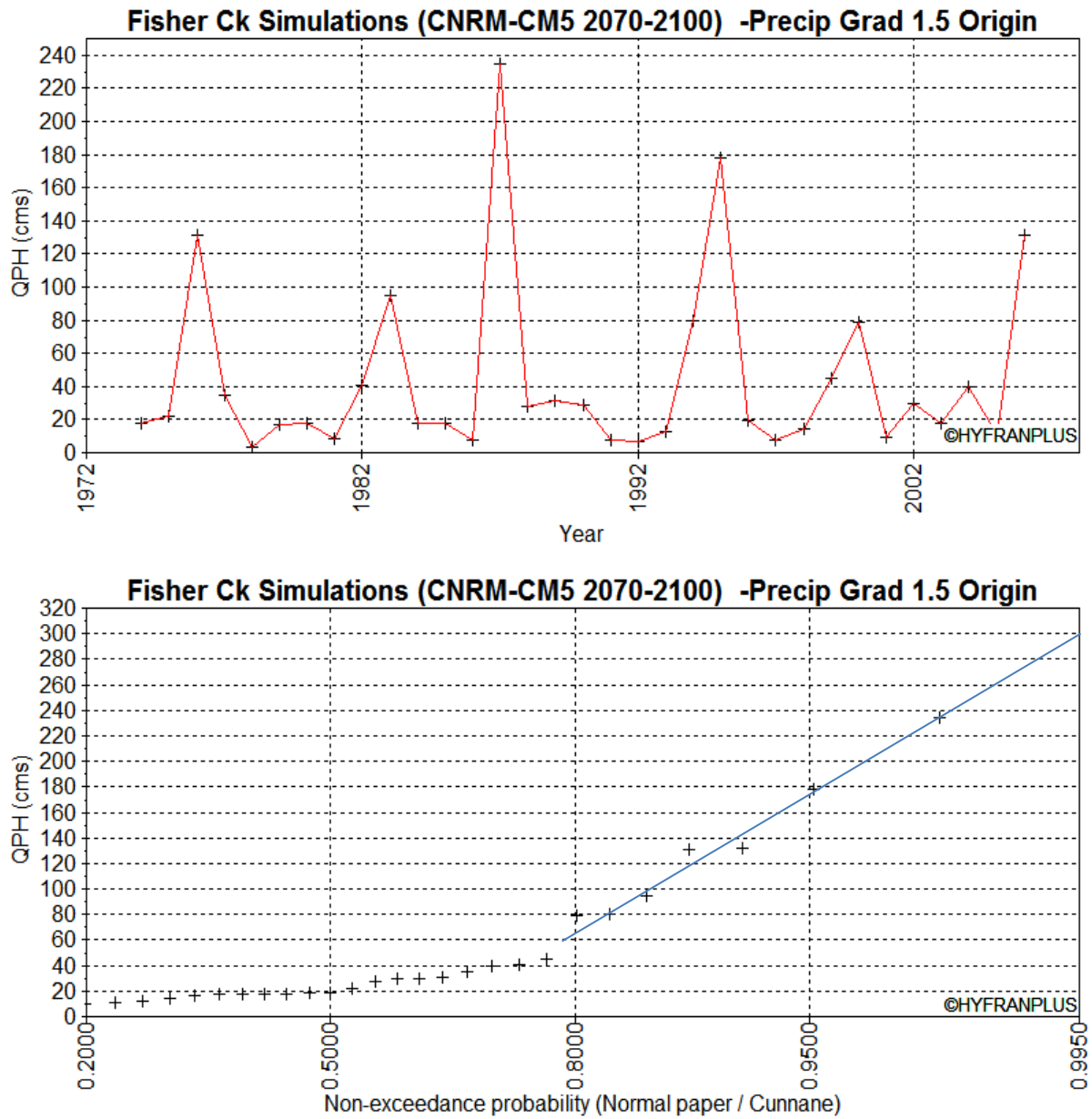


Figure D15. Sensitivity analysis: Fisher Creek HEC-HMS model precipitation gradient set to 150% of original value; simulated Fisher Creek Bridge annual hourly discharge maxima (top panel) and frequency analysis of the annual hourly discharge maxima (bottom panel) for the CNRM-CM5 climate projection for the period 2070-2100.

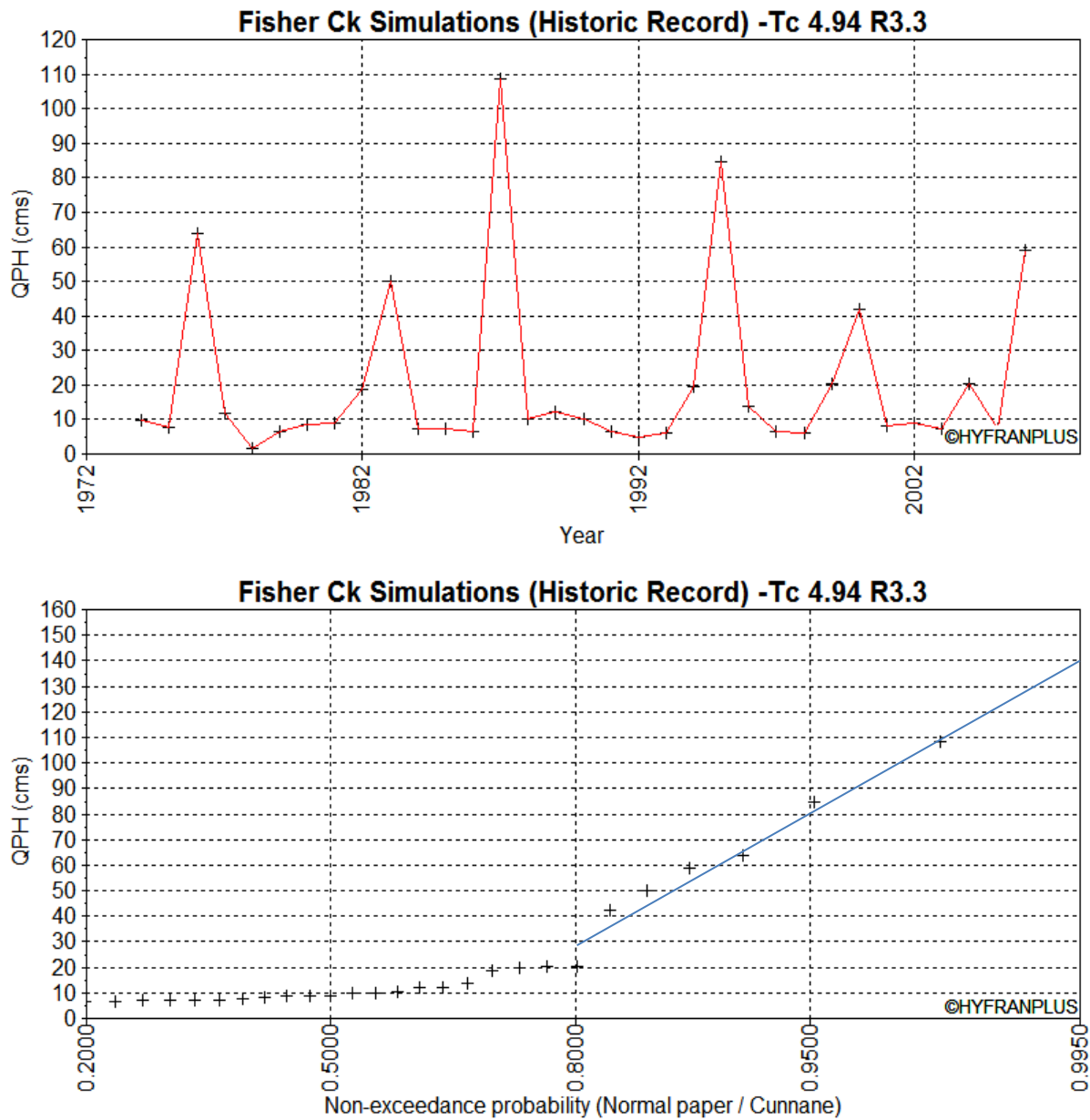


Figure D16. Sensitivity analysis: Fisher Creek HEC-HMS time of concentration set to 4.94 hours; simulated Fisher Creek Bridge annual hourly discharge maxima (top panel) and frequency analysis of the annual hourly discharge maxima (bottom panel) for the historic climate period.

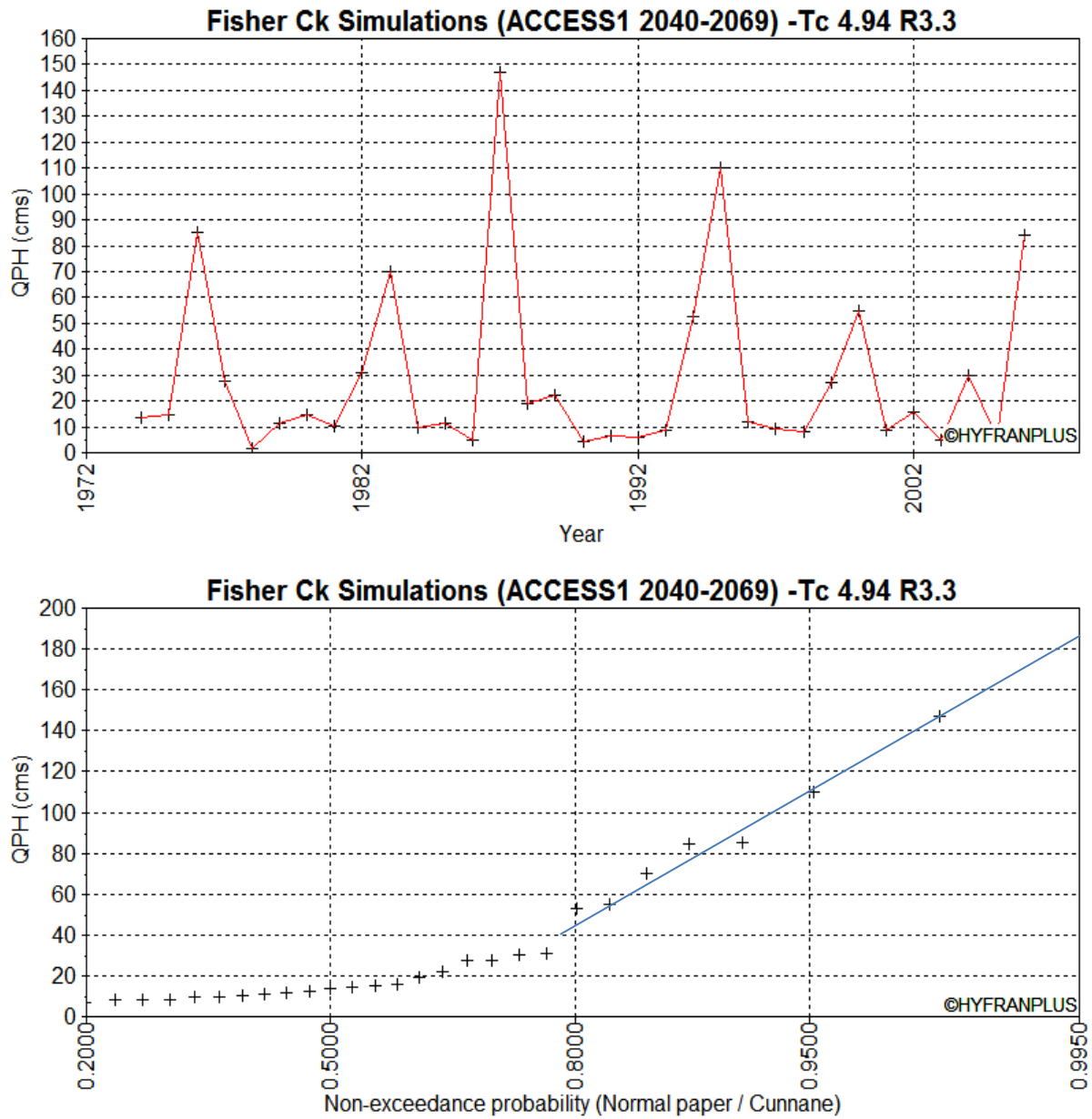


Figure D17. Sensitivity analysis: Fisher Creek HEC-HMS time of concentration set to 4.94 hours; simulated Fisher Creek Bridge annual hourly discharge maxima (top panel) and frequency analysis of the annual hourly discharge maxima (bottom panel) for the ACCESS1 climate projection for the period 2040-2069.

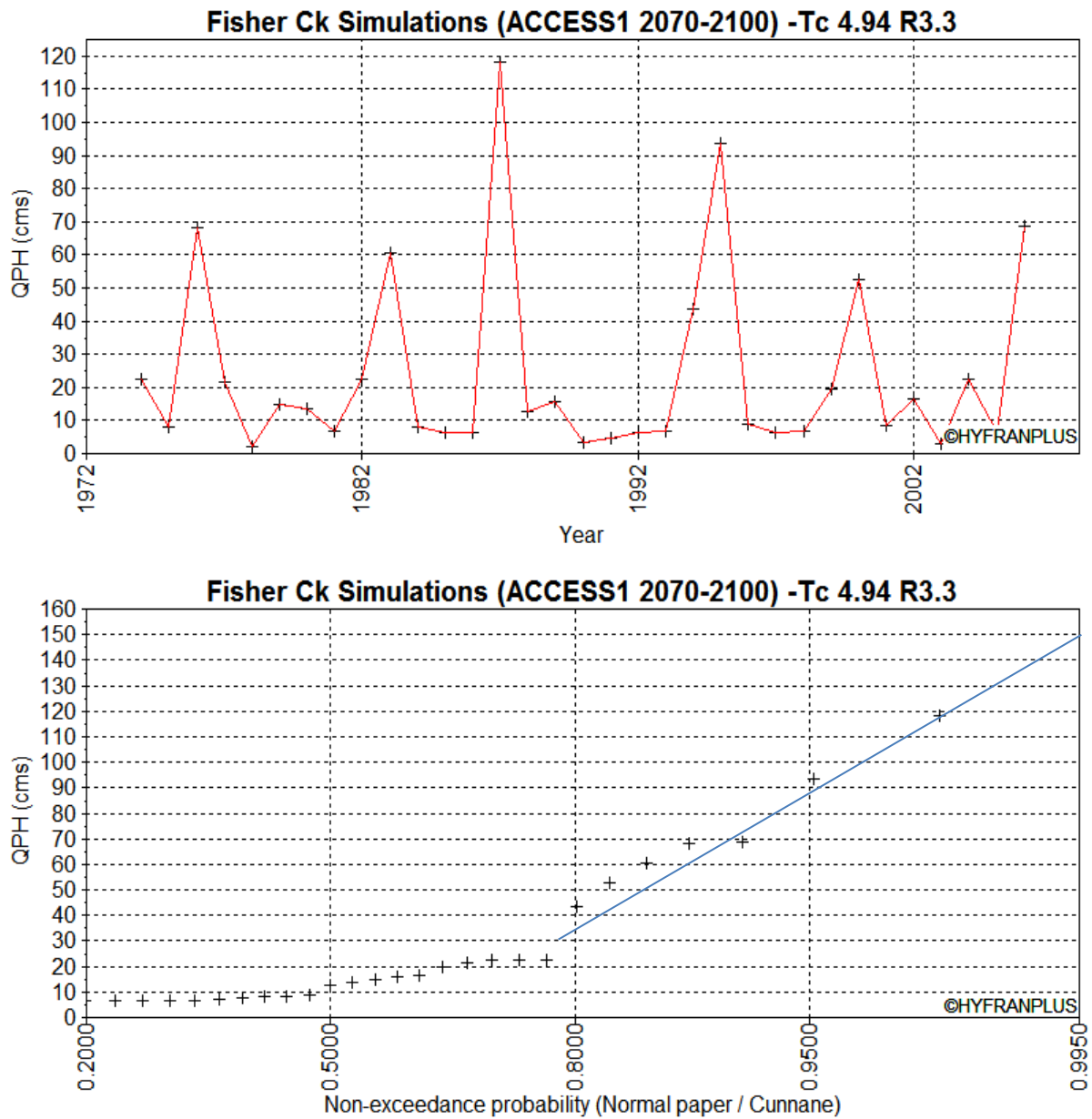


Figure D18. Sensitivity analysis: Fisher Creek HEC-HMS time of concentration set to 4.94 hours; simulated Fisher Creek Bridge annual hourly discharge maxima (top panel) and frequency analysis of the annual hourly discharge maxima (bottom panel) for the ACCESS1 climate projection for the period 2070-2100.

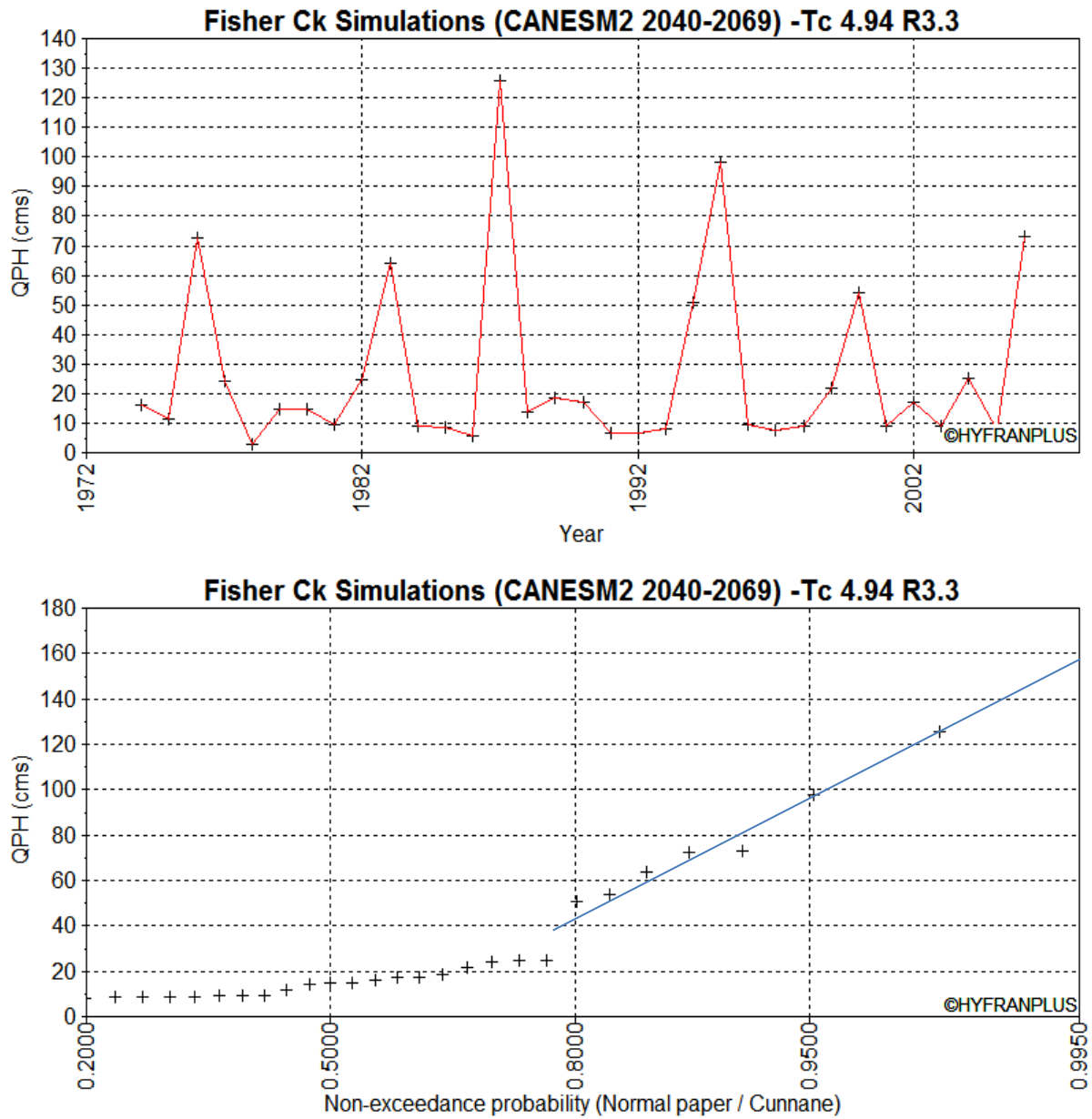


Figure D19. Sensitivity analysis: Fisher Creek HEC-HMS time of concentration set to 4.94 hours; simulated Fisher Creek Bridge annual hourly discharge maxima (top panel) and frequency analysis of the annual hourly discharge maxima (bottom panel) for the CanESM2 climate projection for the period 2040-2069.

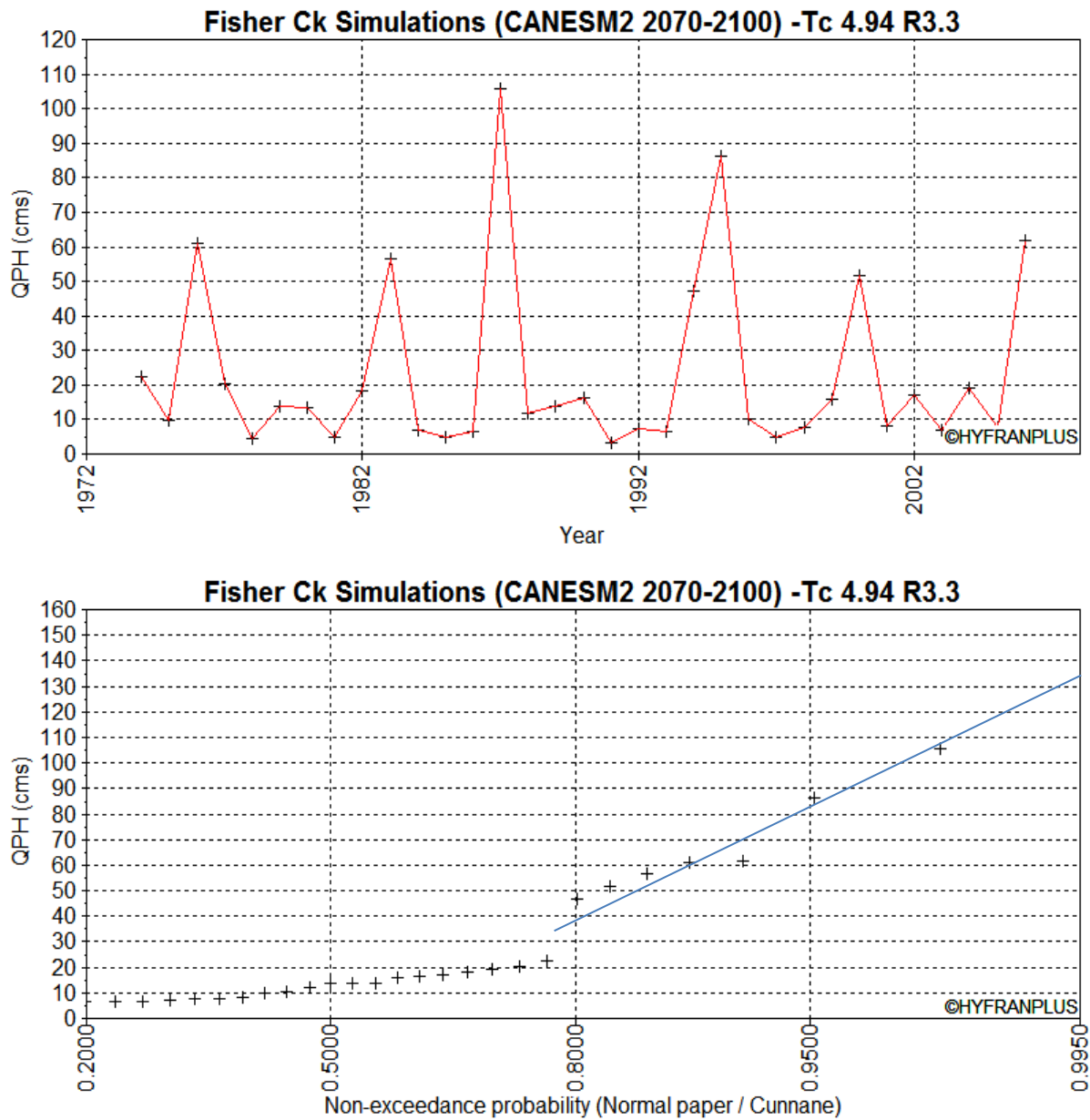


Figure D20. Sensitivity analysis: Fisher Creek HEC-HMS time of concentration set to 4.94 hours; simulated Fisher Creek Bridge annual hourly discharge maxima (top panel) and frequency analysis of the annual hourly discharge maxima (bottom panel) for the CanESM2 climate projection for the period 2070-2100.

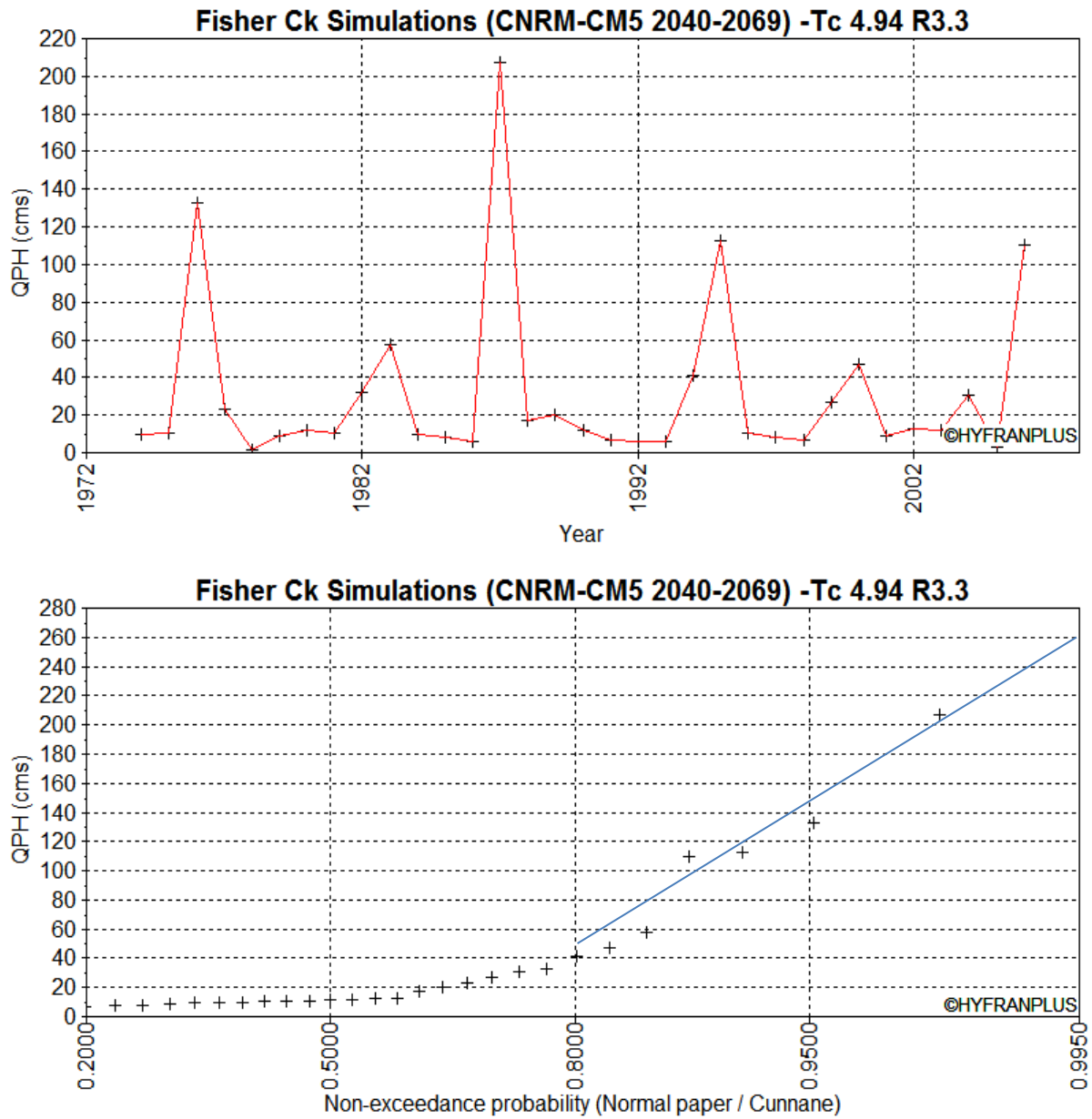


Figure D21. Sensitivity analysis: Fisher Creek HEC-HMS time of concentration set to 4.94 hours; simulated Fisher Creek Bridge annual hourly discharge maxima (top panel) and frequency analysis of the annual hourly discharge maxima (bottom panel) for the CNRM-CM5 climate projection for the period 2040-2069.

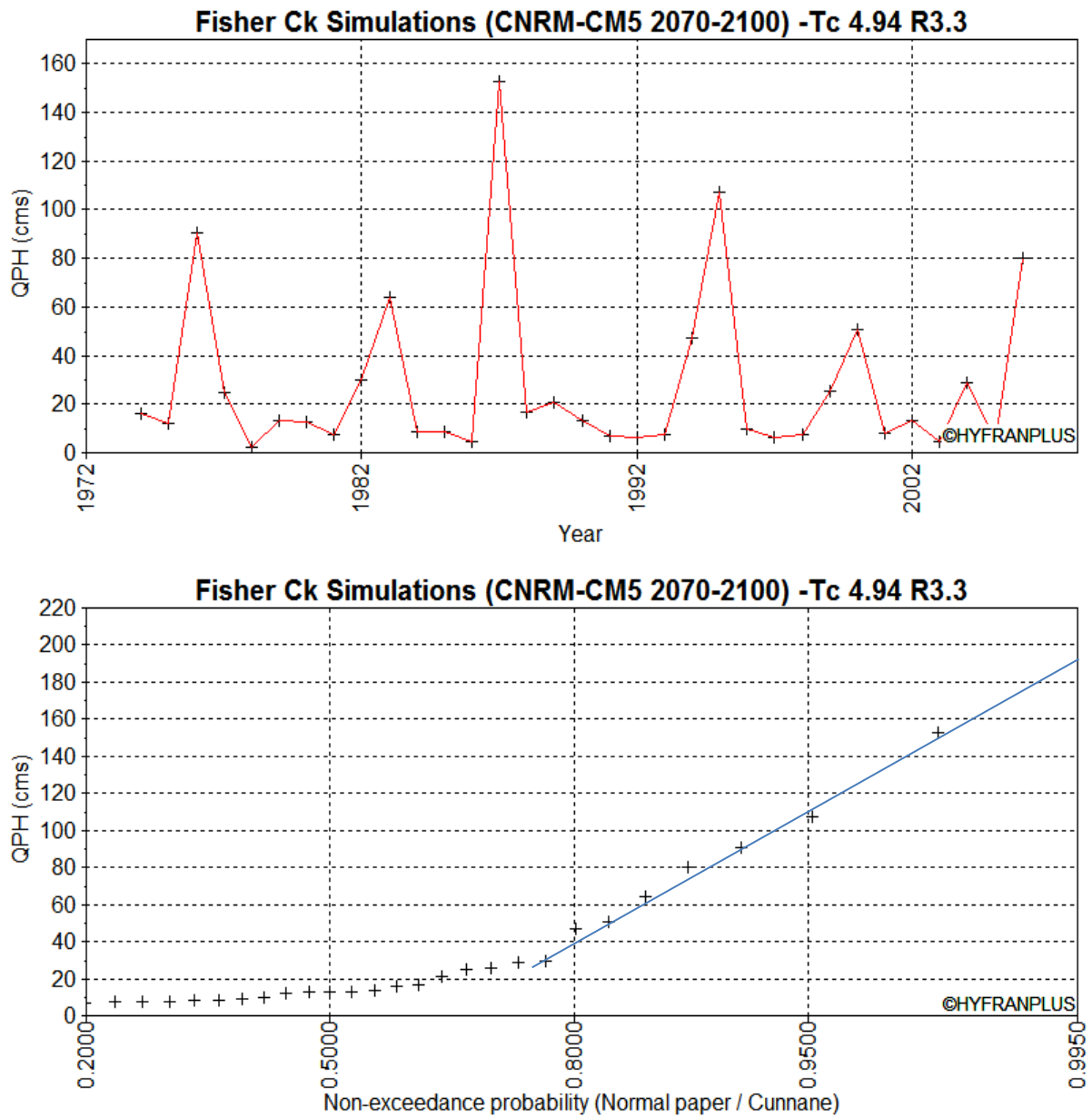


Figure D22. Sensitivity analysis: Fisher Creek HEC-HMS time of concentration set to 4.94 hours; simulated Fisher Creek Bridge annual hourly discharge maxima (top panel) and frequency analysis of the annual hourly discharge maxima (bottom panel) for the CNRM-CM5 climate projection for the period 2070-2100.